

FEB – Fresenius Environmental Bulletin

FOUNDED JOINTLY BY F. KORTE AND F. COULSTON

PRODUCTION BY PSP – PARLAR SCIENTIFIC PUBLICATIONS, ANGERSTR. 12, 85354 FREISING, GERMANY

IN COOPERATION WITH LEHRSTUHL FÜR CHEMISCH-TECHNISCHE ANALYSE UND LEBENSMITTELTECHNOLOGIE,

TECHNISCHE UNIVERSITÄT MÜNCHEN, 85350 FREISING - WEIHENSTEPHAN, GERMANY

COPYRIGHT © BY PSP – PARLAR SCIENTIFIC PUBLICATIONS, ANGERSTR. 12, 85354 FREISING, GERMANY.

ALL RIGHTS ARE RESERVED, ESPECIALLY THE RIGHT TO TRANSLATE INTO FOREIGN LANGUAGE. NO PART OF THE JOURNAL

MAY BE REPRODUCED IN ANY FORM- THROUGH PHOTOCOPYING, MICROFILMING OR OTHER PROCESSES- OR CONVERTED TO A MACHINE LANGUAGE, ESPECIALLY FOR DATA PROCESSING EQUIPMENT- WITHOUT THE WRITTEN PERMISSION OF THE PUBLISHER. THE RIGHTS OF REPRODUCTION BY LECTURE, RADIO

AND TELEVISION TRANSMISSION, MAGNETIC SOUND RECORDING OR SIMILAR MEANS ARE ALSO RESERVED

FEB - EDITORIAL BOARD**Chief Editor:**

PROF. DR. H. PARLAR
 INSTITUT FÜR LEBENSMITTELTECHNOLOGIE UND ANALYTISCHE CHEMIE
 TU MÜNCHEN - 85350 FREISING-WEIHENSTEPHAN, GERMANY
 E-MAIL: PARLAR@WZW.TUM.DE

Co-Editors:**ENVIRONMENTAL ANALYTICAL CHEMISTRY:**

DR. D. KOTZIAS
 COMMISSION OF THE EUROPEAN COMMUNITIES,
 JOINT RESEARCH CENTRE, ISPRRA ESTABLISHMENT,
 21020 ISPRRA (VARESE), ITALY

ENVIRONMENTAL PROTEOMIC AND BIOLOGY:

PROF. DR. A. GÖRG
 FACHGEBIET PROTEOMIK
 TU MÜNCHEN - 85350 FREISING-WEIHENSTEPHAN, GERMANY

PROF. DR. A. PICCOLO
 UNIVERSITÀ DI NAPOLI "FREDERICIO II",
 DIPTO. DI SCIENZE CHIMICO-AGGRARIE
 VIA UNIVERSITÀ 100, 80055 PORTICI (NAPOLI), ITALY

PROF. DR. G. SCHÜÜRMANN
 UFZ-UMWELTFORSCHUNGZENTRUM,
 SEKTION CHEMISCHE ÖKOTOXIKOLOGIE LEIPZIG-HALLE GMBH,
 PERMOSERSTR.15, 04318 LEIPZIG, GERMANY

ENVIRONMENTAL CHEMISTRY:

PROF. DR. M. BAHADIR
 INSTITUT FÜR ÖKOLOGISCHE CHEMIE UND ABFALLANALYTIK
 TU BRAUNSCHWEIG
 HAGENRING 30, 38106 BRAUNSCHWEIG, GERMANY

PROF. DR. M. SPITELLER
 INSTITUT FÜR UMWELTFORSCHUNG UNIVERSITÄT DORTMUND
 OTTO-HAHN-STR. 6, 44221 DORTMUND, GERMANY

PROF. DR. IVAN HOLOUBEK
 RECETOX_TOCOEN
 KAMENICE 126/3, 62500 BRNO, CZECH REPUBLIC

ENVIRONMENTAL MANAGEMENT:

DR. H. SCHLESING
 SECRETARY GENERAL, EARTO,
 RUE DE LUXEMBOURG,3, 1000 BRUSSELS, BELGIUM

PROF. DR. F. VOSNIAKOS
 T.E.I. OF THESSALONIKI, APPLIED PHYSICS LAB.
 P.O. BOX 14561, 54101 THESSALONIKI, GREECE

DR. K.I. NIKOLAOU
 ORGANIZATION OF THE MASTER PLAN &
 ENVIRONMENTAL PROTECTION OF THESSALONIKI (OMPEPT)
 54636 THESSALONIKI, GREECE

ENVIRONMENTAL TOXICOLOGY:

PROF. DR. H. GREIM
 SENATSKOMM. D. DFG Z. PRÜFUNG GESUNDHEITSSCHÄDL.
 ARBEITSSTOFFE
 TU MÜNCHEN, 85350 FREISING-WEIHENSTEPHAN, GERMANY

PROF. DR. A. KETTRUP
 INSTITUT FÜR LEBENSMITTELTECHNOLOGIE UND ANALYTISCHE CHEMIE
 TU MÜNCHEN - 85350 FREISING-WEIHENSTEPHAN, GERMANY

FEB - ADVISORY BOARD**ENVIRONMENTAL ANALYTICAL CHEMISTRY:**

K. BALLSCHMITTER, D - K. BESTER, D - K. FISCHER, D - R. KALLENBORN, N
 D.C.G. MUIR, CAN - R. NIESSNER, D - W. VETTER, D - R. SPACCINI, I

ENVIRONMENTAL PROTEOMIC AND BIOLOGY:

D. ADELUNG, D - G.I. KVESITADZE, GEOR
 A. REICHLMAIR-LAIS, D - C. STEINBERG, D - R. VISWANATHAN, D

ENVIRONMENTAL CHEMISTRY:

J.P. LAY, D - J. BURHENNE, D - S. NITZ, D - R. KREUZIG, D
 D. L. SWACKHAMMER, U.S.A. - R. ZEPPE, U.S.A. - T. ALPAY, TR
 V. LIBRANDO; I

ENVIRONMENTAL MANAGEMENT:

O. HUTZINGER, A - L.O. RUZO, U.S.A - U. SCHLOTTMANN, D

ENVIRONMENTAL TOXICOLOGY:

K.-W. SCHRAMM, D - H. FRANK, D - H. P. HAGENMEIER, D
 D. SCHULZ-JANDER, U.S.A. - H.U. WOLF, D - M. McLACHLAN, S

Managing Editor:

DR. G. LEUPOLD
 INSTITUT FÜR CHEMISCHE-TECHNISCHE ANALYSE UND CHEMISCHE
 LEBENSMITTELTECHNOLOGIE, TU MÜNCHEN
 85350 FREISING-WEIHENSTEPHAN, GERMANY
 E-MAIL: LEU@WZW.TUM.DE

Editorial Chief-Officer:

SELMA PARLAR
 PSP- PARLAR SCIENTIFIC PUBLICATIONS
 ANGERSTR.12, 85354 FREISING, GERMANY
 E-MAIL: PARLAR@PSP-PARLAR.DE - WWW.PSP-PARLAR.DE

Marketing Chief Manager:

MAX-JOSEF KIRCHMAIER
 MASELL-AGENCY FOR MARKETING & COMMUNICATION, PUBLIC-
 RELATIONS
 ANGERSTR.12, 85354 FREISING, GERMANY
 E-MAIL: MASELL@MASELL.COM - WWW.MASELL.COM

Abstracted/ indexed in: Biology & Environmental Sciences, BIOSIS, C.A.B. International, Cambridge Scientific Abstracts, Chemical Abstracts, Current Awareness, Current Contents/ Agriculture, CSA Civil Engineering Abstracts, CSA Mechanical & Transengineering, IBIDS database, Information Ventures, NISC,

Research Alert, Science Citation Index (SCI), SciSearch, Selected
Water Resources Abstracts

CONTENTS

ORIGINAL PAPERS

EFFECT OF LEAD STRESS ON GROWTH AND ACCUMULATION RESPONSE OF <i>PANICUM MAXIMUM</i> IN TROPICAL SOIL Chengjun Ge, Huamei Yu, Wenhao Tang and Cheng Li	1583
HYBRID EFFECT OF CDS AND C ₆₀ MOLECULES ON TiO ₂ AND ENHANCEMENT OF THE PHOTOCATALYTIC ACTIVITY Ze-Da Meng, Lei Zhu, Kwang-Youn Cho and Won-Chun Oh	1589
OFFSHORE ECOSYSTEM HEALTH ASSESSMENT: A CASE STUDY OF JIANGSU OFFSHORE AREA, CHINA Zulin Hua, Benlin Dai, Li Gu, Kejian Chu, Yulong He and Yunzhen Li	1598
THE EFFECT OF BIOLOGICAL PRETREATMENT ON DISSOLVED ORGANIC NITROGEN REMOVAL IN DOWNSTREAM COAGULATION AND THE COUNTERMEASURE Huining Zhang, Li Gu, Bing Liu, Xin Yu and Zihong Fan	1611
IMPACT OF MAGNETIC TREATMENT ON PHYSICOCHEMICAL PROPERTIES OF WASTEWATER TREATMENT PLANTS IN NORTH JORDAN Saleh Shakhatreh and Riad Al Ott	1617
ENHANCED PHOTOCATALYTIC ACTIVITY OF AgNbO ₃ DOPED WITH Fe ³⁺ Hui Xu, Yuanguo Xu, Huaming Li, Guangsong Sun, Ling Liu and Xiangyang Wu	1624
CRITICAL EVALUATION OF THE NATIONAL ALLOCATION PLANS UNDER THE EUROPEAN UNION EMISSION TRADING SCHEME. CASE STUDY GREECE John K. Kaldellis, Dimitris Zafirakis and Nikolaos Mantelis	1629
RADIOACTIVITY MEASUREMENT AND DOSE ASSESSMENT FROM SURFACE SOILS AROUND THE ÇATALAĞZI COAL-FIRED POWER PLANT, TURKEY Hüseyin Aytekin and Rıdvan Baldık	1642
EFFECT OF ADAPTED CONSTRUCTED FLORA ON CONTINUOUS COUPLED AEROBIC-ANAEROBIC PROCESS FOR TREATMENT OF TOMATO PASTE WASTEWATER Peng Cao, Chun Li, Shumei Wen, Yanbin Tong and Jinren Ni	1649
COMPARISON OF ELEMENT CONTENTS IN HAZELNUTS GROWN UNDER ORGANIC AND CONVENTIONAL FARMING REGIMES FOR HUMAN NUTRITION AND HEALTH Uğur Akbaba, Yusuf Şahin and Hasan Türkez	1655
PROTECTIVE ROLE OF TWO LICHENS IN HUMAN LYMPHOCYTES <i>IN VITRO</i> Lokman Alpsoy, Ali Aslan, Elif Kotan, Guleray Agar and Mustafa Anar	1661

MODELLING THE INFLUENCE OF SALINITY AND WATER DEFICIENCY ON GROWTH AND BIOMASS OF <i>GROENLANDIA DENSA</i> (POTAMOGETONACEAE)	1667
Dilek Demirezen Yilmaz and Kadiriye Uruç Parlak	
ASSESSMENT OF RIVER LANDSCAPES IN TERMS OF PRESERVATION AND USAGE BALANCE: A CASE STUDY OF THE BARTİN RIVER FLOODPLAIN CORRIDOR (WESTERN BLACK SEA REGION, TURKEY)	1673
Bülent Cengiz, Richard C. Smardon and Yalçın Memlük	
DEGRADATION OF ORGANIC MATTER AND AMMONIA NITROGEN IN CONSTRUCTED RAPID INFILTRATION SYSTEM	1685
Wenlai Xu, Jianqiang Zhang and Yun Liu	
AEROBIC DEGRADATION PROPERTIES AND BACTERIAL DIVERSITY OF TOLUENE DEGRADED BY DIFFERENT ACCLIMATED BACTERIA	1691
Jianghong Guo, Yun Qi, Lin Zhao, Xiuli Liu and Xin Tan	
EFFECT OF INTERMITTENT ALKALI TREATMENT AND POTATO ADDITION ON ANAEROBIC DIGESTION OF SPARTINA ALTERNIFLORA	1698
Jibiao Zhang, Yan Luo, Xingzhang Luo, Zheng Zheng, Guangyin Chen and Shiguan Yang	
DISTRIBUTION AND CONTAMINATION STATUS OF HEAVY METALS IN SEDIMENTS OF BUNA RIVER AND ADRIATIC SEA	1704
Alma Shehu and Pranvera Lazo	
RELATIONSHIP BETWEEN SOIL NUTRIENTS AND SOIL MICROBIAL BIOMASS, STRUCTURE AND DIVERSITY UNDER DIFFERENT TILLAGE MANAGEMENT IN WHEAT-CORN DOUBLE-CROPPING SYSTEM	1711
Ying Wang, Chunsheng Hu and Wenxu Dong	
INDEX	1719

EFFECT OF LEAD STRESS ON GROWTH AND ACCUMULATION RESPONSE OF *PANICUM MAXIMUM* IN TROPICAL SOIL

Chengjun Ge^{1,2}, Huamei Yu^{3,4}, Wenhao Tang^{2,*}, and Cheng Li⁴

¹ Key Laboratory of Protection and Development Utilization of Tropical Crop

Germplasm Resources, Ministry of Education, Hainan University, Haikou 570228, China

² Department of Environmental Science, Hainan University, Renmin Road, Haikou 570228, China

³ School of Economy and Management, Hainan University, Renmin Road, Haikou 570228, China

⁴ School of Chemical and Environmental Engineering, China University of Mining and Technology, Beijing 100083, China

ABSTRACT

Using tropical plants in heavy metal-polluted environment restoration is a new bio-technique in ecological restoration research of tropical areas. Herein, we report a preliminary research to determine the growth and accumulation response of a typical tropical plant (*Panicum maximum*) on lead pollution. Results showed that Pb pollution in low concentration favored the height growth and dry weight increment of *Panicum maximum*, while in high concentration it disfavored. The addition of Pb increased all forms of Pb content in the soils, among which the residual forms exhibited a great reduction, while the Fe-Mn oxides and organic combined forms showed a great enhancement. The K_{BCF} value of roots of *Panicum maximum* ranged from 0.37 to 1.48. The concentration of lead in underground part was higher than that in aboveground part of *Panicum maximum*. So, this plant could still be a candidate for lead-contaminated soil reclamation.

KEYWORDS:

lead, *Panicum maximum*, growth, accumulation response

1. INTRODUCTION

With the development of urbanization, industrialization and agriculture, soils have been polluted by heavy metals all over the world [1], enhancing the detrimental effects on human health [2]. The heavy metal pollution has drawn much attention because of its nonbiodegradation, toxicity, and amount in nature, which has brought serious adverse effect to the ecosystem [3-7]. Researchers are interested in the iron behavior in soil and plant, phytoremediation technology in polluted soil and iron toxicity [8-10].

Using tropical plants in ecological restoration is a new bio-technique in research on heavy metal-polluted environment restoration [11]. Tropical plants possess the ability to eliminate heavy metal ions from soil by bio-concentration or bio-conversion when they absorb major mineral elements from soil.

Red soil (*granitic Latosol*), most of which shows strong acidity and low organic matter in surface layer of cultivated soils, is one of the most common soil styles in South China. Because of its strong acidity, simple structures of humic substances and weak adsorptive capacity of soil colloids, the red soil has weak cation exchange capacity. Thus, the heavy metal ions absorbed by soil have high biological activities negatively influencing the growth of plants.

In recent years, researchers have explored the effects of heavy metals, such as copper, cadmium and lead [12, 13], on aquatic and terrestrial plants, but there are few reports on tropical plants. In this paper, the Pb absorbing characteristics of *Panicum maximum*, a kind of ordinary tropical plant, were primarily investigated by pot simulation test. Growth response of *Panicum maximum* on Pb pollution in tropical soil was also firstly studied. Plant biomass, bio-accumulation of heavy metals, change of lead forms, and distribution of heavy metals were synchronously reported. This provides a theoretical basis and some available information for further application of *Panicum maximum* to polluted tropical soil reclamation and phytoremediation of toxic metals in polluted soil.

2. MATERIALS AND METHODS

2.1. Experimental Materials

The soil samples (*granitic Latosol*) used for the pot experiments were collected from the agricultural experiment park of Hainan University, Danzhou, China. The basic characteristics of soil samples (depth of 1 to 20 cm) were as follows: organic matter content $2.71 \text{ g} \cdot \text{kg}^{-1}$, pH 5.59, and

* Corresponding author

total nitrogen, organic phosphorus, potassium and lead contents were $0.13 \text{ g} \cdot \text{kg}^{-1}$, $148.51 \text{ g} \cdot \text{kg}^{-1}$, $98.8 \text{ g} \cdot \text{kg}^{-1}$ and $21.16 \text{ mg} \cdot \text{kg}^{-1}$, respectively. Tropical forage plant (*Panicum maximum*. cv. Reyan No.8) was provided by the Institute of Tropical Crops Genetic Resources, Chinese Academy of Tropical Agriculture. Seeds of similar height and biomass were soaked with sulfuric acid (98%) for 3 min to break dormancy. Then, regulating pH to a neutral level was significantly important. Seeds were planted into the pots when the plumule length reached about 2 cm in the Petri dishes bed with filter paper disk.

2.2. Experimental Design

The heavy metal salt used in this study was $\text{Pb}(\text{NO}_3)_2$ (analytical purity), which was diluted in deionized water. Treatments were prepared at lead concentrations of 50, 100, 250, 500, and $750 \text{ mg} \cdot \text{kg}^{-1}$. The soil without exterior lead was used as blank comparison. Each plastic pot (diameter 19 cm) was filled with 3 kg soil sample (28 days after Pb and inorganic fertilizer addition). The detailed content of inorganic fertilizer included $2.25 \text{ g } (\text{NH}_4)_2\text{SO}_4$, $0.93 \text{ g } \text{KH}_2\text{PO}_4$ and $0.24 \text{ g } \text{KCl}$. Only 20 plants were used for each pot, and three replicates in the experiment. The soil without plant cultivation served as control group. During the experiment, the pots were maintained at 70% water capacity of the soil. The pots were conserved in the greenhouse allocated in the Institute of Environment and Plant Protection, Chinese Academy of Tropical Agriculture.

2.3. Indicators and Test Methods

Soil pH was measured in the mixture of soil and water at the ratio of 1:5. Soil organic matters, N, P, and K content were measured according to conventional methods [14].

Sequential extraction procedure was employed to determine Pb content in various forms. The exchangeable, carbonate combined, Fe-Mn oxides combined and organic combined forms were separated according to the methods of Tessier [15] as well as the method of total Pb content developed by Chinese Academy of Science (CAS) [14]. The detailed process is shown in Table 1. The residual form was calculated by subtracting the sum of all other forms from the total Pb content. All containers were dipped in 2% HNO_3 for more than 24 h to avoid possible heavy metal contamination.

During harvest, the aboveground and underground parts were rinsed with distilled water and further separated. The plant samples were dried at 70°C for 48 h to a constant weight, after which dry weights of different parts were determined by electronic balance.

2.4. Calculations of bioconcentration factor

Bioconcentration factor (BCF) value was an important index to estimate a plant's ability of assimilating / concentrating heavy metals. BCF values differed with characteristics of heavy metals, physiological factors and accumulation ability of plants, and environmental conditions. The bioaccumulation ability of *Panicum maximum* was calculated using the following equation:

$$K_{\text{BCF}} = C_p / C_s \quad (1)$$

where C_p is the concentration of Pb in plant, and C_s is concentration of Pb in soil.

2.5. Data Processing

Data were analyzed by using a statistical package SPSS version 11.0. One-way Analysis of Variance (ANOVA) tests with significance levels of 5% were carried out and followed by the LSD test. Regression and correlation analyses were also conducted. Microsoft Office Excel 2003 was also helpful for editing data and charts.

3. RESULTS AND DISCUSSION

Lead is a non-essential element, which can cause a certain toxic consequence when it enters the bodies of plants. For example, lead on low concentration level can result in the disorder of metabolism system, and further inhibiting the growth, while high concentration of lead can even induce death. A previous study showed that the toxicology of Pb stress was to destroy ultrastructure of plant cell nucleus, mitochondria and chloroplasts, reduce the leaf chlorophyll and content of ascorbic acid, and decrease the activity of dehydrogenase [16]. Consequently, it ruined the normal physiological function of plants, such as respirator metabolism, photosynthesis, hydrogen deoxidization and cell division, and, finally, affected the quality and biomass of the plants.

TABLE 1 - Sequential extraction procedure for the different forms of lead.

Form	Extraction agent	Operation conditions
Exchangeable	$1 \text{ mol} \cdot \text{L}^{-1} \text{ Mg}(\text{NO}_3)_2$	Shaken at 25°C for 2 h, separated by centrifugation
Carbonate combined	$1 \text{ mol} \cdot \text{L}^{-1} \text{ HAc} + 1 \text{ mol} \cdot \text{L}^{-1} \text{ NaAc}$ (pH 5.0)	Shaken at 25°C for 2 h, separated by centrifugation
Fe-Mn oxide combined	$0.04 \text{ mol} \cdot \text{L}^{-1} \text{ NH}_3\text{OH} \cdot \text{HCl} + 25\% \text{ HAc}$	Heated in 96°C water-bath for 2 h, supplemented with water, separated by centrifugation
Organic combined	A: $0.02 \text{ mol} \cdot \text{L}^{-1} \text{ HNO}_3 + 30\% \text{ H}_2\text{O}_2$ B: $3.2 \text{ mol} \cdot \text{L}^{-1} \text{ NH}_4\text{OAc} + 20\% \text{ HNO}_3$	Added agent A and evaporated to dryness in 85°C water-baths, then added agent B and shaken for 0.5 h, separated by centrifugation

TABLE 2 - The effects of lead stress on plant height, shoot and root dry weight yield (n=3).

Treatment elements	Treatment concentration (mg/kg)	Plant height (cm)		Dry weight in shoots (g·pot ⁻¹)		Dry weight in roots (g·pot ⁻¹)	
		\bar{x}	SD	\bar{x}	SD	\bar{x}	SD
Pb	0	60.7b	6.1	26.1bc	2.55	7.4ab	1.20
	50	68.1ab	7.0	29.0ab	3.61	8.5ab	0.50
	100	75.3a	14.6	33.4ab	4.04	10.1a	2.00
	250	70.9ab	8.4	29.6ab	4.73	8.0ab	1.80
	500	76.1a	4.5	35.5a	4.40	6.1b	1.20
	750	49.7c	6.3	19.4c	3.21	5.8b	2.00

*: a, b, c, d: Mean values followed with different letters in the rows are significantly different $p<0.05$.

3.1. Influence of Pb on growth of *Panicum maximum*

In this study, we focused on plant height, biomass of shoot and root of *Panicum maximum* in the lead-polluted soils (Table 2).

From Table 2, we could draw the conclusion that the growth of *Panicum maximum* was promoted when Pb concentration was lower than 500 mg/kg. The plant height of these treatments (<500 mg/kg) was much higher than that of control treatment, and the highest increase amplitude could even reach 25%. However, the height of plant would significantly decrease when the concentration of lead in soils was 750 mg/kg.

We also found that the change tendency of biomass was basically identical with that of the plant height. Both of them showed that low concentrations (≤ 500 mg/kg) of lead promoted the growth of *Panicum maximum*, while high concentrations (750 mg/kg) suppressed it. The biomass of aboveground part was 36% higher than control treatment when the concentration of lead was 500 mg/kg, whereas it decreased by 26% in Pb 750 mg/kg treatment. Hereby, we could set Pb concentration in soils at 500 mg/kg or slightly higher as the critical value of toxic effects of Pb on *Panicum maximum*. Through regression analysis of plant height-dry weight in shoots of *Panicum maximum* and soil concentrations, the result showed a significant positive correlation ($R^2=0.9674$). Based on this result, it could be considered that the major influence of Pb on dry weight in aerial parts of *Panicum maximum* was caused by affecting its plant height.

The dry weight in roots of *Panicum maximum* was highest in Pb 100 mg/kg, and decreased by 17 and 21% in the treatments of Pb 500 mg/kg and 750 mg/kg. In the research, we also found that Pb-tolerance ability of *Panicum maximum* was strong; in the meanwhile, we observed that the main root of *Panicum maximum* was deep into the soil and its fibrous root could cover the whole level of the soil, which was extremely beneficial to vegetation rehabilitation in lead-polluted areas and prevention of tropical soil erosion.

In a word, it was obvious that a “low promoting, high restraining” phenomenon happened to the dry weight of aboveground and underground parts of *Panicum maximum*. The result was similar to [11], revealing the ill effect of Cd on *Panicum maximum*. So, the toxic effects of Pb and Cd

on *Panicum maximum* may have some similar mechanism. Low lead concentration promoted the growth of *Panicum maximum*. The reason might be that the addition of Pb replaced the effective adsorption sites of other nutrient elements in soils and desorbed them from soils, so it further prompted other essential nutrient ions in soils which would inevitably accelerate the growth of plant. “High restraining” phenomenon was mainly due to influence in soil fertility, which was caused by a series of physical and chemical actions occurring between excess heavy metals in soils and soil components.

The toxic effects of heavy metals in different plants may differ significantly [17]. Li *et al.* [18] reported that biomass of crops decreased with the increase of heavy metal concentration. In low level heavy metal concentration treatments, growth of tomato and pakchoi were not much inhibited while in high level treatments, some vegetables, such as green capsicum, Chinese kale or water spinach, were detrimentally affected [18]. More information about heavy metal stress on tropical plants is still insufficient.

3.2. Lead accumulation in *Panicum maximum*

As presented in Fig. 1, lead concentrations in the plants increased with rising lead level in the soils. When the concentrations of Pb in soils were 50, 100, 250, 500 and 750 mg/kg, that in the underground part of plant were 1.86, 2.83, 6.02, 7.48 and 9.28 times higher than in control treatment, and that in the aboveground plant part were 1.26, 2.68, 5.83, 9.39 and 8.81 times higher than control. The value of K_{BCF} of underground part of *Panicum maximum* ranged from 0.37 to 1.48. The highest K_{BCF} was achieved when no exterior Pb was introduced to soils, which indicated that the lead accumulating ability of *Panicum maximum* could decrease by adding Pb. The value of K_{BCF} of aboveground *Panicum maximum* to lead in soil varied from 0.22 to 0.94. Ge *et al.* [11] indicated that the enrichment coefficient of *Panicum maximum* to soil Cd ranged from 0.29 to 4.1, which was higher than data in this article. In general, the main factor controlling the translocation of heavy metals from soil to plant is their chemical speciation [18]. Soil physical-chemical characteristics contribute to the variation of K_{BCF} to a certain degree.

In this study, the average absorption coefficient of Pb was 0.76, which significantly decreased with increasing Pb concentration in soils (Fig.1). With increasing Pb concen-

tration added to soil, those of lead in both underground and aboveground parts were basically stable. As a result, the steady accumulation quantity in the aboveground part of *Panicum maximum* could occur. The result indicated that the transfer of Pb from underground to aboveground part was less qualified by high Pb concentration, and the reason needs to be further studied.

As could be seen from Fig. 2, the percentage distribution of lead in underground parts (56-70%) was higher than that in aboveground parts (30-44%).

Furthermore, from the results, we could conclude that the K_{BCF} values of *Panicum maximum* were all lower than 1. So it was not optimistic to apply *Panicum maximum* to

restoring Pb-polluted soils, but Pb-tolerance of *Panicum maximum* has practical significance in wasteland reclamation and pasture cleaner production. There was a lot of tropical plant resources in tropical area, and how to perfect a mechanism to fit with the characteristic and screening standard of hyperaccumulator seemed to be of great importance, through which we could find more hyperaccumulators to provide abundant resources to govern and restore the polluted soil.

The results also indicated that quartic and square model could achieve the highest correlation coefficients between concentration in underground part and that in soils, as well as concentration in aboveground part and that in soils (Table 3).

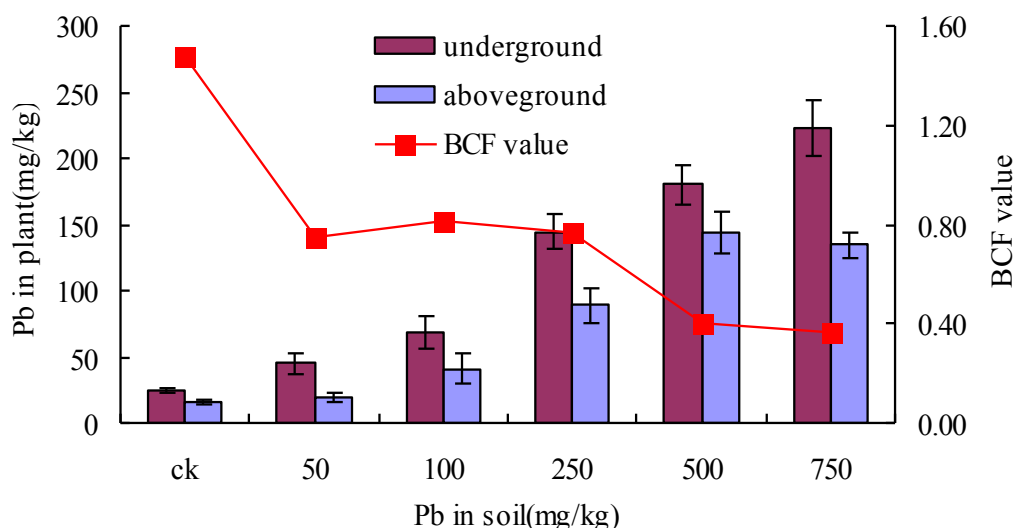


FIGURE 1 - Effect of lead in soils on lead content of *Panicum maximum*.

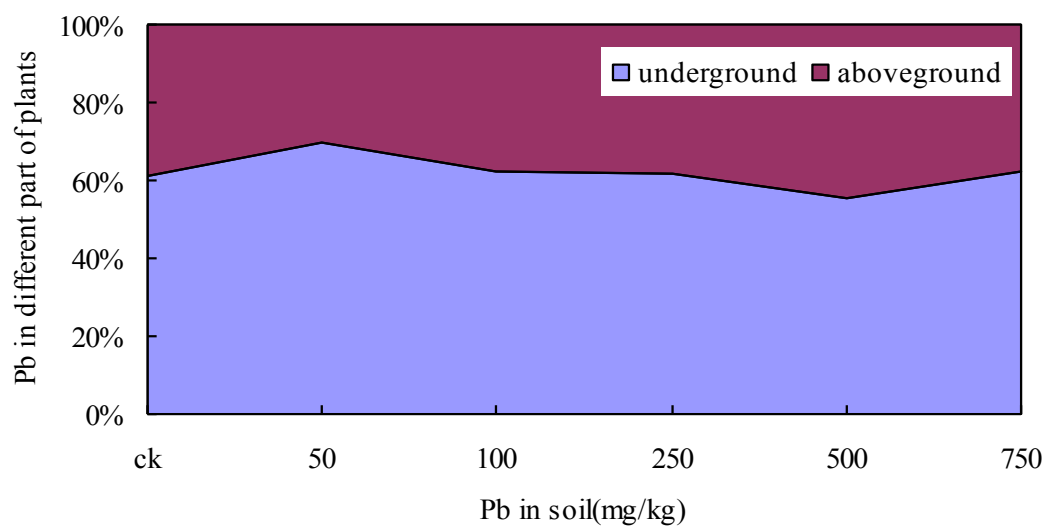


FIGURE 2 - Percentage of lead content in the different parts of *Panicum maximum*.

TABLE 3 - Curve model of accumulating lead in plants under different lead concentrations.

Model	R^2	F value	p
$Y_a = -0.0006x_1^2 + 0.5854x_1 - 2.873$	0.9876	1553.4	0.0001
$Y_u = 2E-08x_1^4 - 2E-05x_1^3 + 0.0047x_1^2 + 0.2921x_1 + 17.397$	0.9994	1798.9	0.0001

*□ Ya means the concentration of lead accumulated in aboveground part of plant (mg/kg); Yu means the concentration of lead accumulated in underground part of plant (mg/kg); X₁ means the concentration of added lead in tropical soils.

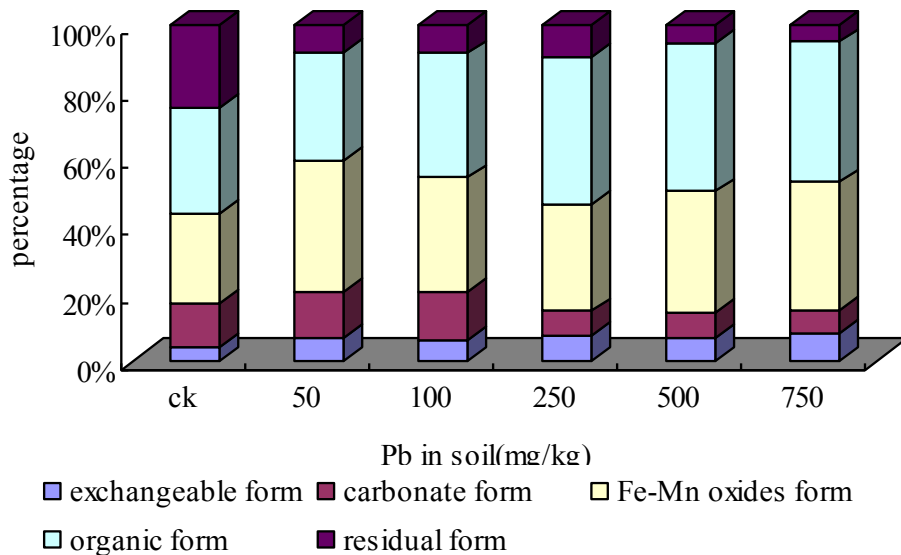


FIGURE 3 - Distribution of forms of Pb in soil (mg/kg).

3.3. Influence of exogenous Pb stress on its forms in soils

Figure 3 shows the contents of different forms of Pb in soils when the growth of plants expired. It indicated that the form of lead in the treatments including control treatment mainly was Fe-Mn oxides combined and organic combined (58-79%), which probably attributed to the high affinity between Pb and organic matter and oxides.

With increasing addition of Pb, the residual forms exhibited a persistent reduction but the Fe-Mn oxide and organic combined forms a great enhancement. The possible reason was that lots of colloids in tropical soils could induce adsorption, complexation and chemical reactions, which would unavoidably transform into certain forms which are difficult to be absorbed. Ge *et al.* [10] reported that with the addition of Cd in various concentrations, Cd forms in the soil varied in that the residual percentage dropped continuously, but organic form increased before decreasing afterwards, and available Cd as well as Fe and Mn oxide forms increased in percentage continuously as well. That is to say, *Panicum maximum* could change the forms of heavy metals in soil. However, different heavy metals displayed special characteristics.

4. CONCLUSION

(1) The effect of “low promoting, high restraining” of Pb concentration on the dry weight of aboveground and underground part as well as plant height of *Panicum maximum* was similar. In this study, *Panicum maximum* grows well in the soil containing 500 mg/kg Pb, indicating that Pb-tolerance ability of *Panicum maximum* was strong when they were in pot culture.

(2) Pb in the treated soils was mainly in Fe-Mn oxide combined and organic combined form. The addition of Pb increased Pb content in all forms in the soil, among which the residual forms exhibited a great reduction while the Fe-Mn oxide and organic combined forms were strongly enhanced. The KBCF value in roots of *Panicum maximum* to lead in soil ranged from 0.37 to 1.48. The concentration of lead in underground part was higher than that in above-ground part of *Panicum maximum*.

(3) Although *Panicum maximum* had the ability to accumulate and tolerate lead, the KBCF was not high. So *Panicum maximum* was not a good candidate as a hyper-accumulation plant in Pb-polluted areas. However, it could still be a candidate for lead-contaminated soil reclamation.

ACKNOWLEDGMENT

This work was financed by the Opened Fund Program of Key Laboratory of Protection and Development Utilization of Tropical Crop Germplasm Resources (Hainan University), Ministry of Education (NO. 2010ckled-09), the Natural Science Fund of Hainan Province, China (NO. 809003), Youth Foundation of Hainan University (NO. qnjj1013), and Scientific Research Foundation for Doctor, Hainan University (NO. kyqd1068).

REFERENCES

- [1] Nilufer C. and Ayten K. (2006) Effect of cadmium, zinc, copper and fluoranthene on soil bacteria. *Fresenius Environmental Bulletin* 15(7), 619-625.
- [2] McLaughlin M. J., Parker D. R. and Clarke J. M. (1999) Metals and micronutrients—food safety issues. *Field Crops Research* 60, 143-163.
- [3] Wang J., Ren H. and Liu J. (2006) Distribution of lead in urban soil and its potential risk in Shenyang City, China. *Chin. Geo. Sci.* 16, 127-132.
- [4] Tiaeva N. A., Grishantseva E. S. and Safronova N. S. (2007) Patterns in the distribution of several chemical elements in bottom sediments and soils of the Ivankovo Reservoir area, Volga River valley. *Moscow University Geology Bulletin* 62, 173-183.
- [5] Duman F., Cicek M., and Sezen G. Seasonal changes of metal accumulation and distribution in common club rush (*Schoenoplectus lacustris*) and common reed (*Phragmites australis*). *Exotoxicology* 16, 457-463.
- [6] Gardner H. S., Brennan L.M., Toussaint M. W., Rosencrance A.B., Boncavage-Hennessey E.M. and Wolfe M. J. (1998) Environmental complex mixture toxicity assessment. *Environ. Health Persp.* 106, 1299-1305.
- [7] Altenburger R., Boedeker W., Faust M. and Grimme L. H. (1996) Regulations for combined effects of pollutants: consequences from risk assessment in aquatic toxicology. *Food Chem. Toxicol.* 34, 1155-1157.
- [8] Chaney R.L., Malik M. and Li Y. M. (1997) Phytoremediation of soil metals. *Curr Opin Biotechnol* 8, 279-284.
- [9] Yan Z.G., He Q.L. and Li F.S. (2007) The application of earthworm in soil risk assessment. *Environmental Science Research* (1), 134-142.
- [10] Kamitani T., Oba H. and Kaneko N. (2006) Microbial biomass and tolerance of microbial community on an aged heavy metal polluted floodplain in Japan. *Water, Air and Soil pollution* 172, 185-200.
- [11] Ge C.J., Yu H.M. and Huang Z.B. (2009) Growth and Accumulation Response of *Panicum maximum* on Cd Pollution. *Progress in Environmental Science and Technology* 2, Science Press USA Inc., 1934-1939.
- [12] Gong Y. L., Yuan J. G., Yang Z. Y., Zhou Y. H., Lu B. Y. and Wang J. L. (2010) Cadmium and lead accumulations by typical cultivars of water spinach under different soil conditions. *Fresenius Environmental Bulletin* 19(2), 190-197.
- [13] Nurcan K. (2004) Determination of heavy metal concentrations in open and protected cropping systems. *Fresenius Environmental Bulletin* 13, 1521-1524.
- [14] Institute of Soil Science, Chinese Academy of Science (1978) Soil physical and chemical analyses. Shanghai, Shanghai Science and Technology Press, China.
- [15] Tessier A. (1979) Sequential extraction procedure for the speciation of particulate, trace metals. *Anal. Chem.* 51 (7), 844-851.
- [16] Lal N. (2005) Toxic effect of lead on certain biochemical parameters in Gram seedlings. *Bull. Environ. Contam. Toxicol.* 75: 67-72.
- [17] Leon A.M., Palma J.M., Corpas F.J., Gomez M., Romero-Puertas M.C., Chatterjee D., Mateos R.M. and Sandalio L.M. (2002) Antioxidative enzymes in cultivars of pepper plants with different sensitivity to cadmium. *Plant Physiol. Biochem.* 40(8), 13-820.
- [18] Li Q.S., Cai S.S., Mo C.H., Chu B., Peng L.H. and Yang F.B. (2010) Toxic effects of heavy metals and their accumulation in vegetables grown in a saline soil. *Ecotoxicology and Environmental Safety* 73, 84-88.

Received: November 11, 2010

Revised: February 23, 2011

Accepted: March 23, 2011

CORRESPONDING AUTHOR

Wenhao Tang

Department of Environmental Science
School of Environment and Plant Protection
Hainan University
Haikou 570228
P. R. CHINA

Phone: +86-898-23301064

Fax: +86-898-23300107

E-mail: twh23301229@163.com

HYBRID EFFECT OF CdS AND C₆₀ MOLECULES ON TiO₂ AND ENHANCEMENT OF THE PHOTOCATALYTIC ACTIVITY

Ze-Da Meng¹, Lei Zhu¹, Kwang-Youn Cho² and Won-Chun Oh^{1,*}

¹Department of Advanced Materials Science & Engineering, Hanseo University, Seosan-si, Chungnam-do, Korea, 356-706

²Korea In statute of Ceramic Engineering and Technology, Seoul, Korea, 153-801

ABSTRACT

CdS-C₆₀, C₆₀-TiO₂ and CdS-C₆₀/TiO₂ composites were prepared using a sol-gel method, and their high photocatalytic activity was evaluated by the degradation of methylene blue (MB) solutions under UV light. The surface area, surface structure, crystal phase and elemental identification of these composites were characterized by Brunauer–Emmett–Teller (BET) surface area, scanning electron microscopy (SEM), transmission electron microscopy (TEM), X-ray diffraction (XRD) and energy dispersive X-ray (EDX) spectroscopy, respectively. The degradation of MB was determined using UV/Vis spectrophotometry. An increase in photocatalytic activity was observed, and it may be attributed to both the increase of photo-absorption effect by the fullerene and the cooperative effect of CdS.

KEYWORDS: CdS-C₆₀/TiO₂, photocatalytic, scanning electron microscopy (SEM), transmission electron microscopy (TEM), methylene blue (MB)

1. INTRODUCTION

C₆₀ have attracted extensive attention for their various interesting properties due to their delocalized conjugated structures and electron-accepting ability. One of the most remarkable properties of C₆₀ in electron-transfer processes is that it can efficiently arouse a rapid photo-induced charge separation and a relatively slow charge recombination [1]. Thus, the combination of photocatalysts and C₆₀ may provide an ideal system to achieve an enhanced charge separation by photo-induced electron transfer. Some of the fullerene-donor linked molecules on an electrode exhibited excellent photovoltaic effects upon photo-irradiation [2–4].

Photocatalytic water splitting over semiconductors is an effective and attractive method for converting solar energy into clean and renewable hydrogen fuel. Titanium dioxide has attracted both industrial and academic attention for potential applications as the gate dielectric in metal oxide semiconductor field effect transistors (surface for

* Corresponding author
solar energy conversion, high efficiency photocatalyst and gas sensor) because of their well-known properties, including high refractive index and transmittance in visible region. TiO₂ is emerging attractive material because of its surface photochemistry as well as peculiar chemical and physical behaviors [5, 6]. To improve the response of TiO₂, transition metal or non-metal atom doped TiO₂ and dye or metal complex sensitized TiO₂ have been developed [7, 8]. Alternative approach for achieving this objective is to couple TiO₂ by using a narrow band gap semiconductor with a higher conduction band (CB) than that of TiO₂. In this sensitized TiO₂, charge injection from the CB of the narrow band gap semiconductor to that of TiO₂ can lead to efficient and longer charge separation by minimizing the electron-hole recombination [9, 10].

For instance, crystalline cadmium sulfide (CdS) has smaller band gap energy (2.42 eV) and can be used to induce photocatalytic water decomposition [11]. It has received considerable attention during the recent years because of proven and potential applications in photoconductor as well as photovoltaic devices. It would be desirable to directly prepare TiO₂ particles with homogeneously dispersed CdS, because the direct formation of these two semiconductors would provide a strong coupling between them [12–15].

Therefore, we developed a new approach to facilitate the direct formation of TiO₂ coupled by highly dispersed CdS and C₆₀ by sol-gel method. Structural variations, surface state and elemental compositions were investigated for preparations of CdS-C₆₀, C₆₀-TiO₂ and CdS-C₆₀/TiO₂ composites. X-ray diffraction (XRD), scanning electron microscopy (SEM), energy dispersive X-ray (EDX) and transmission electron microscopy (TEM) were employed for characterization of these new photocatalysts. The catalytic efficiencies of these composites were evaluated by the photocatalytic degradation of methylene blue (MB, C₁₆H₁₈N₃S·Cl·3H₂O).

2. MATERIALS AND METHODS

Crystalline fullerenes were selected as the support material. The fullerenes were supplied from Tokyo Kasei Kogyo Co. Ltd., Japan, and without further purification.

Crystalline fullerene [C₆₀] powder of 99.9% purity from TCI (Tokyo Kasei Kogyo Co. Ltd., Japan) was used as the carbon matrix. The titanium(IV) n-butoxide (TNB, C₁₆H₃₆O₄Ti) as a titanium source for the preparation of the Pt-fullerene/TiO₂ composites was purchased as reagent-grade from Acros Organics (USA). Cadmium acetate dehydrate [(CH₃COO)₂Cd·2H₂O] was supplied from Dae Jung Chemicals and Metals Co., Ltd (Korea), and sodium sulfide (Na₂S·5H₂O) from Yakuri pure Chemicals. Co., Ltd (Japan). For the oxidization of the surface of the fullerene, m-chloroperbenzoic acid (MCPBA) was used as an oxidized reagent, also purchased from Acros Organics, New Jersey, USA. Methylene blue (MB, C₁₆H₁₈N₃S·Cl·3H₂O, analytical grade) was purchased from Duksan Pure Chemical Co., Ltd. Benzene and ethyl alcohol were purchased as reagent-grade from Duksan Pure Chemical Co (Korea) and Daejung Chemical Co. (Korea), and used without further purification unless otherwise stated.

2.1. Oxidation of C₆₀ surface

MCPBA (m-chloroperbenzoic acid, ca. 1 g) was suspended in 50 ml benzene, followed by the addition of fullerene [C₆₀] (ca. 40 mg). The mixture was then refluxed in an air atmosphere and stirred for 6 h. The solvent was subsequently dried at the boiling point of benzene (353.13 K). After completion, the dark brown precipitates were washed with ethyl alcohol and dried at 323 K, after this the oxidation of C₆₀ was carried out.

2.2. Preparation of CDS-C₆₀

A stoichiometric volume of 30 ml (CH₃COO)₂Cd·2H₂O and ethanol solutions (0.26 M) was mixed with oxidized C₆₀ (A), 50 ml Na₂S aqueous solution (0.16 M), added drop-by-drop to solution (A), at 343 K and stirred for 7 h (flow-rate 6 drops every min). After thorough washing, it was deposited in deionized water for 5 h, and then dried at 353 K. After being heat-treated at 573 K for 1 h, the dark green CdS-C₆₀ powders were obtained.

2.3. Preparation of CDS-C₆₀/TiO₂ composites

CdS-C₆₀ was prepared using pristine concentrations of TNB for the preparation of CdS-C₆₀/TiO₂ composites. CdS-C₆₀ powder was mixed with 3 ml TNB solution in 50 ml benzene. Then, the solutions were homogenized under reflux at 343 K for 5 h, while being stirred in a vial again. After stirring, the solution transformed into CdS-C₆₀/TiO₂ gels, which were heat-treated at 873 K, and then CdS-C₆₀/TiO₂ composites were produced.

2.4. Characterization of CDS-C₆₀/TiO₂ compounds

For the measurements of structural variations, XRD patterns were taken using an X-ray generator (Shimadzu XD-D1, Japan) with Cu K α radiation. SEM was used to observe the surface state and structure of CdS-C₆₀/TiO₂ composites (JSM-5200 JOEL, Japan). EDX was also used for the elemental analysis of the samples. The BET surface area was determined by N₂ adsorption measurements at 77 K (Monosorb, USA). TEM (JEOL, JEM-2010, Japan) analyses were used to observe the surface state and structure of the CdS-C₆₀/TiO₂ composites. At acceleration voltage of 200 kV, TEM was used to investigate the size and distribution of the titanium and iron particle deposit on the fullerene surface of various samples. TEM specimens were prepared by placing a few drops of the sample solution on a carbon grid.

2.5. Photocatalytic degradation of MB

Photocatalytic activities were evaluated by MB degradation in aqueous media under UV irradiation. For UV irradiation, the reaction beaker was located axially and illuminated with UV light (UV lamp 8 W, 365 nm) in a box. The lamp was used at a distance of 100 mm from the aqueous solution in the darkness box. The initial MB concentration (C₀) was 3.0×10⁻⁵ mol/L. 0.05 g CdS-C₆₀, C₆₀-TiO₂ and CdS-C₆₀/TiO₂ compounds were added to 50 ml MB solution and placed for 2 h in the darkness box. Then, the suspension was irradiated with visible light as a function of irradiation time. Samples were then withdrawn regularly from the reactor, and dispersed powders were removed by centrifugation. The clean transparent solution was UV-VIS-analyzed. The concentration of MB in the solution was determined as a function of irradiation time.

3. RESULTS AND DISCUSSION

3.1. Characterization of the products

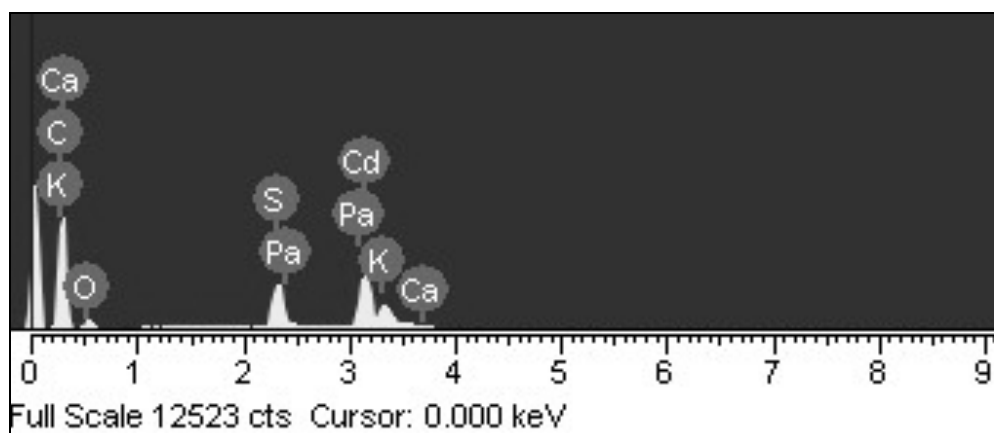
Fig. 1 shows the energy dispersive X-ray investigations carried out with the surface of the CdS-C₆₀, C₆₀-TiO₂ and CdS-C₆₀/TiO₂ compounds. The elemental composition of these samples has been analyzed, and the characteristic elements were identified using an EDX detection spectrometer. Fig. 1 shows that strong K α and K β peaks from Ti element appear at 4.51 and 4.92 keV, while a moderate K α peak of the element O appears at 0.52 keV. Besides all the above peaks, the elements S and Cd can also be found. In Fig. 2, the quantitative microanalyses of C, O, Ti, Cd and S as major elements for the composites were performed by EDX. From the EDX data, all the main elements existed. The numerical results of EDX quantitative microanalysis of the samples revealed the ratios listed in Table 1. In Fig. 1 (c), the spectra show the presence of C, O and Ti as major elements, with strong Cd and S peaks. There were some small impurities, possibly introduced into composites when using the fullerene without purification. In the case of most of the samples, carbon and

titanium were present as major elements with small quantities of oxygen in the composite.

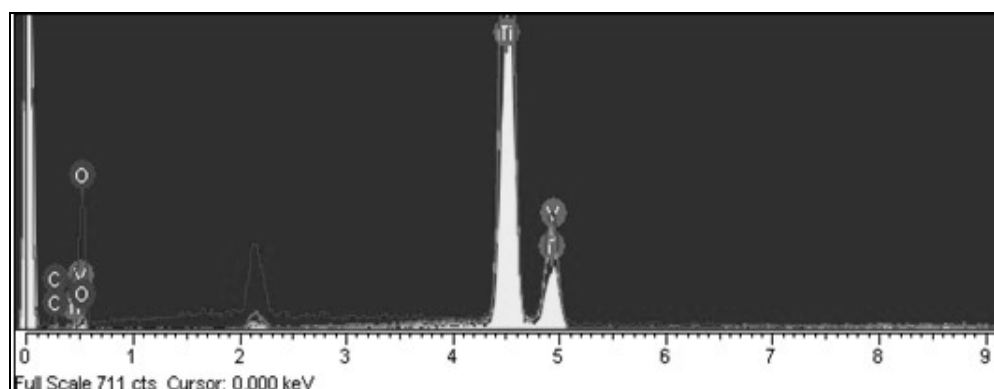
Fig. 2 characterizes the micro-surface structures and morphology of the CdS-C₆₀, C₆₀-TiO₂ and CdS-C₆₀/TiO₂ compounds. C₆₀ and CdS are uniformly coated on the surface of TiO₂ and lead to an enlargement of the nanoparticle size. In the reports of Zhang et al. [16, 17], a good dispersion of small particles could provide more reactive

TABLE 1 - EDX elemental microanalysis and BET surface area values of CdS-C₆₀, C₆₀-TiO₂ and CdS-C₆₀/TiO₂.

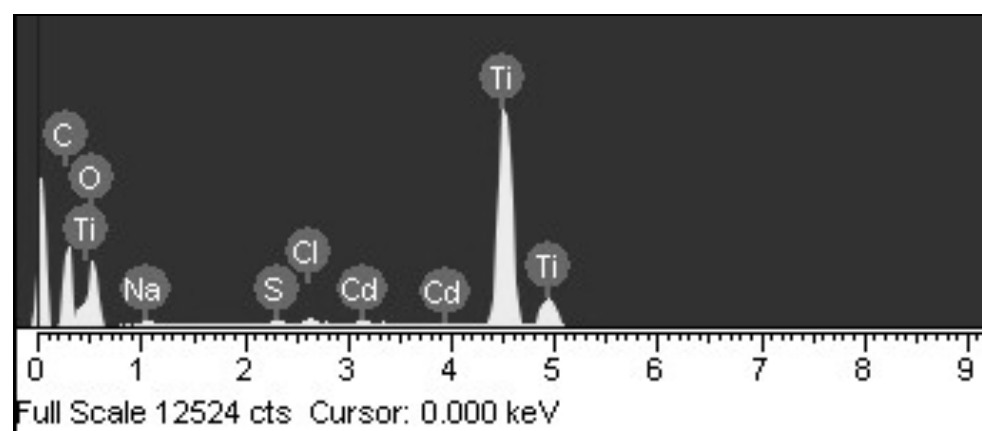
Sample name	C (%)	O (%)	Cd (%)	S (%)	Ti (%)	BET (m ² /g)
C ₆₀	99.99	-	-	-	-	85.05
CdS-C ₆₀	63.03	10.96	1.87	4.80	-	72.37
C ₆₀ -TiO ₂	4.12	42.41	53.47	-	-	80.25
CdS-C ₆₀ /TiO ₂	4.99	57.42	0.24	35.33	0.79	33.33



(a)



(b)



(c)

FIGURE 1 - EDX elemental microanalysis of CdS-C₆₀ (a), C₆₀-TiO₂ (b) and CdS-C₆₀/TiO₂ (c) compounds.

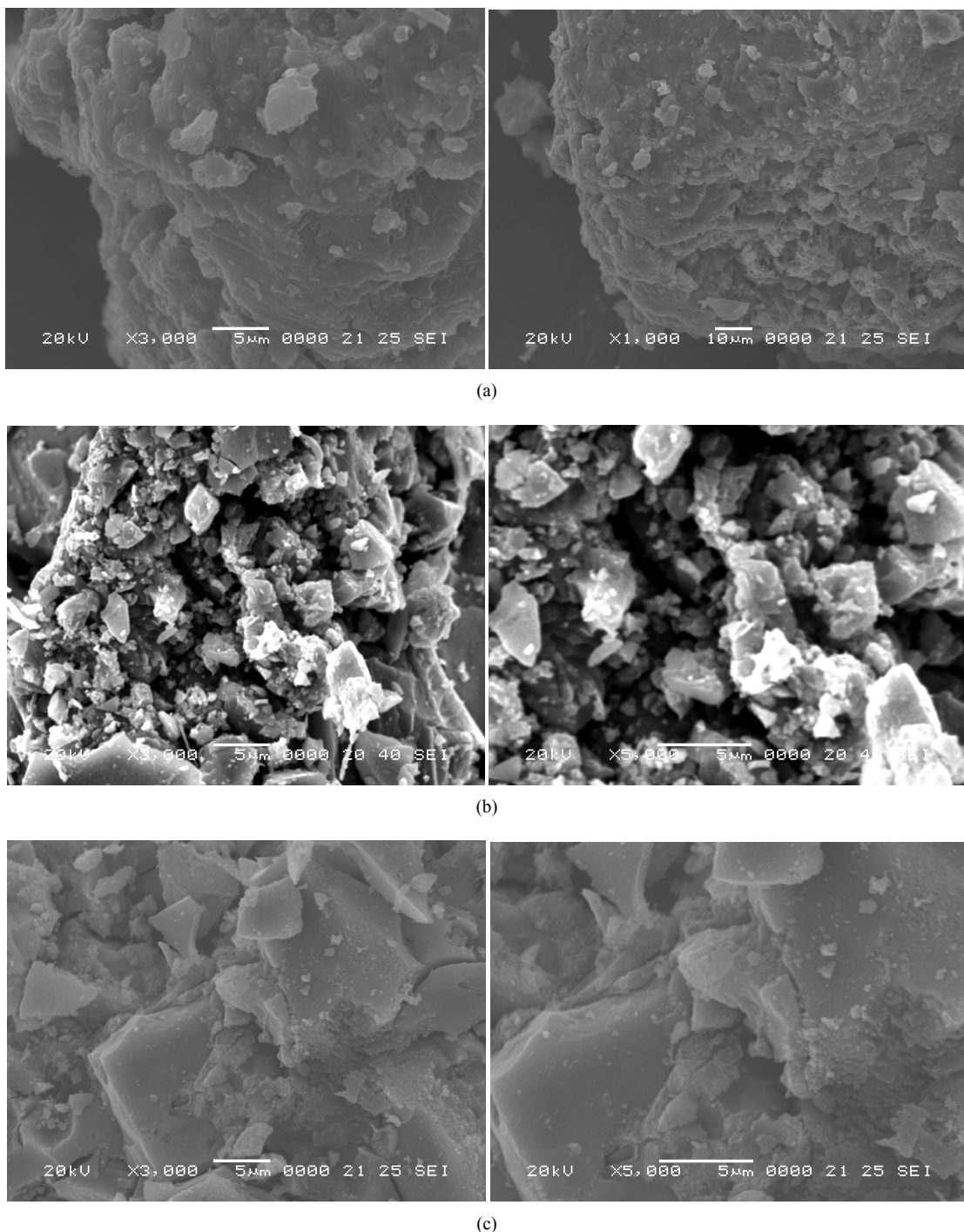


FIGURE 2 - SEM image obtained from CdS-C₆₀ (a), C₆₀-TiO₂(b) and CdS-C₆₀/TiO₂(c) compounds.

sites for the reactants than aggregated particles. The surface roughness seems to be more with little aggregation of grains. Fig. 2 (a) shows CdS-C₆₀, (b) C₆₀-TiO₂ and (c) CdS-C₆₀/TiO₂, and the aggregation phenomenon becomes more and more serious, and CdS addition for doping can make the aggregation serious.

The BET surface areas of the raw CdS-C₆₀, C₆₀-TiO₂ and CdS-C₆₀/TiO₂ photocatalysts are listed in Table 1. The BET value decreases from 85 m²/g of pure fullerene to 33.3 m²/g of CdS-C₆₀/TiO₂. It can be considered that TiO₂ and CdS particles are introduced into fullerene pores, and the value of CdS-C₆₀/TiO₂ decreased. The sample CdS-C₆₀ has the largest area which can affect the adsorption reaction. The BET surface area of CdS-C₆₀ photocatalyst

was decreased by 35% when CdS-C₆₀ particles were loaded on the TiO₂ support. This was because TiO₂ particles can fill into the pores of CdS-C₆₀ particles, and, therefore, the pore size and volume of CdS-C₆₀ particles decreased significantly when the particles were attached on TiO₂ [18].

The TEM images of CdS-C₆₀ and CdS-C₆₀/TiO₂ are shown in Fig. 3. A representative TEM image shown in Fig. 3 reveals that the prepared powders are uniform and some aggregations among the particles are also observed. The average diameter of C₆₀ is estimated to be about 20 nm. In Fig. 3 (a), CdS particles are well-dispersed and attached onto the C₆₀ surface. The image of CdS-C₆₀/TiO₂ compounds (Fig. 3 (b)) shows that all particles were aggregated implying that the presence of TiO₂ could efficiently enhance the agglomeration of CdS-C₆₀ and impair the dispersion of nanoparticles.

XRD patterns of CdS-C₆₀, C₆₀-TiO₂ and CdS-C₆₀/TiO₂ composites are shown in Fig. 4, respectively. C is the characteristic peak corresponding to C₆₀, A is the anatase phase of titanium, and S is CdS. The XRD pattern of the CdS-C₆₀ reveals a crystalline phase of C₆₀ and CdS. The peaks at $2\theta = 24.7, 26.5, 28.3, 36.6, 43.8, 48.1$ and 51.8 can be assigned to the (100), (002), (101), (102), (110), (103) and (112) planes of hexagonal CdS structure [19-21]. For the XRD patterns of CdS-C₆₀/TiO₂, we also can find CdS peaks at $2\theta = 28.3, 43.8$ and 51.8, which can be assigned to the (101), (110) and (112) planes of hexagonal CdS structure due to the presence of low amount of CdS on the TiO₂ reducing the intensity of the peaks related to CdS and the interference of TiO₂ peaks. The content of CdS is only about 1%, observed from the EDX image. The XRD patterns of C₆₀-TiO₂ reveal a crystalline phase of TiO₂, but we cannot find the peaks of C₆₀ due to its low amount and the interference of TiO₂. The major peaks at 25.3, 37.5, 48.0, 53.8, 54.9, 62.5, 68.7, 70.3, 75.1 and 82.6 are diffractions of (101), (004), (200), (105), (211), (204), (116),

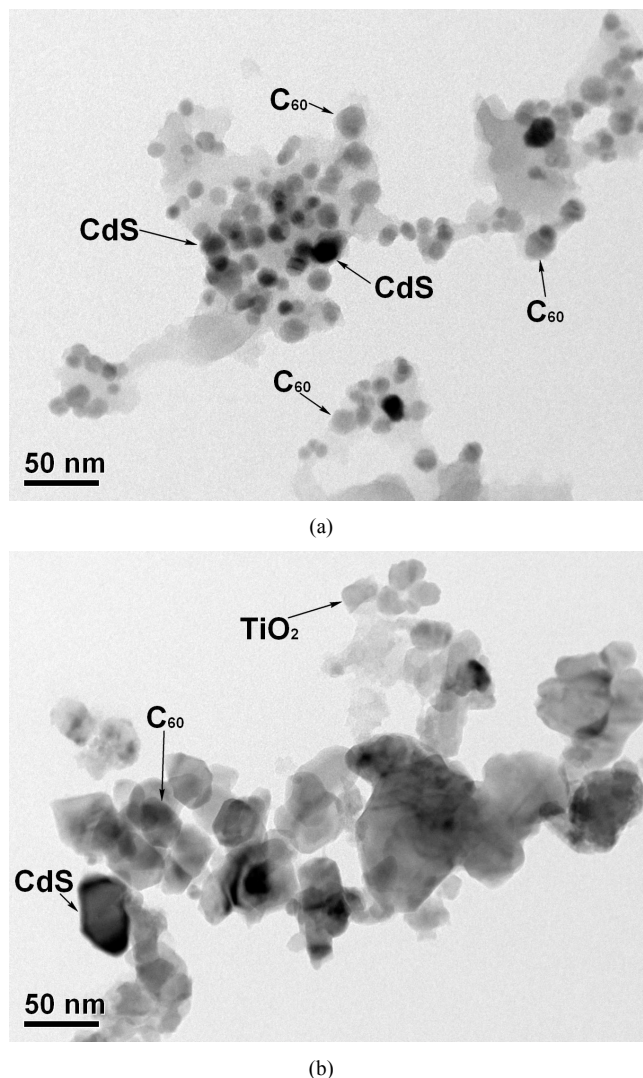


FIGURE 3 - TEM image obtained from CdS-C₆₀ (a) and CdS-C₆₀/TiO₂ (b) compounds.

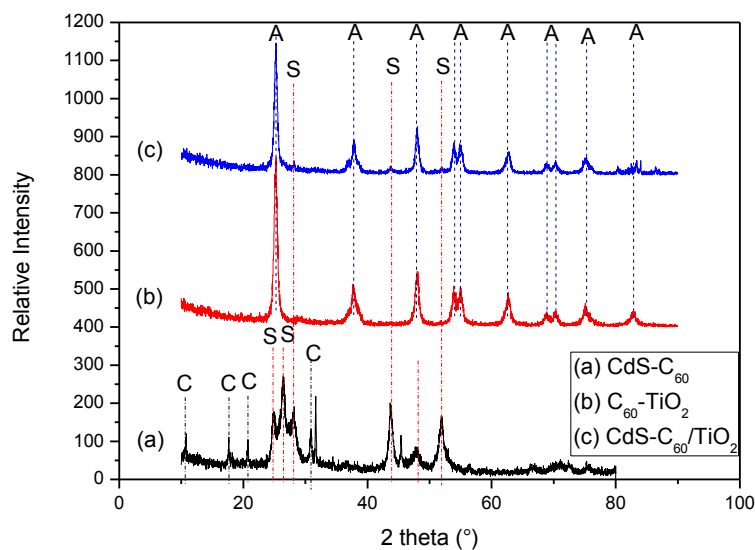


FIGURE 4 - XRD patterns from CdS-C₆₀ (a), C₆₀-TiO₂ (b) and CdS-C₆₀/TiO₂ (c) compounds.

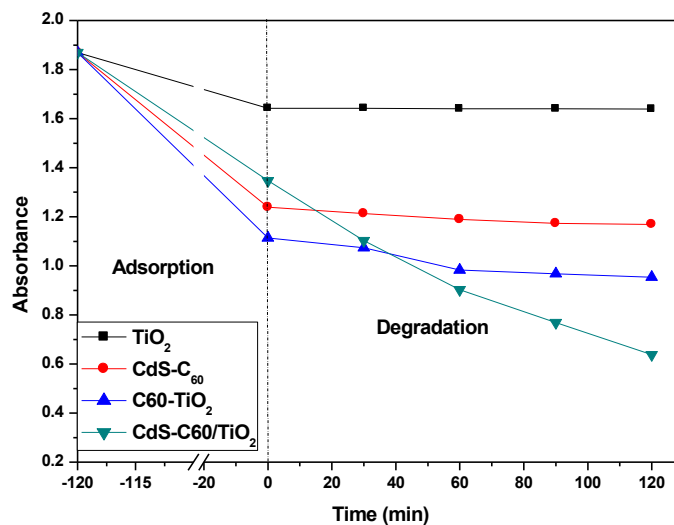


FIGURE 5 - Effect of the methylene blue decolorization for CdS-C₆₀, C₆₀-TiO₂ and CdS-C₆₀/TiO₂.

(220), (215) and (224) planes of anatase indicating that the prepared TiO₂ is an anatase phase [22-24]. In comparison of the XRD patterns between C₆₀-TiO₂ and CdS-C₆₀/TiO₂, the intensity of TiO₂ peak was decreased and the peak at $\theta = 82.6$ cannot be found at the EDX patterns of CdS-C₆₀/TiO₂. We can conclude that introduced CdS prevented the growth of anatase crystals.

3.2. Photodegradation of methylene blue

The degradation effects of MB concentration against the photocatalyst derivatives under various time conditions are shown in Fig. 5. From these spectra for MB solution after photolysis, the relative yields of the photolysis products formed under different irradiation time conditions are shown for the products. The concentration of MB was 3.0×10^{-5} mol/L and the absorbance decreased with an increase of irradiation time. This implies that the light transparency of MB increased greatly by the photocatalytic degradation effect. An effect of the high crystallinity of the anatase phase on photocatalytic degradation of MB has been shown. TiO₂ only has adsorption effects under visible light because, of the wide band gap, TiO₂ particles cannot create electron-holes. In Fig. 5, the adsorption effect of C₆₀-TiO₂ is better than that of CdS-C₆₀ due to the relatively high surface area. However, the adsorption effect of CdS-C₆₀/TiO₂ is the best, although it has the smaller surface area. The BET specific surface area of the adsorbent is only an important factor for adsorption effects. Additionally, the polarity matching between the adsorbent and the adsorbate, pore structure of the adsorbent and the matching of the pore size of the adsorbent with that of the adsorbate are main factors influencing adsorption. The higher adsorption capacity is derived from good matching of pore to molecular diameter [25]. From Fig. 5, we can find that the degradation effect of CdS-C₆₀/TiO₂ is the best. Because the concentration of MB is high, the degradation effects of C₆₀-TiO₂ and CdS-C₆₀ are not outstanding,

and degradation effect of CdS-C₆₀ is not good due to the photo-corrosion of CdS [26-28].

In the C₆₀ coupled TiO₂ system, the photocatalytic activities were mainly enhanced due to the high efficiency of charge separation induced by the synergistic effects of C₆₀ and TiO₂. The processes of photogenerated charge transition during irradiation are shown in Fig. 6. In case of C₆₀ coupled TiO₂, hole and electron pairs were generated and separated on the interface of TiO₂ by UV light irradiation. The level of conduction band in TiO₂ was lower than the reduction potential of C₆₀. So, the photogenerated electrons can easily transfer from the conduction band of TiO₂ to C₆₀ molecules with the interaction between TiO₂ and C₆₀. Simultaneously, the holes in valence band (VB) of TiO₂ can directly transfer to the C₆₀, because the VB of TiO₂ matched well with the C₆₀. The synergistic effects of both C₆₀ and TiO₂ promoted the separation efficiency of photogenerated electron-hole pairs resulting in the high photocatalytic activity of C₆₀-hybridized TiO₂ samples. In this case, C₆₀ coupled TiO₂ system improves the reaction state. In addition, the C₆₀ molecules also played an important role in storing and shuttling photo-induced electrons generated from TiO₂ photocatalyst, which promoted the separation efficiency of photoinduced electron-hole pairs but decreased their recombination rate. Because C₆₀ is a trap-rich conductor, the C₆₀ molecules acted as an electron relay [29, 30], and the role of the injected electrons in this system was not only to increase the density of charge carrier but also to fill trap states, hence increasing the average mobility [31]. When C₆₀ molecules are absorbed on the surface of TiO₂, an immediate and direct route of electron transfer to C₆₀ directly from TiO₂ enhances the rate of hydroxyl radical generation [32].

The photocatalytic activity was not only determined by the amount of C₆₀ transferring the photo-induced electrons, but also related to the contact area between TiO₂

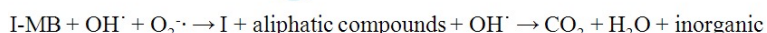
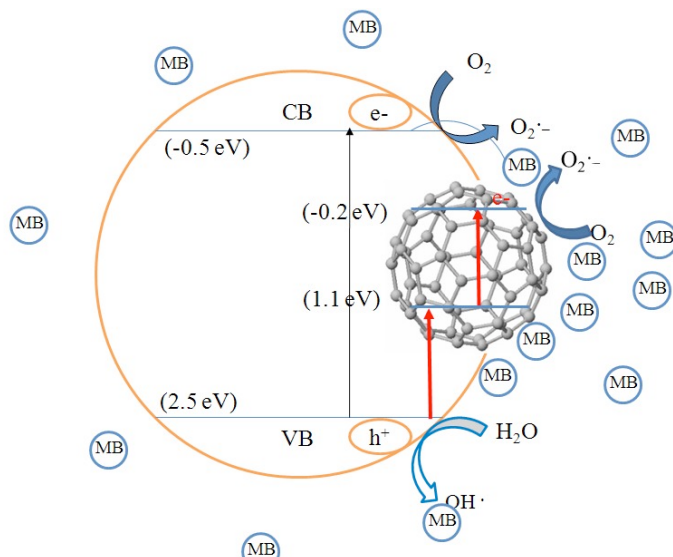


FIGURE 6 - Schematic drawing of separation of photogenerated electrons and holes on the interface of $\text{C}_{60}\text{-TiO}_2$

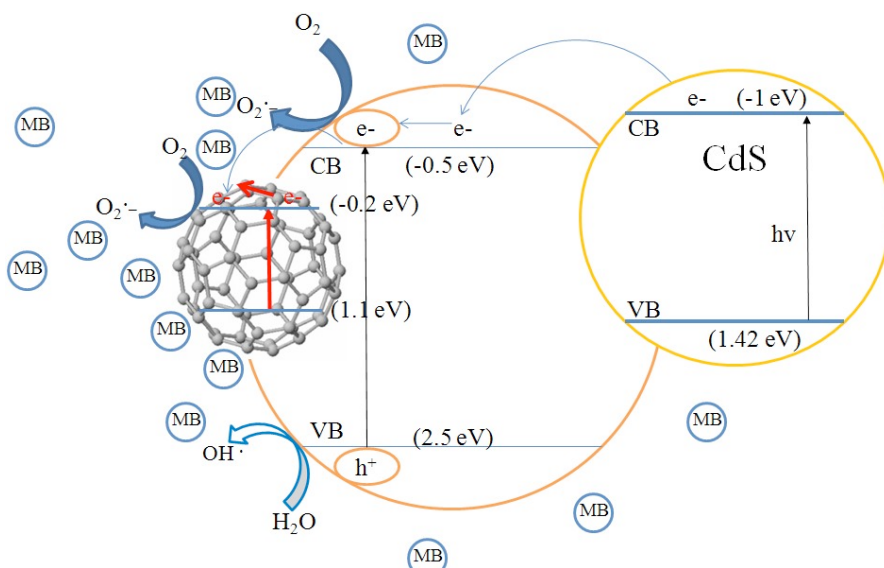


FIGURE 7 - Schematic drawing of separation of photogenerated electrons and holes on the interface of $\text{CdS-C}_{60}\text{/TiO}_2$.

and organic pollutants. C_{60} played the surface area enhancer for TiO_2 , due to its relatively large specific surface area.

In case of C_{60} and CdS coupled TiO_2 systems, semiconductor coupling two components has a beneficial role in improving charge separation and extending TiO_2 in response to UV light. The interparticle electron transfer between C_{60} and TiO_2 semiconductor system above was also described by [33]. We propose a mechanism for the degradation of pollutants on $\text{CdS-C}_{60}/\text{TiO}_2$ photocatalyst under UV light irradiation as shown in Fig. 7. In case of CdS addition as new matter, the excited electrons from the CdS

particles are quickly transferred to a TiO_2 particle since the conduction band of CdS is -1 eV which is -0.5 more negative than that of TiO_2 [34]. The result indicates that the electrons from excited CdS are injected into the conduction band of TiO_2 and then scavenged by molecular oxygen O_2 to yield the superoxide radical anion $\text{O}_2\cdot^-$. This vectorial transfer of charge should, therefore, enhance the photo-oxidation of the adsorbed organic substrate. However, the photo-generated holes in CdS nanocrystals cannot oxidize hydroxyl groups to hydroxyl radicals due to their valence band potential. This results in the photo-

corrosion of CdS, forming cadmium cations [35]. An approach is still pursued to make stable CdS photocatalyst.

4. CONCLUSIONS

The experimental results clearly demonstrate that CdS-C₆₀/TiO₂ photocatalysts have strong combination properties and effective electron transfer between CdS and TiO₂. The surface area of CdS-C₆₀/TiO₂ composites decreased due to CdS and titania particles coated on the surface of C₆₀s. XRD results showed that TiO₂ is in the form of anatase, and CdS can clearly be found. The result of degradation of methylene blue indicated that addition of C₆₀ and CdS enhanced the photocatalytic activity of CdS-C₆₀/TiO₂ composite, due to the synergistic effect of all three particles, and promoted the separation efficiency of photo-generated electron–hole pairs resulting in high photocatalytic activity.

REFERENCES

- [1] Davis J.J., Hill H.A.O., Kurz A., Leighton A.D. and Safronov A.Y. (1997) The aqueous electrochemistry of C₆₀ and methanofullerene films. *J. Ele. Chem.* 429, 7–11.
- [2] Szucs A., Loix A., Nagy J.B. and Lamberts L. (1995) Fullerene film electrodes in aqueous solutions Part 1. Preparation and electrochemical characterization. *J. Ele. Chem.* 397, 191–203.
- [3] Nakashima N., Ishii T., Shirakusa M., Nakanishi T., Murakami H. and Sagara T. (2001) Molecular bilayer-based superstructures of a fullerene-carrying ammonium amphiphile: structure and electrochemistry. *Chem. Eur. J.* 7, 1766–1772.
- [4] Oh W.C. (2010) Review of carbon based titania photocatalysts. *J. Photo. Sci.* 1, 29–34.
- [5] Cheng M.L. and Oh W.C. (2010) Fabrication of Cr/CNT/TiO₂ composites and their photocatalytic activity under visible light. *Fresenius Enciron. Bull.* 19, 2938–2946.
- [6] Oh W.C. and Zhang F.J. (2010) A review-antibacterial activity of CNT/TiO₂, Ag-CNT/TiO₂, and C₆₀/TiO₂. *J. Photo. Sci.* 1, 63–67
- [7] Zhu L., Meng Z.D., Chen M.L., Zhang F.J., Choi J.G., Park J.Y. and Oh W.C. (2010) Photodegradation of MB solution by the metal (Fe, Ni and Co) containing AC/TiO₂ photocatalyst under the UV irradiation. *J. Photo. Sci.* 1, 69–76.
- [8] Meng Z.D., Zhang K. and Oh W.C. (2010) Preparation of different Fe containing TiO₂ photocatalysts and comparison of their photocatalytic activity. *Korean J. Mater. Re.* 20, 228–234.
- [9] Bessekhouad Robert Y.D. and Weber J.V. (2004) Bi₂S₃/TiO₂ and CdS/TiO₂ heterojunctions as an available configuration for photocatalytic degradation of organic pollutant. *J. Photochem. Photobiol. A* 163, 569–580.
- [10] Bessekhouad Y., Chaoui N., Trzpiti M., Ghazzal N., Robert D. and Weber J.V. (2006) UV-vis versus visible degradation of Acid Orange II in a coupled CdS/TiO₂ semiconductors suspension. *J. Photochem. Photobiol. A* 183, 218–224.
- [11] Robert D. (2007) Photosensitization of TiO₂ by M_xO_y and M_xS_y nanoparticles for heterogeneous photocatalysis applications. *Catal. Today* 122, 20–26.
- [12] Fuji H., Ohtaki M., Eguchi K. and Arai H. (1998) Preparation and photocatalytic activities of a semiconductor composite of CdS embedded in a TiO₂ gel as a stable oxide semiconducting matrix. *J. Mol. Catal. A: Chem.* 129, 61–68.
- [13] Mathew X., Enriquez J.P., Romeo A. and Tiwari A.N. (2004) CdTe/CdS solar cells on flexible substrates. *Solar Energy* 77, 831–838.
- [14] Nanda K.K., Sarangi S.N., Mohanty S. and Sahu S.N. (1998) Optical properties of CdS nanocrystalline films prepared by a precipitation technique. *Thin Solid Films* 322, 21–27.
- [15] Li X.Q., Cheng Y., Liu L.F. and Mu J. (2010) Enhanced photoelectrochemical properties of TiO₂ nanotubes co-sensitized with CdS nanoparticles and tetrasulfonated copper phthalocyanine. *Colloids and Surfaces A: Physicochem. Eng. Aspects* 353, 226–231.
- [16] Zhang F.J., Liu J., Chen M.L. and Oh W.C. (2009) Photoelectrocatalytic degradation of dyes in aqueous solution using CNT/TiO₂ electrode. *J. Korean Ceram. Soc.* 46, 263–270.
- [17] Zhang X.W., Zhou M.H. and Lei L.C. (2005) Preparation of photocatalytic TiO₂ coating of nanosized particles supported on activated carbon by AP-MOCVD. *Carbon* 43, 1700–1708.
- [18] Zhang F.J., Chen M.L., Zhang K. and Oh W.C. (2010) Visible light photoelectrocatalytic properties of novel yttrium treated carbon nanotube/titania composite electrodes. *Bull. Korean Chem. Soc.* 31, 133–138.
- [19] Mane R.S., Yoon M.Y., Chung H. and Han S.H. (2007) Co-deposition of TiO₂/CdS films electrode for photoelectrochemical cells. *Solar Energy* 81, 290–293.
- [20] Chi C.F., Lee Y.L. and Weng H.S. (2008) A CdS-modified TiO₂ nanocrystalline photoanode for efficient hydrogen generation by visible light. *Nanotechnology* 19, 125704–125705.
- [21] Gerischer H. and Lubke M. (1986) A particle size effect in the sensitization of TiO₂ electrodes by a CdS deposit. *J. Electroanal. Chem.* 204, 225–227.
- [22] Khan S.U.M., Al-Shahry M. and Ingler Jr W.B. (2002) Efficient photochemical water splitting by a chemically modified n-TiO₂. *Science* 297, 2243–2245.
- [23] Barakat M.A., Schaeffer H., Hayes G. and Ismat-Shah S. (2005) Photocatalytic degradation of 2 chlorophenol by Co-doped TiO₂ nanoparticles. *Appl. Catal. B: Environ.* 57, 23–30.
- [24] Colmenares J.C., Aramendia M.A., Marinas A., Marinas J.M. and Urbano F.J. (2006) Synthesis, characterization and photocatalytic activity of different metal-doped titania systems. *Appl. Catal. A: Gen.* 306, 120–127.
- [25] Yu J.X., Li B.H., Sun X.M., Jun Y. and Chi R.A. (2009) Adsorption of methylene blue and rhodamine B on baker's yeast and photocatalytic regeneration of the biosorbent. *Biochem. Eng. J.* 45, 145–151.
- [26] Wu L., Yu J.C. and Fu X.Z. (2006) Characterization and photocatalytic mechanism of nanosized CdS coupled TiO₂ nanocrystals under visible light irradiation. *J. Molecular Cataly. A: Chem.* 244, 25–32.
- [27] So W.W., Kim K.J. and Moon S.J. (2004) Photo-production of hydrogen over the CdS-TiO₂ nano-composite particulate films treated with TiCl₄. *Int. J. Hydrogen Energy* 29, 229–234.

- [28] Bard A.J. and Wrighton M.S. (1977) Thermodynamic potential for the anodic dissolution of n-type semiconductors. *J. Electrochem. Soc.* 124, 1706-1710.
- [29] Haddon R.C., Hebard A.F., Rosseinsky M.J. and Murphy D.W. (1991) Conducting films of C₆₀ and C₇₀ by alkali-metal doping. *Nature* 350, 320-322.
- [30] Brabec C.J., Sariciftci N.S., and Hummelen J.C. (2001) Plastic Solar Cells. *Adv. Funct. Mater.* 11, 15-26.
- [31] Sun Y.P., Gudure R., Lawson G.E., Mullins J.E., Guo Z., Quinlan J., Bunker C.E. and Gord J.R. (2000) Photophysical and Electron-Transfer Properties of Mono- and Multiple Functionalized Fullerene Derivatives. *J. Phys. Chem. B* 104, 4625-4632
- [32] Yamamoto K., Saunders M., Khong A., Gross R.J., Grayson J.M., Gross M.L., Benedetto A.F. and Weisman R.B. (1999) Isolation and Spectral Properties of Kr@C₆₀, a Stable van der Waals Molecule. *J. Am. Chem. Soc.* 121, 1591-1596.
- [33] Kohtani S., Kudo A. and Sakata T. (1993) Spectral sensitization of a TiO₂ semiconductor electrode by CdS microcrystals and its photoelectrochemical properties. *Chem. Phys. Lett.* 206, 166-170.
- [34] Flood R., Enright B., Allen M., Barry S., Dalton A., Doyle H., Tynan D. and Fitzmaurice D. (1995) Determination of band edge energies for transparent nanocrystalline TiO₂-CdS sandwich electrodes prepared by electrodeposition. *Sol. Energy Mater. Sol. Cells* 39, 83-98.
- [35] Li C., Yuan J., Han B.Y., Jiang L. and Shangguan W.F. (2010) TiO₂ nanotubes incorporated with CdS for photocatalytic hydrogen production from splitting water under visible light irradiation. *Int. J. Hydrogen Energy.* 35, 7073-7079.

Received: December 10, 2010
Revised: March 07, 2011
Accepted: March 23, 2011

CORRESPONDING AUTHOR

Won-Chun Oh
 Department of Advanced Materials Science & Engineering
 Hanseo University
 Seosan-si, Chungnam-do
 KOREA, 356-706

E-mail: wc_oh@hanseo.ac.kr

FEB/ Vol 20/ No 7/ 2011 – pages 1589 – 1597

OFFSHORE ECOSYSTEM HEALTH ASSESSMENT: A CASE STUDY OF JIANGSU OFFSHORE AREA, CHINA

Zulin Hua^{1,2}, Benlin Dai^{1,2,*}, Li Gu^{1,2}, Kejian Chu^{1,2}, Yulong He³ and Yunzhen Li³

¹ Key Laboratory of Integrated Regulation and Resource Development on Shallow Lake of Ministry of Education, College of Environment, Hohai University, 210098 Nanjing, China

² National Engineering Research Center of Water Resources Efficient Utilization and Engineering Safety, Hohai University, 210098 Nanjing, China

³ Faculty of Geosciences and Environmental Engineering, Southwest Jiaotong University, 610031 Chengdu, China

ABSTRACT

Based on the ecosystem responses to natural and anthropogenic pressures, a set of relatively comprehensive assessment indicators covering water quality physico-chemical, residual toxicity in organisms, ecological and sediment aspects was proposed and applied for assessing the Jiangsu offshore ecosystem health. Moreover, an improved method (PPCM-PCAM) which combines projection pursuit cluster model (PPCM) with principal component analysis method (PCAM) was developed to assess offshore ecosystem health. By using these established indicators and this improved method, the relative comparison results show that the Jiangsu offshore ecosystem health status varies temporally from good to bad: autumn > summer > spring > winter; and spatially from good to bad: Radial Sandbank Subzone (RSS) > Haizhou Bay Subzone (HBS) > North Branch of the Yangtze River Estuary and its Adjacent Subzone (NBS). From the findings of the absolute diagnosis, it can be concluded that the Jiangsu offshore ecosystem is generally sub-healthy.

KEYWORDS: Jiangsu offshore ecosystem health; pressure; assessment indicator; relative comparison; absolute diagnosis; projection pursuit cluster model - principal component analysis method (PPCM-PCAM)

1. INTRODUCTION

The offshore ecosystem service functions, such as providing food, primary contact recreation and tourism resource, are extremely important in terms of sustainable social and economic development [1]. However, the offshore ecosystems worldwide continue to be under unrelenting natural and anthropogenic pressures from red tide, biological invasion, continued urban development along shorelines, industrial and agricultural pollution, resource

* Corresponding author

exploration, and extensive fishing or overfishing [2, 3]. These activities may not only affect social-economic development and human health, but also lead to the collapse of offshore ecosystems themselves [4, 5]. Therefore, there is urgent need to set the restoration and maintenance of offshore ecosystem health as a priority in offshore management policy documents [6, 7].

This is evidence by the launches over the past few years of many international and national ocean environmental programs including: (1) “the Global Ocean Observing System’s (GOOS) Health of the Ocean (HOTO) program” and “the Global Investigation of Pollution in the Marine Environment (GIPME)” supported by the Intergovernmental Oceanographic Commission (IOC) of United Nations Educational, Scientific, and Cultural Organization (UNESCO) [8, 9]; (2) “the Coasts under Stress (CUS) project supported by Canada’s Federal Research Granting Agency [10]; (3) the “Assessment on Marine Ecosystem Health” supported by State Oceanic Administration People’s Republic of China (SOAPRC); and (4) “The Guidance for the Assessment of Coastal Marine Ecosystem Health” published by SOAPRC [11]. Increasing special attention has been paid to ocean or offshore ecosystem health in the whole world.

The use of indicator species, which can serve as important barometers of the offshore ecosystem health assessment, has become a mainstream study trend [12]. The offshore ecosystem health can be determined by monitoring the parameters of biomass, residual toxicity in organism, etc. Indicator species that have been successfully applied in the assessment of the offshore ecosystem health include benthic macrofauna [9], meiofauna [13], bottlenose dolphins [14], manatees [15], marine turtles [16], southern sea otter [17], or marine birds [18]. However, the complexity of the offshore aquatic ecosystem means that its health status cannot be completely reflected by using only a single factor, such as indicator species. Thus, a number of integrated indicators have been proposed, such as structure and function indicators [19]; exergy, specific exergy

and ascendancy indicators [20]; stress indicators integrating response indicators [21]; the indicators including productivity, fish and fishery, pollution, socioeconomic conditions and pertinent governance regime aspects [22]; phytoplankton abundance and diversity index [23]; and thermodynamic indicators combining network oriented indicators [24]. Despite the more complete picture of ecosystem health status obtained using the integrated assessment in-dicators system, there is urgent need to develop more comprehensive indicators for the offshore ecosystem health assessment.

In addition to the indicators, the assessment method also plays an important role. In recent years, many integrated methods have been applied to the offshore ecosystem health assessment, including comprehensive index method [25], artificial neural network model [26], fuzzy comprehensive evaluation method [27], and grey system method [28]. However, there are still some limitations, for example, the different dimensions of the indices and the liability of the results to subjective factors [29]. Furthermore, it is difficult to determine the relative weights of the indices, which leads to difficulties in the application of the models.

The projection pursuit cluster model (PPCM) is employed to investigate the offshore health assessment in this paper. The PPCM is an exploring data analysis method which is driven by the sample data directly. It is also an objective weighted method which can avoid the artificial influence factors. High dimensional data is projected into one-dimensional space by computer technology, and then, the feature of high dimensional data is analyzed through the projected characteristics of the one-dimensional space [29-33]. Through this processing route, the limitations in other evaluation methods can be effectively avoided. However, the development of a suitable method to optimize projection index function in practice is a tough task, which may challenge the use of PPCM. With regard to this issue, the principal component analysis method [34] (PCAM) is employed to estimate optimum projection direction.

In this paper, the Jiangsu offshore area is taken as a case study, and the developed indicator and method are used to assess the ecosystem health status of the area. In section 2, a set of more comprehensive quantitative indicators based on the offshore ecosystem responses to the natural and anthropogenic pressures is presented. An improved combined method (the PPCM-PCAM) is also proposed in this section. In section 3, the developed integrated indicator and the method are utilized for the Jiangsu offshore ecosystem health assessment and the results are discussed in detail.

2. MATERIALS AND METHODS

2.1. Study area and sampling sites

Jiangsu offshore area is located in the middle part of East China Sea Continental Shelf, which is dominated by a warm temperate and subtropical humid monsoon climate (Fig. 1). The length of Jiangsu coastline is about 954 km, and its internal water area is about 2.18×10^4 km². From July 2006 to November 2007, the samples were collected at 40 sites. The collection time span was subdivided into four periods: spring, summer, autumn and winter. At these sites, the data were monitored and surveyed according to different methods and standards, and these data are considered to be representative average values of each season. For the purpose of comparative analysis, the Jiangsu offshore area was divided into three parts, namely Haizhou Bay Subzone (HBS), Radial Sandbank Subzone (RSS), and North Branch of the Yangtze River Estuary and its Adjacent Subzone (NBS).

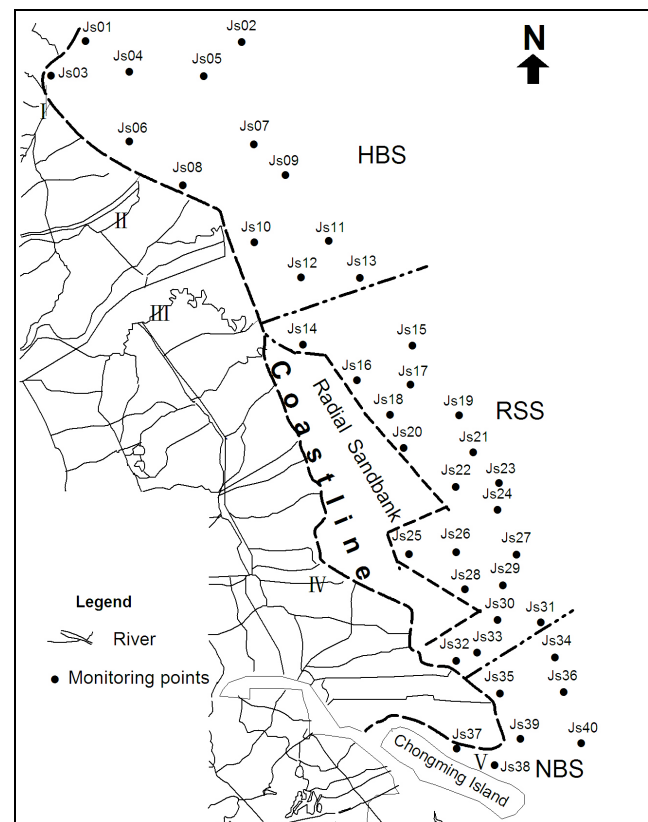


FIGURE 1 - Map of the offshore area, Jiangsu province, China (I: Linhong River; II: Guanhe River; III: Sheyang River; IV: Xiaoyang River; V: North Branch of the Yangtze River Estuary).

2.2. Assessment procedures design

The assessment procedures designed for the offshore ecosystem health are shown in Fig. 2. There are five major steps for the offshore ecosystem health assessment. Firstly, the natural and human-induced threats and disturbances are reviewed, and the corresponding structure and function of the offshore ecosystem are determined. Secondly, the natural and anthropogenic inputs (pressures), components of the offshore ecosystem are analyzed to understand relationships among these elements. Thirdly, the responses of the offshore ecosystem to the pressures

are identified as: water quality physico-chemical, biological, ecological, and sediment responses. Nextly, based on this, the assessment indicators' system, which is a multi-index of water quality, organisms, ecology and sediment, is developed. Finally, the offshore ecosystem health is assessed using the improved ecosystem health assessment method (the PPCM-PCAM).

In the Jiangsu offshore area of China, the major natural and human disturbances are industrialization, urbanization, agricultural development, marine aquaculture, and red tide disaster, which cause primary pressures on water quality and aquatic organisms. The corresponding responses of the offshore ecosystem to the pressures concern physical, chemical, biological, ecological, and sediment aspects. Based on these responses, a set of comprehensive indicators can be established and applied to assess the Jiangsu offshore ecosystem health.

2.3. Integrated evaluation method

Assume x_{ij}^0 ($i = 1, \dots, n; j = 1, \dots, m; n$ is the total number of samples; m is the total index number of sample) is the initial value of the j th factor of the i th sample, the PPCM procedures to assess the offshore ecosystem health can be described as follows [31-33]:

Step 1: Data standardization.

In order to eliminate the effect of dimensions and ranges, the original value will be transformed before it is used by the PPCM. Here, the index value is to be standardized as in the following formula:

$$\text{For a positive index, let: } x_{ij} = \frac{x_{j\min}}{x_{ij}^0}; \quad (1)$$

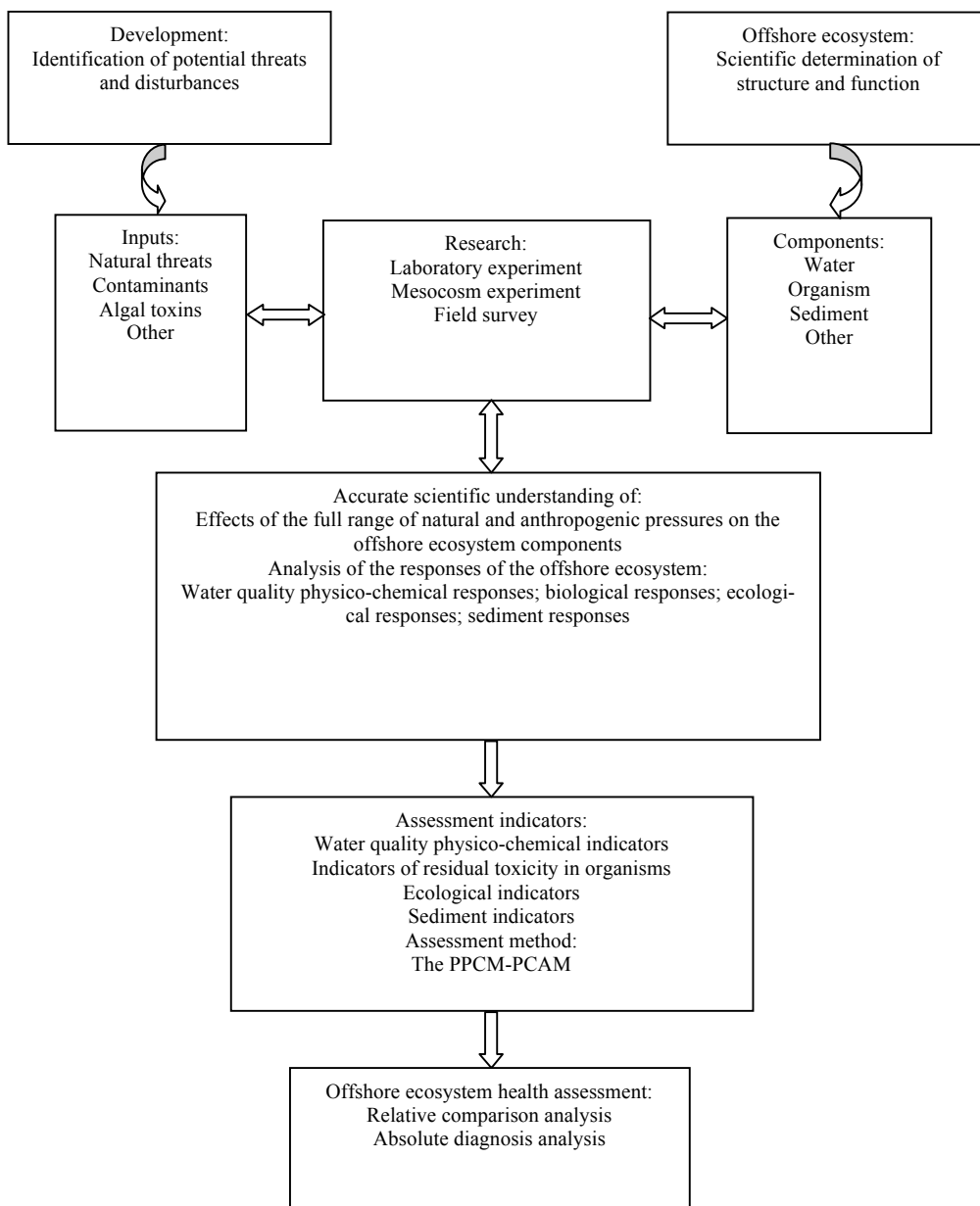


FIGURE 2 - The designed procedure chart for offshore ecosystem health assessment.

$$\text{but for a negative index, let: } x_{ij}^0 = \frac{x_{ij}^0}{x_{j\max}}, \quad (2)$$

where x_{ij} ($i = 1, \dots, n; j = 1, \dots, m$) is the j th index original value of the i th sample by standardizing, $x_{j\max}$ and $x_{j\min}$ are the maximum and minimum values of the j th index, respectively.

Step 2: Linear projection.

Assume a is an m -dimensional unit vector, and z_i is the projection characteristic value of the i th sample, the linear projection of the i th sample can be expressed by:

$$z_i = \sum_{j=1}^m a_j x_{ij}. \quad (3)$$

Step 3: Projection index function.

For synthesizing the projection values, the dispersal characteristic of the projection value z_i is required as follows. The partial projection points should be as intensive as possible, preferably forming individual point regions, and the point regions should be as widely dispersed as possible in the entire region. Then, based on the principle of cluster analysis, the projection index $Q(a)$ can be formulated by: $Q(a) = s(a) \cdot d(a)$. (4)

Here, a is the projection axis, $s(a)$ represents the spread of data, and $d(a)$ describes the “local density” of

the points after projection onto \vec{a} . The bigger the value of $Q(\vec{a})$, the more remarkable the cluster will be.

The value of $s(\vec{a})$ is calculated by the variance of z_i ,

$$\text{as follows: } s(\vec{a}) = \left[\sum_{i=1}^n (z_i - \bar{z}_a)^2 / n \right]^{1/2}. \quad (5)$$

Here, \bar{z}_a is the average value of z_i in axis \vec{a} , and $d(\vec{a})$ is calculated through the distance r_{ik} between two points' projection characteristic value. Let $r_{ik} = |z_i - z_k|$ ($k = 1, \dots, n$), and $d(\vec{a})$ can be expressed by:

$$d(\vec{a}) = \sum_{i=1}^n \sum_{k=1}^n (R - r_{ik}) f(R - r_{ik}), \quad (6)$$

in which $f(R - r_{ik})$ is a unit jumping function, $f(R - r_{ik}) = 1$ when $R > r_{ik}$, or else $f(R - r_{ik}) = 0$. R is the window radius to get the partial density, the selection of which should not only be to ensure that the average number of the projection points in the widow is not extremely small in order to avoid a large moving average deviation, but also to ensure a not-too-rapid improvement of R as m improves. There are indications that the scope of cutoff radius is $\max(r_{ik}) + m/2 \leq R \leq 2m$, and the value of R is taken to be $0.1 s(\vec{a})$.

Step 4: Projection index function optimization.

According to the analysis above, we know that \vec{a} will be the right projection direction when $Q(\vec{a})$ in Eq. (4) reaches its maximum value. It can be found that the \vec{a} can be expressed by the following optimum problem:

$$\max Q(\vec{a}), \|\vec{a}\| = 1. \quad (7)$$

Here, the nonlinear optimization problem described by formula (7) can be resolved by many methods. However, the projection index function may be differentiable and continuous when projection direction is optimized with traditional optimum method [32]. Then, in order to improve the PPCM for overcoming the deficiency, the PCAM is employed to solve the nonlinear optimization problem of the PPCM in this paper. The optimizing procedures by using the PCAM can be described as follows.

Suppose the offshore ecosystem health assessment standards are divided into k categories, the m assessment indicators in each category are expressed as matrix X . Here, each row vector $\{X_i = (x_{i1}, x_{i2}, \dots, x_m)\}$, $i = 1, 2, \dots, k$ is regarded as a data point.

Each variable in the matrix X has been auto-scaled to zero mean and unit variance, the covariance matrix (C) can be defined as:

$$C = \frac{1}{m} XX^T. \quad (8)$$

Where, X^T is the transposed matrix of the matrix X .

According to the related covariance matrix C , we can get its m characteristic roots which are not less than 0, then rank them according to their size, and $\lambda_1 \geq \lambda_2 \geq \dots \geq \lambda_m \geq 0$. Then, the 1st primary component axis (a_1) is the optimal projection direction, namely

$$\begin{aligned} \lambda_1 &= \max(a_1 C a_1^T) = \max\left(\frac{1}{m} a_1 X X^T a_1^T\right), \|a_1\| = 1; \lambda_2 \\ &= \max(a_2 C a_2^T) = \max\left(\frac{1}{m} a_2 X X^T a_2^T\right), \|a_2\| = 1; \dots \lambda_m = \\ &\max(a_m C a_m^T) = \max\left(\frac{1}{m} a_m X X^T a_m^T\right), \|a_m\| = 1; \text{ and} \\ &a_m \perp a_{m-1}, \dots, a_1. \end{aligned} \quad (9)$$

The analyses in this study are conducted in MATLAB 7.1 system.

Step 5: Integrated evaluation analysis.

As z_i is able to reflect the comprehensive evaluation index of samples, we can analyze the data feature and draw a reasonable conclusion according to the discrepancy of z_i between each grade of the standard and the assessment sample.

3. RESULTS AND DISCUSSION

3.1. Major natural and anthropogenic disturbances

Through relevant investigation and analysis, major natural and anthropogenic disturbances and possible associated pressures are shown in Table 1. Among these disturbances, marine aquaculture, industrialization and urbanization have caused the most serious pressures to the Jiangsu offshore ecosystem. Major physical pressures are caused by marine aquaculture, red tide and resource exploration, while major chemical and ecological pressures are caused by various pollutions from human daily life, industrial activities and agricultural irrigation. The COD_{cr} and NH₃-N loads from various anthropogenic pollution sources had increased considerably from 2006 to 2007; however, the phosphate salts loads decreased slightly over the same time period (Table 2).

3.2. Indicators for assessing Jiangsu offshore ecosystem health

The assessment indicators in the Jiangsu offshore ecosystem are discussed with regard to the afore-mentioned assessment procedures, and the responses of the Jiangsu offshore ecosystem to these natural and anthropogenic pressures. Key indicators include water quality indicators, indicators of residual toxicity in organisms, ecological indicators, and sediment indicators.

In order to discover the overall trend and degree of offshore pollution easily, the comprehensive pollution index (CPI) [12] are used in this study (Eq. (10)):

$$P_i = \frac{1}{n} \sum_{j=1}^n \frac{C_{ij}}{C_{sj}}. \quad (10)$$

Where, P_i is the value of CPI at i site, C_{ij} is the value of j th parameter at i th site, and C_{sj} is the Level 2 value of j th parameter. The Level 2 value is determined according to the marine function zoning, Jiangsu province, China (2001-2010), sea water quality standard (GB3097-1997, China); marine biological quality (GB18421-2001, China); marine sediment quality (GB18668-2002, China). The nutrient factors and heavy metals are indicated by CPI in this paper, and the lower CPI value, the healthier the offshore water area is.

Diversity index is calculated by the Shannon-Wiener Index, and abundance index is calculated by the Margalef Index.

3.3. Water quality physical indicators

The main physical responses of the Jiangsu offshore ecosystem to the pressures are changes in transparency and suspended solids (SS) (Fig. 3). These are, therefore, selected as the water quality physical indicators to assess the Jiangsu offshore ecosystem. Fig. 3a shows that the general temporal order from good to bad with regard to transparency is: summer > spring > autumn > winter. The transparency (Secchi Disc depth) at many monitoring points is lower than 1 m, which may reflect the influence of attached algae. At some monitoring points, the concentrations of SS are even higher than the criteria of Category 4, which is the poorest category according to sea water quality standard (GB3097-1997) of China (Fig. 3b). This may be caused by extensive coastal marine aquaculture and urbanization.

TABLE 1 - Major natural and anthropogenic disturbances and associated pressures in the Jiangsu offshore water area, China.

Disturbances	Pollution caused by the disturbance	Pressures
Red tide	Transparency reduction; water quality and ecological damage	P, C, E
Biological invasion	Ecological damage	E
Marine aquaculture	Changes of DO, pH, turbidity, nutrient salts; influences of phytoplankton, benthic organisms	P, C, E
Industry	Water quality degradation	C, E
Agriculture	Water quality degradation	C, E
Resource exploration	Ecosystem degradation	P, C
Urbanization	Water quality and ecosystem degradation	P, C, E

Note: DO: dissolved oxygen; P: physical pressures; C: chemical pressures; E: ecological pressures.

TABLE 2 - Pollutant loadings into the Jiangsu offshore water area, in 2006 and 2007 (tons per year).

Major river pollutants dumped into the Jiangsu offshore water area, China	COD_{cr}		Phosphate salts		NH₃-N	
	2006	2007	2006	2007	2006	2007
HBS	Linhong River	3617	103542	2144	1061	67
	Guanhe River	N	32543	N	921	N
	Sheyang River	25964	59216	3283	533	374
RSS	Xiaoyang River	4158	N	1020	N	111
	North Branch of the Yangtze River Estuary	N	575255	N	1695	N
Total	33739	770556	6447	4210	552	36726

Note: data from bulletin of marine environmental quality in Jiangsu province, China (2006, 2007). N: no statistics.

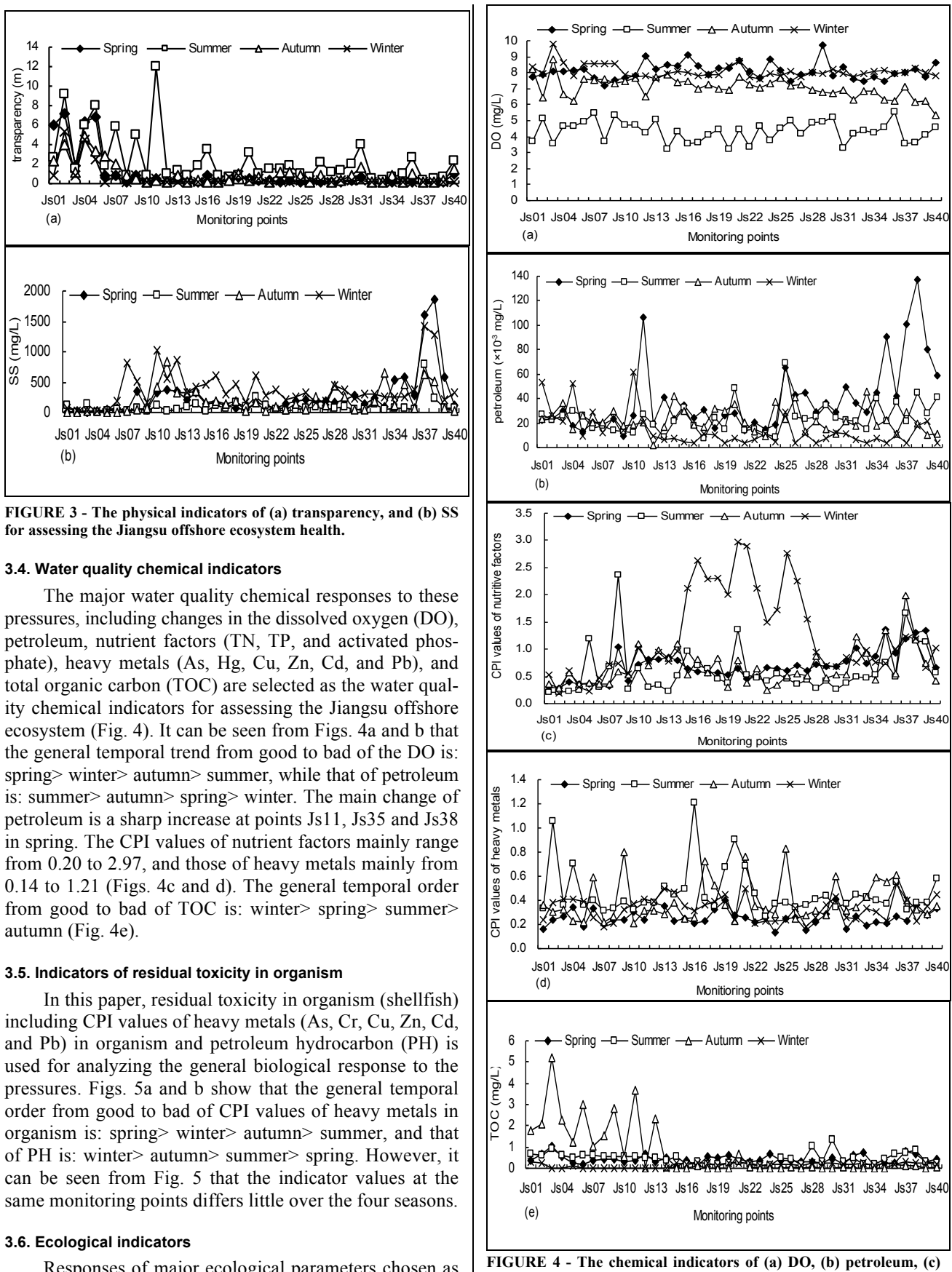


FIGURE 3 - The physical indicators of (a) transparency, and (b) SS for assessing the Jiangsu offshore ecosystem health.

3.4. Water quality chemical indicators

The major water quality chemical responses to these pressures, including changes in the dissolved oxygen (DO), petroleum, nutrient factors (TN, TP, and activated phosphate), heavy metals (As, Hg, Cu, Zn, Cd, and Pb), and total organic carbon (TOC) are selected as the water quality chemical indicators for assessing the Jiangsu offshore ecosystem (Fig. 4). It can be seen from Figs. 4a and b that the general temporal trend from good to bad of the DO is: spring > winter > autumn > summer, while that of petroleum is: summer > autumn > spring > winter. The main change of petroleum is a sharp increase at points Js11, Js35 and Js38 in spring. The CPI values of nutrient factors mainly range from 0.20 to 2.97, and those of heavy metals mainly from 0.14 to 1.21 (Figs. 4c and d). The general temporal order from good to bad of TOC is: winter > spring > summer > autumn (Fig. 4e).

3.5. Indicators of residual toxicity in organism

In this paper, residual toxicity in organism (shellfish) including CPI values of heavy metals (As, Cr, Cu, Zn, Cd, and Pb) in organism and petroleum hydrocarbon (PH) is used for analyzing the general biological response to the pressures. Figs. 5a and b show that the general temporal order from good to bad of CPI values of heavy metals in organism is: spring > winter > autumn > summer, and that of PH is: winter > autumn > summer > spring. However, it can be seen from Fig. 5 that the indicator values at the same monitoring points differs little over the four seasons.

3.6. Ecological indicators

Responses of major ecological parameters chosen as the ecological indicators for assessing the Jiangsu offshore

FIGURE 4 - The chemical indicators of (a) DO, (b) petroleum, (c) CPI values of nutritive salts, (d) CPI values of heavy metals, and (e) TOC for assessing the Jiangsu offshore ecosystem health.

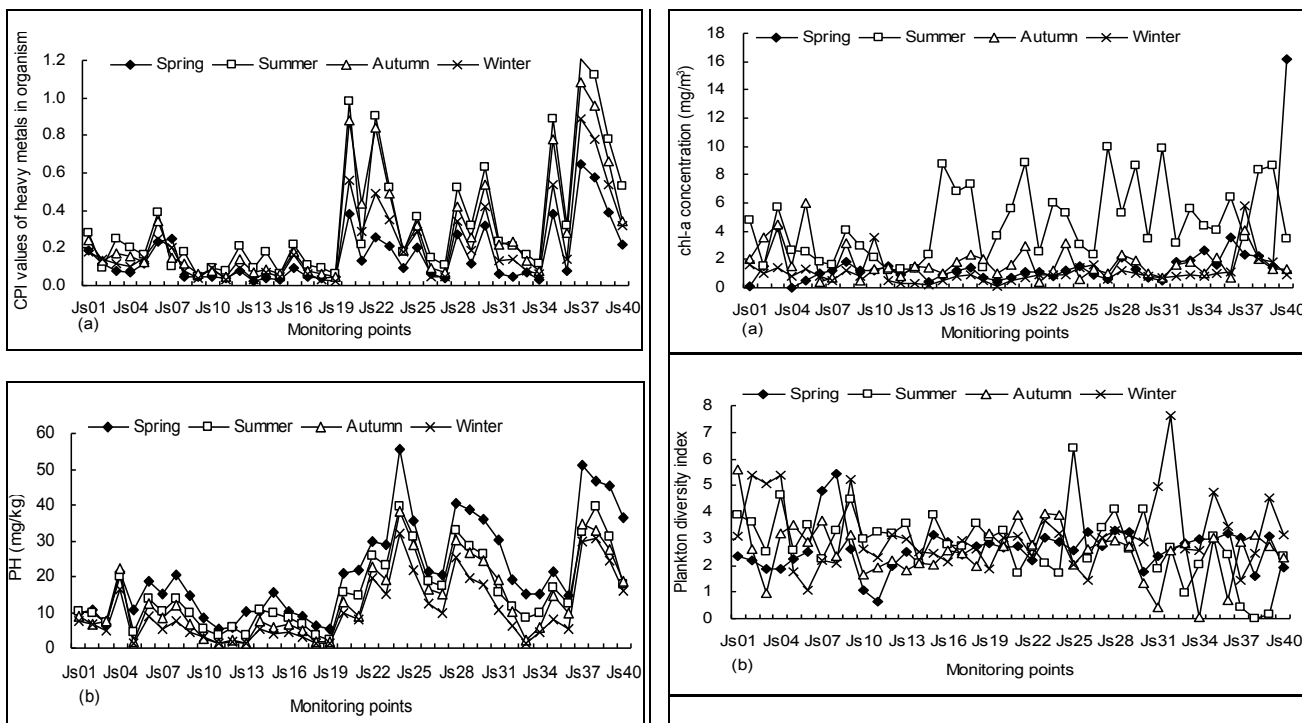


FIGURE 5 - The indicators of residual toxicity in organism of (a) CPI values of heavy metals in organism, and (b) petroleum hydrocarbon (PH) for assessing the Jiangsu offshore ecosystem health.

ecosystem in this paper include Chl-a concentration, plankton diversity index, plankton abundance index, benthonic organism diversity index, and benthonic organism abundance index (Fig. 6). Fig. 6a shows that the Chl-a concentration values mainly vary from 0.03 to 16.2 mg/m³, with the highest recorded at point Js40 in spring. It can be seen from Figs. 6b and d that the maximum values of plankton and benthonic organism diversity index are measured at point Js32 in winter and in spring, respectively. In contrast, the minimum values of plankton and benthonic organism diversity index are monitored at points Js38 and Js09 in summer, respectively. The plankton abundance index mainly ranges from 1.13 to 18.72, and that of the benthonic organism abundance index mainly ranges from 0.33 to 6.32 (Figs. 6c and e). The main changes of plankton diversity and abundance index have considerable increases at points Js32 in winter and Js25 in summer, respectively (Figs. 6b and c).

3.7. Sediment Indicators

Due to the long-term anthropogenic contamination of the offshore water quality, a variety of contaminants were accumulated in sediment, such as organic carbon (OC), petroleum, heavy metals (As, Cr, Cu, Zn, Cd, and Pb), sulfide, etc. These parameters are, therefore, chosen as the sediment indicators to assess the Jiangsu offshore ecosystem in this paper. The specific indicator values and general change trends of OC, petroleum in sediment, CPI values of heavy metals in sediment, and sulfide are shown in Fig. 7.

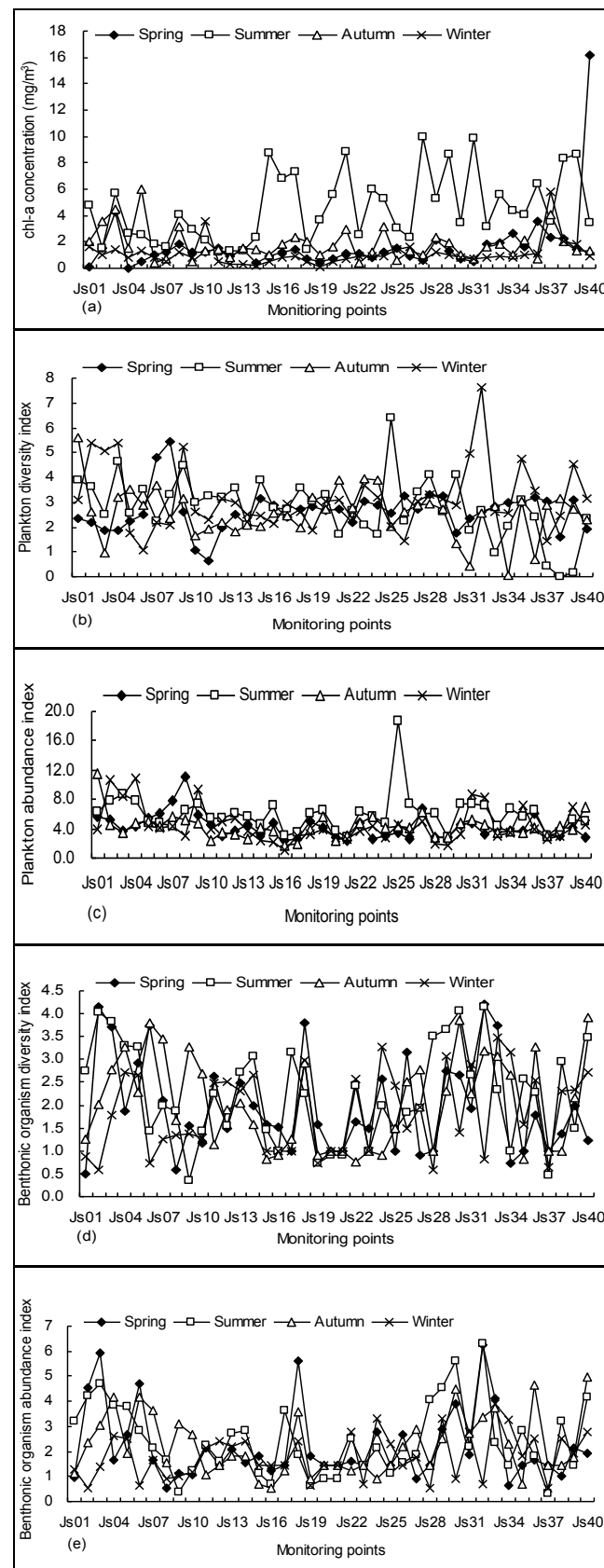


FIGURE 6 - The ecological indicators of (a) Chl-a concentration, (b) plankton diversity index, (c) plankton abundance index, (d) benthonic organism diversity index, and (e) benthonic organism abundance index for assessing the Jiangsu offshore ecosystem health.

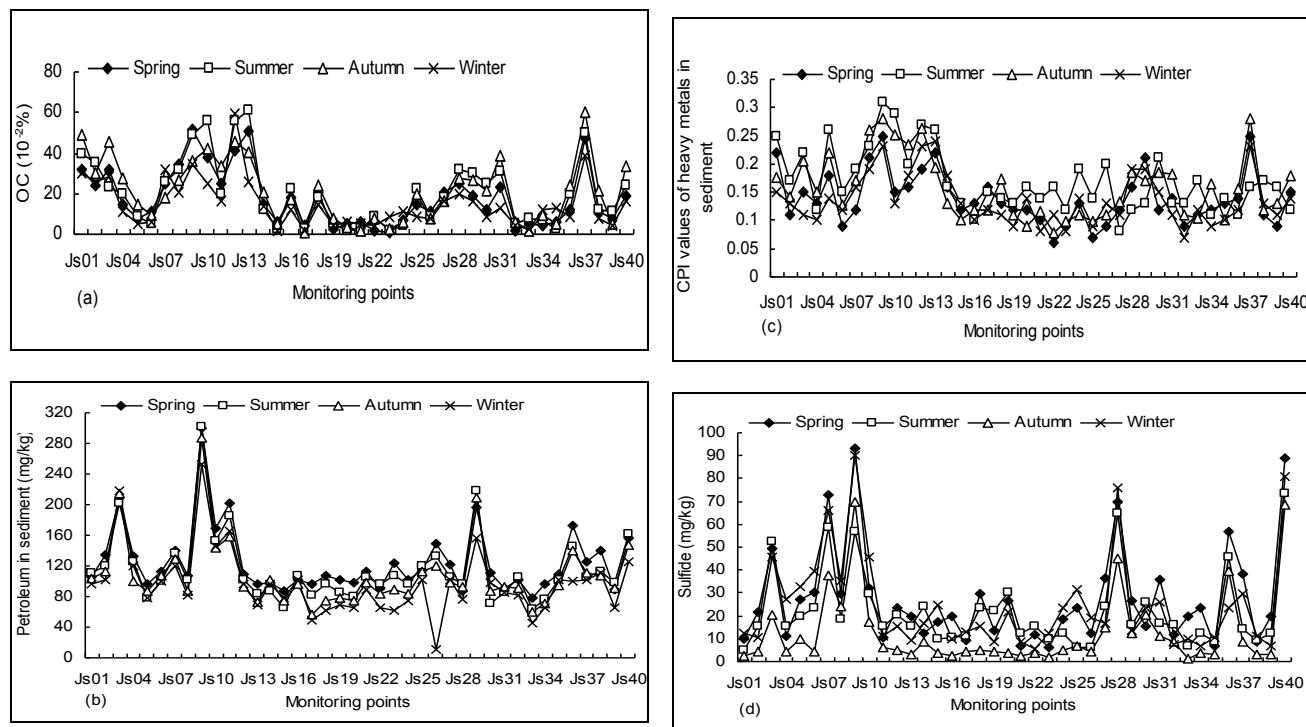


FIGURE 7 - The sediment indicators of (a) OC, (b) petroleum in sediment, (c) CPI values of heavy metals in sediment, and (d) sulfide for assessing the Jiangsu offshore ecosystem health.

TABLE 3 - The indicators for assessing the Jiangsu offshore ecosystem health, China.

Elements	Assessing indicators	Relative healthy state		Methods for obtaining indicator values	
		Healthy	Sick		
Water Quality indicators	Physical indicators	Transparency SS	Deeper Lower	Shallower Higher	Measure Measure
	Chemical indicators	DO Petroleum	Higher Lower	Lower Higher	Measure Measure
		CPI values of nutritive salts CPI values of heavy metals	Smaller Smaller	Larger Larger	Measure and calculate Measure and calculate
		TOC	Smaller	Larger	Measure
	Indicators of residual toxicity in organism	CPI values of heavy metals in organism petroleum hydrocarbon (PH)	Smaller Smaller	Larger Larger	Measure and calculate Measure
	Ecological indicators	Chl-a concentration Plankton diversity index Plankton abundance index Benthonic organism diversity index Benthonic organism abundance index	Lower Higher Higher Higher Higher	Higher Lower Lower Lower Lower	Measure Measure and calculate Measure and calculate Measure and calculate Measure and calculate
	Sediment indicators	Organic carbon (OC) Petroleum in sediment CPI values of heavy metals in sediment Sulfide	Smaller Lower Smaller Smaller	Larger Higher Larger Larger	Measure Measure Measure and calculate Measure

3.8. Aggregation of assessment standard

Based on the afore-mentioned analysis, a set of comprehensive assessment indicators in the Jiangsu offshore ecosystem are presented in Table 3. The indicators encompass the ecosystem response indicators to the pressures including physical, chemical, residual toxicity in organism, ecological, and sediment aspects. The indicator values can be obtained through measurement and/or calculation.

The determination of the assessment standards is the basis of ecosystem health assessment [35], so that the final evaluation results are directly affected by these standards. Especially for the offshore ecosystem, there is no general understanding and uniform standard at present [36]. The assessment standard is usually altered according to offshore locations, sizes, types and phases of ecological succession, and social expectations of different stakeholders, thus, it is a relative standard. In this paper, there are

five major reference criteria for determining ecosystem health assessment standards for the Jiangsu offshore water area: (1) judgment according to historical data and cross-reference methods; (2) on-the-spot investigation; (3) application of national and regional standards and relevant research results for references; (4) critical levels related to the health property values of organism; (5) public participation, and expert consultation [36-39].

According to the afore-mentioned criteria, in terms of the uncertainty and relativity of the offshore ecosystem health, the health assessment standard for the Jiangsu offshore ecosystem is divided into 4 levels: “healthy”, “sub-healthy”, “unhealthy” and “sick”. The details of the health assessment standards for the Jiangsu offshore ecosystem are shown in Table 4.

3.9. Health assessment of the Jiangsu offshore ecosystem

According to the data of 4-grade offshore ecosystem health assessment standard (Table 4) and assessment samples (40 monitoring points, Figs. 3-7), the projective index function for assessing the Jiangsu offshore ecosystem health is established by using the PCAM to solve the optimum problem of Eq. (7). The maximum projective index function value is obtained as 1.5063, the optimal projective direction is $\vec{a} = (0.2389, 0.2160, 0.2648, 0.2083, 0.2505, 0.2505, 0.2464, 0.2505, 0.1989, 0.2269, 0.2409, 0.2394, 0.2409, 0.2394, 0.2212, 0.2212, 0.2505, 0.2269)$, and cluster standards based on the projection characteristic values z_i are: grade healthy ($z_i: 1.0193$), grade sub-healthy ($z_i: 1.7797$), grade unhealthy ($z_i: 3.0049$), and grade sick ($z_i: 4.2079$) (Fig. 8a). It can be seen from Fig. 8a that the model precision is high, so it can be used to describe the relationship between offshore ecosystem health assessment standard and indicator. The projection characteristic values of monitoring points can also be calculated using aforementioned model, and the results are shown in Fig. 8b.

TABLE 4 - Four-grade health assessment standard for the Jiangsu offshore ecosystem.

Indicators	Healthy	Sub-healthy	Unhealthy	Sick
Transparency (m) ^a	9.0	6.0	3.0	1.0
SS (mg/L) ^b	6	10	100	150
DO (mg/L) ^c	8.0	6.0	4.0	3.0
Petroleum ($\times 10^{-3}$ mg/L) ^{b, c}	25	50	300	500
CPI values of nutritive salts ^b	1	1.5	2.5	3
CPI values of heavy metals ^b	1	1.5	2.5	3
TOC (mg/L) ^c	1.5	3.0	3.0	3.0
CPI values of heavy metals in organism ^d	1	1.5	2.5	3
pH (mg/kg) ^d	15	50	80	100
Chl-a concentration (mg/m ³) ^b	1.5	3.0	5.0	6.0
Plankton diversity index ^c	3	2	1	0.5
Plankton abundance index ^a	5.0	3.0	2.0	1.0
Benthonic organism diversity index ^c	3	2	1	0.5
Benthonic organism abundance index ^a	5.0	3.0	2.0	1.0
OC ($\times 10^{-2}\%$) ^{c, e}	50	100	200	300
Petroleum in sediment (mg/kg) ^{c, e}	250	500	1000	1500
CPI values of heavy metals in sediment ^e	1	1.5	2.5	3
Sulfide (mg/kg) ^e	150	300	500	600

Note: ^a Determined or judged according to the long-term statistical data by Ocean and Fishery Bureau of Jiangsu Province in China, National Marine Data and Information Center and state oceanic administration people's republic of China. ^b referred or judged from assessment standards by “Sea water quality standard” (GB3097-1997, China), and/or “Environment quality standard for surface water” (GB3838-2002, China), and/or “The guidance for the assessment of coastal marine ecosystem health” (HY/T 087-2005, China). ^c cited in reference [28] by Li et al. (2010). ^d calculated or judged from assessment standards by “Marine biological quality” (GB 18421-2001, China). ^e referred or calculated from assessment standards by “Marine sediment quality” (GB 18668-2002, China).

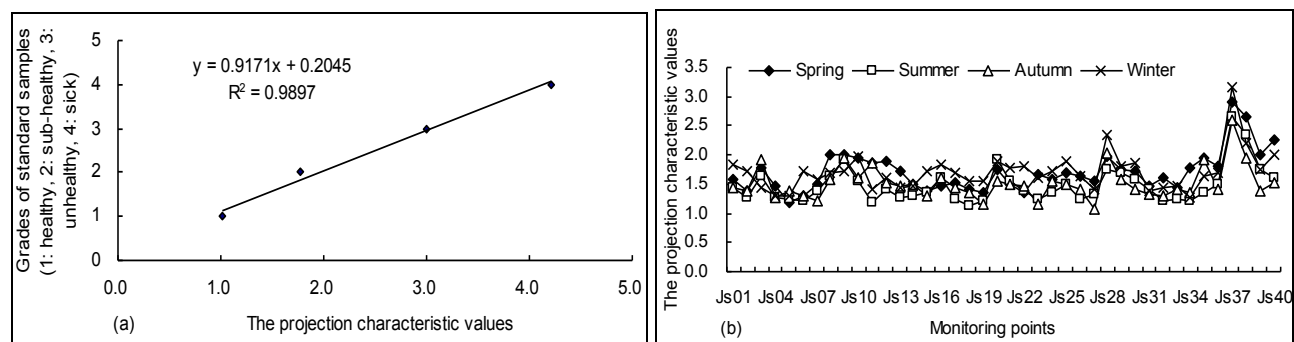


FIGURE 8 - Relationship between the projection characteristic values and grades (a), and the projection characteristic values of monitoring points (b).

TABLE 5 - Health Assessment results of the Jiangsu offshore ecosystem.

Season	Health assessments results							
	Js01	Js02	Js03	Js04	Js05	Js06	Js07	Js08
Spring	sub-healthy	healthy	sub-healthy	sub-healthy	healthy	healthy	sub-healthy	sub-healthy
Summer	sub-healthy	healthy	sub-healthy	healthy	healthy	healthy	healthy	sub-healthy
Autumn	sub-healthy	healthy	sub-healthy	healthy	healthy	healthy	healthy	sub-healthy
Winter	sub-healthy	sub-healthy	sub-healthy	healthy	healthy	sub-healthy	sub-healthy	sub-healthy
Season	Health assessments results							
	Js09	Js10	Js11	Js12	Js13	Js14	Js15	Js16
Spring	sub-healthy	sub-healthy	sub-healthy	sub-healthy	sub-healthy	sub-healthy	healthy	sub-healthy
Summer	sub-healthy	sub-healthy	healthy	sub-healthy	healthy	healthy	healthy	sub-healthy
Autumn	sub-healthy	sub-healthy	sub-healthy	sub-healthy	sub-healthy	sub-healthy	healthy	sub-healthy
Winter	sub-healthy	sub-healthy	sub-healthy	sub-healthy	sub-healthy	sub-healthy	sub-healthy	sub-healthy
Season	Health assessments results							
	Js17	Js18	Js19	Js20	Js21	Js22	Js23	Js24
Spring	sub-healthy	sub-healthy	healthy	sub-healthy	sub-healthy	healthy	sub-healthy	sub-healthy
Summer	healthy	healthy	healthy	sub-healthy	sub-healthy	healthy	healthy	sub-healthy
Autumn	sub-healthy	healthy	healthy	sub-healthy	sub-healthy	sub-healthy	sub-healthy	sub-healthy
Winter	sub-healthy	sub-healthy	sub-healthy	sub-healthy	sub-healthy	sub-healthy	sub-healthy	sub-healthy
Season	Health assessments results							
	Js25	Js26	Js27	Js28	Js29	Js30	Js31	Js32
Spring	sub-healthy	sub-healthy	sub-healthy	sub-healthy	sub-healthy	sub-healthy	sub-healthy	sub-healthy
Summer	sub-healthy	healthy	healthy	sub-healthy	sub-healthy	sub-healthy	sub-healthy	healthy
Autumn	sub-healthy	sub-healthy	healthy	sub-healthy	sub-healthy	sub-healthy	healthy	healthy
Winter	sub-healthy	sub-healthy	sub-healthy	sub-healthy	sub-healthy	sub-healthy	sub-healthy	sub-healthy
Relative comparison results	Temporal order from good to bad					Spatial order from good to bad		
	Autumn> Summer> Spring> Winter					RSS> HBS> NBS		

TABLE 6 - Health Assessment results by three methods.

The randomly selected samples		The PPCM-PCAM		Fuzzy comprehensive evaluation method		Grey system method	
Spring	Js04	sub-healthy		sub-healthy		sub-healthy	
	Js17	sub-healthy		sub-healthy		sub-healthy	
	Js33	sub-healthy		sub-healthy		sub-healthy	
	Js38	unhealthy		sub-healthy		sub-healthy	
Summer	Js06	healthy		healthy		healthy	
	Js20	sub-healthy		sub-healthy		sub-healthy	
	Js25	sub-healthy		sub-healthy		sub-healthy	
	Js37	unhealthy		unhealthy		unhealthy	
Autumn	Js09	sub-healthy		sub-healthy		sub-healthy	
	Js15	healthy		healthy		sub-healthy	
	Js22	sub-healthy		sub-healthy		sub-healthy	
	Js35	sub-healthy		sub-healthy		sub-healthy	
Winter	Js11	sub-healthy		sub-healthy		sub-healthy	
	Js29	sub-healthy		sub-healthy		sub-healthy	
	Js32	healthy		sub-healthy		healthy	
	Js40	sub-healthy		sub-healthy		sub-healthy	

Health assessment results from different points and different seasons of Jiangsu offshore ecosystem are listed in Table 5. There are 7, 12, 14 and 4 points categorized as healthy in spring, summer, autumn and winter, respectively. Most points are sub-healthy, accounting for 80.0, 67.5, 62.5 and 87.5% of all points in spring, summer, autumn and winter, respectively. Only one or two points are unhealthy in some seasons, and no points are categorized as being in a sick state in any season. The relative compari-

son results show that the temporal order of the Jiangsu offshore ecosystem health status from good to bad is: autumn> summer> spring> winter; while the spatial order of health status from good to bad is determined as follows: RSS> HBS> NBS. In general, the Jiangsu offshore ecosystem is in a sub-healthy state.

Meanwhile, in order to verify the PPCM-PCAM effectiveness, the assessment results of some randomly selected samples by fuzzy comprehensive evaluation method

and grey system method have been presented, as Table 6 shows. Compared with the other methods, the PPCM-PCAM has similar assessment results with most of the randomly selected samples, while small difference with few samples exist. Therefore, the assessment result from the PPCM-PCAM is effective and reasonable.

3.10. Assessment indicators and methods

Based on the ecosystem responses to the natural and anthropogenic pressures, the indicators presented in this paper cover water quality physico-chemical, residual toxicity in organism, ecological, and sediment aspects of the offshore ecosystem health. These indicators can show the early warning signs of ecosystem malfunction as well as confirm the presence of significant ecosystem pathology [6, 7, 21]. The changes of water quality physico-chemical indicators represent the first response of an offshore ecosystem to external disturbances. These are followed by organism, ecology and sediment environment changes. It is more effective to apply the indicators simultaneously. These indicators may be used for the health assessment of similar offshore ecosystems.

Compared with other similar studies (e.g. references [21, 24, 28, 37]), a set of more comprehensive quantitative indicators is provided in this study. However, only a set of quantitative indicators is considered. Then, qualitative indicators for assessing the offshore ecosystem health, such as aesthetic enjoyment, water surface cleanliness, ornamental value of tourism resources and recreational facilities, etc., will be considered in a future study. Moreover, owing to the lack of data, two extensive used ecological indicators that include exergy and specific exergy [40-42] for assessing aquatic ecosystem health are also not considered in this study. Since the domain of the offshore ecosystem health is vast and it encompasses not only water quality, organism, ecology dimensions, etc., but also socio-economic and human aspects [43, 44], and different indicators cover different aspects of offshore ecosystem health [45], it may be necessary to develop several indicators simultaneously to get a sufficient image of the offshore ecosystem health.

Both relative comparison and absolute diagnosis are very important for the ecosystem health assessment, and it is necessary to apply the two methods simultaneously. Xu et al. [21, 46] put forward that absolute diagnosis will be the key topic for future researches on ecosystem health. However, the present researches (reviewed by references [21, 24]) on the offshore ecosystem health assessment have mainly focused on the relative comparison aspect.

In response to it, we investigated not only relative comparison, but also absolute diagnosis by using an improved method (the PPCM-PCAM) in the Jiangsu offshore ecosystem health assessment. The method can be used to describe the continuous changes in offshore ecosystem health status. Furthermore, the assessment standards for different health status can be also obtained applying PPCM-PCAM (Table 4). The PPCM-PCAM is a valuable

method with the advantage of simple principle, uncomplicated calculation procedure, objective and reliable results, etc. It is expected that the PPCM-PCAM will be widely used for assessing offshore ecosystems and other watershed ecosystem health status.

4. CONCLUSIONS

In the present study, detailed procedures for assessing the offshore ecosystem health status were designed. The assessment indicators that include water quality physico-chemical, residual toxicity in organism, ecological, and sediment aspects were suggested. Based on the projection pursuit cluster model combining principal component analysis method, an improved method (the PPCM-PCAM) was also developed. The fitted and compared results have proven that the method has a high precision, and it can be easily used for the relative comparison and absolute diagnosis for assessing ecosystem health status. In addition, comparison of the obtained results with other methods, the PPCM-PCAM is also effective and reliable. However, there still exist some limitations by using the PPCM-PCAM to assess offshore ecosystem health (it is difficult to find the optimal projection direction when the assessment indicators are too much by using the PCAM; and different methods for standardizing the data may lead to different assessment results, etc). Then, these issues will be improved in the future study.

As a case study, the health status of the Jiangsu offshore ecosystem was evaluated using the developed integrated indicators and the PPCM-PCAM. The assessment results showed that almost all the points were categorized as healthy and sub-healthy level in four seasons. Only one or two points were at an unhealthy level in some seasons, no points were categorized as the sick level in any season. On the whole, the Jiangsu offshore ecosystem was assessed as being in a sub-healthy state.

ACKNOWLEDGEMENTS

The research work was partly supported by National Basic Research Program of China (2008CB418202), the Water Special Project (Grant No. 2009ZX07103-006), National Natural Science Foundation of China (Grant No: 50979026 and 51009048), China National Funds for Distinguished Young Scholars (Grant No. 50925932), National Key Technologies R&D Program of China (2006BAA01A24), Social Science and Technology Development Project of Jiangsu Province (BS2006095), The Project of “Six Talent Peak” of Jiangsu Province (08-C), the Fundamental Research Funds for the Central Universities of China (2009B18314, SWJTU09CX058 and SWJTU09ZT26) and 908 Special Foundation of Jiangsu Province in China (JS-908-02-06).

REFERENCES

- [1] Xu, F. L., Zhao, Z. Y., Zhan, W., Zhao S. S., Dawson R. W. and Tao, S. (2005) An ecosystem health index methodology (EHIM) for lake ecosystem health assessment. *Ecological Modelling* 188 (2-4): 327-339.
- [2] Wells, P. G. (1999) Biomonitoring the health of coastal marine ecosystem – the roles and challenges of microscale toxicity tests. *Marine Pollution Bulletin* 39 (1-12): 39-47.
- [3] Ha Al-Madfa (2002) Metals accumulation in the marine ecosystem around Qatar (Arabian Gulf). *Fresenius Environmental Bulletin* 11 (12A): 1042-1047.
- [4] Cairns, Jr. J. (1997) Sustainability, ecosystem services, and health. *International Journal of Sustainable Development and World Ecology* 4 (3): 153-165.
- [5] Daily, G. C. (1997) Nature's service: societal dependence on natural ecosystem. Island Press, Washington, DC.
- [6] Xu, F. L., Lam, K. C., Hao, J. Y., Chen, Y. Q. and Tao, S. (2004) Restoring marine coastal ecosystem health as a new goal for integrated catchment management in Tolo Harbor, Hong Kong, China. *Chinese Journal of Population, Resources and Environment (China)* 2 (2): 11-18.
- [7] Xu, F. L., Hao, J. Y., Tao, S. and Dawson, R. W. (2006) Restoration of marine coastal ecosystem health as a new goal for integrated catchment management in Tolo Harbor, Hong Kong, China. *Environmental Management* 37 (4): 540-552.
- [8] Strain, P. M. and Macdonald R. W. (2002) Design and implementation of a program to monitor ocean health. *Ocean & Coastal Management* 45 (6-7): 325-355.
- [9] Magni, P. (2003) Biological benthic tools as indicators of coastal marine ecosystems health. *Chemistry and Ecology* 19 (5): 363-372.
- [10] Dolan, H. A., Taylor M., Neis B., Ommer R., Eyles, J., Schneider, D. and Monteverchi, B. (2005) Restructuring and health in Canadian coastal communities. *EcoHealth* 2 (3):195-208.
- [11] Len, Y. S. (2008) Ecosystem health assessment of Jiaozhou Bay in China. Master Thesis, the First Institute of Oceanography of State Oceanic Administration People's Republic of China (in Chinese).
- [12] Meng, W., Zhang, N., Zhang, Y. and Zheng, B. H. (2009) Integrated assessment of river health based on water quality, aquatic life and physical habitat. *Journal of Environment Science (China)* 21(8): 1017-1027.
- [13] Kennedy, A. D. and Jacoby, C. A. (1999) Biological indicators of marine environmental health: meiofauna – a neglected benthic component? *Environmental Monitoring and Assessment* 54 (1): 47-68.
- [14] Wells, R. S., Rhinehart, H. L., Hansen, L. J., Sweeney, J. C., Townsend, F. I., Stone, R., Casper, D. R., Scott, M. D., Hohn, A. A. and Rowles, T. K. (2004) Bottlenose dolphins as marine ecosystem sentinels: developing a health monitoring system. *EcoHealth* 1 (3): 246-254.
- [15] Bonde, R. K., Aguirre, A. A. and Powell J. (2004) Manatees as sentinels of marine ecosystem health: are they the 2000-pound canaries? *EcoHealth* 1 (3): 255-262.
- [16] Aguirre, A. A. and Lutz, P. L. (2004) Marine turtles as sentinels of ecosystem health: is fibropapillomatosis an indicator? *EcoHealth* 1 (3): 275-283.
- [17] Jessup, D. A., Miller, M., Ames, J., Harris, M., Kreuder, C., Conrad P. A., and Mazet, J. A. K. (2004) Southern sea otter as a sentinel of marine ecosystem health. *EcoHealth* 1 (3): 239-245.
- [18] Mallory, M. L., Gilchrist, H. G., Braune B. M. and Gaston, A. J. (2006) Marine Birds as indicators of Arctic marine ecosystem health: linking the northern ecosystem initiative to long – term studies. *Environmental Monitoring and Assessment* 113 (1-3): 31-48.
- [19] Boesch, D. F. and Paul J. F. (2001) An overview of coastal environmental health indicators. *Human and Ecological Risk Assessment* 7 (5): 1409-1417.
- [20] Fabiano, M., Vassallo, P., Vezzulli, L., Salvo, V. S. and Marques, J. C. (2004) Temporal and spatial change of exergy and ascendancy in different benthic marine ecosystems. *Energy* 29 (11): 1697-1712.
- [21] Xu, F. L., Lam, K. C., Zhao, Z. Y., Zhan, W., Chen, Y. D. and Tao, S. (2004) Marine coastal ecosystem health assessment: a case study of the Tolo Harbour, Hong Kong, China. *Ecological Modelling* 173 (4): 355-370.
- [22] Yáñez-Arancibia, A. and Day, J. W. (2004) The Gulf of Mexico: towards an integration of coastal management with large marine ecosystem management. *Ocean & Coastal Management* 47 (11-12): 537-563.
- [23] Polat, S. (2007) Seasonal dynamics of phytoplankton in a coastal marine ecosystem: Iskenderun Bay, northeastern Mediterranean Sea. *Fresenius Environmental Bulletin* 16 (7): 756-763.
- [24] Vassallo, P., Fabiano, M., Vezzulli, L., Sandulli, R., Marques, J. C. and Jørgensen S. E. (2006) Assessing the health of coastal marine ecosystem: a holistic approach based on sediment micro and meio-benthic measures. *Ecological Indicators* 6 (3): 525-542.
- [25] Yang, J. Q., Cui, W. L., Zhang H. L. and Xu Z. J. (2003) Marine ecosystem health structure and function index assessment in the west of Laizhou Bay, China. *Marine Science Bulletin* 22 (5): 58-63 (in Chinese).
- [26] Mo, M. H., Wang, X. L., Wu, H. J., Cai S. M., Zhang, X. Y. and Wang, H. L. (2009) Ecosystem health assessment of Honghu Lake Wetland of China using artificial neural network work approach. *Chinese Geographical Science (China)* 19 (4): 349-356.
- [27] Yin, L. Q., Han, Z. G. and Long, Y. (2009) Health Assessment on Hengshui Lake Wetland ecosystem. *Environmental Science and Management* 34 (11): 136-140 (in Chinese).
- [28] Li, Q. X., Zhu, L. and Chen, Z. Z. (2010) Ecosystem health assessment of marine sublittoral ecosystem by grey system method. *Acta Scientiarum Naturalium Universitatis Nankaiensis* 43 (1): 39-43 (in Chinese).
- [29] Jin, J. L., Li, L., Wang, W. S. and Zhang M. (2006) A genetic fuzzy analytical hierarchy process based projection pursuit method for selecting schemes of water transportation projects. *Journal of Ocean University of China (Oceanic and Coastal Sea Research) (China)* 30 (5): 289-294.
- [30] Yang, S. L., Wang, S. and Gong, D. N. (2006) Approach to weighted geometric evaluation based on projection pursuit. *Engineering Sciences (China)* 4 (1): 85-88.
- [31] Wang, S., Yang, S. L. and Ma, X. J. (2008) On grey relation projection model based on projection pursuit. *Engineering Sciences (China)* 6 (4): 49-52.

- [32] Wang, S. J., Yang, Z. F. and Ding, J. (2004) Projection pursuit cluster model and its application in water quality assessment. *Journal of Environmental Sciences (China)* 16 (6): 994-995.
- [33] Wang, S. J. and Ni, C. J. (2008) Application of projection pursuit dynamic cluster model in regional partition of water resources in China. *Water Resources Management* 22 (10): 1421-1429.
- [34] Li, Z. Y., Ding, J. and Peng, L. H. (2004) Principles and methods of environmental quality assessment. Chemical Industry Press, Beijing, China (in Chinese).
- [35] Ma, K. M., Kong, H. M., Guan, W. B. and Fu, B. J. (2001) Ecosystem health assessment: methods and directions. *Acta Ecologica Sinica* 21 (12): 2106-2116 (in Chinese).
- [36] Zhao, Y. W. and Yang, Z. F. (2009) Integrative fuzzy hierarchical model for river health assessment: a case study of Yong River in Ningbo City, China. *Communications in Non-linear Science and Numerical Simulation (China)* 14 (4): 1729-1736.
- [37] Ye, S. F., Liu, X. and Ding, D. W. (2007) Ecosystem health assessment of the Changjiang River Estuary: indicator system and its primarily assessment. *Acta Oceanologica Sinica* 29 (4): 128-136 (in Chinese).
- [38] Lin, Q., Zhang, S. S. and Liu, S. L. (2010) Health diagnosis of the wetland ecosystem of Liaohe Estuary. *Journal of Ecology and Rural Environment* 26 (1): 41-46 (in Chinese).
- [39] Troussellier, M., Got, P., Bouvy, M., M'Boup, M., Arfi, R., Lebihan, F., Monfort, P., Corbin, D. and Bernard C. (2004) Water quality and health status of the Senegal River estuary. *Marine Pollution Bulletin* 48 (9-10): 852-862.
- [40] Jørgensen, S. E. (1988) Use of models as experimental tool to show that structural changes are accompanied by increased exergy. *Ecological Modelling* 41 (1-2): 117-126.
- [41] Jørgensen, S. E. (1995) Exergy and ecological buffer capacities as measures of ecosystem health. *Ecosystem Health* 1 (3), 150-160.
- [42] Jørgensen, S. E. (2000) Application of exergy and specific exergy as ecological indicators of coastal areas. *Aquatic Ecosystem Health & Management* 3 (3): 419-430.
- [43] Karr, J. R. (1992) Ecological integrity: protecting earth? Life support systems. In: Costanza, R., Norton, B. G., Haskell, B. D. (Eds), *Ecosystem health: new goals for environmental management*. Island Press, Washington DC.
- [44] Rapport, D. J. (1995) Ecosystem health: exploring the territory. *Ecosystem Health* 1 (1): 5-13.
- [45] Xu, F. L., Jørgensen S. E. and Tao, S. (1999) Ecological indicators for assessing freshwater ecosystem health. *Ecological Modelling* 116 (1): 77-106.
- [46] Xu, F. L., Tao, S., Dawson, R. W., Li, P. G. and Cao, J. (2001) Lake ecosystem health assessment: indicators and methods. *Water Research* 35 (13): 3157-3167.

Received: December 13, 2010

Revised: March 04, 2011

Accepted: March 23, 2011

CORRESPONDING AUTHOR

Benlin Dai

College of Environment
Hohai University
183 Mailbox
1st Xikang Road
210098 Nanjing, Jiangsu Province
P.R. CHINA

E-mail: benlindai@163.com; dbl0@hhu.edu.cn

THE EFFECT OF BIOLOGICAL PRETREATMENT ON DISSOLVED ORGANIC NITROGEN REMOVAL IN DOWNSTREAM COAGULATION AND THE COUNTERMEASURE

Huinong Zhang, Li Gu, Bing Liu, Xin Yu* and Zihong Fan

Key Lab of Urban Environment and Health, Institute of Urban Environment, Chinese Academy of Sciences, 1799 Jimei Road, Xiamen, 361021, China

ABSTRACT

The effect of biological pretreatment in downstream coagulation on dissolved organic nitrogen (DON) removal was investigated under different process conditions including different coagulant doses and enhanced coagulation with cationic polymer. The results showed that DON removal in coagulation was reduced by the biological pretreatment. It was found that biological fluidization pretreatment could change the composition of the compounds and generate more nitrogen-enriched compounds. It might be the reason of the lower DON removal of biological pretreated water in downstream coagulation. As a countermeasure, adding cationic polymer could effectively promote removal of DON in coagulation, and particularly the promotion of biologically pretreated water was more obvious.

KEYWORDS: Biological pretreatment, cationic polymer, coagulation, dissolved organic nitrogen (DON)

1. INTRODUCTION

Nitrogenous organic matter consists mainly of NH classes and amino categories including nitriles, purines, pyrimidines and nitro compounds. It was reported that in approximately 23,000 samples, median DON concentration in surface water was about 0.37 mg/L [1], with the ratios of DOC/DON (C/N) averaged at 18.0 mg C/mg N [2].

Disinfectants, such as chlorine and chloramines, form mutagenic disinfection byproducts (DBPs) of potential human health concerns in water treatment plants [3]. The carbon-based DBPs, such as trihalomethanes and haloacetic acids, have received great attention over the past decades. However, the nitrogenous DBPs (N-DBPs) usually with higher toxicity were found in recent years [4]. N-DBPs are

formed during the interactions between chlorine and DON [5, 6]. So, DON is becoming a hot issue for the research of drinking water now.

As a conventional process widely applied in drinking water production, coagulation is designed to remove suspended and colloid substances. However, the removal of DOC in coagulation was limited [7] and nitrogenous compounds can hardly be removed by this progress [8]. It was reported that an average decrease of DON concentrations was 20% across the full-scale water treatment plants (WTPs) [2]. In some developing districts, the source water is highly polluted by organic matters. So, pretreatment is urgently needed. Biological pretreatments are utilized most frequently in China. It is acknowledged the biological pretreatment is of great benefit to the following coagulation process in removing the organic substances by changing the organic molecular and colloidal Zeta potential [9, 10]. However, the studies about DON removal in coagulation are still limited. And the impact of biological pretreatment on DON removal in coagulation has rarely been studied.

Hence, it is the first time that research quantified the effects of biological pretreatment on DON removal in coagulation and discussed the reasons.

2. MATERIALS AND METHODS

2.1. Study site and sampling

The research was carried out in a Water Plant located at Pinghu, Zhejiang province, China. The source water was seriously polluted with DOC concentration of 8.5 mg/L and DON concentration of 2.0 mg/L, in average during this study. The conventional process could not make the finished water quality meet the national criteria. Thus, biological pretreatment was applied and two biological fluidization tanks with suspended carriers in parallel were included. Each tank was divided into three contact oxidation sub-tanks in series with a designed hydraulic retention time of 1 h. The coarse pore aeration system was built at the bottom of the tanks with the ratio of air to water at (0.8–

* Corresponding author

1.5);1. Source water (SW) and biologically pretreated water (BPW) were collected from the inlet and outlet of biological fluidized bed, respectively.

2.2. Jar tests

Coagulation was performed in a jar test apparatus (DBJ-621, No. 4332 Factory, China). Each sample (1.0 L) was mixed rapidly at 180 rpm for 2 min, mixed slowly at 40 rpm for 15 min, and then settled for 30 min. During the rapid mixing, aluminum sulfate and/or a cationic polymer (cationic polyacrylamide, Heng Yi Chemical Co., Ltd, China) were spiked. Coagulant dosages ranged from 0 to 10 mg Al/L. Cationic polymer dosages were 0 to 3 mg/L. At the end of each jar test, turbidity of supernatant was measured (AQ4500, Orion, US). Samples were also taken and filtered through 0.45- μ m pore-sized membranes for the following analysis. Zeta potential was measured by a Zetasizer (Malvern Nano-ZS ZEN3600, UK).

2.3 Analytical methods

A TOC-VCHS analyzer (Shimadzu, Japan) was used to measure DOC. UVA₂₅₄ was determined by a spectrometer (UV-2000 UNICO, China). Ammonia, nitrite, nitrate and total dissolved nitrogen (TDN) were measured using salicylate-hypochlorite method, N-(1-naphthyl)-ethylenediamine photometric method, UV spectrophotometric method and alkaline potassium persulfate digestion-UV spectrophotometric method, respectively. These determinations were carried out according to the Chinese National Standard Methods [11]. DON was quantified as TDN minus ammonia, nitrite and nitrate. A turbidity-meter (AQ4500, Orion, US) for turbidity and a pH-meter (HQ40d, HACH, US) for pH were calibrated prior to use.

Fluorescence spectrophotometry (F-4600 FL, Hitachi, Japan) was applied to characterize the organic matters in water by three-dimensional excitation-emission matrix (EEM). Excitation (Ex) wavelength and emission (Em) wavelength were set from 200 to 500 nm and from 280 to 500 nm at 5 nm sampling intervals, respectively. To eliminate second order Rayleigh light scattering, a 290 nm emission cutoff filter was used in scanning. The spectrum of double-distilled water was recorded as the blank. To express the fluorescence intensity at an interval of 5 nm, the contour line was shown for each EEM spectrum. Software Origin 8.0 (OriginLab Corporation, MA, USA) was employed to process the data.

3. RESULTS AND DISCUSSION

3.1 Performance of biological pretreatment

SW was treated by the biological fluidized bed. The pH values of SW and BPW were 7.6. It was widely acknowledged that biological processes could utilize biological available matters, such as biodegradable organics and ammonia, which might be ineffectively removed by

conventional treatment. It was confirmed by the results in this study, too (Fig. 1). Both DOC and NH₄⁺-N concentrations were decreased. DOC was reduced from 10.0 to 9.3 mg/L, and NH₄⁺-N from 2.87 to 0.79 mg/L. NO₃⁻-N was increased dramatically from 2.83 to 4.89 mg/L. NO₂⁻-N concentration remained at about 0.22~0.27 mg/L. C/N decreased from 5.25 to 4.45 mg C/mg N. However, the DON concentration of the effluent was about 1.57 mg/L which was quite close to that of the influent.

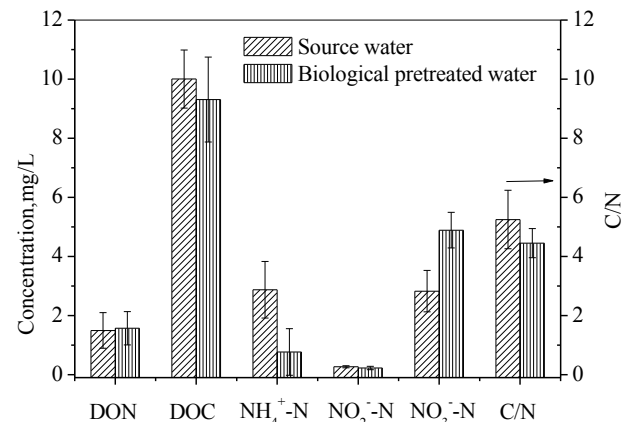


FIGURE 1 - The effect of biological pretreatment on the quality of the water (n=14).

The SW average of DON was much higher than in other countries [1]. The low C/N ratio found herein revealed that nitrogen-enriched dissolved substances predominated in the water. The biological pretreatment posed highly efficiency in NH₄⁺ removal (73.4%). It confirmed that the biological pretreatment had the potential to remove pollutants, such as biodegradable organics, synthetic organic compounds and ammonia, which might be ineffectively removed by conventional treatment [12, 13].

During biological treatment, the variation of NH₄⁺-N and NO₃⁻-N could be attributed to nitrification during which the former was transformed to the latter. Biodegradable organic matters (BOM) could be utilized for energy production and synthesis of the cellular components by the microorganisms, which could be observed through the reduction of DOC. However, DON did not show the same tendency though the biodegradable DON was a fraction of BOM, strongly implying the generation of new nitrogen-enriched species during the biological pretreatment. So it was interesting to investigate the track of DON and what the new species were.

3.2 Soluble microbial products (SMPs) responsible for newly generated DON

To acquire potential changes of the dissolved organic matters (DOM), EEM was applied. The spectra are shown in Fig. 2. It was obvious that the intensities of the both peaks (peak A and peak B) were increased after the biological pretreatment. The intensity of peak A increased from 1134 to 1633, while peak B increased from 757 to

1160. The intensity ratios of peak A and B were measured, increasing from 1.44 to 1.53. It implied that some DOM was formed during the biological pretreatment and the composition of the compounds was changed.

In brief, peak A was associated with the aromatic protein substances and peak B with SMP-like substances including tyrosine-, tryptophan- and protein-like compo-

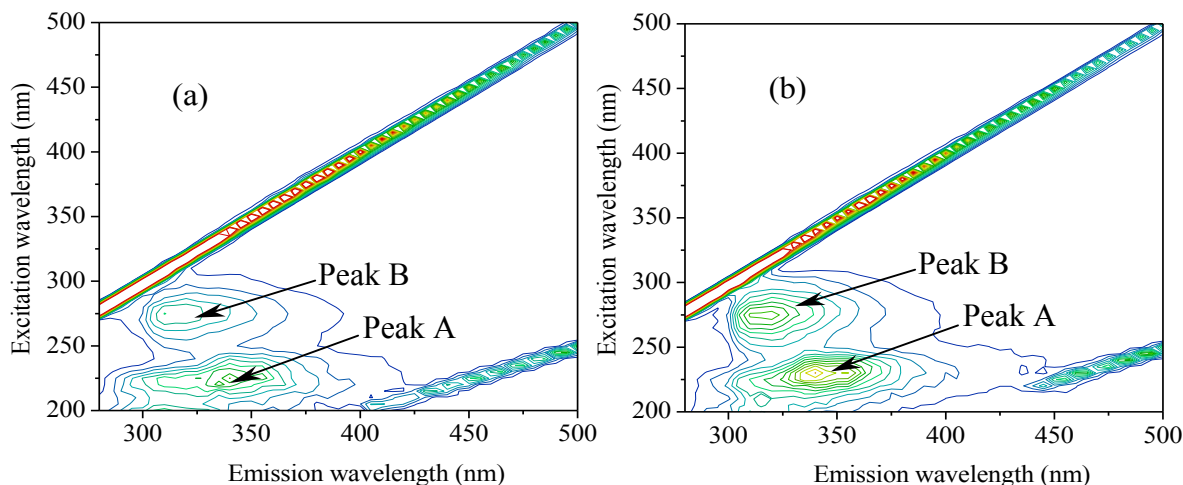


FIGURE 2 - Contour plots of excitation emission matrices of (a) source water and (b) biologically pretreated water.

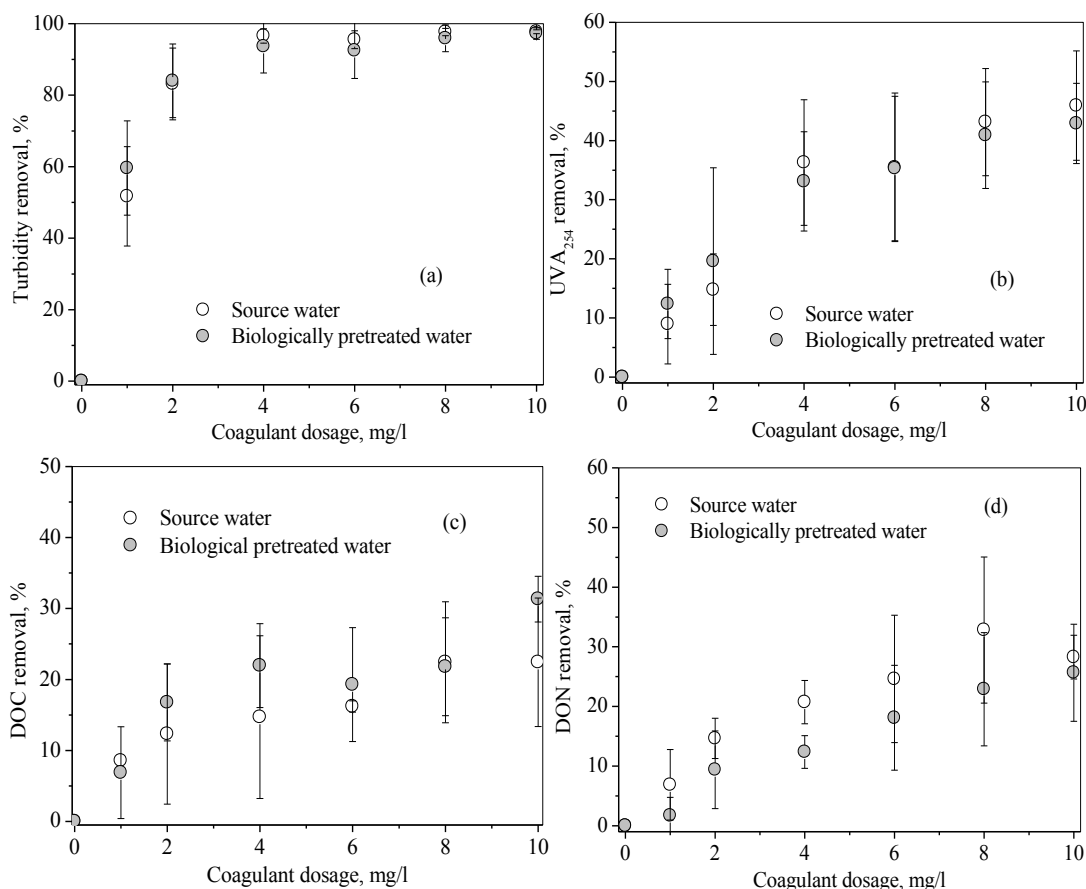


FIGURE 3 - Comparison of (a) turbidity, (b) UVA₂₅₄, (c) DOC and (d) DON removals after coagulation with aluminum sulfate between source water and biologically pre-treated water.

nents, respectively [14]. The aromatic protein substances and the SMP-like substances could be called SMPs herein, and they were nitrogenous. So, there was a good relationship between DON and the intensity of the peaks in the EEM figure. Previous studies had shown that the formation of the aromatic protein-like substances had direct relationship with microbial activity [15]. Due to the microbial activity in biochemical processes, the SMPs could be formed and released. SMPs resulted from intermediates or end-products of substrate degradation and endogenous cell decomposition [16]. The majority of effluent soluble organic carbon (SOC) was SMP, while only a small fraction of the effluent SOC was the residual original substrate according to the experimental results [17]. SMPs were nitrogen-enriched compounds and contained groups of organic matters, such as polysaccharides, proteins, nucleic acids, amino acids and steroids [18]. It was also reported that these SMPs presented a lower biodegradability and lower C/N [19], and had a strong fluorescence. Hence, the EEM spectra confirmed that though DON was co-removed with DOC during the biological pretreatment, new nitrogen-enriched substances (SMPs) were synthesized and released again, which resulted in almost the same DON concentration of the BPW compared with the SW.

Above results revealed that changes of structural properties of DON had taken place during the biological pretreatment, and the problem brought by them to coagulation would be discussed in section 3.3.

3.3 Effect of biological pretreatment on removals of DON and related species in downstream coagulation

Jar tests were conducted to investigate the effect of biological pretreatment on removals of DON and related species in coagulation. Fig. 3 presents that the index concentrations of waters varied as a function of different coagulant doses.

The biological pretreatment affected turbidity and UVA₂₅₄ removals slightly (Figs. 3(a, b)). UVA₂₅₄ measured the amount of aromatic humic fraction of organic matter, and was correlated with aromatic carbon and hydrophobic acid content [20]. It indicated that the biological pretreatment had no obvious removal effect on aromatic fraction of organic matter in coagulation.

Biological pretreatment enhanced DOC removal over the entire range of coagulant dosages tested (Fig. 3(c)). Coagulation could be generally explained in terms of two distinct mechanisms: charge neutralization and sweep flocculation [21]. The aluminum coagulant removed NOM mainly due to charge neutralization. The charge neutralization occurred between surface complexes of negatively charged functional groups on NOM molecules and the positively charged acceptor sites on the aluminum hydroxide surface [22].

Although the DOC removal was enhanced, DON removal was reduced by the biological pretreatment as shown in Fig. 3 (d). It was noticed that the DON removal

in coagulation was reduced. The biological pretreatment exhibited a negative effect on DON removal in downstream coagulation, which was inconsistent with the traditional view that the biological pretreatment was helpful for the following coagulation.

It was believed that biological pretreatment would enhance coagulation through the following means. 1) Sticky secretions (extracellular polymeric substances, EPS, mainly polysaccharides) were generated in the microbial metabolism. The released EPS could act as biopolymer flocculants. Under the adsorption bridging action of the EPS, suspended solids and colloidal particles tend to be bonded together [23]. 2) Biological pretreatment markedly altered the particle size distribution, shifting the granulometric distribution toward larger sizes [17, 24]. The average particle size increased from 169.0 to 179.2 nm in this study. 3) Biological pretreatment decreased the absolute Zeta potential value of particles in water, which made colloidal particles more easily destabilized and agglomerated in the water [10]. The Zeta potential values of particles increased from -16.4 to -13.8 mV. So, the DOC removal in coagulation was strengthened by biological pretreatment.

As mentioned above, DON could be categorized into aromatic and aliphatic nitrogen, and the later was preferentially to be removed for its polarity and ability to bind with metals [1]. The higher proportion of aromatic nitrogenous substances in the BPW could be one of the reasons for the reduced DON removal during coagulation. Another reason might be the different behavior of the specific aliphatic nitrogen species. The aliphatic nitrogenous substances contain basic, neutral and acid functional groups. Commonly, the neutral fractions were considered to be nitrogen-enriched substances and present lower C/N ratios than acid fractions [1]. They were considered as proteinaceous, and generated in the form of SMP-like components during the biological pretreatment. Basic fractions are also enriched in nitrogen, but represent a rather small portion of the DON. They might be of minor significance to the DON in the bulk water [1]. Many tests showed that the neutral fractions were more difficult to be removed during the coagulation than acid fractions [1]. Consequently, the increase of these two types of DON fractions in biological pretreatment resulted in the lowered DON removal efficiency in downstream coagulation for BPW.

So, it was a problem that biological pretreatment hampered DON removal in downstream coagulation. How can it promote the coagulation effect? Cationic polymer was added in the coagulation process (part 3.4).

3.4 Effect of cationic polymer on DON removal during coagulation

DON removals with different cationic polymer doses are presented in Fig. 4. The pH value of water was 7.6. Cationic polymer could significantly raise the removal efficiency of DON. Moreover, this promotion would be augmented, especially if the water was pretreated biologically. The augment was significantly larger with the BPW.

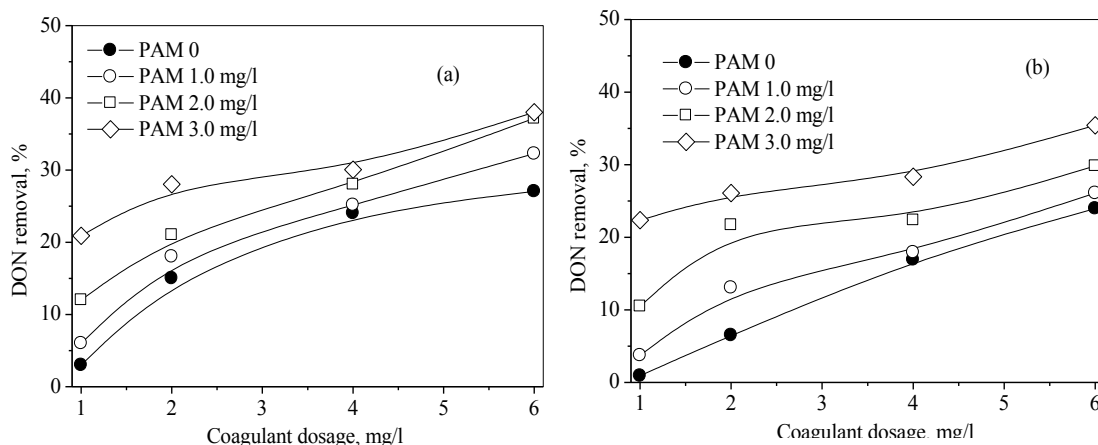


FIGURE 4 - Effect of biological pretreatment on DON removal during coagulation with cationic polymer addition:(a) source water and (b) biologically pretreated water.

The anionic charge carried by SMPs played a major part in their interaction with metal ions and other cationic species. Addition of cationic polymers during coagulation could help neutralize the negative charge on more polar NOM [25]. More polar NOM fractions were nitrogen-enriched and be related to SMP-like components [1]. The polymer molecule was combined with aromatic protein substances and SMP-like components (including neutral fractions) by the effect of Van der Waals force between cationic polar groups on the polymer and DON negative functional group. The effect of Van der Waals force became stronger when the polymer was added. However, at the same specific charge dose, addition of cationic polymers exhibited a synergic effect with aluminum sulfate on DON removal [26]. The polymer could act as a bridge between the polar molecules and the surface of the aluminum hydroxide, and result in a fast precipitation of the flocs [25]. Because the SMPs-like turned more as mentioned above, the effect of polymer on augment DON removal was greater on BPW than SW. Hence, close DON removal was obtained in coagulation of the both waters at the polymer dosage of 3.0 mg/L.

4 CONCLUSIONS

(1) The DON removal in coagulation was reduced by biological pretreatment.

(2) It was found that biological fluidization pretreatment could change the composition of the compounds and generate more nitrogen-enriched compounds. It might be the reason of the lower DON removal of BPW in downstream coagulation.

(3) As a countermeasure, adding cationic polymer could effectively promote removal of DON in coagulation, and particularly the promotion of BPW was more obvious.

ACKNOWLEDGEMENTS

The authors would like to acknowledge financial support provided by National Natural Science Foundation of China (NSFC) (No. 50678080 & 51078343), Fujian Provincial Natural Science Foundation (2009J06028), and the Hundred Talents Program & Knowledge Innovation Program (KZCX2-YW-JC406, KZCX2-YW-452, KZCX2-YW-T08), Chinese Academy of Sciences.

REFERENCES

- [1] Westerhoff, P. and Mash, H. (2002) Dissolved organic nitrogen in drinking water supplies: a review. *Journal of Water Supply Research and Technology-Aqua.* 51(8), 415-448.
- [2] Lee, W., Westerhoff, P., and Esparza-Soto, M. (2006) Occurrence and removal of dissolved organic nitrogen in US water treatment plants. *Journal American Water Works Association.* 98(10), 102-110.
- [3] Richardson, S.D. (2003) Disinfection by-products and other emerging contaminants in drinking water. *TrAC Trends in Analytical Chemistry.* 22(10), 666-684.
- [4] Muellner, M.G., Wagner, E.D., McCalla, K., Richardson, S.D., Woo, Y.T., and Plewa, M.J. (2007) Haloacetonitriles vs. regulated haloacetic acids: Are nitrogen-containing DBPs more toxic? *Environmental Science & Technology.* 41(2), 645-651.
- [5] Chu, W.H., Gao, N.Y., and Deng, Y. (2010) Formation of haloacetamides during chlorination of dissolved organic nitrogen aspartic acid. *Journal of Hazardous Materials.* 173(1-3), 82-86.
- [6] Lee, W., Westerhoff, P., and Croue, J.P. (2007) Dissolved organic nitrogen as a precursor for chloroform, dichloroacetonitrile, N-Nitrosodimethylamine, and trichloronitromethane. *Environmental Science & Technology.* 41(15), 5485-5490.
- [7] Wang, G.S., Kang, S.F., Yang, H.J., Pai, S.Y., and Chen, H.W. (2002) Removal of dissolved natural organic matter from source water with Alum coagulation. *Environmental Technology.* 23(12), 1415-1423.

- [8] Vilge-Ritter, A., Masion, A., Boulange, T., Rybacki, D., and Bottero, J.Y. (1999) Removal of natural organic matter by coagulation-flocculation: A pyrolysis-GC-MS study. *Environmental Science & Technology*. 33(17), 3027-3032.
- [9] Li, W. J., Xing, Y. and Lu, S. Y. (2006) Study on biological aerated filter as pretreatment process of coagulation and sedimentation. *China water & wastewater*. 22(21), 50-52
- [10] Liu, W. J., He, B. P. and Zhang, X. H. (1996) Research of influence of biological pretreatment on colloidal Zeta potential in water polluted by organic matter. *China Water and Wastewater*. 12(4), 27-29..
- [11] SEPA. (2002) *Water and Wastewater Monitoring Methods*. China Environmental Science Publishing House: Beijing.
- [12] Bouwer, E.J. and Crowe, P.B. (1988) Biological Processes in Drinking-Water Treatment. *Journal American Water Works Association*. 80(9), 82-93.
- [13] Rittmann, B.E. and Snoeyink, V.L. (1984) Achieving Biologically Stable Drinking-Water. *Journal American Water Works Association*. 76(10), 106-114.
- [14] Chen, W., Westerhoff, P., Leenheer, J.A., and Booksh, K. (2003) Fluorescence excitation - Emission matrix regional integration to quantify spectra for dissolved organic matter. *Environmental Science & Technology*. 37(24), 5701-5710.
- [15] Parlanti, E., Worz, K., Geoffroy, L., and Lamotte, M. (2000) Dissolved organic matter fluorescence spectroscopy as a tool to estimate biological activity in a coastal zone submitted to anthropogenic inputs. *Organic Geochemistry*. 31(12), 1765-1781.
- [16] Boero, V.J., Eckenfelder, W.W., and Bowers, A.R. (1991) Soluble Microbial Product Formation in Biological-Systems. *Water Science and Technology*. 23(4-6), 1067-1076.
- [17] Namkung, E. and Rittmann, B.E. (1986) Soluble Microbial Products (SMP) Formation Kinetics by Biofilms. *Water Research*. 20(6), 795-806.
- [18] Rittmann, B.E., Bae, W., Namkung, E., and Lu, C.J. (1987) A Critical-Evaluation of Microbial Product Formation in Biological Processes. *Water Science and Technology*. 19(3-4), 517-528.
- [19] Ciner, F. and San, H.A. (2001) Soluble microbial product formation in biological systems. *Fresenius Environmental Bulletin*. 10(2), 160-164.
- [20] Korshin, G.V., Li, C.W., and Benjamin, M.M. (1997) Monitoring the properties of natural organic matter through UV spectroscopy: A consistent theory. *Water Research*. 31(7), 1787-1795.
- [21] Duan, J.M. and Gregory, J. (2003) Coagulation by hydrolysing metal salts. *Advances in Colloid and Interface Science*. 100, 475-502.
- [22] Kummert, R. and Stumm, W. (1980) The Surface Complexation of Organic-Acids on Hydrous γ -Al₂O₃. *Journal of Colloid and Interface Science*. 75(2), 373-385.
- [23] Salehizadeh, H. and Shojaosadati, S.A. (2001) Extracellular biopolymeric flocculants - Recent trends and biotechnological importance. *Biotechnology Advances*. 19(5), 371-385.
- [24] You, H.S., Huang, C.P., Cheng, H.S., and Pan, J.R. (2005) Effect of biofiltration on particle characteristics and flocculation behavior. *Journal of Chemical Technology and Biotechnology*. 80(6), 705-711.
- [25] Lurie, M. and Rebhun, M. (1997) Effect of properties of polyelectrolytes on their interaction with particulates and soluble organics. *Water Science and Technology*. 36(4), 93-101.
- [26] Lee, W. and Westerhoff, P. (2006) Dissolved organic nitrogen removal during water treatment by aluminum sulfate and cationic polymer coagulation. *Water Research*. 40(20), 3767-3774.

Received: December 21, 2010

Revised: March 01, 2011

Accepted: March 23, 2011

CORRESPONDING AUTHOR

Xin Yu

Key Lab of Urban Environment and Health
Institute of Urban Environment
Chinese Academy of Sciences
1799 Jimei Road
Xiamen, 361021
P.R. CHINA

E-mail: xyu@iue.ac.cn

IMPACT OF MAGNETIC TREATMENT ON PHYSICOCHEMICAL PROPERTIES OF WASTEWATER TREATMENT PLANTS IN NORTH JORDAN

Saleh Shakhatreh* and Riad Al Ott

Al Balqa' Applied University, Al Huson University College, P.O.Box 50, Al-Huson, Jordan

ABSTRACT

The magnetic field treatment of water exiting three wastewater treatment plants in north Jordan is discussed and investigated with respect to the effects it has not only on removal of scale formation ingredients from the water treated but also on a variety of its physicochemical properties. A single pass of water is performed through a reactor using moderate but varying field strengths (ranging from 0.3 to 0.9 T) and several observables of water quality, generally related to its total hardness are measured both prior and after the treatment.

KEYWORDS: Magnetic Water Treatment (MWT), Antiscale Magnetic Treatment, Magnetic Water Softening

1. INTRODUCTION

Minor ingredients of drinking water like Ca and Mg improve its quality but cause technical problems as they enhance hardness and provoke deposition of scale in evaporators and especially in boilers. Scale deposit is a common and costly problem in many industrial [1, 2] and domestic applications of water and although its major constituents are Ca and Mg carbonates, phosphates and sulfates can be also formed.. Traditional methods of removing or controlling scale use chemicals, which although effective add to cost and the chemical load on evacuated water streams after disposal. Magnetic treatment of water has been proposed in order to circumvent problems arising from the chemical treatment [3]. This is not a water softening process, since no chemical exchange or reaction takes place. There are certain drawbacks however, in the application of the magnetic treatment of water. The main ones reported in the literature include the complicated physicochemical phenomena involved and subsequently the lack of theoretical background for optimization [4].

The results of this initial study are of vital importance to Northern Jordan, where the three wastewater treatment plants tested, as shown in Figure 1, since the country ranks among the ten countries with worst water shortage supply [5] and most of its towns have to rely on groundwater for human and agricultural consumption. It is therefore of great importance to search for low cost but effective means by which to treat wastewater and make it possible to be re-used mainly for agricultural processes.

In the following study, our interest was not simply just to relate the applied magnetic field with the amount of deposited solids, but also with other properties of the treated water, which might make it possible to be used even for animal and human consumption. Therefore the main interest does not lie in the form of the deposited solids [6] but mainly on other properties of water, which undergo alterations due to the removal of scale producing ingredients.

2. MATERIALS AND METHODS

The experimental apparatus was designed to satisfy mainly the following criteria:

- recirculation solution and over control fluid flow with respect to the magnetic field orientation.
- exposure of the samples to magnetic fields of strength higher than 0.30 up to 0.90 Tesla.
- a powerful electromagnet bobbin, which can deliver up to 1.00 Tesla, is incorporated into the set-up to ensure the desired magnetic field strength. Provided with a flexible water circulating system.

A general scheme presenting the device by which the studied samples were magnetically treated is given in Figure 2.

Measurements on both untreated and magnetically treated water samples include TH (total hardness), pH, TSS (total suspended solids), TDS (total dissolved solids), VSS (volatile suspended substances), COD (chemical oxygen demand) and BOD₅ (biological oxygen demand after 5 days).

* Corresponding author

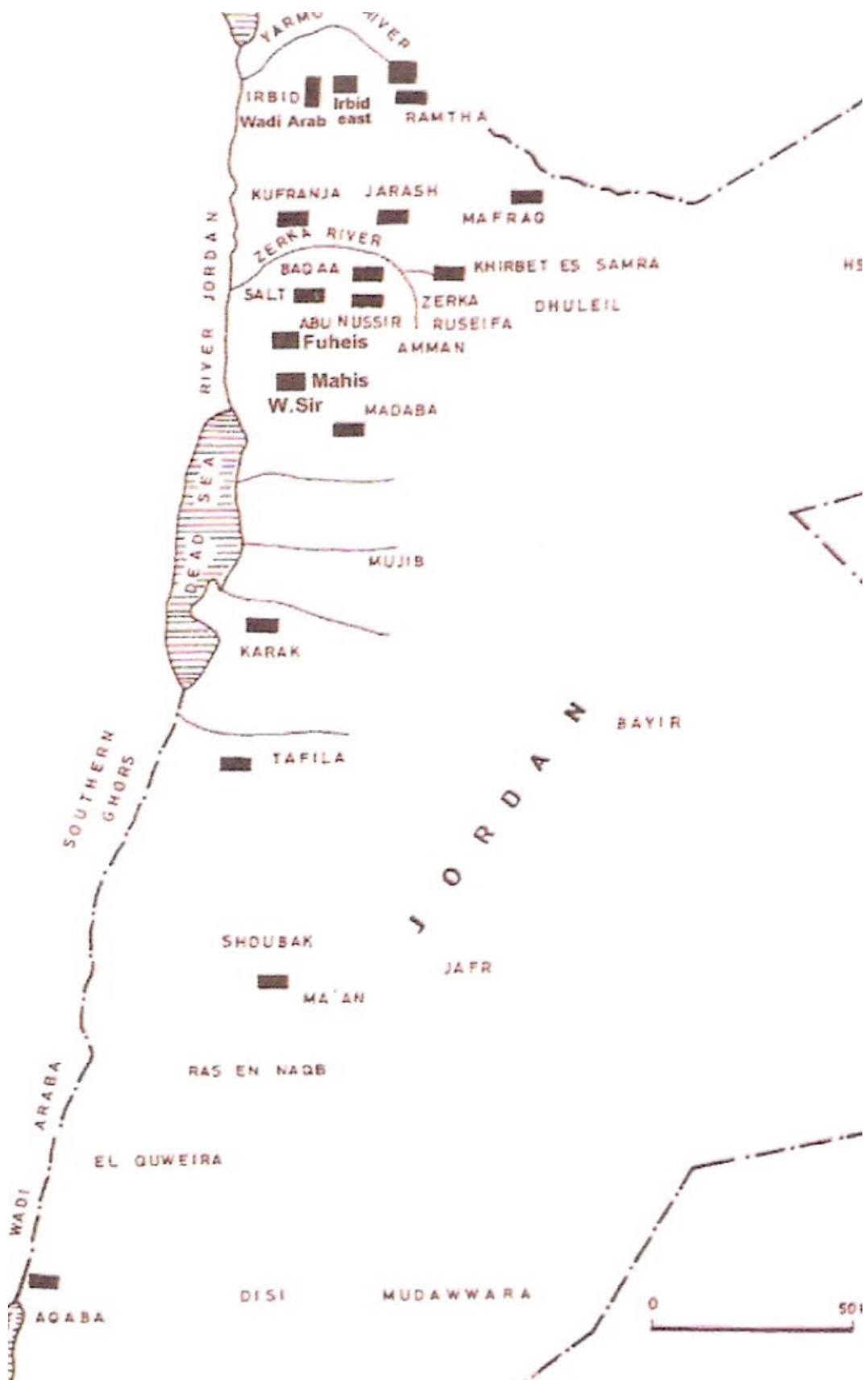


FIGURE 1 - Location of the wastewater treatment plants in Jordan.

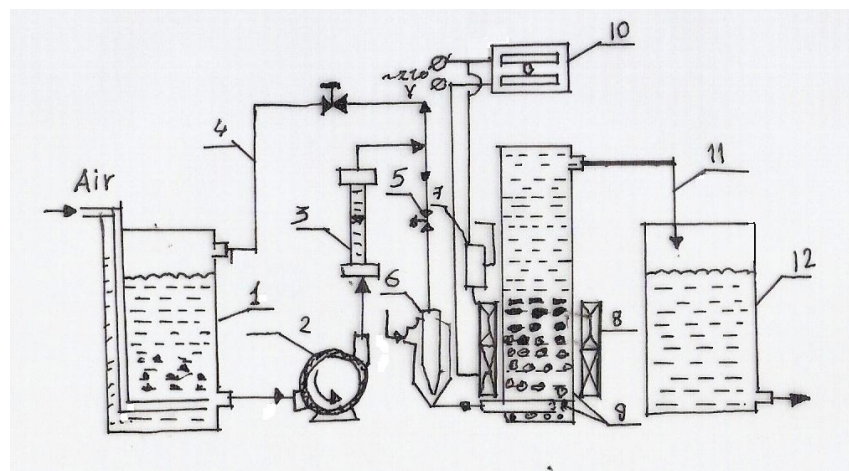


FIGURE 2 - Scheme of installation for water treatment with Magnetic Field. 1- reservoir, 2- pump, 3- flow meter, 4- recycling pipe, 5- regulating valve, 6- ejector, 7-rheostat, 8- magnetic field, 9- magnetized particles, 10- power source, 11- evacuation pipe, 12- collecting reservoir.

Total hardness is expressed as the total dissolved amount of Calcium and Magnesium and is evaluated as

$$GH = \left(\frac{Ca \text{ (mg L}^{-1})}{0,4} + \frac{Mg \text{ (mg L}^{-1})}{0,24} \right) \times 10^{-2} \text{ (mmol L}^{-1})$$

The rest of the properties are presented in the usual units.

Three samples from the outlet water streams, of three dissimilar sewage plants in Northern Jordan were taken to be treated, namely from Al-Ekeder, Hassan and Irbid sites. All the samples were circulated through the apparatus at a flow rate of 0.3 to 0.5 m³ s⁻¹ and were treated using a magnetic field with variable magnetic induction (0.3 T, 0.6 T and 0.9 T respectively).

3. RESULTS AND DISCUSSION

In the following, raw water refers to the water samples that are collected at the exit point of the corresponding water treatment plant and the values of the properties measured are listed under the appropriate columns which represent the magnetic field strength applied to the samples.

The results certainly reveal an impact of the magnetic field strength on the various properties of the water treated. We believe, however, that there is some merit in trying to discover some more firm relationships, between these functions, if there are any and in this respect we tabulated their values and treated them by least squares regression methods applying simple models as to their dependency on the field.

TABLE 1 - Results from the magnetic antiscale treatment of the water samples according to their origin. First line, Al-Ekeder plant, second line, Hassan plant, third line, Irbid plant.

Test	Raw Water	Magnetic field 0.3 T	Magnetic field 0.6 T	Magnetic field 0.9 T
pH	8.3	7.3	7.3	7.3
	8.1	7.8	7.7	7.5
	7.8	7.5	7.3	7.3
TH	813	800	790	774
	520	501	488	473
	567	560	556	547
VSS	345	339	333	329
	32	32	30	30
	32	30	28	26
TDS	1430	1420	1404	1389
	976	969	962	955
	1028	1003	992	984
TSS	407	395	377	365
	40	39	39	38
	45	41	37	36
COD	800	770	756	740
	135	134	132	130
	172	169	164	158
BOD ₅	190	178	169	153
	21	20	20	19
	34	33	32	30

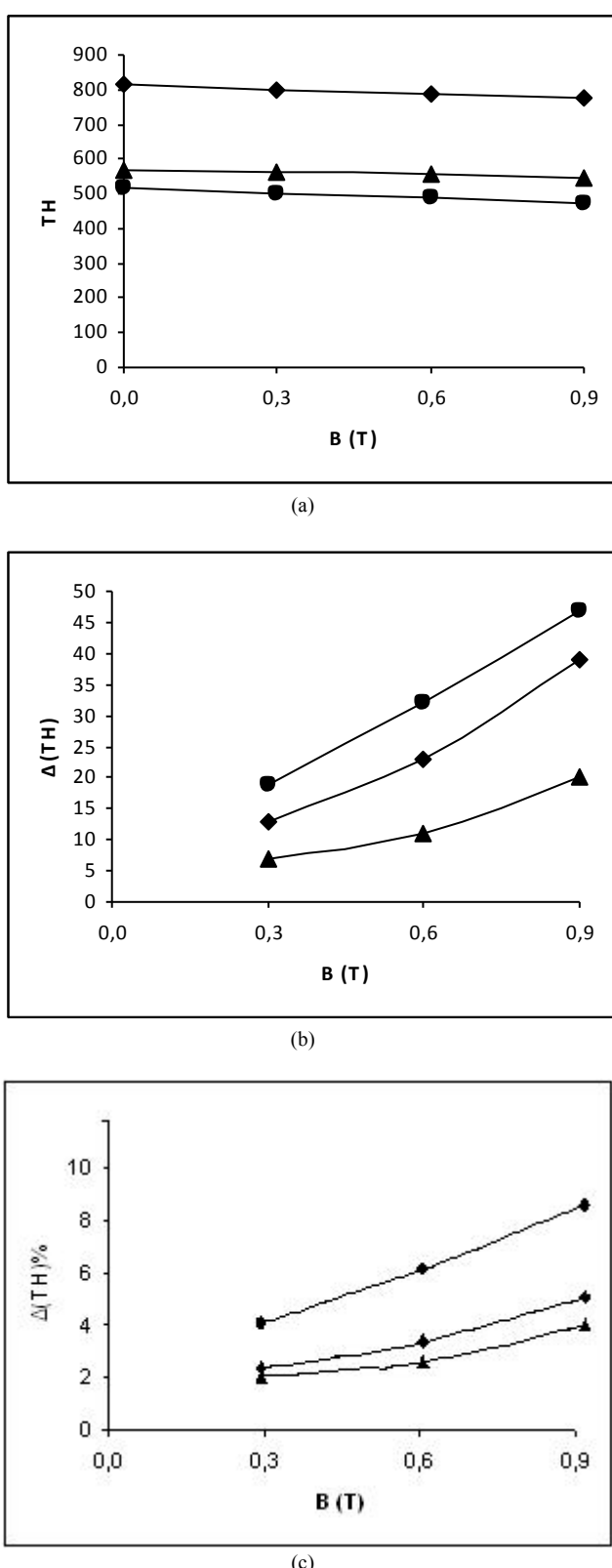


FIGURE 3 - Total hardness alteration with respect to the applied magnetic field. a) The absolute values of total hardness, b) the gradient of total hardness change ($\Delta(\text{TH})/\Delta B$) and c) the percent relative change of the measured quantity. Squares, circles and triangles represent the values obtained from the Al-Ekeder, Hassan and Irbid samples respectively.

3.1. Total hardness variation with applied magnetic field

Percent changes in the TH values range from 1% to 10% depending on the field strength although not in a linear fashion, however the absolute values of TH vary linearly with the applied field but not uniformly. The best results, viewed as the variation of the TH relative to the applied field is presented by the Hassan sample (slope of -51.3) while the worst are reported for that of Irbid (slope of -21.3). The latter also presents the least consistency as the regression of the data gives a value for R^2 equal to 0.98. The gradient of the total hardness with respect to the applied field (Fig. 3b) also give the same general indication. In the case of a free linear fitting of the data (in our case not including the 0,0 point as a point of each diagram) Irbid plant shows the smallest gradient (21.6) while the two other plants are more close in their performance (gradients calculated as 43.3 and 46.6 respectively). However, the best fit for the relative change of the total hardness appears to be an exponential one for all the samples without any solid conclusion being drawn from the form of the resulting equations.

3.2. Total suspended solids variation with applied magnetic field

The values observed are deteriorating monotonically with increasing field strength although the fields applied may be regarded as low-to-medium ones [7]. The Al-Ekeder sample behaves distinctively different from the other two samples in that the initial value is at least eight-fold higher from the nearest one and that its variation with the field strength is also very much higher than the other two samples. Besides the proximity of their initial TSS values the two other samples behave differently upon magnetic treatment, the Irbid sample being the most affected by the field strength (by a five-fold TSS slope relative to the next sample) achieving a 20% drop from its initial value at the highest field applied. The three samples behave distinctively different as far as the relative deterioration of TSS is regarded with respect to the applied field and they do not appear to be amenable to the same type of mathematical simulation. In fact Al-Ekeder and Irbid results appear to follow an exponential and those of Hassan a linear relation towards the B values and in this respect no clear conclusions can be drawn besides the obvious differentiation in the sample contents as far as the TSS constitution is concerned.

3.3. Total dissolved solids variation with applied magnetic field

Usually the sum of TSS and TDS (termed TS, i.e. total solids) corresponds well with the observed values for TH and in fact, in all our measurements the ratio of the sum of the first two over the later is almost equal to 2 (actually 2,050, ranging between 2,26 and 1,87 averages for Al-Ekeder and Irbid samples respectively). In this respect there is expectation that the TDS values will either parallel those of TH and TSS or will add to the later in order to follow the trend of the former. In fact, there is a general similarity in the obtained values in the observation

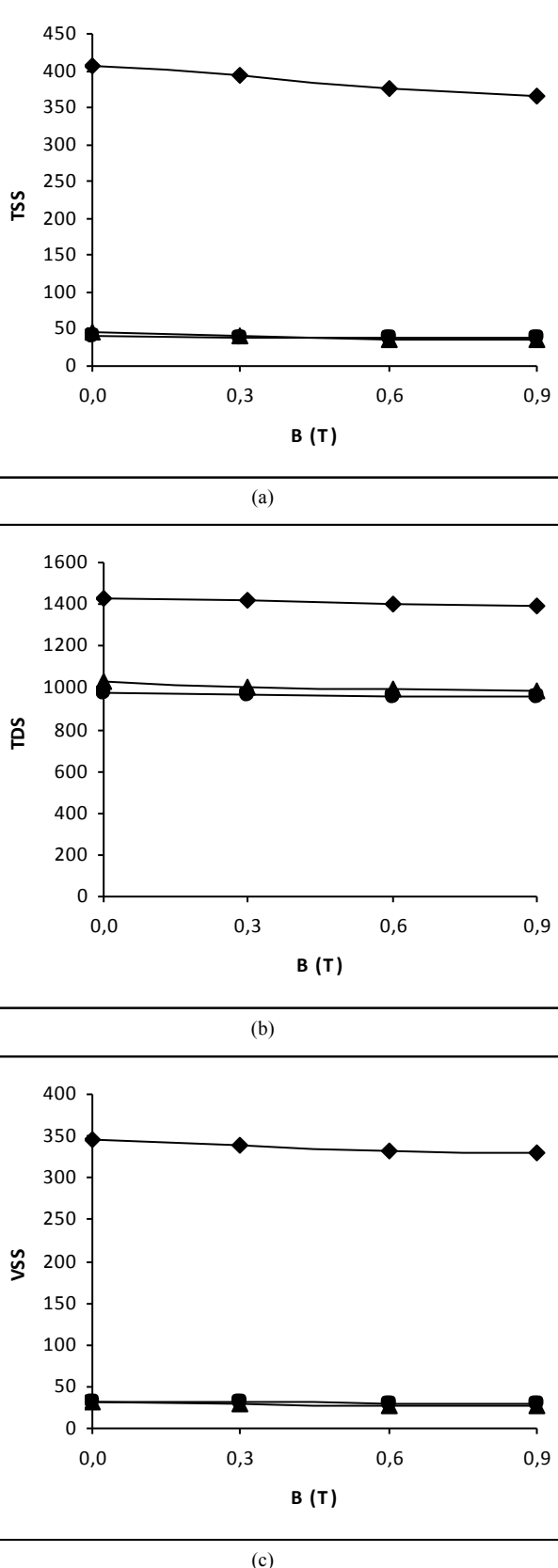


FIGURE 4 - Variation of TSS (a), TDS (b), VSS (c) with the applied magnetic field. The notation of the points in each graph is the same as in Fig. 2.

that Al-Ekeder plant shows the highest absolute values and the Irbid one is the most affected by the field action.

The effect on the TSS values on all samples is much smaller than that on the corresponding TDS (percent changes not exceeding 4.5%). Interestingly enough, the Al-Ekeder and Irbid samples appear to behave almost identically as far as the rate of deterioration with increasing magnetic field is concerned, which is double that of the third sample. Since in the TSS data presented above there is a different response of the samples to the magnetic field the conclusion drawn is that the three samples treated cannot be categorized in a single or even in two groups regarding their inorganic material content.

3.4. pH dependence on applied magnetic field

Although in several bibliographic references there is considerable effort placed on the retention of the pH within small regimes there have been studies where the pH was kept uncontrolled. During such an experiment the pH of the magnetically treated system was found to fall by 0.5 units and then towards the end of the experiment slowly to return to its original value [8]. In our study there was no attempt to control the pH, since the results in previous studies indicates that retention of pH will not make a valuable changes. Therefore there was a measurement of its value right after the magnetic treatment. There is clear indication that our results compare well with the literature and that the largest drop in the pH value is observed in the more “salty” water sample from the Al-Ekeder plant which corresponds with the massive removal of carbonates and phosphates, therefore provoking a larger impulse on the hydrolysis equilibria occurring within the sample.

It is evident from the values obtained that the field strength used has not reached a threshold value beyond which no further effect on pH is observed. In all cases, the pH values obtained are within the generally accepted limits of drinkable water.

3.5. BOD and COD changes with applied magnetic field

The values of BOD5 and COD are apparently affected by the application of magnetic field and this is certainly due to the inclusion of the corresponding organic material into the agglomerates formed upon the magnetic treatment of the water sample. BOD is affected more intensely, the largest percent change approaching 20% while the corresponding one for COD is near 9%. Once again the water sample from Al-Ekeder is different than the other two samples both in the very higher values and the higher rate of deterioration with applied field strength. However, in terms of relative value alteration the Irbid sample shows the most appreciable trend, in the case of COD even surpassing that of the most loaded sample of Al-Ekeder. These results however, cannot be directly and only related to the applied field strength as factors like the form of the deposited scale and its formation process are of key importance in the amount and form of the organic material

that will be incorporated into their sediment. Indeed,
as ex-

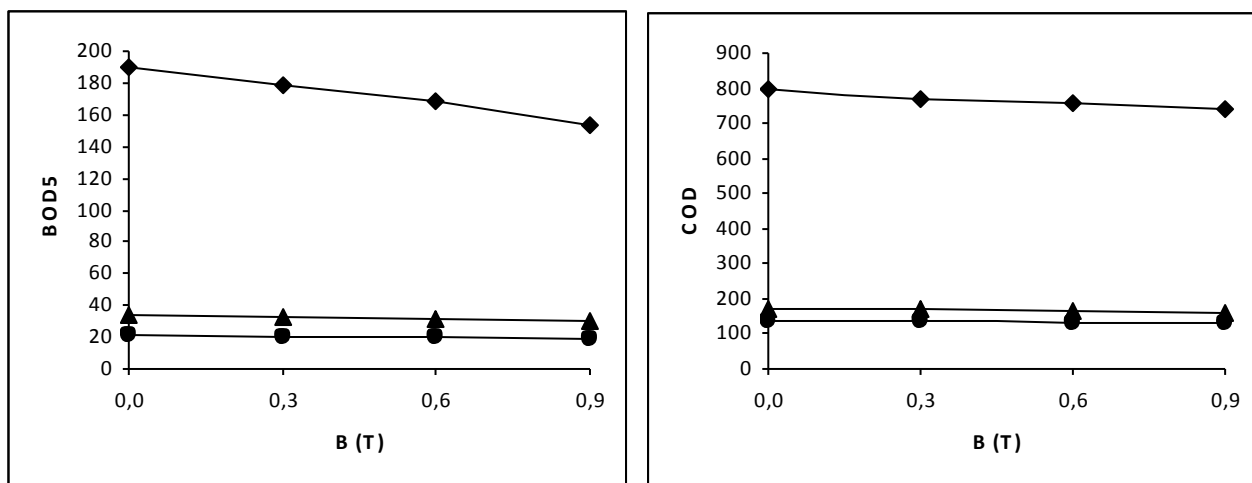


FIGURE 5 - Variation of BOD5 (a), COD (b), with the applied magnetic field. The notation of the points in each graph is the same as in the previous figures.

TABLE 2 - Correlation and linear regression between raw water and magnetic field for the three samples.

X	Y1	Y2	Y3	X*Y1	X*Y2	X*Y3	X^2	
8.3	7.3	7.3	7.3	60.59	60.59	60.59	68.89	
8.1	7.8	7.7	7.5	63.18	62.37	60.75	65.61	
7.8	7.5	7.3	7.3	58.5	56.94	56.94	60.84	
813	800	790	774	650400	642270	629262	660969	
520	501	488	473	260520	253760	245960	270400	
567	560	556	547	317520	315252	310149	321489	
345	339	333	329	116955	114885	113505	119025	
32	32	30	30	1024	960	960	1024	
32	30	28	26	960	896	832	1024	
1430	1420	1404	1389	2030600	2007720	1986270	2044900	
976	969	962	955	945744	938912	932080	952576	
1028	1003	992	984	1031084	1019776	1011552	1056784	
407	395	377	365	160765	153439	148555	165649	
40	39	39	38	1560	1560	1520	1600	
45	41	37	36	1845	1665	1620	2025	
800	770	756	740	616000	604800	592000	640000	
135	134	132	130	18090	17820	17550	18225	
172	169	164	158	29068	28208	27176	29584	
190	178	169	153	33820	32110	29070	36100	
21	20	20	19	420	420	399	441	
34	33	32	30	1122	1088	1020	1156	
7611.2	7455.6	7331.3	7198.1	6217679	6135721	6049658	6323166	SUM
362.4381	355.0286	349.1095	342.7667					AVER
B	0.986228	0.975874	0.965274					
A	-2.41799	-4.58439	-7.08526					
CORR	0.999887	0.999761	0.999531					

pected, the COD results show an appreciable linear relationship to the field both as absolute and relative values, with R^2 not below 0.997 in all cases considered.

The relation between raw water X and magnetic field was studied for the three samples. They are illustrated in the above table, where X denotes raw water, Y₁ denote magnetic field of (0.3), Y₂ denote magnetic field of (0.6), and Y₃ denote magnetic field of (0.9).

Two sides of this study namely; correlation and linear regression as follows:

A) regarding Correlation concept , it is found that :

1) corr. Coeff. between the two variables X and Y₁ $\text{Corr}(X,Y_1) = 0.9998$ that indicates a strong positive corr. between the two variables

2) $\text{Corr}(X,Y_2) = 0.9997$ means the relationship between X and Y₂ is little weaker than between X and Y₁.

3) $\text{corr}(X,Y_3) = 0.9995$

B) regarding regression concept ,there are three regression equations of Y₁ ,Y₂ and Y₃ on X,depending on the following formulas;

$$B = \sum \frac{x_i y_i - n \bar{x} \bar{y}}{x_i^2 - n \bar{x}^2}$$

Where $n = 22$, \bar{x} is the arithmetic mean of the first column (raw water) and \bar{y} is the arithmetic mean for Y_i , $i=1, 2, 3$, and $A = \bar{y} - B \bar{x}$. Which in using the general formula for regression, using the two parameters A and B ($y(\text{est.}) = A + Bx$) give the following results:

- 1) $Y_1(\text{est.}) = -2.42 + 0.986 X$
- 2) $Y_2(\text{est.}) = -4.58 + 0.975 X$
- 3) $Y_3(\text{est.}) = -7.085 + 0.965 X$

And finally the estimated error regarding any regression equation from the above will be:

$$\text{Est. error} = Y_i(\text{real}) - Y_i(\text{est.}), i = 1, 2, 3.$$

4. CONCLUSIONS

The total hardness of the treated water samples drops apparently by the applied field strength as it is expected. The hardness of the water samples studied is expected since they originate from wastewater treatment plants. The exceptionally high hardness of the Al-Ekeder samples may be directly related to the nearby solid waste and sewage dumping site which is regarded as a major contributor in the deterioration of the water quality of the Yarmuk river. Along this line lies also the dramatic difference in total suspended solids between the Al-Ekeder and the other two samples studied. The most affected sample however, appears to be the one from Irbid, since except TH reveals the largest final percentage change in the measured properties.

In view of the complexity and the non-uniformity of the samples which were not pretreated, there is no firm and straightforward relation between any two measured quantities and the magnetic field strength, however it appears that the fields used have not reached the critical point after which they provoke no effect on the treated water [9].

ACKNOWLEDGEMENT

The authors would like to acknowledge the useful suggestions of Dr. P. D. Akrivos, Aristotle University of Thessaloniki, in the course of the preparation of the present manuscript.

REFERENCES

- [1] Glater, J. York, J. L. and Campbell, K.S. (1980) Scale formation and prevention. In Principles of Desalination Part B, 2nd edn (Edited by Spiegler K. S. and Laird A. D. K.), pp. 627-678. Academic Press, New York.
- [2] Grutsch, J.F. and McClintock, J.W. (1984) Corrosion and deposit control in alkaline cooling water using magnetic water treatment at Amoco's largest refinery. Paper No. 330, Corrosion 84th National Association of Corrosion Engineers, New Orleans.
- [3] Eliassen, R. Skrinde, R.T. and Davis, W.B. (1958) Experimental performance of 'miracle' water conditioners. J. Am. Wat. Wks Assoc. 50, 1371-1385.
- [4] Baker, J.S. and Judd, S.J. (1996) Magnetic amelioration of scale formation. Wat. Res. 30, 247-260.
- [5] Scott, C.A. El-Naser, H. Hagan, R.E. and Hijazi, A. (2003) Facing water scarcity in Jordan: Reuse, demand reduction, energy, and transboundary approaches to assure future water supplies. Water Int. 28, 209-216.
- [6] Higashitani, K. Kage, A. Katamura, S. Imai, K. and Hatade, S. (1993) Effects of magnetic field on formation of CaCO_3 particles. J. Coll. Int. Sci. 156, 90-95.
- [7] Gehr, R. Zhai, Z.A. Finch, J.A. and Rao, R. (1995) Reduction of soluble mineral concentrations in CaSO_4 saturated water using a magnetic field. Wat. Res. 29, 933-940.
- [8] Parsons S.A., Wang B.-L., Judd S.J. and Stephenson T., 1997. Wat. Res. 31, 339-342.
- [9] Higashitani, K. Okuhara, K. and Hatade, S. (1992) Effects of magnetic fields on stability of nonmagnetic ultrafine colloidal particles. J. Coll. Int. Sci. 152, 125-131.

Received: January 19, 2011

Revised: March 23, 2011

Accepted: April 05, 2011

CORRESPONDING AUTHOR

Saleh K. Shakhatreh

Al Balqa' Applied University
Al Huson University College
P.O.Box 50, Al-Huson
JORDAN

Phone: 009622 7010400 int 222

Fax: 009622 7010397

E-mail: shakhatreh_s@yahoo.com

ENHANCED PHOTOCATALYTIC ACTIVITY OF AgNbO₃ DOPED WITH Fe³⁺

Hui Xu, Yuanguo Xu, Huaming Li*, Guangsong Sun, Ling Liu and Xiangyang Wu

School of the Environment, School of Chemistry and Chemical Engineering, Jiangsu University, Zhenjiang 212013, P. R. China

ABSTRACT

Fe³⁺-AgNbO₃ composites were prepared by impregnation method. The physicochemical properties of the catalysts were characterized by X-ray diffraction (XRD), field emission scanning electron microscopy (FESEM) and UV-vis diffuse reflectance spectrum (DRS). The photocatalytic activity of the samples was evaluated by photocatalytic degradation of methylene blue dye under UV light irradiation. The result revealed that the photocatalytic degradation efficiency was increased by introduction of Fe³⁺. The highest photocatalytic activity was obtained when the sample calcined at 300°C with 2 wt% Fe³⁺ under UV light irradiation with 3 h.

KEYWORDS:
Fe³⁺-AgNbO₃; Photocatalytic; Degradation

1. INTRODUCTION

In order to meet the increasingly stringent standards of environmental regulation, many techniques have been used in the environmental protection. Environmental photocatalysis is one technique that has great potential to treat organic contaminates in the environment. Recently, AgNbO₃ with a perovskite structure has been found to show photocatalytic activity for water splitting and pollutants treatment [1, 2]. However, the photocatalytic activity of AgNbO₃ generally depends on a competition between the transfer rate of surface charge carriers [3]. High recombination rate of photo-generated electron and holes can result in low efficiency and slow down the photocatalytic degradation process. In order to increase the photocatalytic activity, some methods are used. In semiconductor systems, doping semiconductor with foreign ions is one of the most promising strategies for enhancing separated rate of pairs (electron and holes) and photocatalytic activity of the catalysts.

Many ions have been used in modification TiO₂ and the other semiconductor materials, such as Fe [4], Au [5], Ag [6], Sn [7], Ni [8], Cu [9], N [10], C [11], S [12] and so on. Among many candidates, iron(III) ion seems to be the most promising due to its cost-effectiveness. Zhou et al. [13] prepared the mesoporous Fe-doped TiO₂ powders. It was indicated that a small amount of Fe³⁺ ions in TiO₂ powders could obviously enhance their photocatalytic activity. The photocatalytic activity of Fe-doped TiO₂ powders prepared by this method and calcined at 400°C exceeded that of Degussa P25 (P25) by a factor of more than two times at an optimal atomic ratio of Fe to Ti of 0.25. The high activity of the Fe-doped TiO₂ powders could be attributed to the results of the synergistic effects of Fe-doping, large BET specific surface area and small crystallite size. Naeem et al. [14] synthesized the Fe³⁺-doped and undoped TiO₂ nanoparticles. The results showed that the Fe³⁺-doped TiO₂ possessed the anatase structures. The 0.5 mol% Fe doping exhibited enhancing photocatalytic activity. Yu [15] also prepared the Fe-doped TiO₂ nanorods. The results showed that Fe-doping greatly enhanced the visible-light photocatalytic activity of mesoporous TiO₂ nanorods, and when the atomic ratio of Fe/Ti was in the range of 0.1-1.0%, the photocatalytic activity of the samples was higher than that of Degussa P25 and pure TiO₂ nanorods. At Fe=0.5%, the photocatalytic activity of Fe-TiO₂ nanorods was two times higher than that of P25. In addition, Fe-doped non-TiO₂ catalysts also showed the increasing photocatalytic activity for water splitting and pollutant degradation. Zielinska indicated that introduction of Fe could enhance the photocatalytic activity of the NaNbO₃ [16]. Fe could also increase the photocatalytic activity of the CeVO₄ [17], SrTiO₃ [18], LaCoO₃ [19], CuGa₂O₄ [20], BiVO₄ [21], and so on. Therefore, it could be inferred that loading proper Fe as co-catalysts should enhance the activity of the photocatalysts. In this work, Fe-doped AgNbO₃ powders were prepared by a simple impregnating-calcination method. The photocatalytic activity of the catalysts was evaluated by the photocatalytic oxidation of methylene blue (MB). To the best of our knowledge, this is the first time to report the preparation and photocatalytic activity of Fe-doped AgNbO₃ photocatalyst. The effect of Fe on the enhanced photocatalytic activity of the pure AgNbO₃ was also investigated.

* Corresponding author

2. MATERIALS AND METHODS

2.1. Material

All chemicals were analytical grade and used as received without purification. All chemicals were purchased from Sinopharm Chemical Reagent Co. Ltd.

2.2. Synthesis of Fe^{3+} - AgNbO_3 photocatalysts

AgNbO_3 powders were prepared by conventional solid-state reactions. Starting materials AgNO_3 and Nb_2O_5 were mixed in a stoichiometric ratio. The mixtures were calcined at 880°C for 5 h.

A suitable amount of $\text{Fe}(\text{NO}_3)_3 \cdot 9\text{H}_2\text{O}$ solution was added to the synthesized AgNbO_3 to form suspension solution of Fe^{3+} - AgNbO_3 . The suspension was stirred by using a glass rod during evaporation of water on a water bath. The dried powders were calcined at 300°C for 4 h. Then the Fe^{3+} - AgNbO_3 photocatalyst was obtained.

2.3. Photocatalysts characterization

The crystalline phases of the prepared catalysts were analyzed by X-ray diffraction (XRD) by Bruker D8 diffractometer with $\text{Cu K}\alpha$ radiation ($\lambda=1.5418 \text{ \AA}$) in the range of $2\theta=10\text{--}80^\circ$. The morphology and particle size of the powders were obtained by field-emission microscope (S-4800IIFESEM, Hitachi, Japan). The chemical composition of the samples was determined by X-ray energy dispersion spectrum (EDS) attached to the SEM. The diffuse reflectance spectra (DRS) was performed on a UV-2450 (Shimadzu) instrument in the range of 240 nm to 800 nm. BaSO_4 was used as the reflectance standard material.

2.4. Photocatalytic activity

The photocatalytic activity of Fe^{3+} - AgNbO_3 composites was evaluated by degradation of MB dye. Experiments were carried out in Pyrex photocatalytic reactor with two 125 W mercury lamps as UV source. 100 mg of Fe^{3+} - AgNbO_3 was added to a 100 mL solution containing the MB dye (10 mg/L) solution. Prior to UV illumination, the suspension was strongly magnetically stirred for 30 min in the dark for adsorption/desorption equilibrium between the photocatalyst and the MB dye. The photocatalytic degradation efficiency (E) of MB was calculated by formula: $E = \frac{C_0 - C}{C_0} \times 100\% = \frac{A_0 - A}{A_0} \times 100\%$, where C_0

$$E = \frac{C_0 - C}{C_0} \times 100\% = \frac{A_0 - A}{A_0} \times 100\%, \text{ where } C_0$$

was the adsorption equilibrium concentration of MB, C was the concentration of MB solution at time t, and A_0 and A were the corresponding values for the absorbance. The absorbance of MB was determined by spectrophotometer at 664 nm.

3. RESULTS AND DISCUSSION

3.1. XRD analysis

Fig. 1A showed the XRD patterns of materials calcined at 300°C with different Fe contents. It was found that the

XRD patterns of all the Fe^{3+} - AgNbO_3 catalysts were almost similar to that of pure AgNbO_3 (JCPDS files: 52-0405), indicating that there was no change in the crystal structure after Fe loading. However, no diffraction peaks of iron oxides appeared when the samples were calcined at 300°C, which might be because the content of iron oxides was below the detection limit of XRD analysis. This also indicated that Fe^{3+} was uniformly dispersed on AgNbO_3 particles.

The XRD spectra of the series catalysts under different calcination temperature were shown in Fig. 1B. It was indicated that there was no observation of iron oxides phase. All the catalysts calcined at various temperatures were present in AgNbO_3 standard structure.

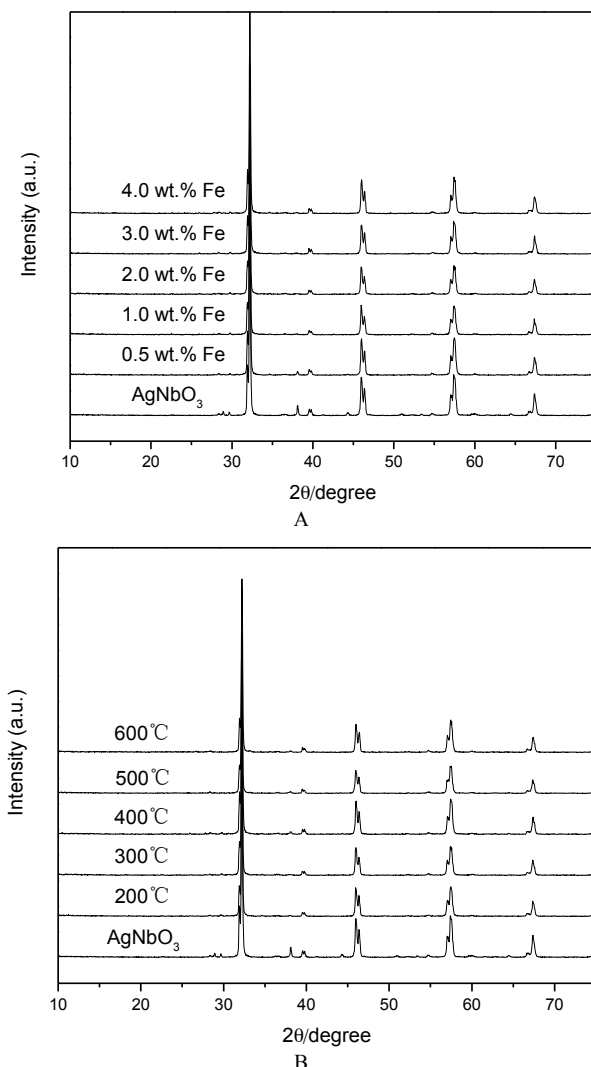


FIGURE 1 - XRD of Fe^{3+} - AgNbO_3 with (A) different contents of Fe loading (B) different calcination temperature.

3.2. Scanning electron microscopy and EDS analysis

SEM images of the synthesized pure AgNbO_3 and Fe^{3+} - AgNbO_3 photocatalyst were shown in Fig. 2. It could be seen that the size distribution of the neat AgNbO_3 var-

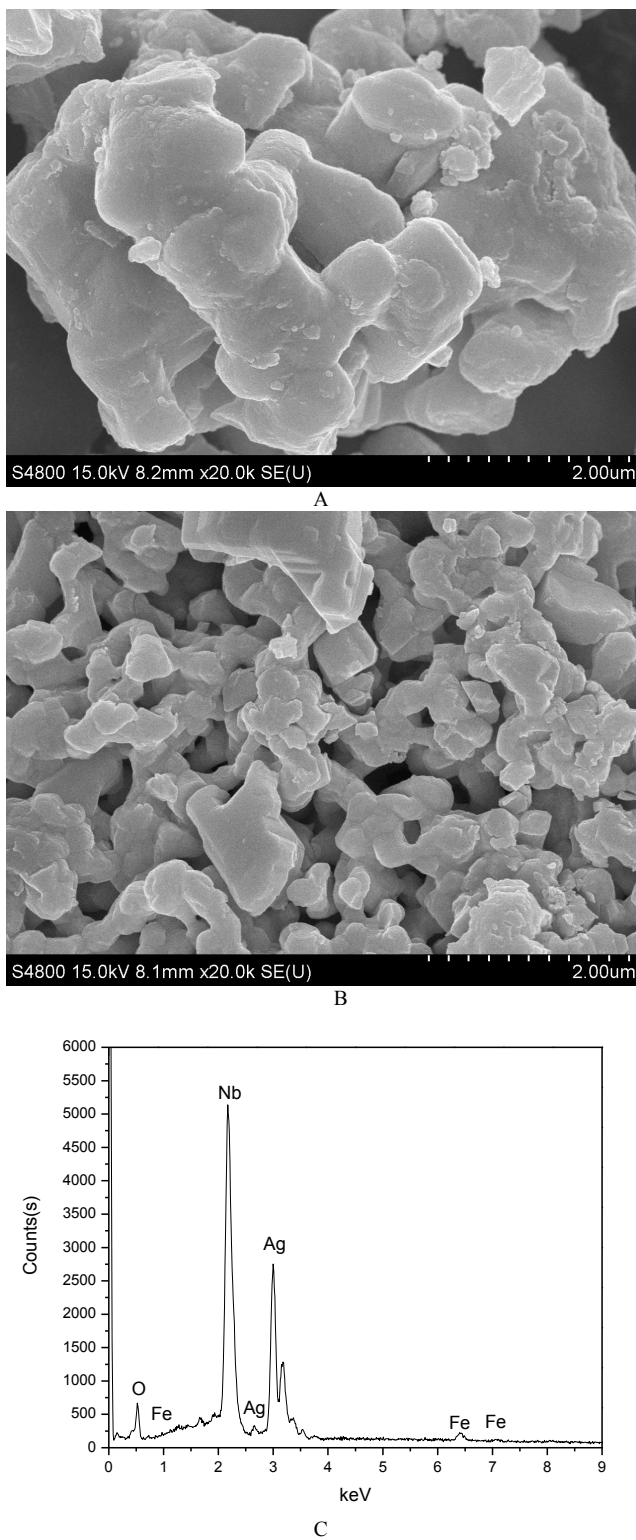


FIGURE 2 - SEM image of Fe^{3+} - AgNbO_3 (A), AgNbO_3 (B) and (C) EDS image of Fe^{3+} - AgNbO_3 .

ied in the range of 0.5–2.5 μm (Fig. 2B). It was found that the morphology of Fe^{3+} - AgNbO_3 was different from the pure AgNbO_3 (Fig. 2A). The Fe^{3+} - AgNbO_3 particles were bigger than the pure AgNbO_3 . In Fig. 2A, there were many small particles covered on the face of the pure AgNbO_3 ,

which were speculated to be iron oxides. According to the results of the EDS analysis (Fig. 2C), iron ions were present in the Fe^{3+} - AgNbO_3 sample.

3.3. DRS analysis

For photocatalysis application, UV-visible light absorption property is very important. Fig. 3 showed the DRS of different samples. The pure AgNbO_3 showed absorption band from UV to 450 nm. Fe^{3+} - AgNbO_3 samples showed some differences with pure AgNbO_3 . It could be seen that the Fe doping had greatly changed the light absorption of the photocatalyst. In the wavelength range of 400–800 nm, the reflectance of Fe^{3+} - AgNbO_3 samples was lower than that of pure AgNbO_3 . However, in the ultraviolet region, it was not obvious because of the very high absorption of ultraviolet light for the pure AgNbO_3 . It was also indicated that with the increasing Fe content, the visible absorption of the Fe^{3+} - AgNbO_3 photocatalysts enhanced, which could be beneficial to increase photocatalytic activity.

By plotting $(Ahv)^2$ versus hv , in which A and hv was the absorption coefficient and photons' energy, respectively. The band gap energies of pure AgNbO_3 and Fe^{3+} - AgNbO_3 with different Fe content were calculated to be 2.86, 2.75, 2.72, 1.85, 1.89 and 2.65 eV, respectively (Fe content: 0–4 wt%). This result indicated that Fe^{3+} loading could narrow the band gap of the catalysts.

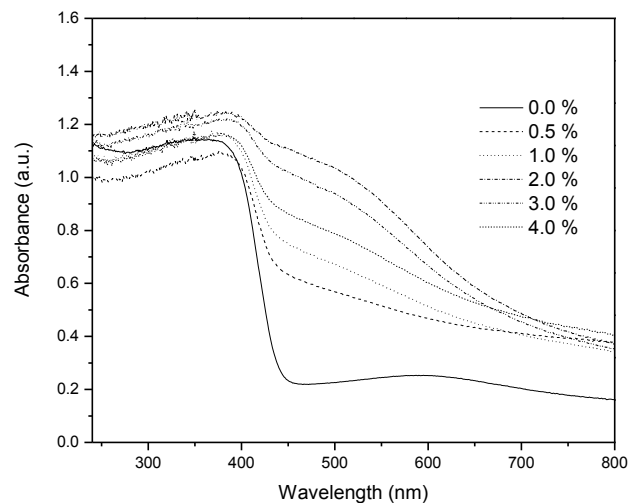


FIGURE 3 - DRS of Fe^{3+} - AgNbO_3 with different content of Fe loading.

3.4. Photocatalytic activity

The effect of loading Fe on the photocatalytic activity of AgNbO_3 was evaluated by measuring the degradation of MB in an aqueous solution under UV light irradiation. Fig. 4 showed the photocatalytic activity of different Fe content catalysts. It was found that the photocatalytic reactivity increased with the increasing amounts of Fe. The optimum Fe content was found to be 2 wt%. However, after reaching the maximum value, the activity of the photocatalysts decreased by further loading of Fe ions. These results showed that the activity of the Fe loading photocatalysts strongly depended on the contents of Fe.

From Fig. 4, it could be seen that the photocatalytic degradation efficiency of MB by the pure AgNbO_3 was 50% for 3 h. For the 2 wt% Fe^{3+} - AgNbO_3 , the photocatalytic degradation efficiency of MB after 3 h irradiation was 86%. When the Fe content was increased at 4 wt%, the efficiency was only 65%. The excess Fe (>2 wt%) covering on the surface of AgNbO_3 could increase the number of recombination centers, thus decreased photocatalytic activity.

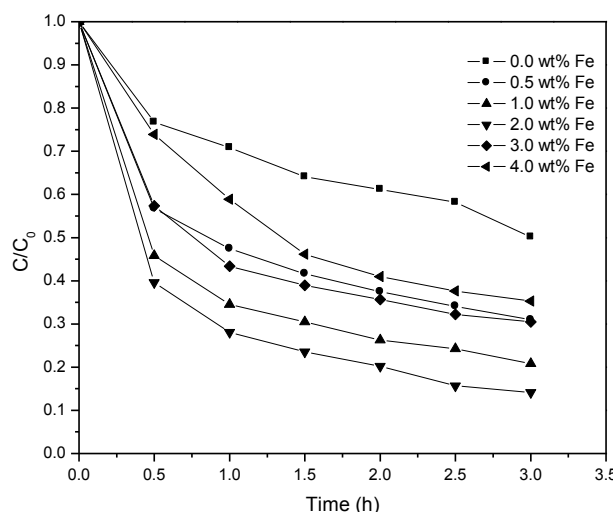


FIGURE 4 - Effect of the different Fe content on MB photocatalytic degradation efficiency.

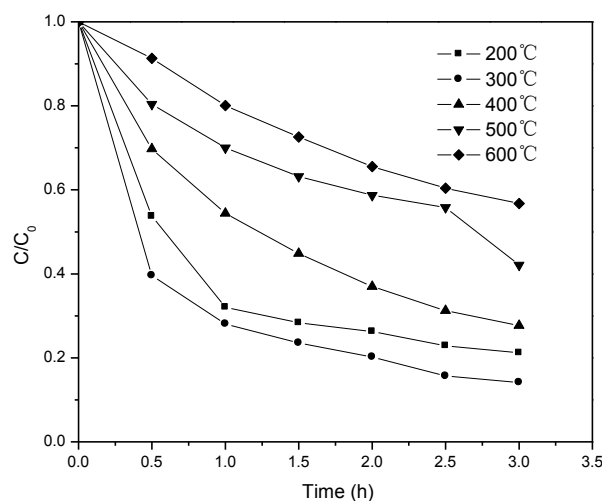


FIGURE 5 - Effect of the different calcination temperature on MB photocatalytic degradation efficiency.

The relationship between the photocatalytic activity of Fe^{3+} - AgNbO_3 composites and calcination temperature were shown in Fig. 5. It was indicated that the photocatalytic degradation efficiency decreased with the increasing calcination temperature. With increase the calcination temperature, the $\text{Fe}(\text{NO}_3)_3$ could decompose into iron oxides, and the crystallinity of iron oxides could increased with increasing temperatures. The highly crystallized structure

could favor migration of electron-hole pairs, so as to high photocatalytic activity. However, at higher calcination temperatures (>300°C), the iron oxides would agglomerate into large bulk. The large particles with low activity species would decrease photocatalytic activity. Therefore, it could conclude that the 2 wt% Fe^{3+} - AgNbO_3 calcined at 300°C had the highest activity under UV illumination.

Fig. 6 showed temporal evolution of the spectral changes during photocatalytic degradation of MB over AgNbO_3 and Fe^{3+} - AgNbO_3 with Fe concentration of 2 wt%. From Fig. 6B, it could be seen that the intensity of the absorption peak at 664 nm decreased drastically in the 3 h of UV irradiation, which indicated that Fe^{3+} - AgNbO_3 catalyst exhibited high photocatalytic activity. However, Fig. 9A showed that the comparing test confirmed that MB could only be slightly degraded by AgNbO_3 catalysts. It was indicated that the Fe^{3+} - AgNbO_3 catalyst showed higher photocatalytic activity than the pure AgNbO_3 .

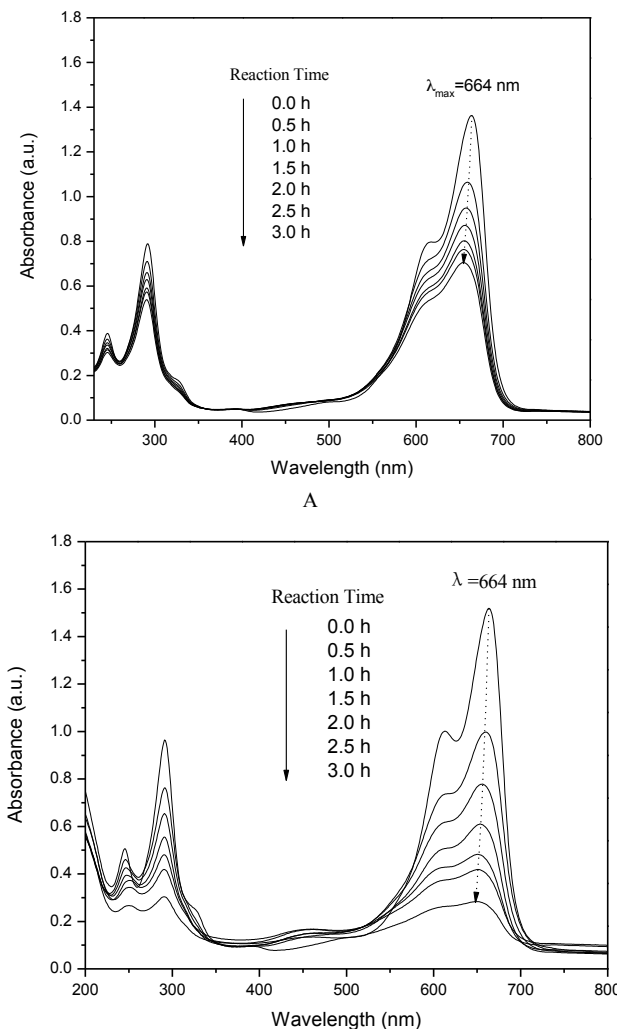


FIGURE 6 - Absorption spectral changes of MB under UV light irradiation: (A) AgNbO_3 as photocatalyst (B) Fe^{3+} - AgNbO_3 as photocatalyst.

4. CONCLUSIONS

In this study, Fe^{3+} -modified AgNbO_3 photocatalysts were prepared by impregnation method and used for the photocatalytic oxidization of MB. The Fe^{3+} - AgNbO_3 (2 wt%) calcined at 300°C showed the highest activity under UV illumination. The presence of the Fe on the AgNbO_3 could accept the photogenerated electrons, and then electrons and holes were efficiently separated, which lead to the improvement of photocatalytic activity.

ACKNOWLEDGMENT

The authors genuinely appreciate the financial support of this work from the the National Nature Science Foundation of China (No. 21007021 and 21076099) and Research Foundation of Jiangsu University (10JDG128), Society Development Fund of Zhenjiang (SH2010006), Agricultural Science and Technology Fund of Zhenjiang (NY2010030) and Doctoral Innovation Fund of Jiangsu (CX10B-275Z).

REFERENCES

- [1] Kudo, A. (2006) Development of photocatalyst materials for water splitting. *Int. J. Hydrogen Energy*, **31**, 197-202.
- [2] Kato, H., Kobayashi, H. and Kudo, A. (2002) Role of Ag^+ in the Band Structures and Photocatalytic Properties of AgMO_3 (M: Ta and Nb) with the Perovskite Structure. *J. Phys. Chem. B*, **106**, 12441-12447.
- [3] Li, G., Kako, T., Wang, D., Zou, Z. and Ye, J. (2009) Enhanced Photocatalytic Activity of La-doped AgNbO_3 under Visible Light Irradiation. *Dalton Trans.*, 2423-2427.
- [4] Nemmar, A., Melghit, K., Al-Salam, S., Zia, S., Dhanasekaran, S., Attoub, S., Al-Amri, I. and Ali, B. H. (2011) Acute respiratory and systemic toxicity of pulmonary exposure to rutile Fe-doped TiO_2 nanorods. *Toxicology*, **279**, 167-175.
- [5] Kumar, P. S. S., Sivakumar, R., Anandan, S., Madhavan, J., Maruthamuthu, P. and Ashokkumar, M. (2008) Photocatalytic degradation of Acid Red 88 using Au- TiO_2 nanoparticles in aqueous solutions. *Water Res.*, **42**, 4878-4884.
- [6] Wu, C. D., Xu, H., Li, H. M., Chu, J. Y., Yan, Y. S. and Li, C. S. (2007) Photocatalytic decolorization of methylene blue via Ag-deposited BiVO_4 under UV-light irradiation. *Fresen. Environ. Bull.*, **16**, 242-246.
- [7] Li, X., Xiong, R. and Wei, G. (2009) Preparation and photocatalytic activity of nanoglued Sn-doped TiO_2 . *J. Hazard. Mater.*, **164**, 587-591.
- [8] Wu, T., Yan, Q. and Wan, H. (2005) Partial oxidation of methane to hydrogen and carbon monoxide over a Ni/TiO_2 catalyst. *J. Mol. Catal. A: Chem.*, **226**, 41-48.
- [9] Sun, J., Chen, G., Li, Y., Zhou, C. and Zhang, H. (2011) A novel photocatalyst and improvement of photocatalytic properties by Cu doping. *J. Alloy. Compd.*, **509**, 1133-1137.
- [10] Bangkedphol, S., Keenan, H. E., Davidson, C. M., Sakultantima, A., Sirisaksoontorn, W. and Songsasen, A. (2010) Enhancement of tributyltin degradation under natural light by N-doped TiO_2 photocatalyst. *J. Hazard. Mater.*, **184**, 533-537.
- [11] Chang, C. P. and Lin, Y. C. (2009) Enhancement Effect of double-layer TiO_2 /activated carbon film for the photocatalytic oxidation of gaseous acetone. *Fresen. Environ. Bull.*, **18**, 968-974.
- [12] Li, H., Zhang, X., Huo, Y. and Zhu, J. (2007) Supercritical Preparation of a Highly Active S-Doped TiO_2 Photocatalyst for Methylen Blue Mineralization. *Environ. Sci. Technol.*, **41**, 4410-4414.
- [13] Zhou, M., Yu, J. and Cheng, B. (2006) Effects of Fe-doping on the photocatalytic activity of mesoporous TiO_2 powders prepared by an ultrasonic method. *J. Hazard. Mater.*, **137**, 1838-1847.
- [14] Naeem, K. and Ouyang, F. (2010) Preparation of Fe^{3+} -doped TiO_2 nano particles and its photocatalytic activity under UV light. *Physica B*, **405**, 221-226.
- [15] Yu, J., Xiang, Q. and Zhou, M. (2009) Preparation, characterization and visible-light-driven photocatalytic activity of Fe-doped titania nanorods and first-principles study for electronic structures. *Appl. Catal. B: Environ.*, **90**, 595-602.
- [16] Zielinska, B., Borowiak-Palen, E. and Kalenczuk, R. J. (2011) Preparation, characterization and photocatalytic activity of metal-loaded NaNbO_3 . *J. Phy. Chem. Solids*, **72**, 117-123.
- [17] Deshpande, P. A. and Madras, G. (2010) Photocatalytic degradation of phenol by base metal-substituted orthovanadates. *Chem. Eng. J.*, **161**, 136-145.
- [18] Puangpetch, T., Srerethawong, T. and Chavadej, S. (2010) Hydrogen production over metal-loaded mesoporous-assembled SrTiO_3 nanocrystal photocatalysts: Effects of metal type and loading. *Int. J. Hydrogen Energy*, **35**, 6531-6540.
- [19] Jia, L., Li, J. and Fang, W. (2009) Enhanced visible-light active C and Fe co-doped LaCoO_3 for reduction of carbon dioxide. *Catal. Commun.*, **11**, 87-90.
- [20] Gurunathan, K., Baeg, J. O., Lee, S. M., Subramanian, E., Moon, S. J. and Kong, K. (2008) Visible light active pristine and Fe^{3+} -doped CuGa_2O_4 spinel photocatalysts for solar hydrogen production. *Int. J. Hydrogen Energy*, **33**, 2646-2652.
- [21] Xu, H., Li, H., Wu, C., Chu, J., Yan, Y. and Shu, H. (2008) Preparation, characterization and photocatalytic activity of transition metal-loaded BiVO_4 . *Mater. Sci. Eng. B*, **147**, 52-56.

Received: January 24, 2011

Revised: February 28, 2011

Accepted: April 05, 2011

CORRESPONDING AUTHOR

Huaming Li

School of the Environment

School of Chemistry and Chemical Engineering

Jiangsu University

Zhenjiang 212013

P. R. CHINA

Phone: +86-511-88791800

Fax: +86-511-88791708

E-mail: lihm@ujs.edu.cn

CRITICAL EVALUATION OF THE NATIONAL ALLOCATION PLANS UNDER THE EUROPEAN UNION EMISSION TRADING SCHEME. CASE STUDY GREECE

John K. Kaldellis*, Dimitris Zafirakis and Nikolaos Mantelis

Lab of Soft Energy Applications & Environmental Protection, TEI of Piraeus, P.O. Box 41046, Athens 12201, Greece

ABSTRACT

Since the operation of the EU Emission Trading Scheme (ETS) in 2005, a number of industrial and energy sector installations that are according to the 2003/87/EC Directive exceeding given capacity limits are liable to a certain set of rules concerning abatement of climate change. As a result, greenhouse gas (GHG) emission allowances were distributed for each liable installation on the basis of national allocation plans (NAPs), issued during the first stage of the ETS (2005-2007), while during the time the second stage of the ETS is in force (2008-2012), based on the application of updated NAPs. In this context, a critical review is currently undertaken concerning the implementation of the first and the second NAP in Greece, emphasizing on the performance of the three main polluting sectors (i.e. energy, cement and refineries). For this purpose, verified emission data of the first ETS stage is collected at the installation level and a comparison is performed with the allowances provided during both the first and the second stage of the ETS. Finally, based on the quantified determination of performance at the installation level through the estimation of emission factors, implications of the NAPs' implementation in Greece are analyzed in view of the country's current economic state.

KEYWORDS: carbon dioxide emissions; industrial sector; electricity generation; cement industry; refineries.

1. INTRODUCTION

Since ratifying the Kyoto Protocol in May 2002, Greece committed to restrict its greenhouse gas (GHG) emissions by the year 2010 to the levels of +25% in comparison with

the respective emission production of the base year 1990. In this context, according to the latest official data announced by the Greek Ministry of the Environment, Physical Planning and Public Works [1] for the years 1990-2008 (see also Figure 1), the relative increase of national GHG emissions for 2008 is found only marginally lower than the respective +25% limit (~23%), while the total amount of emissions reaches approximately 127Mt of CO₂-eq. Throughout this period, contribution of the energy sector is found to be clearly the catalyst with a long-term average of 78% contribution, followed by the industry and the agriculture sectors with 10% and 9% long-term average contribution respectively. On top of that, since the year 2005, industrial and energy sector installations that are according to the 2003/87/EC Directive exceeding given capacity limits are liable to the EU Emission Trading Scheme (ETS) and the implementation of National Allocation Plans (NAPs), according to which liable installations are obliged to comply with certain emission allowances provided.

At the same time, the Greek gross domestic product (GDP) composition [2], as a reflection of the local economy state, is mainly based on the services' sector (78.5% contribution), with the industrial and agricultural sectors representing 17.6% and 4% respectively. In this context, despite the fact that the national energy intensity presents a constant reduction [3] since the end of the '90s (see also Figure 2), the respective primary energy consumption constantly increases [3]. Considering this, a trend towards the gradual abandonment of energy intensive activities such as industrial ones [4] (although considerable reduction of energy intensity has been encountered in the Greek industrial sector as well [5], mainly deriving from the implementation of more efficient energy consumption strategies such as adoption of CHP units [6]) and the dominance of the services' sector approximating 80% of the GDP may be reflected. Besides, the conclusion drawn above is further established by the data of Figure 3, where the time evolution of the relative national industry production is depicted for the period between 2005 and 2010 [7]. As one may see, a reduction of approximately 15% may be recorded for the last two years of the period, coinciding with the period of economic recession for Greece [8].

* Corresponding author

Time Evolution of GHG Emissions in Greece (1990-2008)

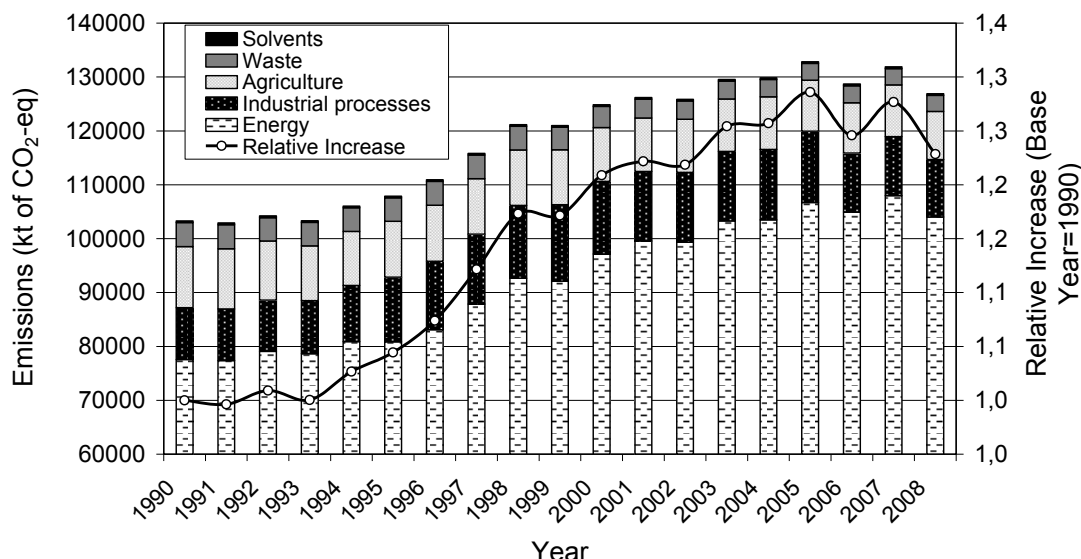


FIGURE 1 - Time evolution of GHG emissions in Greece and relative increase in relation to the base year 1990

Time Evolution of Energy Intensity Vs Primary Energy Consumption in Greece (1990-2008)

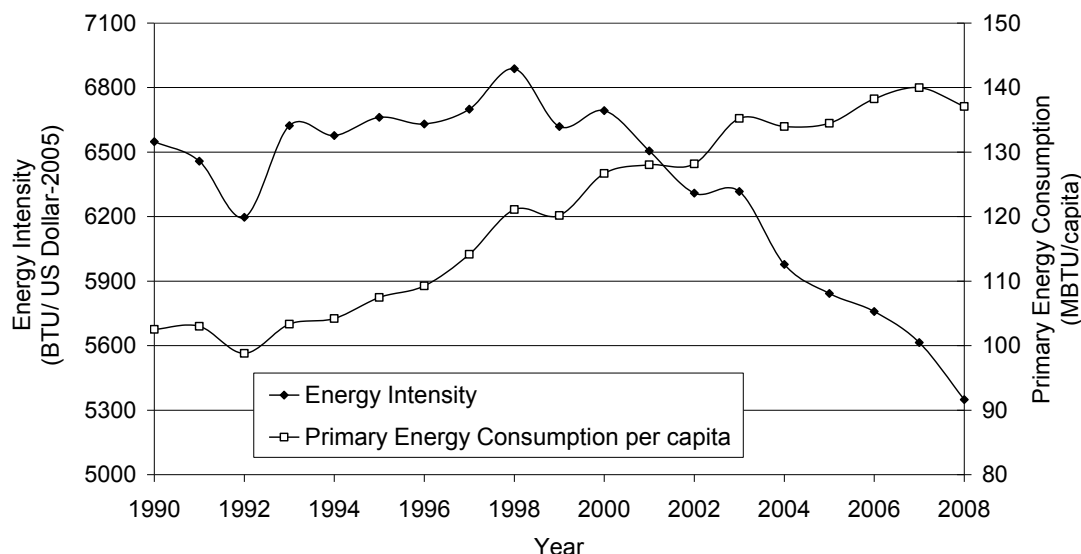


FIGURE 2 - Time evolution of energy intensity and primary energy consumption per capita in Greece

Considering the state of the local economy as well as the national obligations to maintain GHG emissions below a certain ceiling, a critical review of the first stage of the ETS implementation along with an evaluation of the second stage allowances are currently provided for Greece, in the context of giving some policy directions that may both safeguard the local industry and establish the grounds for the revival of the national economy.

2. MATERIALS AND METHODS

2.1. Implementation of NAPs in Greece

As already mentioned, since the operation of the EU ETS in 2005, a number of industrial and energy sector installations that are according to the 2003/87/EC Directive exceeding given capacity limits are liable to a certain set of rules concerning abatement of climate change, i.e.:

- Determination of allowances for the emissions of these liable to the ETS installations is a priori allocated on the basis of certain considerations
- Number of allowances decided has to be lower than the emissions that these installations would produce if the ETS was not applied, so that emission reduction can be ensured
- During the first (2005-7) and the second (2008-12) implementation periods, trading of the allowances is limited only to CO₂ and to installations that as mentioned before are found to exceed certain capacity limits, although in the future the system shall include both other gases (such as perfluorocarbons and nitrous oxide) and polluting installations (Directive 2009/29/EC)
- Distribution of the emission allowances for each participating Member State is performed in accordance with the respective NAP, which following the stage of consultation needs to be completed before the beginning of the trading period
- Enforcement of a strict monitoring framework for the participating installations, so as to ensure satisfaction of targets set or provision of substantial fines in case of non-compliance (i.e. installations fail to both reduce their emissions under the allowances provided by the NAP and buy the allowances required in case of excess)
- Transactions of allowances have to be recorded in both national and interconnected community-wide registries.

In this context, the first NAP of Greece (first published in December 2004 and then amended in April 2005), basing its determination of allowances on the predictions of

the business as usual (BaU) scenario during the time (using historical data of the 2000-2003 period), called for the reduction of emissions for the period 2005-7 by 2.1% in comparison with the respective expected emission production [9]. More specifically, the first NAP requested the reduction of CO₂ emissions by 1.9MtCO₂ in 2005, 3MtCO₂ in 2006 and 4.4MtCO₂ in 2007, while the number of Greek installations under the ETS for the specific period amounted to 141. Moreover, allocation of allowances was first distributed at the sector level and secondly at the level of installations, with the electricity generation sector concentrating a total of 156,194kt for the 3-year period (or 52,064kt/year) out of the entire assigned amount of approximately 213.4Mt (see also Figure 4). On the other hand, the cement industries were provided with a total of more than 33Mt while the refineries' sector concentrated a total of more than 10Mt for the entire first stage. Finally, for the rest of industrial plants, allowances of approximately 7Mt/year should be taken into account.

Subsequently, according to the official information concerning the implementation of the second NAP [10] during the period 2008-2012, a total amount of almost 347MtCO₂ for the entire second stage of the ETS should be considered (see also Figure 5). The total number of liable installations during this second stage has increased to 150, while as it accrues (see also Figure 6), stricter allowances have been imposed in most of the sectors, excluding refineries, sintering, lime and ceramics (see also Figure 6). In this context, the greatest reduction is faced by the sector of glass, owed however to the reduction of liable installations from three to one. Less considerable reduction is encountered in the sectors of paper and electricity generation (in the order of 5%), while the greatest reduction per liable installation concerns the sector of other combustion plants, owed to the increase of the liable installations' number.

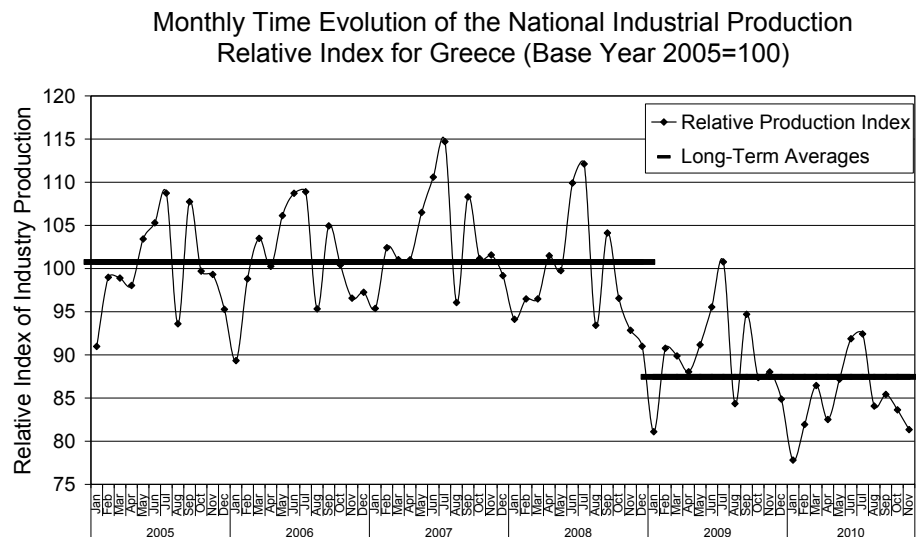


FIGURE 3 - Time evolution of industry production in Greece

Distribution of CO₂ Allowances by Sector for the 1st NAP
Period in Greece (a total of 213.4 MtCO₂-eq)

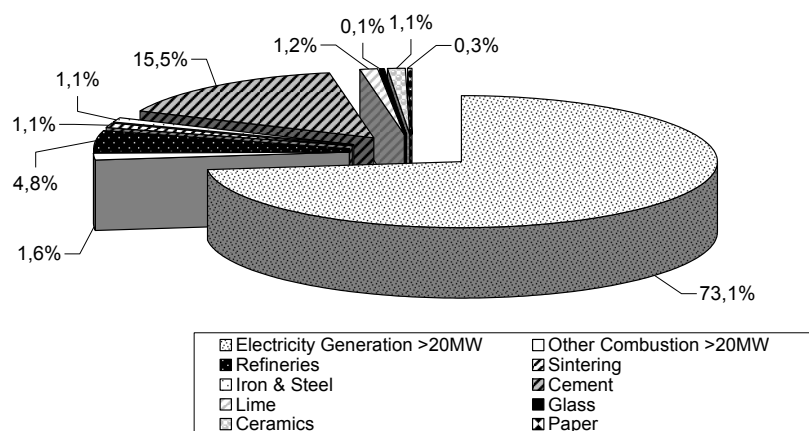


FIGURE 4 - Distribution of allowances by sector for the first period of the NAP

Distribution of CO₂ Allowances by Sector for the 2nd NAP
Period in Greece (a total of 346.73 MtCO₂-eq)

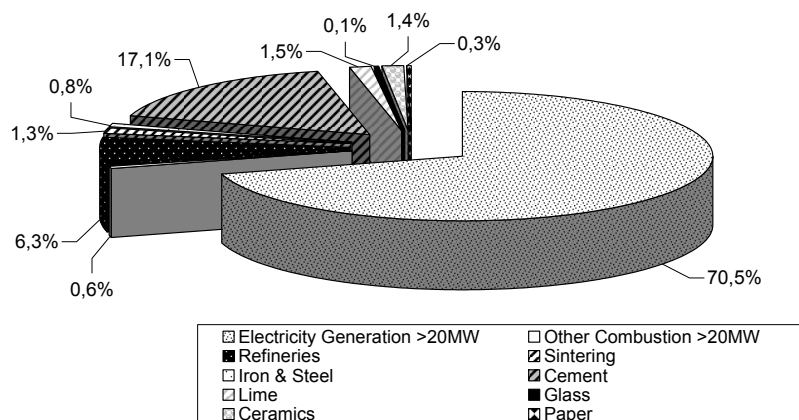


FIGURE 5 - Distribution of allowances by sector for the second period of the NAP

Annual Change in the Allocation of Allowances per Sector
between the 1st and the 2nd Period of the ETS in Greece

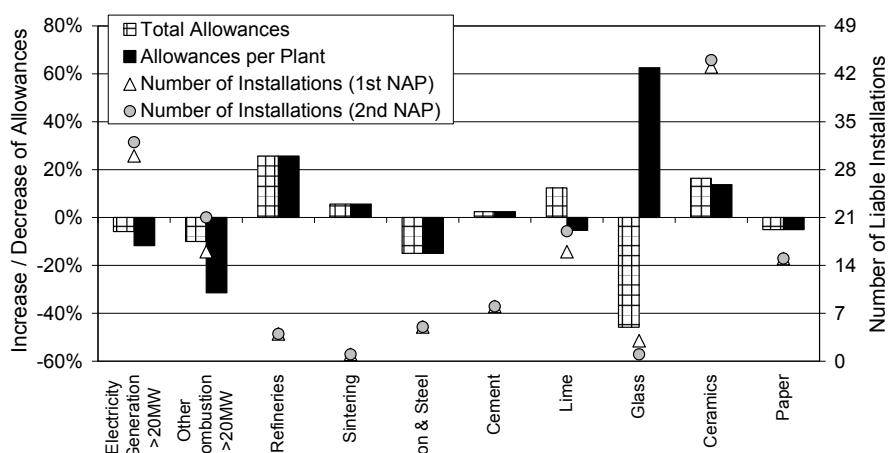


FIGURE 6 - Comparison between NAP allowances for the first and the second period by sector

Similar to the methodology of the allowances' allocation adopted in the first NAP, the BaU scenario of emission's production for the 2008-12 period was based on the exploitation of historical data that in the specific case dated back to the period between 2000 and 2004 (the second NAP was published in the September of 2006), and thus verified emissions for the first NAP period obtained in the meantime were not used during the determination of the 2008-12 allowances. Considering the above, in order to properly evaluate both the performance of liable installations and the allowances provided by the two NAPs, comparison of allowances with the respective verified emission data concerning the 2005-2007 period (not taken into account during the configuration of the second NAP) along with the estimation of emission factors for the liable installations are thought to be necessary.

3. RESULTS AND DISCUSSION

3.1. Performance of Greek installations during the first NAP

Acknowledging the need to evaluate both the distribution of allowances provided by the first and the second NAP as well as the performance of participating installations, verified emissions for the first period of the ETS are currently gathered for all liable Greek installations [11]. In this context, in Figure 7 one may obtain a comparison between the allowances provided during both stages and the verified emissions of the first period at the sector level, with emphasis given on the sectors of electricity generation, cement and refineries. Based on the results obtained, considerable violation for the first NAP period may be recorded for the sector of refineries (~16.5% or 670ktCO₂ per year), followed by electricity generation plants with a

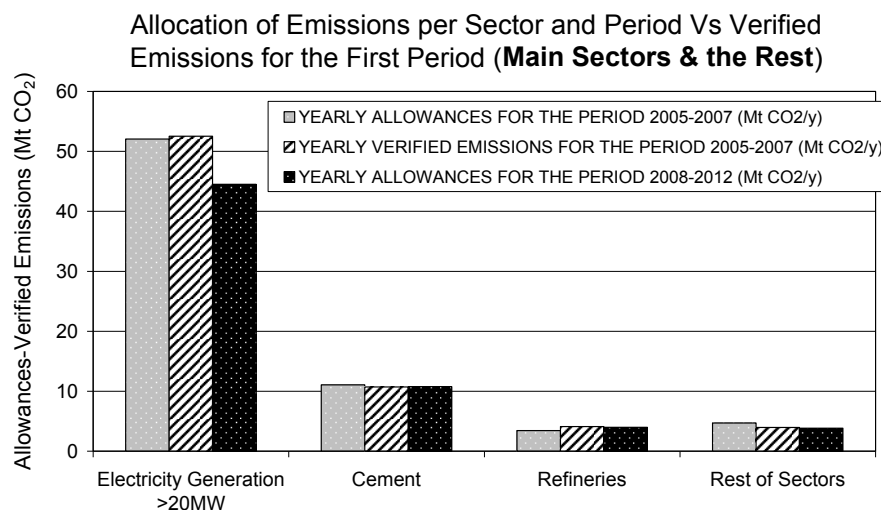


FIGURE 7 - Comparison of NAP allowances by sector and period of implementation with the verified emissions of the first period, emphasizing on the performance of the three main sectors

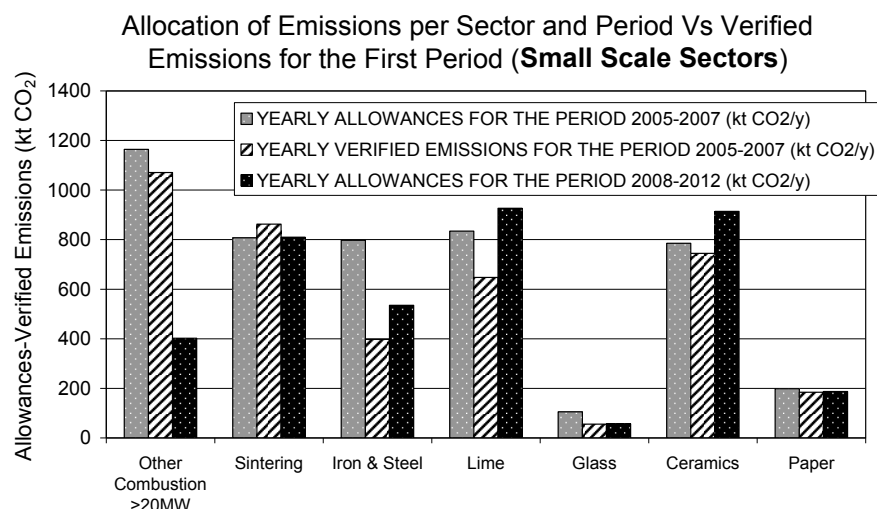


FIGURE 8 - Comparison of NAP allowances by sector and period of implementation with the verified emissions of the first period for the small scale sectors

violation of 458ktCO₂ per year. Contrariwise, the cement industry managed to comply with the assigned allowances, similar to the majority of small scale sectors appearing in Figure 8, where one should note the stock of emissions accruing from the performance of iron & steel and lime industries. In fact, as one may see in Figure 8, it is only the sintering sector that exceeded the given allowances, with all other small scale sectors presenting a cumulative stock of 0.78MtCO₂/year. Nevertheless, the overall performance of Greek installations during this first stage of the ETS is determined by a marginal violation of 53ktCO₂/year, configured however on the basis of a relatively uneven distribution of allowances. Besides that, if also proceeding to the comparison of verified emissions with the allowances provided during the second stage, the ability of certain sectors (e.g. other combustion plants and the electricity generation sector) to comply with the reduced –in most cases- allowances seems rather uncertain.

Further analysis of the up to now situation may also be described in terms of allowance classification. More specifically, by dividing the liable installations in classes of allowances, results of Figures 9-10 may be obtained. As one may see, serious violation is recorded in the case of big-scale polluters (allowances exceeding 100kt/year) where more than 57% of the installations (a total of 37 plants) exceed their allowances (Figure 10), leading to an excess of almost 1.6MtCO₂ for the entire period (Figure 9). On the other hand, considerable is the contribution of the class between 50 and 100ktCO₂/year, where a net stock of approximately 1.36MtCO₂ may be noted, although 44% of the class installations appear to violate their allowances (see also Figure 10). Finally, situation appears to be more balanced for the rest of classes where although the violating installations exceed 60% at all times, a marginal net stock is achieved for all three classes. As a result, it becomes evident that marginal violation of the total emis-

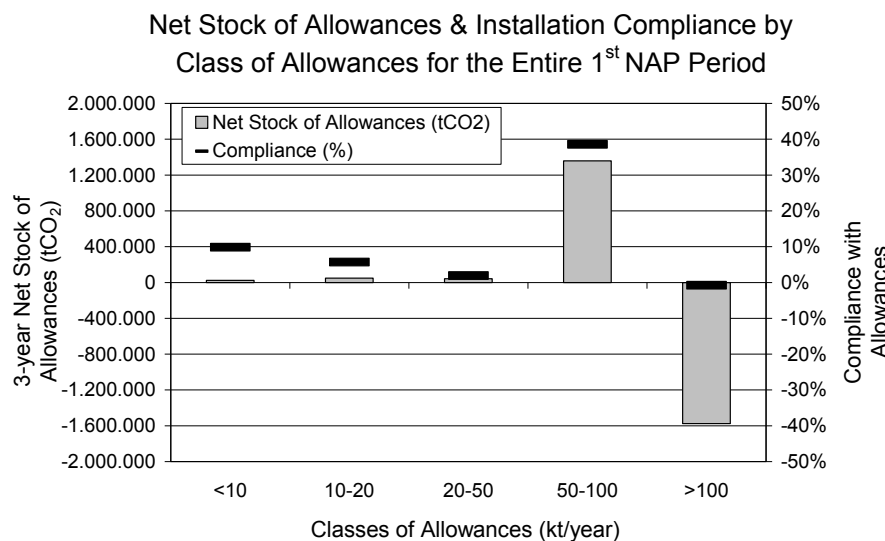


FIGURE 9 - Compliance of Greek installations liable to the allowances provided by the first NAP

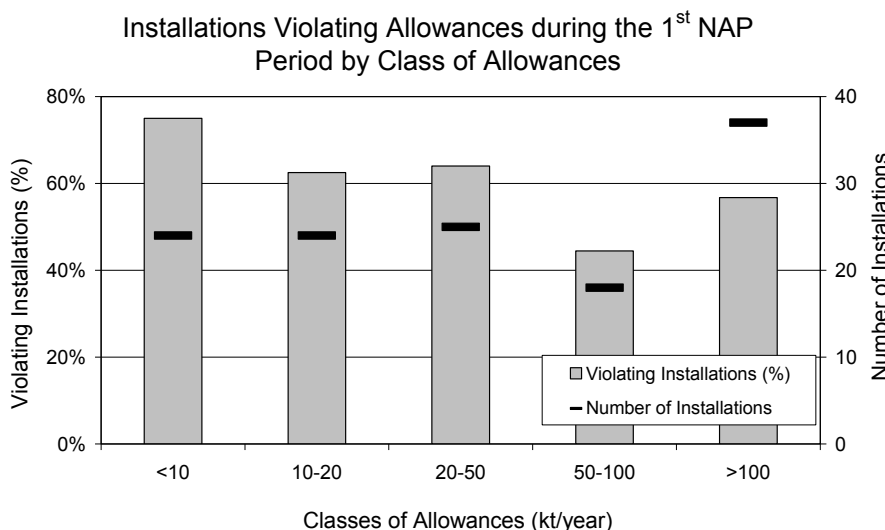


FIGURE 10 - Installations violating the allowances provided by the first NAP

sion allowances provided by the first NAP is largely configured by a certain number of big scale polluters rather than by an even distribution of violation noted for all classes. On the other hand, what should also noted is that although in terms of quantities small scale polluters seem less violating, the percent of violators is considerably increased for small classes of up to 50kt/year. In this context, taking into account that 31 out of 37 big-scale polluters belong to the sectors of electricity generation, cement and refineries, an evaluation of performance and allowances at the installation level is accordingly provided for each one of them.

3.2. Installations of the electricity generation sector

As already mentioned, the electricity generation sector comprises the main polluter among the NAP sectors, being also responsible for a violation of almost 1.4MtCO₂ during the first stage of the ETS implementation. In this context, the electricity generation system of Greece may be divided in two main sectors, i.e. the mainland and the island sub-systems. As far as the mainland electricity grid (interconnected system) is concerned, centralized power generation based mainly on the indigenous lignite reserves should be considered (~50%), while on the other hand the numerous isolated electrical grids of the island region (35 autonomous power stations operating), on top of the Crete island, rely mainly on oil imports [12]. National dependence on fossil fuels may be presently validated by the employment of approximately 6.1GW of steam turbines using local lignite reserves [13] and heavy oil (mazut) imports, 2.3GW of combined cycle power plants using imported natural gas (NG), and a total of 1.3GW of oil based-generation (gas turbines and internal combustion engines), mainly used for the service of non-interconnected Aegean island grids [12]. Following, as far as the energy contribution of renewable energy sources (RES) installations

is concerned (currently in the order of 10-11%), of critical importance is the operation of large-hydro plants that have during the past allowed for the total RES share to reach a maximum of almost 13%, while the respective wind energy share is equal to approximately 3% of the total gross electricity production.

Considering the situation described, a total number of 32 electricity power stations are currently liable to NAP obligations in comparison with a total of 30 plants during the first period of the ETS [9,10]. Performance of liable power stations is accordingly provided in Figures 11-12, where division of power stations into small- and large-scale is attempted, in order to facilitate presentation of the results obtained concerning the comparison of allowances (for both NAPs) with the verified emissions of the first stage.

As far as the small-scale installations are concerned (Figure 11), all stations except for two (i.e. Heron Therm. S.A. and Liptol being currently under retirement and included only for comparison purposes) violated their allowances for the first period, with the thermal power station of Soroni, operating on the island of Rhodes, presenting the greatest emission excess (almost 95kt/year more than permitted) and being largely responsible for the aggregate net excess of 217kt/year of all small-scale power stations. On the other hand, as it may be seen in Figure 12, the situation is more balanced in the case of big-scale power stations, where 6 out of 13 installations managed to comply with their allowances. In fact, according to the comparison results obtained between the allowances and the verified emissions, a net emission stock of 206kt/year recorded in the case of big-scale installations illustrates the efficient performance of the four largest ones, apart from Agios Dimitrios, where a marginal excess of 34kt/year is noted.

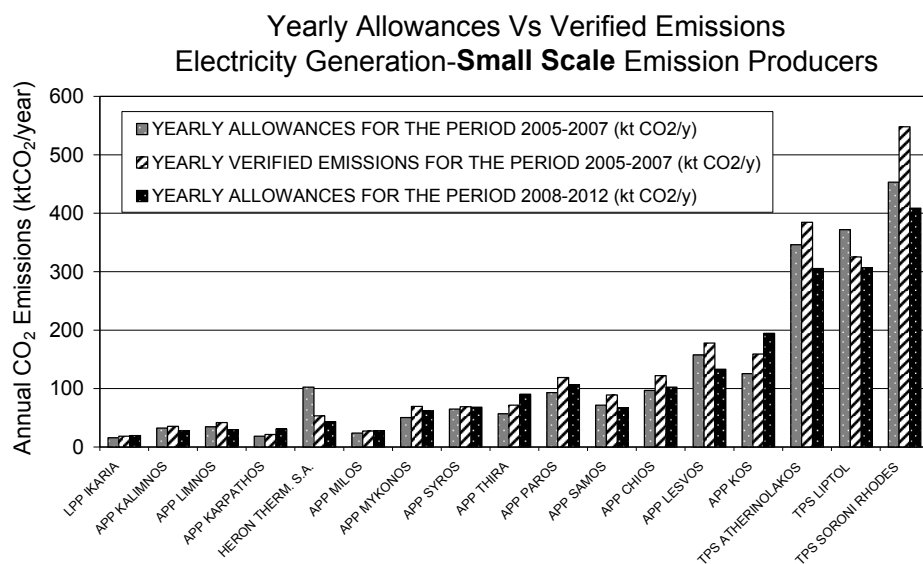


FIGURE 11 - Comparison of NAP allowances with the verified emissions of the first period for small scale electricity power stations

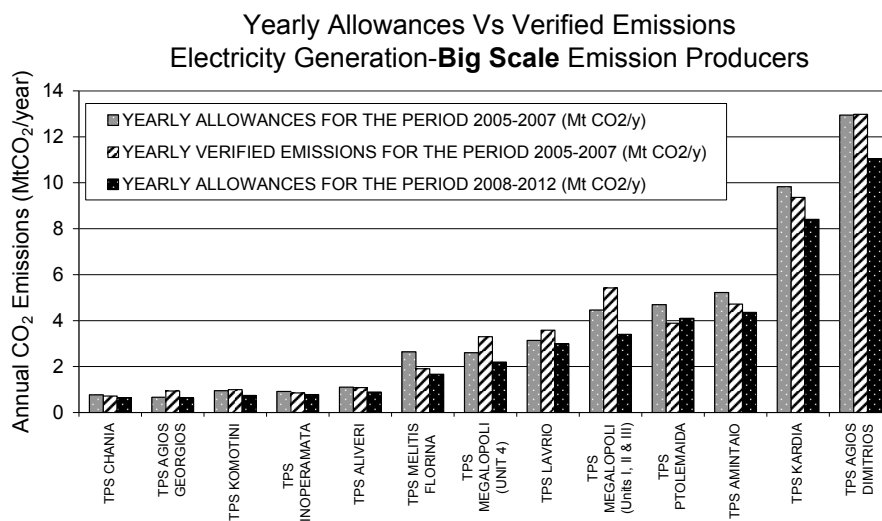


FIGURE 12 - Comparison of NAP allowances with the verified emissions of the first period for big scale electricity power stations

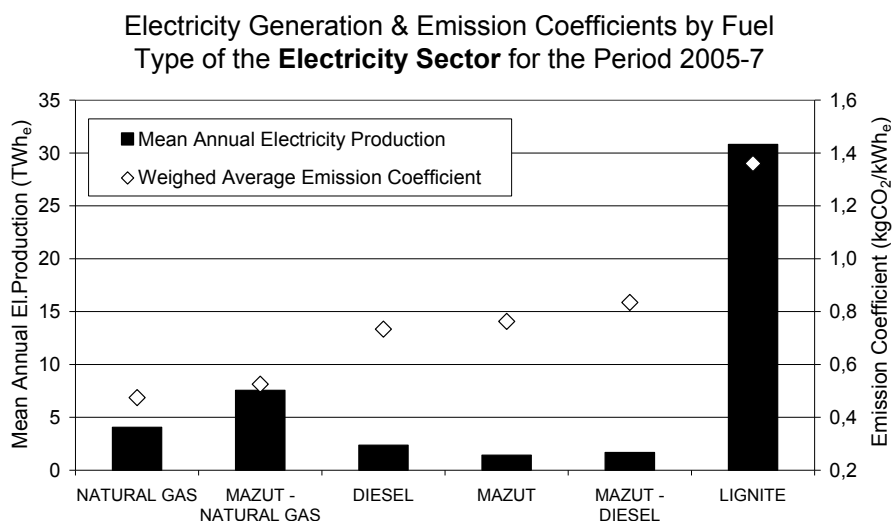


FIGURE 13 - Production rates and emission factors of the electricity generation sector during the 2005-2007 period.

Finally, in Figure 13, estimation of the average emission coefficient by fuel type plotted against the respective mean annual electricity generation during the period 2005-7 reveals the critical role of the local lignite in the annual national balance of the CO₂ emissions' production. On the other hand, NG and mazut-NG installations are kept under 600grCO₂/kWh_e with oil-based installations being responsible for the emission of 720grCO₂/kWh_e to 830grCO₂/kWh_e, while it should be noted that the weighed average emission factor of all installations liable to the NAP for this 3-year period (2005-7) corresponds to 1.09kgCO₂/kWh_e of gross electricity production.

3.3. Installations of the cement industry sector

The Greek cement industry, comprising one of the main exporting sectors of Greece, is determined by a long history beginning in 1902 with the establishment of the first Greek

firm, i.e. Titan. Up until 1983, the sector presented a constant increase rate (mainly due to the increased demand for exports during the time) leading to the annual production peak of 1983, exceeding 14Mt of cement [14]. Accordingly, a stable demand configured by both indigenous needs and the need for exports still preserved (mainly towards USA, EU, the Middle East and North African countries) has led to a long-term production in the order of 13-16Mt of cement per year.

Performance of the liable cement industry installations is presented in Figure 14, where similar to the previous figures, verified emissions are compared with the allowances of both the first and the second stage of the ETS for all 8 participating installations. According to the results obtained, three are the violating stations, this however leading to an overall aggregate of almost 350ktCO₂/year emission excess for the Greek cement sector. On the other

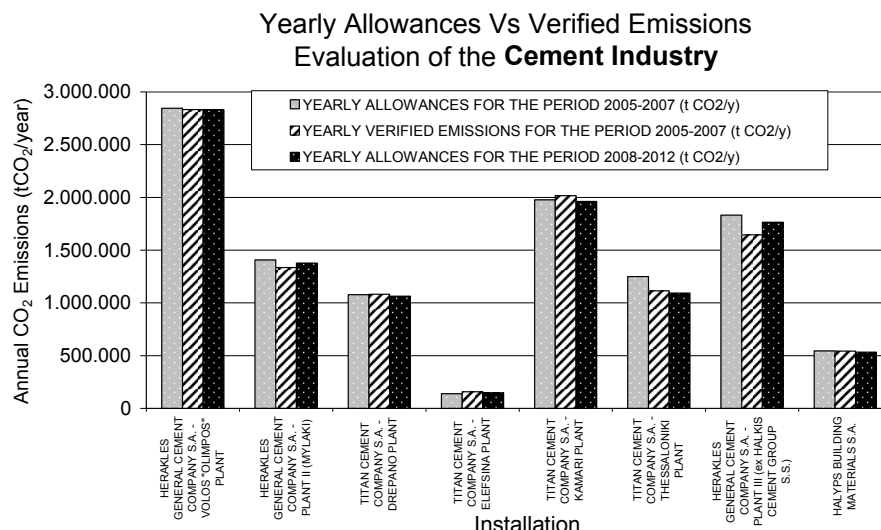


FIGURE 14 - Comparison of NAP allowances with the verified emissions of the first period for the Greek cement industry installations

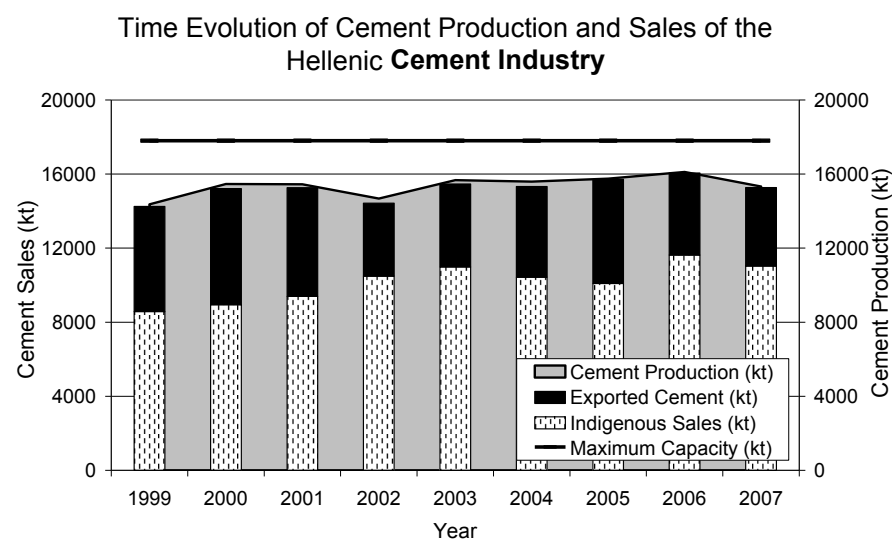


FIGURE 15 - Time evolution, distribution and maximum capacity of cement production in Greece

hand, what should be noted is that in all cases examined, allowances provided for the second ETS stage are more or less identical to the respective of the first.

Furthermore, based on the long-term production data [14] of the cement industry (see also Figure 15), the corresponding emission factor per product unit for the period between 2005-2007 is also estimated per industrial firm (Figure 16). In this context, although the respective coefficient is kept within the anticipated standards, considerable difference noted between different industries (i.e. from 624kgCO₂/t to 720kgCO₂/t) reveals the potential for emission reduction for the heavy emitting plants. However, due to the fact that the specific sector is described by relatively flat production rates (an annual production of 15Mt should be considered during the past decade), compliance with the allowances of the second ETS stage is ex-

pected, although the resulting stock (based on the yearly verified of the first stage) is only 47kt/year. On the other hand, if operation at maximum capacity is encountered, i.e. 17.8Mt/year (see also Figures 15 and 16), it is quite possible that allowance ceilings will be exceeded, especially if considering that the highest emission factors are attributed to the plants with the highest production capacity (see also Figure 16).

3.4. Installations of the refineries' sector

The sector of refineries in Greece is based on two companies, namely Hellenic Petroleum and Motor Oil Hellas; the first operating three refineries found in Thessaloniki, Elefsina and Aspropyrgos (66% of total capacity in 2007) and the second operating one refinery located at Corinthos (34% of total capacity in 2007). In this context,

CO₂ Production Performance of Cement Industry Installations in Greece for the Period 2005-2007

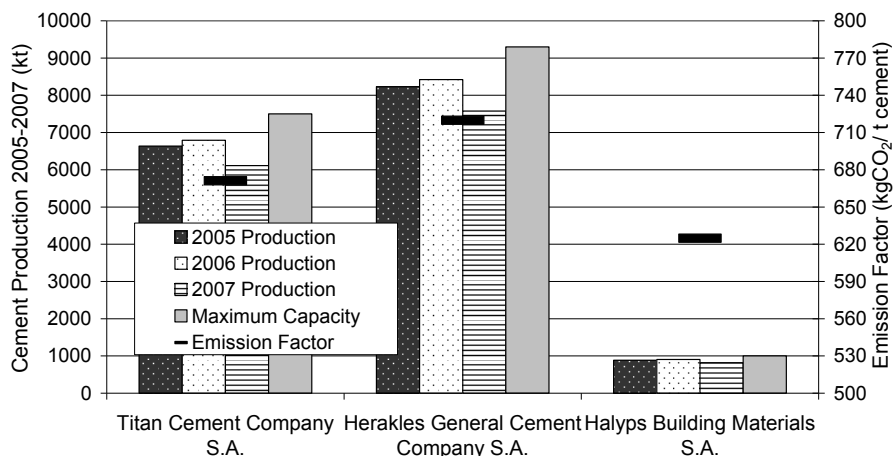


FIGURE 16 - Production rates and emission factors of the cement industry sector during the 2005-2007 period

Yearly Allowances Vs Verified Emissions Evaluation of the Refineries' Industry

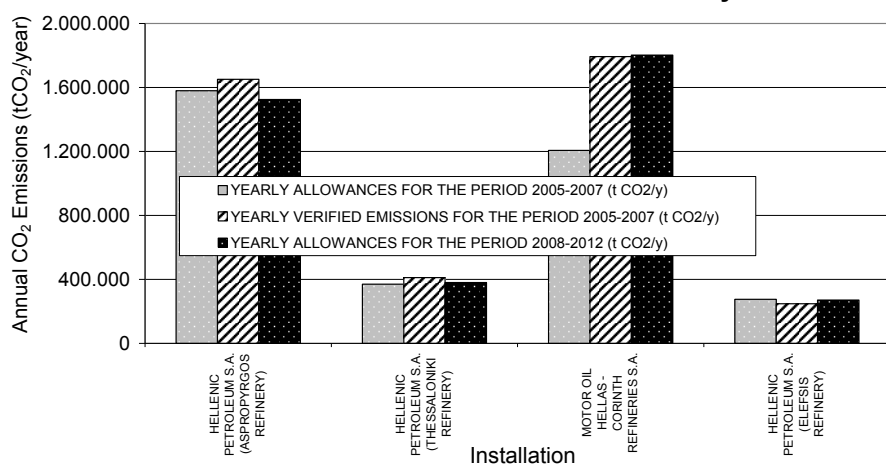


FIGURE 17 - Comparison of NAP allowances with the verified emissions of the first period for the Greek refineries

CO₂ Production Performance of Greek Refineries for the Period 2005-2007

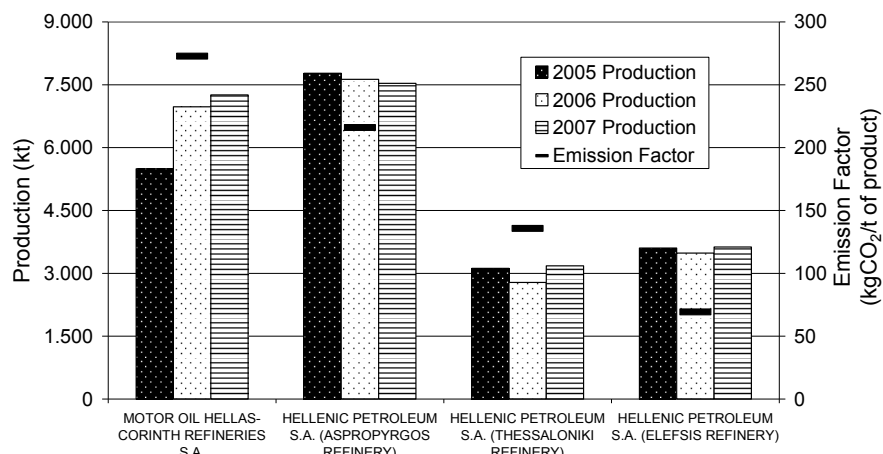


FIGURE 18 - Production rates and emission factors of the refineries' sector during the 2005-2007 period

since the first Greek refinery plant started operating in Aspropyrgos in 1958, the sector met tremendous rates of growth, reaching nowadays an annual turnover in the order of 15 billion €/year [15,16], at the same time employing more than 7500 people and thus comprising one of the keystones of the national economy.

Performance of the refineries' sector at the level of installation for all four plants is given in Figure 17. What accrues from the results obtained is that three out of four installations violated their allowances during the first period of implementation, with an overall violation of 670kt/year. Furthermore, based on the production data of 2005-2007 and the respective verified emissions, considerable imbalance is also recorded in terms of emission factors with the respective values ranging from 70 to 270 kgCO₂ per ton of product; the highest ones attributed to the refineries with the biggest production capacity (see also Figure 18). At the same time, the production of refineries during these 3-year period presents a mean annual increase of 3.8%, strongly questioning compliance with the allowances of the second NAP, violated (by approximately 125kt/year) even in the case of maintaining the verified annual emissions of the first stage.

4. DISCUSSION

Based on the results obtained for each of the three main polluting sectors, the following conclusions may be drawn in view of the second NAP implementation for Greece.

- Concerning the electricity generation sector, unless considerable changes are encountered in the current national electricity generation fuel mix, remarkable violation is anticipated even in the case of zero increase rates in the national electricity consumption. More specifically, if the levels of electricity consumption remain the same, an annual violation of 8 MtCO₂/year should be expected if maintaining the current production patterns. On the other hand, unless the ongoing economic recession considerably affects the energy consumption habits of the local population, even an increase rate of 1% for the respective energy production (see also Figure 13) shall lead to further violation of the given allowances, taking however into account that the maximum possible production capacity of the specific units during the period between 2005-2007 (approximately equal to 52.5 TWh) cannot be exceeded. In fact, based on some rough calculations, an increase of 1% would entail a remarkable 5-year period violation of 52 MtCO₂. As a result, increased adoption of RES -already dictated by the EU [17,18]- along with further promotion of NG and application of the clean coal concept suggesting among others increased energy production efficiency and CO₂ capture and storage (CCS) [19-21], are all required in order for the electricity generation sector to adhere to the second NAP. Note that according to re-

cent studies [22], opportunities for the introduction of CCS in Greece have been identified for five power stations, one refinery plant and one cement plant, that if implemented could reduce national CO₂ emissions by a remarkable 25%-28%. On the other hand, according to the most recent official data [23], the Greek Public Power Corporation (owning 29 out of the 30 power stations presented in Figures 11 and 12) has in the meantime (years 2008 and 2009) spent a total of 150 M€ for the purchase of emission allowances, thus both verifying the projections of emission excess and reflecting the delay met in the shift to alternative fuels and RES.

- As far as the cement industry is concerned, compliance achieved during the first stage of the ETS can only be described as marginal, with the long-term steady production rates implying analogous results for the second stage as well. Nevertheless, if current production capacity is exploited at its full, the fact that the biggest producers are determined by the highest emission factors leads to an overall of 12.35 MtCO₂/year, i.e. an excess of approximately 1.6 MtCO₂/year for the second NAP period. Hence, to achieve maximum production capacity, adoption of more energy efficient production methods and other CO₂ emission abatement measures [24, 25] need to be introduced in the Greek cement industries as well (especially in those determined by the highest emission factors).
- Finally, with regards to the refineries' sector, considerable violation noted during the first ETS stage led to the decision for the increase of allowances in the second NAP, especially for the major producer. At the same time, increasing production rates of the field's companies along with the fact that again –similar to the cement sector- highest emission factors are attributed to the industries with the higher production capacity, still jeopardize compliance with the allowances of the 2008-2012 period. In fact, if assuming that the recent years' increase rate of production (an average of 3.8% has been estimated) is maintained, a total excess of 24 MtCO₂ may be estimated for the entire 5-year period, this leading to a violation of approximately 4.2 MtCO₂. Thus, in the extreme scenario of a constant annual increase rate for the local refineries' production, energy efficiency techniques and CO₂ emission abatement measures [26] need to be set forth.

Considering the situation described, it becomes evident that unless radical changes are implemented in the three major polluting sectors of the Greek economy, the corresponding violation of CO₂ allowances during the second period of the ETS may even reach a total of 65 Mt, largely configured by the electricity generation sector (80% contribution) and less affected by the contribution of the cement (14%) and the refineries' (6%) sectors. In this context, if also taking into account the immediate impacts that the economic crisis may yield for the large-scale national industry as well, promotion and support of the so called green development [27] becomes essential, since not only

obligations of the country concerning promotion of RES at the EU level would be satisfied, but also violation of the second NAP emissions could be counterbalanced [28]. In fact, as one may argue, through the support of a national plan for considerable diffusion of RES in the electricity generation sector, i.e. where the greatest part of excess emissions is recorded, compensation of emission violation may also be achieved for the other two major polluting sectors, thus allowing local cement and refineries' plants to not incorporate any CO₂ emission abatement costs and also maximize their production rates. In this context, although such a strategy would shield the local refineries and cement industries against the economic crisis effects, several scenarios need to be first investigated, this however comprising the subject of a forthcoming research work.

5. CONCLUSIONS

Recapitulating, a critical review of the first and the second Greek NAP was currently undertaken, emphasizing on the major polluting sectors of electricity generation, cement industry and refineries. Evaluation of the performance of the liable installations as well as of the emission allowances provided during the first and the second stage of the ETS was carried out by using verified emission data of the first period and by estimating the respective emission factors. According to the results obtained, violation or marginal compliance during the first stage of the ETS, recorded for most of the installations, questions satisfaction of allowances given for the second period, especially for the sectors of electricity generation and refineries. To confront the situation encountered, liable installations – especially those presenting the greatest violation and the highest emission factors- should either adopt CO₂ emission abatement measures or reduce their production rates, both scenarios however thought to much affect the current economic state of liable plants during this period of economic recession. On the other hand, large-scale promotion of green development projects in the electricity generation sector may both ensure compliance of the specific sector with the second NAP allowances and at the same time allow for maximum capacity production in the cement and the refineries' industrial sectors, this option however requiring further investigation concerning its implications.

REFERENCES

- [1] Greek Ministry for the Environment, Physical Planning and Public Works (2009) Annual Inventory Submission under the Convention and the Kyoto Protocol for Greenhouse and other Gases for the Years 1990-2007. Athens, 2009. Available at: <http://www.ypeka.gr>.
- [2] Central Intelligence Agency (2010) The World Factbook. Greece Economy Overview. Available at: <https://www.cia.gov/library/publications/the-world-factbook/geos/gr.html>.
- [3] Energy Information Administration (2010). Independent Statistics and Analysis. Indicators. Available at: <http://www.eia.doe.gov>.
- [4] Alcántara, V. and Duarte, R. (2004) Comparison of energy intensities in European Union countries. Results of a structural decomposition analysis. Energy Policy 32, 177-189.
- [5] European Commission-Market Observatory for Energy (2010) EU-27 info, Greece. Available at: <http://ec.europa.eu/energy/observatory/>
- [6] Hellenic Petroleum (2011) Environmental Protection. Available at: <http://www.hellenic-petroleum.gr>.
- [7] Greek Foundation for Economic and Industrial research (2010) Report on Greek Economy. Available at: http://www.iobe.gr/index.asp?a_id=122.
- [8] De Grauw, P. (2010) The Greek Crisis and the Future of the Euro-Zone. Eurointelligence. Available at: <http://www.euro-intelligence.com>.
- [9] Greek Ministry for the Environment, Physical Planning and Public Works (2005) National Allocation plan for the Period 2005-2007 (Amended Version). Athens, 2005. Available at: <http://www.ypeka.gr>.
- [10] Greek Ministry for the Environment, Physical Planning and Public Works (2006) National Allocation plan for the Period 2008-2012. Athens, 2006. Available at: <http://www.ypeka.gr>.
- [11] European Commission (2008) Climate Action-Emissions Trading System. Available at: http://ec.europa.eu/clima/documentation/ets/index_en.htm.
- [12] Kaldellis, J.K. and Zafirakis, D. (2007) Present situation and future prospects of electricity generation in Aegean Archipelago islands. Energy Policy 35, 4623-4639.
- [13] Kaldellis J.K., Zafirakis, D. and Kondili, E. (2009) Contribution of lignite in the Greek electricity generation: Review and future prospects. Fuel 88, 475-489.
- [14] Hellenic Cement Industry Association (2010) Evolution of Cement Production in Greece. Available at: <http://www.hcia.gr/7a.html>.
- [15] Hellenic Petroleum (2010) Financial Calendar. Available at: <http://www.hellenic-petroleum.gr>.
- [16] Motor Oil Hellas (2010) Human Resources. Available at: <http://www.moh.gr/resources>.
- [17] Verhaegen, K., Meeus, L., Delvaux, B. and Belmans, R. (2007) Electricity produced from renewable energy sources- What target are we aiming for? Energy Policy 35, 5576-5584.
- [18] Kalampalikas, N.G. and Pilavachi, P.A. (2010) A model for the development of a power production system in Greece, Part II: Where RES meet EU targets. Energy Policy 38, 6514-6528.
- [19] Campbell, P.E., McMullan, J.T. and Williams, B.C. (2009) Concept for a competitive coal fired integrated gasification combined cycle power plant. Fuel 79, 1031-1040.
- [20] Mori, Y., Masutani, S.M., Nihous, G.C., Vega, L.A. and Kinoshita, C.M. (1993) Pre-combustion removal of carbon dioxide from hydrocarbon-fuelled power plants. Fuel 72, 1293-1299.

- [21] Pires, J.C.M., Martins, F.G., Alvim-Ferraz, M.C.M. and Simões, M. (2011) Recent developments on carbon capture and storage: An overview. *Chemical Engineering Research and Design*, In Press, Corrected Proof. Available at: <http://www.sciencedirect.com>.
- [22] Koukouzas, N., Ziogou, F. and Gemeni, V. (2009) Preliminary assessment of CO₂ geological storage opportunities in Greece. *International Journal of Greenhouse Gas Control* 3, 502-513.
- [23] Greek Public Power Corporation (2010) Annual Reports 2008-2009. Available at: <http://www.dei.gr/>
- [24] Hasanbeigi, A., Menke, C. and Price, L. (2010) The CO₂ abatement cost curve for the Thailand cement industry. *Journal of Cleaner Production* 18, 1509-1518.
- [25] Mandal, S.K. and Madheswaran, S. (2010). Environmental efficiency of the Indian cement industry: An interstate analysis. *Energy Policy* 38, 1108-1118.
- [26] Holmgren, K. and Sternhufvud, C. (2008) CO₂-emission reduction costs for petroleum refineries in Sweden. *Journal of Cleaner Production* 16, 385-394.
- [27] Pagoulatos, G. (2010) Friedrich-Ebert-Stiftung I. International Policy Analysis. The Greek Economy and the Potential for Green Development. Available at: <http://library.fes.de/pdf-files/id/ipa/07097.pdf>.
- [28] Kaldellis, J.K., Kondili, E. and Paliatsos, Ath. (2008) The Contribution of Renewable Energy Sources on Reducing the Air Pollution of Greek Electricity Generation Sector. *Fresenius Environmental Bulletin* 17, 1584-1593.

Received: January 25, 2011

Revised: April 11, 2011

Accepted: April 14, 2011

CORRESPONDING AUTHOR

John K. Kaldellis

Lab of Soft Energy Applications
& Environmental Protection
Mechanical Engineering Department
Technological Educational Institute of Piraeus
P.O. Box 41046
Athens 12201
GREECE

Phone: +30-210-5381237
Fax: +30-210-5381467
E-mail: jkald@teipir.gr

RADIOACTIVITY MEASUREMENT AND DOSE ASSESSMENT FROM SURFACE SOILS AROUND THE ÇATALAĞZI COAL-FIRED POWER PLANT, TURKEY

Hüseyin Aytekin* and Ridvan Baldık

Department of Physics, Zonguldak Karaelmas University, 67100, Zonguldak, Turkey

ABSTRACT

This paper presents a study on radioactivity measurements in surface soils around the Çatalağzı coal-fired power plant (ÇCFPP/ÇATES) near the city of Zonguldak on the west of the Black Sea cost of Turkey. Soil samples were collected from 25 locations around the ÇCFPP and the activity concentrations of ^{226}Ra , ^{232}Th and ^{40}K in the samples were determined using a gamma ray spectrometric system with an HPGe detector. The mean activity concentrations in soil samples were found as 47, 50 and 440 Bq kg^{-1} for ^{226}Ra , ^{232}Th and ^{40}K respectively. In order to evaluate the radiological hazard of the natural radioactivity, the radium equivalent activity (Ra_{eq}), the absorbed dose rate (D) and the annual effect dose rate (AED) were calculated and compared with the internationally approved values. Our findings were also compared with the similar studies done in Turkey and other countries in the world.

KEYWORDS:

Radioactivity, Radium, thorium, potassium, soil, Çatalağzı, Turkey

1. INTRODUCTION

Coal contains primordial radionuclides ^{40}K , ^{238}U , ^{235}U , ^{232}Th and the members of decay series of ^{238}U , ^{235}U and ^{232}Th . As a result of coal combustion in a thermal power plant, natural radionuclides and their products and the heavy metals are released and distributed between gaseous and solid combustion products. The natural radionuclides and heavy metals are enriched in solid products, which are bottom and fly ashes. The fly ash is carried through the furnaces with gaseous flow toward a stack. Depending on the emission control system of the stack, most of the fly ash is collected, while the rest is released into atmosphere and deposited on the soil around the coal-fired power plant. The fly ashes from CFPPs escape into

atmosphere in quantities of about 0.5-2% [1]. The average concentrations of ^{238}U , ^{232}Th and ^{40}K were estimated to be 20, 20 and 50 Bq kg^{-1} , respectively, based on the analysis of coal samples from 15 countries, with a variation of more than two order of magnitude [2]. On the other hand, the arithmetic averages of reported concentrations that in the escaping fly ashes are 265 Bq kg^{-1} for ^{40}K , 200 Bq kg^{-1} for ^{238}U , 240 Bq kg^{-1} for ^{226}Ra , 70 Bq kg^{-1} for ^{232}Th [2]. Therefore, burning coal in the power plants is one of the main reasons behind the release of radioactive residues to the environment and exposure of technological enhanced radionuclides to population. In order to provide appropriate protection for population, it is necessary to monitor the released radioactivity from coal-fired power plant (CFPP) into environment and assess the radiological hazards. For this aim, the environmental radioactivity around the CFPP has been investigated in a continuous concern in the recent years [3-9]. Also, there are some studies state possible impacts of the CFPP on the natural radioactivity level around the power plant [3, 10, 11].

Coal is widely used for the electric power generation in Turkey. While most of the coal-fired power plants in Turkey use lignite, ÇCFPP/ÇATES (ÇATES is the local abbreviation of ÇCFPP) uses bituminous coals. The Çatalağzı CFPP ($41^{\circ}30'48.4''N$ and $(31^{\circ}53'41.5''E)$) is located at ~13 km North-East of Zonguldak city on the West Black Sea coast of Turkey (Figure 1). In order to evaluate the environmental impact of the ÇCFPP some studies were carried out: The radon concentration measurements in and around the plant was made by Aytekin et al. [12], and radiological character of the fly ash of the plant and radiological safety aspect of concrete materials which uses these fly ashes were made by Turhan et al. [13, 14]. On the other hand, ^{238}U , ^{232}Th and ^{40}K concentration measurements for soil samples collected from the sites around the plant were made by Aytekin and Baldık [15]. Aytekin and Baldık found that samples collected in the dominant wind direction (southwest of the plant) generally have more radioactivity than that of the other directions.

On the other hand, heavy metal deposition by mosses, as a bio-indicator plant in the vicinity of the ÇCFPP was

* Corresponding author

determined by Uyar et al. [16]. Uyar et al. also determined the most polluted twenty five sites (Figure 2) around the ÇCFPP in their study. In order to decide the sites to be sampled using meteorological data for investigation of the heavy metal contamination around the ÇCFPP, they used the Industrial Source Complex Short Term (ISC-ST) modeling, which have been extensively used over the past two decades for varied application [16]. In the present work, in order to evaluate the radiological impact of ÇCFPP in the surrounding, twenty five surface soil samples were collected from the selected sites, which were defined as the most polluted areas given by ref. [16], as shown in Figure 2. The publication is also the continuation of ref. [15]. In this aim, the radioactivity concentrations of ^{226}Ra , ^{232}Th and ^{40}K radionuclides from these samples were analyzed using a gamma spectrometric system with an HPGe detector.

2. MATERIALS AND METHOD

2.1. The study area

The Çatalağzı CFPP ($41^{\circ}30'48.4''\text{N}$ and $31^{\circ}53'41.5''\text{E}$) is located at ~ 13 km North-East of Zonguldak city (Figure 1) on the West Black Sea coast of Turkey and has been operated since 1946. The plant is located at nearest the sea, frosty fields and the dwellings, and covers a total area of $233,250 \text{ m}^2$, out of which the plant area is $104,050 \text{ m}^2$. There are two units of 150 MW each. These units consume about $1.6 \times 10^6 \text{ t}$ of coal per year. The plant fires coal sludge generated from washing processes and its mixture with low-rank bituminous coal produced in Zonguldak basin as the main fuel. Analysis shows that the characteristics of the coal burnt in the plant are: They have $3573\text{-}5146 \text{ kcal/kg}$, $9.0\text{-}15.4 \text{ wt\%}$ moisture, $30.1\text{-}46.0 \text{ wt\%}$ ash, $0.4\text{-}0.6 \text{ wt\%}$ sulphur, $016.8\text{-}20.9 \text{ wt\%}$ volatile matter and $31.3\text{-}42.9 \text{ wt\%}$ fixed carbon [17].

2.2. Sampling

In order to decide the sites (Figure 2) to collect soil samples from, the modeling aforementioned in the second paragraph of the introduction and given ref. [16] was applied. The modeling was briefly explained in this reference as follows: “The study area was divided into $22 \times 16 \text{ km}^2$ grids with 22 grids along the x-axis and 16 grids along y-axis. The parameters employed in this model, such as dust emission of 532 g s^{-1} (single sinter stack), stack height of 120 m , stack diameter of 6.5 m , stack gas temperature of 150°C and gas velocity: 12 ms^{-1} , stability classes (compiled from Turner’s [18] table), mixing height (determined using the Holzworth [19] technique) and the mean meteorological values (obtained from Turkish Meteorological Department) were used as required input data” [16]. According to the model results, only 48 km^2 of the area was decided to be the most polluted sites, which consists of 25 grids as shown in Figure 2. Surface soil samples were collected from 25 locations (nearby the plant and accessible sites) around the Çatalağzı CFPP, which are not agricultural areas, in the period of April-June 2008. The coordinates of the locations were determined by GPS.

2.3. Measurement of natural radioactivity levels by gamma spectrometry technique

Collected soil samples were crushed at about 1 mm size and dried for 6 h in air circulation oven at 105°C in the laboratory. Dried samples were mixed and prepared as homogenous samples and put in polyethylene bags (9 cm diameter and 4 cm height). About $250\text{-}300 \text{ g}$ of each sample was sealed for 25 days to achieve secular equilibrium between ^{222}Rn and ^{226}Ra . The activities of ^{214}Pb and ^{214}Bi in equilibrium with their parents were assumed to represent the ^{226}Ra activity, while the activities of ^{228}Ac and ^{208}Tl were assumed to represent the ^{232}Th activity.



FIGURE 1 - Geographical location of the study area.

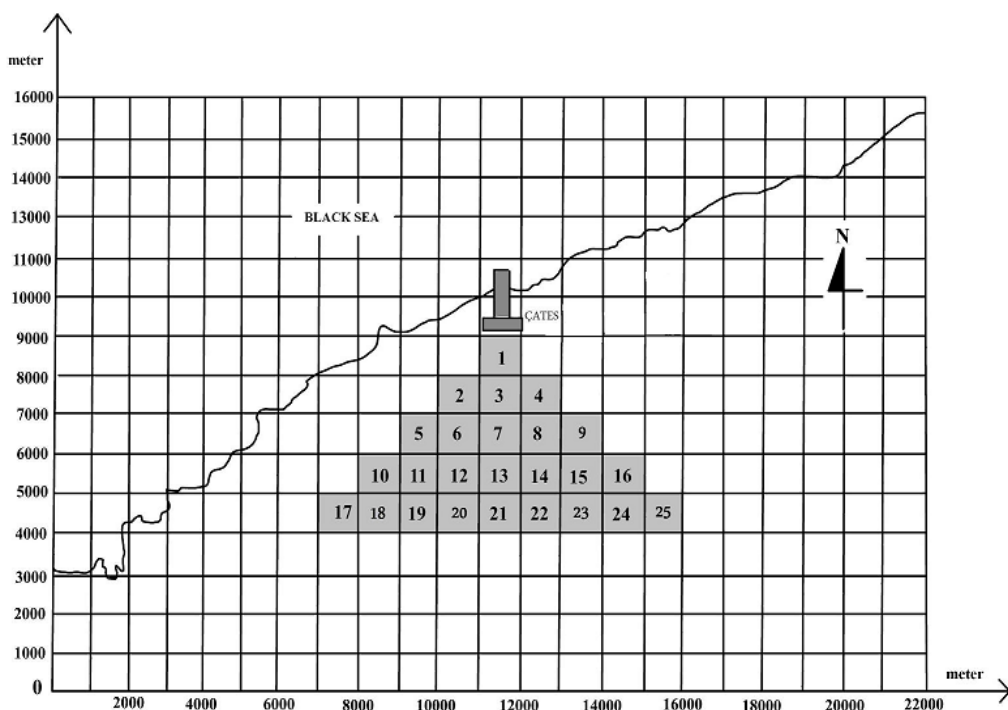


FIGURE 2 - Map of Çatalağzı region [16].

Gamma spectrometry measurements were made with the high purity p-type crystal of coaxial Ge detectors of 150% (Ortec), 110% (Canberra) and 20% (Canberra) of relative efficiency and resolution 1.9–2.2 keV at the 1332 keV gamma of ^{60}Co , and the high purity n-type crystal of coaxial Ge detectors of 70% (Ortec) of relative efficiency. The detectors were shielded in 10 cm thick lead well internally lined with 1 mm Cu and Cd foils. The detector output was connected to an amplifier (Canberra, Model 2025). The energy calibration and relative efficiency calibration of the spectrometer were carried out using calibration sources which contain ^{210}Pb , ^{241}Am , ^{57}Co , ^{137}Cs , ^{60}Co , ^{88}Y and ^{40}K peaks for energy range between 40 and 1850 keV. The activity concentrations of ^{226}Ra have been calculated by means of weighted mean of gamma-ray lines ^{214}Pb ($E_{\gamma} = 295.1$ keV and 351.9 keV) and ^{214}Bi ($E_{\gamma} = 609.3$, 1120.3 keV and 1764.5 keV). In the case of ^{232}Th series, the activities were calculated by using the gamma-ray lines of ^{228}Ac ($E_{\gamma}=338.4$ keV, 911.2 keV and 969 keV), ^{212}Pb ($E_{\gamma} = 238.6$ keV and 300 keV), ^{212}Bi ($E_{\gamma}=1620.7$ keV and 727.2 keV) and ^{208}Tl ($E_{\gamma} = 583.2$ keV). The ^{40}K activity concentration was determined by measuring the ($E_{\gamma} = 1460.8$ keV) gamma-ray line. ^{137}Cs concentration was analyzed by its 662 keV peak.

Assaying was carried out by the gamma spectrometry located at Sarayköy Nuclear Research and Training Centre of Turkish Atomic Energy Agency. The specific activity of each sample was calculated by using the following formula:

$$A = \frac{C_{NET}}{\varepsilon I \Delta t m} \quad (1)$$

where C_{NET} is the net area of total absorption line, A is the activity of the isotope in Bq kg^{-1} , I is the absolute intensity of the transition, Δt is the sample measurements time, ε is the full energy peak efficiency, and m is the mass of the sample. In the analysis, the net peak areas (C_{NET}) are found by the following formula,

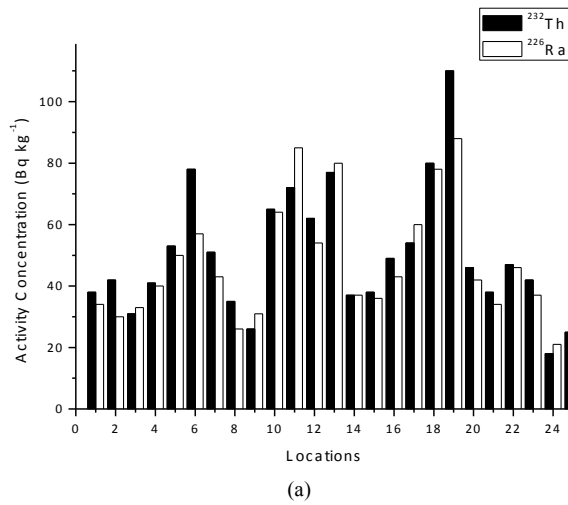
$$C_{NET}=C-B_{PBC} \Delta t \quad (2)$$

where C is the count accumulated over Δt count time (sec), B_{PBC} is the background peak count per second. The counting times were 6×10^4 s for each sample and 2.5×10^5 s for background. If the peak is clear the statistical error is less than 1%. Genie 2000 (CANBERRA) software automatically chooses the areas and fits them to the Gaussians, and the net peak areas are evaluated by subtracting the background counts. If the interested peak is smeared with the other, the peak areas are chosen and fitted to the Gaussians, and the peaks are separated by using the interactive peak search. In case of the analysis using the Gamma Vision (ORTEC), the same procedure is valid.

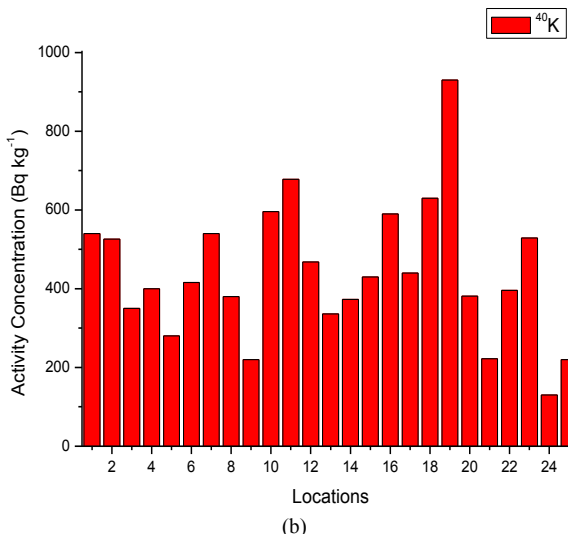
3. RESULTS AND DISCUSSIONS

Distribution of the measured activity concentrations for ^{40}K , ^{226}Ra and ^{232}Th , in surface soils around the CCFPP are shown in Figure 3. As shown in Figure 3 (a), distributions of ^{226}Ra and ^{232}Th activity are significantly similar to each

other and having generally higher values in the south and southwest direction (dominant wind direction). ^{40}K concentrations are also generally higher in the south and southwest direction. The activity concentrations in the soil samples around the ÇCFPP ranges from 20 to 88 Bq kg $^{-1}$, 18 to 110 Bq kg $^{-1}$ and 130 to 930 Bq kg $^{-1}$ for ^{226}Ra , ^{232}Th and ^{40}K , respectively.



(a)



(b)

FIGURE 3 - Concentrations of ^{226}Ra , ^{232}Th and ^{40}K radionuclides in soil samples collected around the Çatalağzı CFPP, Turkey (Bq kg $^{-1}$).

The correlation analyses were made among the measured ^{226}Ra , ^{232}Th and ^{40}K activity concentrations in the collected soil samples (Figure 4). These analysis showed that strongest correlation is between ^{40}K and ^{232}Th activity concentrations with the significant level of $R=0.93$. This strong correlation indicates that the measured activity concentrations for any of these radionuclides are good predictors of the activity concentration of each other. However, there were positive correlations of 0.74 between ^{40}K and ^{226}Ra concentrations and 0.66 between ^{40}K and ^{226}Ra concentrations.

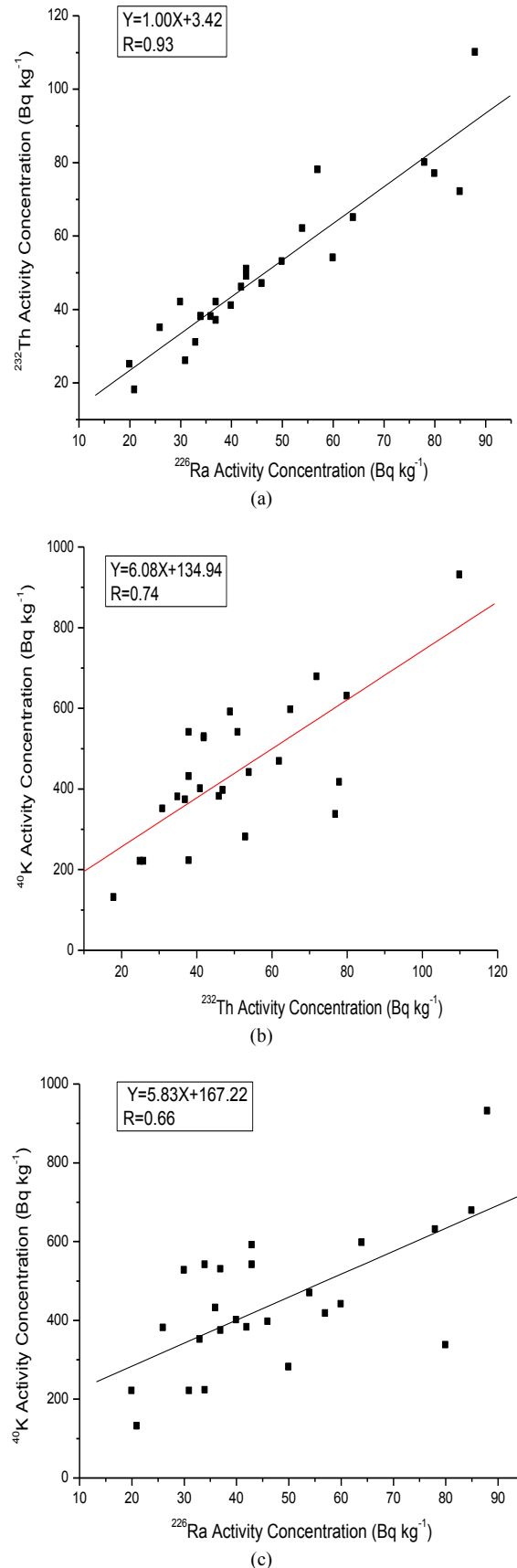


FIGURE 4 - Correlations between (a) ^{232}Th and ^{226}Ra , (b) between ^{40}K and ^{232}Th and (c) between ^{40}K and ^{226}Ra

TABLE 1 - Comparison of ^{226}Ra , ^{232}Th and ^{40}K activity concentrations measured in soils around the Catala^zı CFPP with that of from the soils collected around the CFPPs' from Turkey and the other countries in the world.

Location	^{226}Ra	^{232}Th	^{40}K	Ref.
Mean	47	50	440	Present study
Median	42	46	416	Present study
Min	20	18	130	Present study
Max	88	110	930	Present study
SD	20	21	173	Present study
Poland	9-23	9-20	221-435	Bem [10]
India	14-15.6	18-156	11-707	Mishra [6]
China	13-40	38-73	498-1127	UNSCEAR [20]
Brazil	18-84	18-43	93-223	Flues <i>et al.</i> [11]
Afşin-Elbistan (Turkey)	7-78	26-49	304-744	Çevik <i>et al.</i> [9]
West Anatolia (Turkey)	25-38	26-37	298-517	Gür [22]
Çayırhan (Turkey)	28	25	371	Çevik <i>et al.</i> [21]

In Table 1, the obtained activity concentrations for ^{226}Ra , ^{232}Th and ^{40}K were compared with the results measured from the soil samples collected around the CFPPs' from Turkey and the other countries in the world [6, 9-11, 20-22]. As seen from Table 1, our average concentration values for ^{226}Ra , ^{232}Th and ^{40}K are higher than the world's average values 35, 30 and 400 Bq kg⁻¹ for ^{226}Ra , ^{232}Th and ^{40}K , respectively [23]. While the ^{226}Ra activity concentrations in this study are higher than the concentrations for Poland, China, Afşin-Elbistan (Turkey), Çayırhan (Turkey), and West Anatolia (Turkey), they are consistent with the values of India and Brazil. For ^{232}Th activity concentrations, the observed values are higher than those of Poland, Brazil and Afşin-Elbistan (Turkey), Çayırhan (Turkey), West Anatolia (Turkey). On the other hand our values for ^{232}Th are consistent with India and China. The activity concentration values of ^{40}K are higher than those of Poland, Brazil and Afşin-Elbistan (Turkey), Çayırhan (Turkey), and West Anatolia (Turkey) but lower than those of China. Our findings for ^{40}K are consistent with the values of India and higher than those of Çayırhan (Turkey), Afşin-Elbistan (Turkey) and West Anatolia (Turkey).

The outdoor air absorbed dose rates (D) due to terrestrial gamma rays for soil were calculated because the plant is situated near the sea, frosty fields and the dwellings. The calculation of outdoor absorbed dose rates due to terrestrial gamma rays in air 1 m above the ground surface- from ^{226}Ra , ^{232}Th and ^{40}K concentrations was made on the basis of guidelines provided by UNSCEAR and Veiga *et al.* [23, 24]. The conversion factors were used to compute D in air per unit activity concentration in Bq kg⁻¹ and correspond to 0.462 nGy h⁻¹ for ^{226}Ra , 0.621 nGy h⁻¹ for ^{232}Th and 0.0417 nGy h⁻¹ for ^{40}K , respectively:

$$D(\text{nGy h}^{-1}) = 0.462C_{\text{Ra}} + 0.621C_{\text{Th}} + 0.0417C_{\text{K}}. \quad (3)$$

Where, C_{Ra} , C_{Th} and C_{K} are the average activity concentrations of ^{226}Ra , ^{232}Th , and ^{40}K in Bq kg⁻¹, respectively. The dose values are shown by Table 2. The evaluated absorbed dose rates due to terrestrial radionuclides ^{226}Ra , ^{232}Th , and ^{40}K ranges from 26 to 146 nGy h⁻¹ with the mean value of 70 nGy h⁻¹. This average value is about 1.2 times higher than the global average value of 57 nGy h⁻¹ [25].

In order to estimate the annual effective dose (AED) rates, the conversion coefficient from absorbed dose in air to effective dose rates (0.7 Sv Gy^{-1}) and outdoor occupancy factor (0.2) proposed by UNSCEAR [25] were used. The AED was calculated from absorbed dose in air to those received by adults, considering that people in Turkey spent about 20% of their times outdoors [9],

$$\text{AED}(\mu\text{Sv y}^{-1}) = D(\text{nGy h}^{-1}) \times 8760 \text{ h y}^{-1} \times 0.7 \times \frac{10^6 \mu\text{Sv}}{10^9 \text{nGy}} \times 0.2. \quad (4)$$

The results of AED from soil also given in (Table 2). The AED values, due to terrestrial radionuclides ^{226}Ra , ^{232}Th , and ^{40}K in the samples range from 32 to 179 $\mu\text{Sv y}^{-1}$ with an average value 86 $\mu\text{Sv y}^{-1}$. This average value is higher than the outdoor terrestrial world average AED 70 $\mu\text{Sv y}^{-1}$ [23, 26].

TABLE 2 - The calculated absorbed gamma dose rate (D), annual effective dose rates (AED) and Radium Equivalent Activity (Ra_{eq}) from soil samples around ÇCFPP.

Sample No	D (nGy h ⁻¹)	AED ($\mu\text{Sv y}^{-1}$)	Ra _{eq} (Bq kg ⁻¹)
C01	61	75	130
C02	61	75	131
C03	49	60	104
C04	60	73	129
C05	67	82	147
C06	91	111	201
C07	73	90	158
C08	49	60	105
C09	39	48	85
C10	94	115	203
C11	111	136	240
C12	82	100	179
C13	97	120	216
C14	55	67	119
C15	58	71	123
C16	74	91	159
C17	79	96	171
C18	111	136	241
C19	146	179	317
C20	63	77	137
C21	48	59	105
C22	66	81	144
C23	65	79	138
C24	26	32	57
C25	34	41	73
Mean	70	86	152

To assess the radiological hazard of terrestrial gamma dose, the radium equivalent activity (Ra_{eq}) was calculated. This was defined according to the estimation that 1 Bq kg⁻¹ ^{226}Ra , 0.7 Bq kg⁻¹ of ^{232}Th and 13 Bq kg⁻¹ of ^{40}K procedure the same γ – ray dose [8, 27].

$$Ra_{eq} = C_{Ra} + (C_{Th} \times 1.43) + (C_K \times 0.077), \quad (5)$$

where C_{Ra} , C_{Th} and C_K are the activities in Bq kg⁻¹ of ^{226}Ra , ^{232}Th and ^{40}K respectively. The results of radium equivalent activity are presented in Tables 2. Ra_{eq} in soil samples around ÇCFPP ranges from 57 to 317 Bq kg⁻¹ with an average 152 Bq kg⁻¹, which is lower than the suggested maximal admissible value of 370 Bq kg⁻¹ recommended by the Organization for Economic Cooperation and Development [27].

4. CONCLUSION

This paper presents a study on the determination of the radioactivity measurements in surface soils around the ÇCFPP, Turkey. In this aim, the concentrations of ^{226}Ra , ^{232}Th and ^{40}K radionuclides were measured in surface soils using a gamma spectrometry system with an HPGe detector. The dose estimations from the surface soil samples around the plant were also made. The most polluted areas were determined given by C05-C07, C11-13 and C18 codes, which are located especially on the south west of ÇCFPP. While ^{40}K average concentration is 1.1 times higher than the world average, the ^{232}Th and ^{226}Ra average concentrations are 1.7 and 1.3 times higher than the world averages reported in UNSCEAR [23], respectively. The calculated average absorbed dose rate (70 nGy h⁻¹) due to terrestrial radionuclides ^{226}Ra , ^{232}Th and ^{40}K around the ÇCFPP is about 1.2 times higher than the world average value 57 nGy h⁻¹. However, all the calculated Ra_{eq} values representing the environmental effect of natural radionuclides caused by ÇCFPP do not exceed the suggested maximal admissible value 370 Bq kg⁻¹.

Since the new coal-fired power plants are being constructed in our region, the outcomes of this study will supply important data for the future studies. The periodic measurements of radioactivity of soils in the region should be made to evaluate the trends of the radionuclide concentrations.

ACKNOWLEDGEMENTS

The authors would like to thank to Zonguldak Karaelmas University since this work was supported by under the project numbered 2006-70-01-01. The authors would like to thank Sarayköy Nuclear Research and Training Centre of Turkish Atomic Energy Agency for the gamma spectrometric analysis assaying. The authors also would like to thank to Zonguldak Forest Management Directorate for accessing to the sample sites.

REFERENCES

- [1] Papastefanou, C. and Charamalpous, S. (1978) On the radioactivity of fly ashes from coal power plants. *Z. Naturf.*, 34a, 533-537.
- [2] UNSCEAR: United Nations Scientific Committee on the Effects of Atomic Radiation, Sources, Effects Risks of Ionizing Radiation, United Nation, New York, 1988.
- [3] Baba, A. (2002). Assessment of radioactive contaminants in by-products from Yatağan (Muğla, Turkey) coal-fired power plant. *Environ. Geol.* 41, 916-921.
- [4] Pap Z., Dezso Z. and Daroczy, S. J. (2002) Significant radioactive contamination of soil around a coal-fired thermal power plant. *Environ. Radiat.* 59, 191-205.
- [5] Mandal A. and Sengupta D. (2003) Radioelemental study of Kolaghat, thermal power plant, West Bengal, India: possible environmental hazards. *Environ. Geol.* 44, 180-186.
- [6] Mishra, U. C. (2004) Environmental impact of coal industry and thermal power plants in India. *J. Environ. Radiat.* 72, 35-40.
- [7] Mandal A. and Sengupta, D. (2005) Radionuclide and trace element contamination around Kolaghat Thermal Power Station, West Bengal-Environmental implications. *Curr. Sci.* 88, 617-624.
- [8] Wang, L and Lu, X. (2007) Natural radionuclide concentrations in soils around Baoji coal-fired power plant, China. *Radiation. Effect. Defect. Solid.* 162, 677-683.
- [9] Çevik, U., Damla, N., Koz B. and Kaya, S. (2008) Radiological characterization around the Afsin-Elbistan Coal-Fired Power Plant in Turkey. *Energy & Fuel.* 22, 428-432.
- [10] Bem, H., Wieczorkiewska, P. and Budzanowski, M. (2002) Evaluation of technologically enhanced natural radiation near the coal-fired power plants in the Lodz region of Poland. *J. Environ. Radiat.* 61, 191-201.
- [11] Flues, M., Moraes V. and Mazili, B. P. (2002) The influence of a coal-fired power plant operation on radionuclide concentrations in soil. *J. Environ. Radiat.* 63, 285-294.
- [12] Aytekin, H. Bayata, S. Baldık R. and Çelebi N., (2008) Radon measurements in the Çatalağzı thermal power plant, Turkey. *Radiat. Protect. Dosim.* 128, 251-253.
- [13] Turhan, S. , Parmaksız, A., Köse, A., Yüksel, A., and B. Yücel (2010), Radiological characteristics of pulverized fly ashes produced in Turkish coal-burning thermal power plants, *Fuel*, 89, 2528–2535.
- [14] Turhan, S., Arıkan İ.H., Yücel B., Varinlioğlu A. and Köse, A. (2010) Evaluation of the radiological safety aspects of utilization of Turkish coal combustion fly ash in concrete production. *Fuel*, 89, 3892-3900.
- [15] Aytekin, H. and Baldık, R. (2008) On the radiological character of a coal-fired power plant at the town of Çatalağzı, Turkey. *Tr. J. of Phys.* 32, 101-105.
- [16] Uyar G., Ören, M., Yıldırım, Y. and İnce, M. (2007). Mosses as indicators of atmospheric heavy metal deposition around a coal-fired power plant in Turkey. *Fresen. Environ. Bull.* 16, 182-192.
- [17] Durgun D. and Genç A., (2009) Effects of coal properties on the production rate of combustion solid residue, *Energy*, 34, 1976-1979.

- [18] Turner, D. B. (1994) Workbook of Atmospheric Dispersion Estimates: An Introduction to Dispersion Modeling, (Second Edition), CRC Press, Florida.
- [19] Holzwarth, G. C. (1967) Mixing Depths, Wind Speeds and Air Pollution Potential for Selected Locations in the United States. *J. Appl. Met.* 6, 1039-1044
- [20] Dai, L., Wei, H. and Wang, L. (2007) Spatial distribution and risk assessment of radionuclides in soils around a coal-fired power plant: A case study from the city of Baoji, China. *Environ. Res.* 104, 201-208.
- [21] Cevik, U., Damla, N. and Nezir, S. (2007) Radiological characterization of Cayirhan coal-fired power plant in Turkey. *Fuel*. 86, 2509-2513
- [22] Gür, F. (2006) Determination of radioactive and heavy metal pollution by biomonitoring around west Anatolia coal fired power plants. PhD Thesis (in Turkish) pp. 247.
- [23] UNSCEAR (2000) (United Nations Scientific Committee on the Effects of Atomic Radiation), Exposures from Natural radiation Sources, United Nations, New York.
- [24] Veigaa, R., Sanches, N., Anjos, R.M., Macario, K., Bastos, Iguatemy, J. M., Aguiar, J.G., Santos, A.M.A., Mosquera, B., Carvalho, Baptista Filho, C.M., Umisedo, N.K. (2006) Measurement of natural radioactivity in Brazilian beach sands. *Radiat. Meas.* 41, 186-189.
- [25] UNSCEAR (1993) (United Nations Scientific Committee on the Effects of Atomic Radiation). *Exposure from natural sources of radiation*, United Nations, New York.
- [26] Karahan G. and Bayulkem A. (2000) Assessment of gamma dose rates around Istanbul (Turkey). *J. Environ. Radioact.* 47, 213–221
- [27] OECD (1979) (Organisation for Economic Cooperation and Development). Exposure to radiation from the natural radioactivity in building materials. Report by a Group of the OECD Nuclear Energy Agency, OECD, Paris, France,

Received: January 24, 2011

Accepted: April 06, 2011

CORRESPONDING AUTHOR

Hüseyin Aytekin
 Zonguldak Karaelmas University
 Sciences and Arts Faculty
 Department of Physics
 67100 İncivez, Zonguldak
 TURKEY

Phone: +90372 2574010/1751
 Fax: +90372 2574181
 E-mail: aytekin@karaelmas.edu.tr;
 huseyinaytekin@gmail.com

EFFECT OF ADAPTED CONSTRUCTED FLORA ON CONTINUOUS COUPLED AEROBIC-ANAEROBIC PROCESS FOR TREATMENT OF TOMATO PASTE WASTEWATER

Peng Cao^{1,2}, Chun Li³, Shumei Wen², Yanbin Tong² and Jinren Ni^{1,*}

¹Department of Environmental Engineering, Peking University; The Key Laboratory of Water and Sediment Sciences, Ministry of Education, Beijing 100871, China

²School of Chemistry and Chemical Engineering of Shihezi University; Xinjiang Key Laboratory for Green Processing of Chemical Engineering of Xinjiang Bingtuan, Shihezi 832003, China

³College of Life Science of Beijing Institute of Technology, Beijing 100081, China

ABSTRACT

Adapted flora was constructed to increase the efficiency of tomato paste wastewater treatment in a continuous coupled aerobic-anaerobic process. Four aerobic strains, i.e. *Bacillus subtilis* (JH642), *Pseudomonas putida* (KT2440), *Bacillus megaterium* (DSM319), and *Comamonas testosteroni* (CNB-2), were mixed with other three aerobic strains such as *Bacillus cereus* (F65185), *Bacillus* sp. (B-14911), and *Micrococcus* (FJ1443) to modify the settling property in the aerobic flora, whilst six anaerobic strains including *Clostridium bartletti* (DSM16795), *Alkaliphilus metallireducens* (QYMF), *Clostridium botulinum* (ATCC19397), *Bacillus thuringiensis* (IBL200), *Bacteroides* sp. (controll168), and *Bacillus cereus* (NVH0597-99) were used for sludge reduction in the anaerobic flora. It was found that aerobic strains led to a mean COD removal ratio of 84.98% solely by the aerobic flora for a given influent COD of 700 to 1900 mg/L. Moreover, the addition of anaerobic flora for the given influent COD of 1000 to 1900 mg/L resulted in a higher mean COD removal ratio of 93.33% and considerably reduced the sludge production ratio from 0.3107 g SS/g COD to 0.0167 g SS/g COD. Therefore, the adapted constructed flora is of significance not only to efficient treatment of tomato paste wastewater but also to reduction of excess sludge discharge which has been harassed to environmental engineers.

KEYWORDS: artificially constructed flora, aerobic process, anaerobic process, coupled, cell disruption, wastewater treatment

1. INTRODUCTION

Million tons of untreated tomato paste wastewater was discharged every year in Xinjiang, China, which definitely led to serious pollution and water resource shortage [1] and thus limited the normal development of tomato paste processing industries.

The distinctive characteristic of tomato paste wastewater is seasonal dependent. In general, the tomato harvesting and processing season lasts about 90 days each year. Especially in Xinjiang, one of the major areas with tomato paste processing industries, the harvesting and processing season lasts only 40 to 60 days. The short period of tomato production also implies a short period of operation of tomato paste wastewater treatment system. In fact, efforts have been made on tomato paste wastewater treatment at laboratory scale, such as the bench- and pilot-scale an-aerobic/ aerobic system [2], upflow anaerobic sludge blanket UASB-anoxic-oxic system [3], and coupled aerobic-anaerobic system [4]. More work needs to be done to utilize these systems for engineering practice. One of the most difficult issues is related to the adaptation and conservation of sludge due to seasonal requirements.

In recent years, effective microorganisms (EM) have been widely used in treatment of domestic wastewater, landfill leachate and high-concentration industrial wastewater [5, 6]. Moreover, high solution bacteria (HSB) have been reported for its strong degradation capability. The strains in HSB display not only individual functional behavior but also synergy with one another. Hence, HSB has been recombined into different floras to degrade particular pollutant constituents [7].

As far as tomato paste wastewater treatment system is concerned, mixed activated sludge aeration tank in-series plays a key role. Therefore, appropriate sludge becomes a primary limiting factor for an efficient system. To improve

* Corresponding author

the system, a flora consisting of seven aerobic and six anaerobic strains was constructed for treating tomato paste wastewater in coupled aerobic-anaerobic system. In our previous study [8], the aerobic flora treated tomato paste wastewater efficiently in shaking flask. The total organic carbon (TOC) removal ratio reached to 78.92%. The anaerobic flora accelerated the lysis of aerobic cells in anaerobic environment. The use of adapted flora could ensure a good treatment effect each year and make the sludge be stored safely, conveniently and cheaply during the non-production season.

To verify the efficiency of adapted flora observed at shaking flask stage, a continuous coupled aerobic-anaerobic system was constructed which was analogous to the practical completely-mixed activated sludge aeration tank in-series in tomato paste wastewater treatment plants. By adding aerobic and anaerobic strains respectively to the corresponding regions, the performance of reactor was evaluated in terms of chemical oxygen demand (COD) removal, mixed liquor suspended solids (MLSS) concentration, and suspended solid (SS) concentration with varying dissolved oxygen (DO) during continuous operation.

2. MATERIALS AND METHODS

2.1. Experimental apparatus and procedure

Figure 1 shows a schematic diagram of continuous coupled aerobic-anaerobic system, consisting of a reservoir, reactor, secondary sedimentation tank, influent pump, effluent pump, and aeration pump. The reactor tank measured 54 cm×54 cm×59 cm (L×W×H), and the whole volume was 172 L.

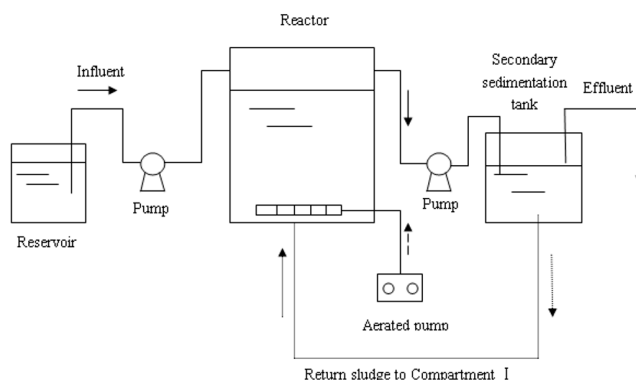


FIGURE 1 - Schematic diagram of the continuous coupled aerobic-anaerobic process.

Figure 2 shows the structure of reactor which was divided into four compartments. The central part in each compartment was the anaerobic region surrounded by wire netting and fully packed by slag. The remaining part was the aerobic regions. Along with aeration impulses from bubbles entering the tank, flow circulations developed between the aerobic and anaerobic regions, thus producing a simultaneous coupled aerobic-anaerobic treatment. It was found that this coupled aerobic-anaerobic treatment pro-

cess led to improved treatment efficiency and very low sludge yields [4].

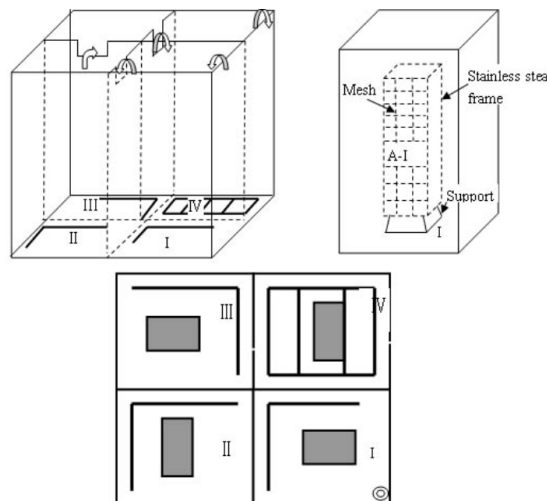


FIGURE 2 – Reactor structure. The thick solid lines indicate the location of the aeration tubes immediately below the base of the reactor, the shaded areas refer to the anaerobic regions. □ is the inlet. Arrows indicate the flow direction. A-I refers to the anaerobic region in compartment 1.

Continuous treatment was achieved due to the liquid-level difference between adjacent compartments. The liquid levels in four compartments were 52, 49, 46, and 46 cm, respectively, corresponding to treatment volumes of 38, 36, 34, and 34 L. The total treatment volume was 142 L before adding the anaerobic regions. The anaerobic region volumes were 5.8, 6.2, 6.4, and 6.8 L, respectively, corresponding to porosities of 55.2%, 54.8%, 54.7%, and 54.4%. Hence, the anaerobic treatment volume was 13.8 L, and the aerobic treatment volume was 116.8 L after coupling the anaerobic regions. Aeration tubes were located with their openings at the base of reactor, as shown in Figure 2. Each aeration tube had a 2–3 mm diameter opening through which bubbles passed to induce circulatory flow. The aeration rate of whole reactor was 6.0 m³/h throughout the whole treatment process. The volume of the secondary sedimentation tank was 11.8 L.

Table 1 lists the characteristics of tomato paste wastewater continuously pumped into the reactor throughout the start-up and test periods. Influent and effluent flows were controlled by peristaltic pumps.

TABLE 1 – Characteristics of wastewater from tomato paste processing

Constituent	Concentration (mg/L)
COD	600 – 2000
BOD	350 – 1000
TN	< 0.5
TP	2 – 5
SS	50 – 80

The culture of anaerobic flora in tomato paste production plant is relatively difficult and expensive. However,

using aerobic flora in a completely-mixed activated sludge aeration tank in-series is relatively simple. To identify the effects of aerobic and anaerobic flora respectively, the treatment process was divided into two stages with total period of 65 days.

Test I was comprised solely by aerobic treatment process. Seven aerobic strains were cultured in shaking flask. About 2000 ml of aerobic liquid (0.4633 g DCW/L) was added into four compartments. The start-up period lasted three days. Test I was run for the next 33 days, with wastewater influent at a rate of 9.6 L/h. However, at day 27, the anaerobic region of Compartment I was tentatively added. At the conclusion of Test I, the other anaerobic regions were added. The volume of anaerobic liquid added into each anaerobic region was 500 ml (0.3874 g DCW/L).

Test II commenced for evaluating the coupled aerobic-anaerobic effects, which lasted for another 32 days with influent at rate of 8.8 L/h.

In the previous screening process, the treatment time was set to 12 h or 24 h. The flora effected within 12 h [8]. The hydraulic retention time (HRT) of treatment system in tomato paste production plant was generally 12 to 18 h. Consequently, the HRT during the period of operation was initially set to 15 h and then adjusted to 14.79 h for better control of the pump. The HRTs of each reactor in Test I were 3.96, 3.75, 3.54, and 3.54 h, whereas those in Test II were 4.01, 3.76, 3.52 and 3.50 h, respectively. During the actual treatment of tomato paste wastewater, the temperature was not controlled. Hence, the treatment temperature in this research was the room temperature ranged from 20 °C to 38 °C. The pH of tomato paste wastewater was generally from 4.5 to 6.0. According to the previous study, lower pH did not influence the treatment effect. Thus the influent pH was not adjusted. Activated sludge, except a small part of excess sludge discharged, in the secondary sedimentation tank was returned to Compartments I. In addition, DO variation in the aerobic and anaerobic regions during Test II was given in Table 2.

TABLE 2 - DO concentrations in aerobic and anaerobic regions at the end of Test II .

Aerobic region	Concentration (mg/L)	Anaerobic region	Concentration (mg/L)
I	0.43 – 0.69	A-I	0.02 – 0.05
II	2.15 – 2.63	A-II	0.03 – 0.07
III	2.76 – 2.95	A-III	0.04 – 0.12
IV	3.04 – 4.10	A-IV	0.11 – 0.24

2.2. Adapted constructed flora

The flora consisted of seven aerobic strains and six anaerobic strains. These strains were screened from acclimated sludge in tomato paste wastewater drainage pipe in Shihezi, China. Capabilities of aerobic strains estimated in terms of TOC removal rate (in 12h), sludge yield (expressed by the increment of cell growth/TOC removal rate), and settling property (expressed by OD₆₀₀ of the supernate

stand for 30 min after treating tomato paste wastewater for 12h). A fundamental flora includes four strains, i.e. *Bacillus subtilis* (JH642), *Pseudomonas putida* (KT2440), *Bacillus megaterium* (DSM319), and *Comamonas testosteroi* (CNB-2), which corresponds to OD₆₀₀ of 0.48 and re-sults in TOC removal rate and sludge yield of 82.06% and 0.97, respectively. The final aerobic flora was constructed by adding three settlement-promoting strains such as *Bacillus cereus* (F65185), *Bacillus sp.* (B-14911), and *Micrococcus* (FJ1443). As results, minor decrease of TOC re-moval rate in the modified aerobic flora occurred with a slight reduction of sludge yield and considerable drop of OD₆₀₀ [8].

The anaerobic flora was constructed from six strains identified as *Clostridium bartlettii* (DSM16795), *Alkaliphilus metallireducens* (QYMF), *Clostridium botulinum* (ATCC19397), *Bacillus thuringiensis* (IBL200), *Bacteroides sp.* (controll 168), and *Bacillus cereus* (NVH0597-99). Selection of these strains was based on their capability to lyse aerobic cells and use the degraded products of aerobic cells in anaerobic environment. When treating a mixture of aerobic cells and wastewater treated by aerobic strains, the anaerobic flora can effectively degrade aerobic cells and fully use degraded products.

2.3 Analytical methods

Samples were collected daily from the inlet, Compartment IV, and the secondary sedimentation tank. COD, MLSS, and SS were measured by standard methods [9]. DO was measured using a DO electrode connected to a DO meter (sension156, HACH COMPANY, American). All measurements were repeated three times.

3. RESULTS AND DISCUSSION

3.1 Test I: COD removal

Figure 3 shows the influent COD and effluent COD during Test I. For influent COD ranged from 700 to 1900 mg/L, the mean effluent COD was 205.01 mg/L. The mean removal rate was 84.98% with deviation of ± 0.0424 implied a fair performance of the aerobic flora, but it was still not up to the discharge standard of COD ≤ 150 mg/L [10]. The COD removal rate was slightly lower than expected due to small number of strains in the flora and the simple biological chain. The simple chain limited the degradation of the metabolites and prevented the further decrease of the effluent COD.

3.2 Test I: MLSS

The returned sludge was fed to the first compartment and distributed to other chambers with water flow. The sludge in Compartment IV was barely influenced by the returned sludge and received sludge from the anterior compartments. Thus, the sludge concentration in Compartment IV could accurately reflect the sludge concentra-

tion in the reactor. Figure 4 shows the rapid increase of MLSS in Compartment IV during Test I. MLSS reached

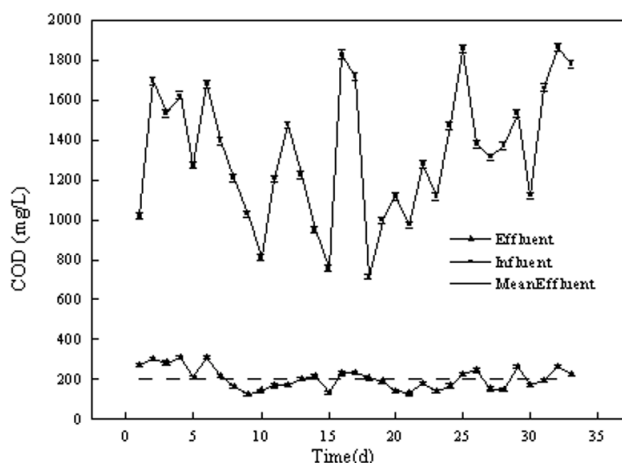


FIGURE 3 - Variation of the COD concentrations in the influent and effluent during test I.

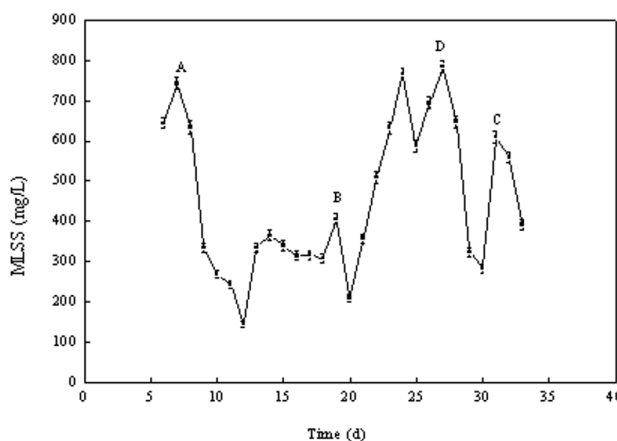


FIGURE 4 – Variation of the MLSS in the compartment IV during test I. A, B and C are the time of sludge discharge. D is the time of adding anaerobic region in compartment I of the reactor.

to 743 mg/L just after 8 days which implied that sludge discharge was necessary. During Test I, sludge discharge was implemented three times. The total discharged sludge was 1304 g (centrifugation at 3600 rpm for 20 min to remove water). The sludge discharge did not mean an immediate reduction of MLSS to a low level in Compartment IV, considering that 11.4 h was entailed for Compartment IV to be adjusted to the reduced sludge concentration after receiving sludge from Compartments I, II, and III. However, the sludge reaccumulation in reactor would result in increase of MLSS again. In the aeration tank of the conventional activated sludge process, the MLSS is usually 1.5 to 3.0 g/L [11]. Nevertheless, the MLSS in the present system was only 0.2 to 0.8 g/L, reduced about 1/3 to 1/2 comparing with that in conventional activated sludge systems. The added flora into open reactor became dominant stock. The proportion of degrading dominant strains in the sludge was higher than that in conventional activat-

ed sludge. This may have contributed to the lower MLSS values compared with those obtained from conventional activated sludge treatment process.

On the other hand, the food/wastewater (F/M) in Test I (day 6 to day 28) ranged from 2.4 to 8.22 kg COD/kg MLSS·d with the sludge retention time (SRT) of 1.81 d at the stationary phase. The average F/M was 4.07 kg COD/kg MLSS·d, which was about 5.09 to 10.17 times of that in conventional activated sludge system. The unit quality sludge could treat more pollutants because of higher proportion of degrading dominant strains, thereby producing a higher F/M.

3.3 Test I: SS

Figure 5 shows the effluent SS from secondary sedimentation tank during Test I. The concentration was slightly high (a mean value of 149.39 mg/L), and sometimes exceeded the discharge standard of SS≤150 mg/L [10]. Although the surface load of secondary sedimentation tank was increased to 0.31 m³/ (m²·h), it did not reduce the SS of effluent because of the presence of fine floccules which were difficult to settle down. Although settling-dominant strains were included in the flora, the other degradation-dominant strains kinds nevertheless limited the resulting improvements to the settling process. On the other hand, there was a positive correlation between the SS and the MLSS. At day 20, the sludge discharge caused the reduction in SS concentration. Subsequently, SS increased to its top as MLSS reached peak at Day 26.

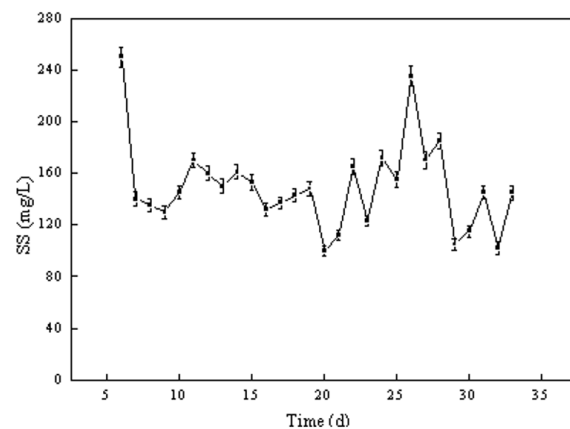


FIGURE 5 - Variation of the SS of the effluent during test I.

The excess sludge yield in Test I included the discharged sludge and the effluent SS. The sludge production ratio (from day 6 to day 28) was 0.3107 g SS/g COD, only about 41.43 to 82.85% of that in conventional activated sludge system [12, 13]. In conventional activated sludge process, many useless strains of microorganisms to degrade pollutants were propagated and produced a considerable amount of excess sludge. However, using the aerobic flora, most of the microorganism strains contributed to the degradation process, and fewer strains were found to be useless.

3.4 Test II: COD removal

Figure 6 shows the influent and effluent COD during Test II. For influent COD ranged from 1000 to 1900 mg/L, the effluent COD was invariably below 150 mg/L with its mean value of 96.45 mg/L and mean removal rate of 93.33% with deviation of ± 0.026 , considerably improved comparing with Test I. Throughout Test II, the effluent quality met the requirement of $\text{COD} \leq 100 \text{ mg/L}$ by Chinese National First-Grade Effluent Standard [10].

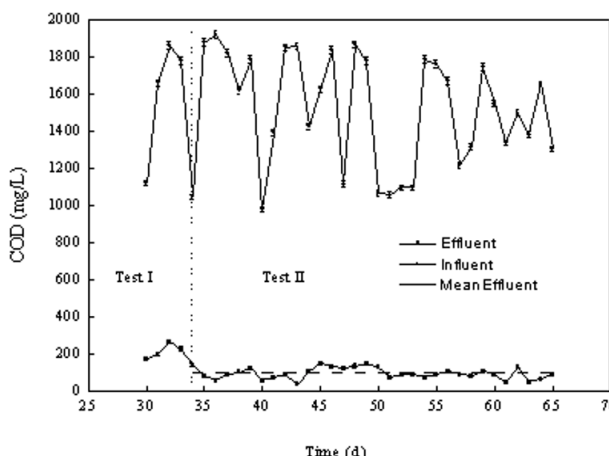


FIGURE 6 - Variation of the COD concentrations in the influent and effluent during test II.

The primary components of effluent COD in Test I were a few pollutant constituents, metabolites of aerobic cells, and fine floccules composed of microorganism strains. Symbiotically, the anaerobic strains used the metabolites produced by the aerobic strains, whereas the aerobic strains used the metabolites produced by the anaerobic strains. Together, the aerobic and anaerobic strains formed a complex degrading chain that effectively reduced the metabolic content of the effluent. Meanwhile, fine floccules of aerobic microorganism strains were degraded by the anaerobic strains after entering anaerobic regions. This was also confirmed by the SS results (see later). Consequently, the overall capability of the system to degrade pollutants was enhanced, thus leading to the lower effluent COD obtained in Test II.

3.5 Test II: MLSS

Figure 7 shows the MLSS in Compartment IV during Test II. After coupling anaerobic regions, MLSS quickly decreased to a stable value around 120 mg/L 5 days before it reached a peak of about 317 mg/L on the 16th day from the start-up of the Test II. This increase was attributed to the growth of aerobic organisms at the surface of anaerobic regions. These organisms blocked some of the flow channels into anaerobic regions as the washing degree was not sufficiently strong. Hence, there was a decrease in aerobic cell decay causing aerobic sludge accumulation. After cleaning the surface of anaerobic regions

and adjusting the aeration angle (increasing the washing degree on the surface of anaerobic regions), the MLSS decreased again to stable levels (100 to 150 mg/L). During Test II, sludge discharge was not implemented.

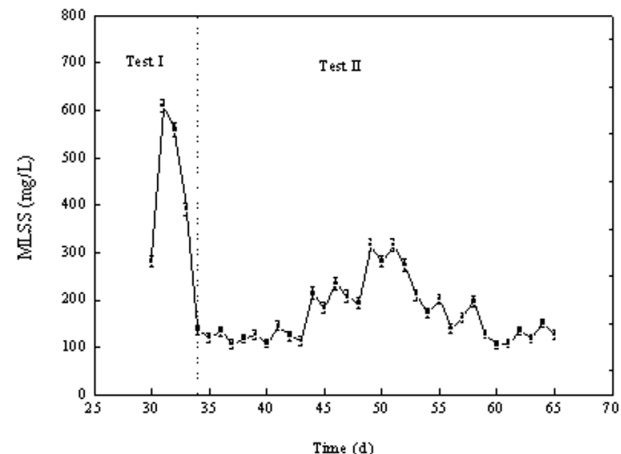


FIGURE 7 – Variation of the MLSS in the compartment IV during test II.

In Test II, the quantity of aerobic microorganisms reached dynamic equilibrium when coupled with anaerobic strains. The aerobic microorganisms consumed pollutants while producing new cells. At the same time, the aerobic cells were continuously degraded after entering anaerobic regions. As a result, accumulation of aerobic strains did not occur in Test II, rendering sludge discharge unnecessary.

3.6 Test II: SS

Figure 8 shows variation of the effluent SS during Test II. After coupling anaerobic regions, SS quickly decreased and stabilized to a mean value of 20.51 mg/L (with a decrease of 86.27% compared with Test I) after 4 days, completely meeting the requirement of $\text{SS} \leq 70 \text{ mg/L}$ by Chinese National First-Grade Effluent Standard [10]. Fine floccules, mostly composed of aerobic cells, were eliminated after entering anaerobic regions, thus causing the reduction in effluent SS in Test II.

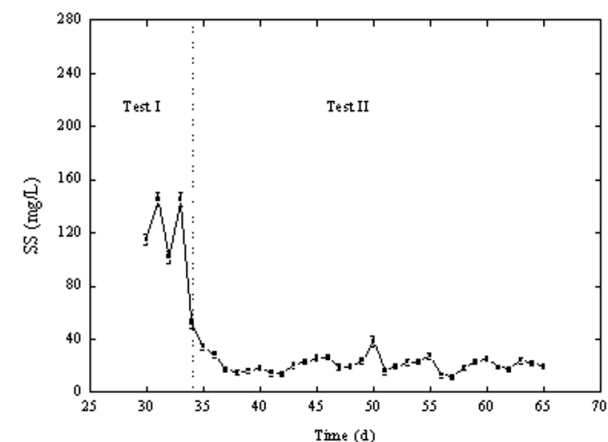


FIGURE 8 - Variation of the SS of the effluent during test II.

No sludge discharge was made in Test II. The effluent SS reflected the level of excess sludge yield in the whole system. In fact, the sludge production ratio was only 0.01667 g SS/g COD in Test II, about 2.22% to 4.45% of that in conventional activated sludge systems. There was no occurrence of sludge blockage and accumulation during Test II. The sludge could be eliminated in the reactor, thereby causing on-site sludge reduction. In addition, the sludge production ratio in Test II was just 27.78% of that in a similar coupled aerobic-anaerobic process (a fixed-bed bioreactor capable of repeatedly coupling aerobes and anaerobes) [14]. Therefore, the adapted anaerobic flora had stronger aerobic cell lytic capability.

4. CONCLUSIONS

The treatment efficiency of adapted constructed flora, which consisted of seven aerobic strains and six anaerobic strains, was examined in a continuous coupled aerobic-anaerobic system which was analogous to a completely-mixed activated sludge aeration tank in-series. The aerobic and anaerobic strains formed a complex degrading chain and effectively degraded pollutants and metabolites, leading to a lower effluent COD. The aerobic cells were degraded by the anaerobes in anaerobic regions, and the lysis products were used by aerobes and anaerobes together, thus leading to much lower sludge production.

Using only aerobic flora, the mean effluent COD was 205.01 mg/L (mean removal rate of 84.98%), and the mean effluent SS was 149.39 mg/L. However, coupling of aerobic and anaerobic flora would further reduce the mean effluent COD to 96.45 mg/L (mean removal rate of 93.33%), and the mean SS to 20.51 mg/L, satisfactorily meeting requirements of Chinese National First-Grade Effluent Standard (GB 8978-1996). The sludge production ratio was reduced to 0.01667 g SS/g COD, and sludge discharge was almost not required. The adapted constructed flora was of great help to tomato paste wastewater treatment in engineering applications.

ACKNOWLEDGMENTS

This study is partially supported by the National Natural Science of China (grant No. 20776017), Bingtuan Doctor Foundation (grant No. 04BSZJ05), and the High-level Talent Start Fund Project of Shihezi University (grant No. RCZX2004-YS10).

REFERENCES

- [1] Han, Q.Q., Yang, Y.H., and Jiang, F.Q. (2006). Disposal and utilization measures of the wastewater produced in the tomato paste production in Xinjiang. *Arid Environ. Monito.*, 97-103.
- [2] Xu, Z.D., and Nakhla, G. (2007). Prefermentation to overcome nutrient limitations in food processing wastewater: Comparison of pilot-and bench-scale systems. *Biochem. Eng. J.*, 16-25.
- [3] Gohil, A. and Nakhla, G. (2006). Treatment of tomato processing wastewater by an upflow anaerobic sludge blanket-anoxic-aerobic system. *Bioresour. Technol.*, 2141-2152.
- [4] Li, W.J., Cao, P., Li, C., and Lu, J.J. (2006). Treatment of organic wastewater from tomato paste processing by coupled aerobic-anaerobic process. *J. Chem. Indus. Eng.*, 2970-2975.
- [5] Jin, M., Wang, X.W., Gong, T.S., Gu, C.Q., Zhang, B., Shen, Z.Q., and Li, J.W. (2005). A novel membrane bioreactor enhanced by effective microorganisms for the treatment of domestic wastewater. *Appl. Microbiol. Biotechnol.*, 229-235.
- [6] Qiu, Z.P., Liu, Y.Y., Yang, L.Z., Wu, M., and Wang, Y.J. (2009). Treatment of landfill leachate by effective microorganism. *Int. J. Environ. Pollut.* 39-47.
- [7] Wang, Y.B. (2001). Characteristics of high solution bacteria technique and its application to high-concentration wastewater treatment. *Water Res. Prot.*, 23-24.
- [8] Wen, S.M., Li, C., Lu, J.J., and Cao, P. (2009). Comparative study on the properties of aerobic strains in an aerobic-anaerobic coupled reactor. *J. Chem. Indus. Eng.*, 2067-2073.
- [9] Wei, F.S. (2002). National environmental protection agency, monitoring, and analysis method of water and wastewater. Beijing: China Environmental Science Press.
- [10] Chinese Environment Protection Agency. (1996). Integrated wastewater discharge standard (GB 8978-1996). Beijing: China Environmental Science Press.
- [11] Galapate, R.P., Agustiani, E., Baes, A.U., Ito, K., and Okada M. (1999). Effect of HRT and MLSS on THM precursor removal in the activated sludge process. *Water Res.*, 131-136.
- [12] Low, E. W., and Chase, H. A. (1999). Reducing production of excess biomass during wastewater treatment. *Water Res.*, 1119-1132.
- [13] Tchobanoglous, G., and Burton, F.L. (1991). Wastewater engineering: treatment, disposal and reuse, Third edition. New York: McGraw-Hill, Inc.
- [14] Feng, Q., Yu, A.F., Chu, L.B., and Xing, X.H. (2008). Performance study of the reduction of excess sludge and simultaneous removal of organic carbon and nitrogen by a combination of fluidized- and fixed-bed bioreactors with different structured macroporous carriers. *Biochem. Eng. J.*, 344-352.

Received: January 31, 2011

Accepted: April 06, 2011

CORRESPONDING AUTHOR

Jinren Ni

Department of Environmental Engineering
Peking University
Beijing 100871

P.R. CHINA

Phone.: 0086-10-62751185
Fax: 0086-10-62756526;
E-mail: nijinren@iee.pku.edu.cn

FEB/ Vol 20/ No 7/ 2011 – pages 1649 – 1654

COMPARISON OF ELEMENT CONTENTS IN HAZELNUTS GROWN UNDER ORGANIC AND CONVENTIONAL FARMING REGIMES FOR HUMAN NUTRITION AND HEALTH

Uğur Akbaba^{1,*}, Yusuf Şahin² and Hasan Türkez³

¹Ministry of National Education, 25100, Erzurum, Turkey

²Department of Physics, Faculty of Science, Atatürk University, 25240, Erzurum, Turkey

³Department of Biology, Faculty of Science, Atatürk University, 25240, Erzurum, Turkey

ABSTRACT

A comparative study on elemental composition of various hazelnut (*Corylus avellana* L.) samples was conducted by using a sensitive method, wavelength dispersive X-ray fluorescence (WDXRF). Twenty-eight elements, such as Al, As, Bi, Ca, Cd, Cu, Fe, Mn, Ni, P, S, Sr, Zn, Cl, Pb, K, Mg, Na, Ba, Rb, Si, Br, Cr, F, La, Se, Ti and Zr, were determined in hazelnut samples (n=10) grown under organic and conventional farming regimes. The obtained results from each group were analyzed statistically by using SPSS statistic program. It was observed that the concentration and peak intensity values of Ca, Fe, Mn, P, Mg, Zn, Cl, Na, Br, Rb, F, K and Se elements were higher in hazelnut samples grown under organic farming regime but Al, Cr and Ni levels were found to be higher in samples grown under conventional farming regime. As, Bi, Cd, Pb, Ti and Zr contents were below the detection limits. Our findings clearly revealed that organic hazelnuts are likely to have higher nutritional mineral content. And the hazelnuts samples grown under conventional farming regime could contain harmful metals like Al, Cr and Ni that might affect the various systems and/or organs of humans and animals.

KEYWORDS: Quantitative determination, elemental analysis, hazelnut, organic farming, conventional farming.

1. INTRODUCTION

Organic farming is a kind of production in which the use of synthetic fertilizers, pesticides, growth regulators, and livestock feed additives is prohibited or minimized. Organic farming has become a highly popular notion in recent years. In particular, the claims that food obtained by conventional farming methods cause some health prob-

lems, claims which have been scientifically proven, have increased the growing interest in organic farming [1]. The rate of birth defects is increased in the regions where chemicals, such as pesticides, fungicides, and herbicides, are extensively used [2]. Moreover, cancers of the throat, breast, stomach, eye, and nose were found to be common among farmers who are directly exposed to chemicals [3]. In fact, in Minnesota, cancer rates were statistically found to be higher in agricultural regions where chemicals are extensively used [4]. Traces of synthetic flavorings and colorings were observed in elemental analyses of the blood, hair and skin samples of hyperactive children [5]. In a study carried out with preschool children, a group of children consumed conventional diets, while another group received organic diets, and subsequent examinations of their blood and urine samples revealed that pesticide residues were six times higher in those from children consuming conventional diets [6].

Organic farming is also important for sustainable agriculture, food quality, soil and environmental health. It was observed that conventional farming reduces organic soil content and decreases biological activity in soil; on the contrary, organic farming increases microbiological activity in soil [7]. Soil quality has been investigated chemically and biologically in soils receiving long-term conventional and organic farming activities and, as a result, soils receiving organic farming were observed to have much better nutritional status [8]. At this point, consumers are looking for variety in their diets and are aware of the health benefits of fruits and vegetables. Of special interest are food sources rich in elemental nutrients including Ca, Mg and K. In fact, the intakes of these nutrient elements are associated with reduced risk of cardiovascular disease, stroke, and cancers of the mouth, pharynx, esophagus, lungs, stomach, and colon [9]. On the contrary, ingestion of metals, especially heavy metals, through fruits or vegetables can cause accumulation in organisms, producing serious health hazards, such as injury to the kidney, symptoms of chronic toxicity, renal failure and liver damage [10].

* Corresponding author

To our best knowledge, there is no report on the elemental contents of hazelnuts which were grown under organic and conventional farming regimes in literature. In the present study, the Al, As, Bi, Ca, Cd, Cu, Fe, Mn, Ni, P, S, Sr, Zn, Cl, Pb, Cl, K, Mg, Na, Ba, Rb, Si, Br, Cr, F, La, Se, Ti and Zr element contents of hazelnuts grown under organic and conventional farming regimes are determined by wavelength-dispersive X-ray fluorescence spectrometry (WDXRF) method for the first time, since the advantages of X-ray fluorescence spectrometry are increasingly relevant in applications to the analysis of clinical and biological materials as demand increases for non-destructive and/or spatially resolved determinations [11].

2. MATERIALS AND METHODS

2.1. WDXRF system

WDXRF system consists of detector, amplifier, discriminator, counter and printer units. The detector converts the falling X-rays into measurable pulses (X-ray detectors used in the following three spectrometers: proportional, gas flow and scintillation detectors). Discriminator filters allow the pulses coming from the detector to pass through a gate of certain pulse height. These pulses are saved in a recorder. If required, the number of pulses (of violence) against the wavelength and the angle of reflection spectrum is obtained by drawing the figure. Fig. 1 shows the used WDXRF system and its units.

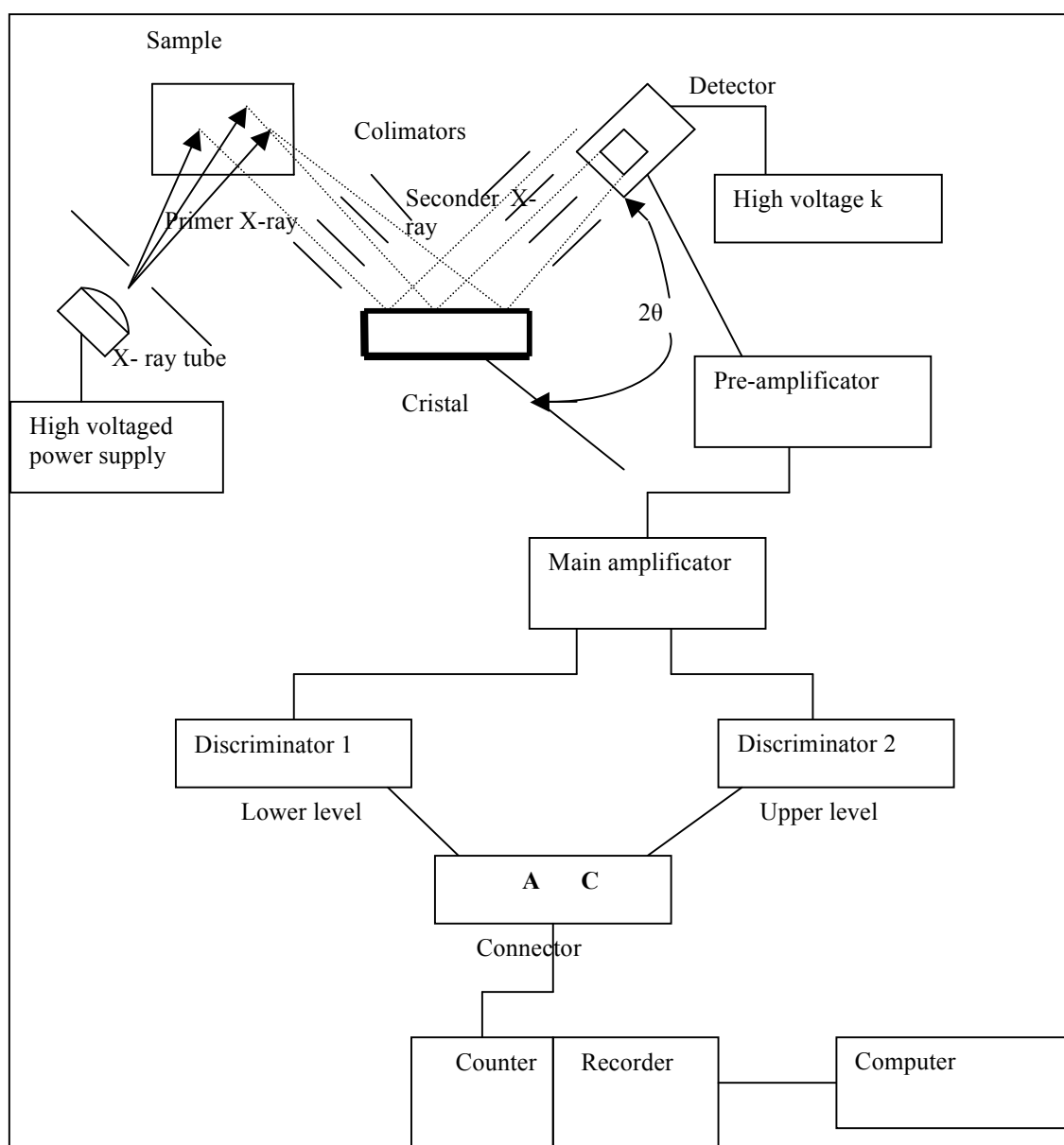


FIGURE 1 - The used WDXRF system and its units.

2.2. The Use of the WDXRF System in Elemental Analysis of Plant Samples

In this study, an agate mortar, a digital scale (Ohaus TS 120, USA), a hydraulic press (Spex P_{max}=3.5×10³ kg/m²), a WDXRF spectrometer (ZSX-100e with rhodium target X-ray controlled by a software ZSX computer) were used. Both hazelnut samples were purchased from a local certified company in Ordu City, Turkey. They were picked up from closer regions during the same harvest period. Under organic farming regime area, chemical inputs, synthetic chemical pesticides, growth regulators, synthetic compound fertilizers, hormones, preservatives, colorings or artificial additives were not used in processing for at least seven years but, in contrast, these inputs were used in conventional farming regime.

2.3. Sample Preparation

The hazelnut samples were ground and mixed in an agate mortar. Since the vacuum conditions of the sample chamber of the system were affected by humidity, the samples were dried at 60 °C for 35 min. The amount of dry matter can decrease as a result of annealing process. Annealing time was short and annealing temperature was low. Because of these reasons, a serious reduction in the quantity and content was not observed. Since the hazelnut samples are oily, a Mylar film was used. The samples were prepared between the Mylar film sheets, and the effect of the films were eliminated by using an analysis

program in the system. 10 organic and 10 conventional samples of 770 mg were analyzed on the sequential ZSX 100e WDXRF spectrometer equipped with a Rh X-ray tube. Matrix-correction process was made automatically by this system. Room temperature was 20-21 °C (on average) and environment was relatively dry. The elementary differences were investigated between the hazelnuts grown under organic and conventional farming regimes. The obtained spectra were drawn using Origin 7.0 software. Ten samples from each of the two groups were prepared for good counting statistics.

2.4. Statistics

The obtained results were statistically examined using SPSS statistical software and t-test to investigate whether the differences observed between element concentrations and peak intensities in each group were statistically significant.

3. RESULTS

Concentrations and peak intensities of Al, As, Bi, Ca, Cd, Cu, Fe, Mn, Ni, P, S, Sr, Zn, Cl, Pb, Cl, K, Mg, Na, Ba, Rb, Si, Br, Cr, F, La, Se, Ti and Zr were measured for each sample. The results of the measurements are given in Table 1. The intensities were plotted as the function of diffraction angle for some elements in the organic sam-

TABLE 1 - Concentrations and peak intensities of 28 elements for hazelnut samples.

ELEMENTS	CONCENTRATION (%)		PEAK INTENSITY (counts per second)		DETECTION LIMITS (ppm)	
	Organic	Conventional	Organic	Conventional	Organic	Conventional
Al	0.0022	0.0037 [#]	0.0911	0.0345 [#]	0.0002	0.0002
Bi	ND	ND	ND	ND	ND	ND
As	ND	ND	ND	ND	ND	ND
Cd	ND	ND	ND	ND	ND	ND
Ca	0.1331	0.1308 [#]	52.7800	52.1357 [#]	0.0001	0.0002
Cu	0.0011	0.0009	1.9553	1.7464	0.0001	0.0001
Fe	0.0182	0.0151 [#]	12.2149	10.2159 [#]	0.0001	0.0001
Mn	0.0114	0.0080 [#]	4.5948	2.2311 [#]	0.0007	0.0003
Ni	0.0005	0.0005 [#]	0.7625	0.7861 [#]	0.0001	0.0001
P	0.1089	0.1063 [#]	32.095	31.4342 [#]	0.0001	0.0002
S	0.0614	0.0633	0.0002	0.0002	16.0537	15.2587
Sr	0.0001	0.0002	1.4861	1.5185	0.0000	0.0000
Zn	0.0657	0.0588 [#]	156.6867	140.1591 [#]	0.0001	0.0001
Cl	0.0113	0.0043 [#]	0.5225	0.1967 [#]	0.0008	0.0011
Pb	ND	ND	ND	ND	ND	ND
K	0.4718	0.4544 [#]	189.3847	182.8199 [#]	0.0002	0.0002
Mg	0.0154	0.0112 [#]	0.2407	0.1762 [#]	0.0005	0.0008
Na	0.0080	0.0059 [#]	0.0444	0.0334 [#]	0.0009	0.0010
Ba	0.0022	0.0022	0.8982	0.9086	0.0006	0.0006
Rb	0.0004	0.0002 [#]	3.3999	1.9943 [#]	0.0000	0.0000
Si	0.0013	0.0013	0.1301	0.1327	0.0002	0.0002
Br	0.0014	0.0005 [#]	4.0123	1.8160 [#]	0.0001	0.0001
Cr	0.0006	0.0009 [#]	0.1830	0.2545 [#]	0.0002	0.0002
F	0.0308	ND	0.0045	ND	0.0163	ND
La	0.0031	0.0029	0.9068	0.8783	0.0008	0.0008
Se	0.0003	ND	0.0001	ND	1.1148	ND
Ti	ND	ND	ND	ND	ND	ND
Zr	ND	ND	ND	ND	ND	ND

Results of the analysis are given as "average ± standard deviation", as 10 samples from each of the two groups were prepared; ND: Not detected; # means statistically different from organic farming regime at the level of 0.05 for same elements.

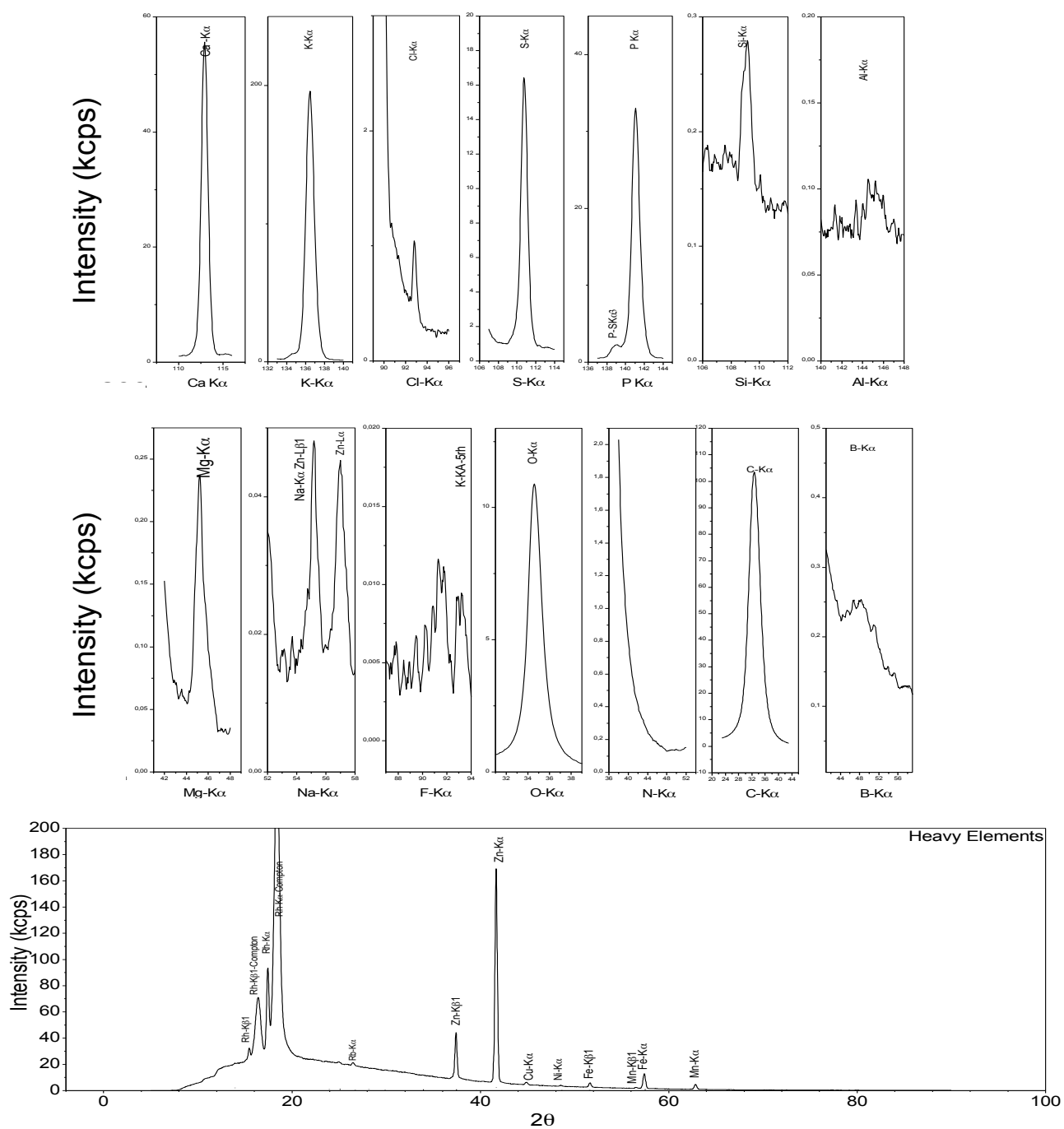


FIGURE 2 - The intensities of some elements versus diffraction angle obtained from the hazelnut sample grown under organic farming regime.

ples (Fig. 2). The statistical analyses of our findings revealed that Ca, Fe, Mn, F, P, Cl, K, Mg, Br, Rb, Na, Zn and Se element contents were higher in hazelnut samples grown under organic farming regime but those of Al, Cr and Ni were found to be lower. However, the amounts of some elements (Cu, S, Sr, Ba, Si and La) did not show any alterations as compared to each other. On the other hand, As, Bi, Cd, Pb, Ti and Zr were not detected in both samples.

4. DISCUSSION AND CONCLUSIONS

Elemental analysis of plant samples is essential in monitoring plants' development, determination of their nutritional value and nutrient insufficiency, and to check for diseases. In the present study, we determined element contents of hazelnut samples by WDXRF method since analytical performance of this method previously proposed proved to be effective and robust [12]. Only a very lim-

ited number of studies in which elemental analyses were carried out on agricultural products could be found. The mineral contents of several products like mulberry [13], chickpea [14], tea [15], tobacco [16] and beans [17] but not hazelnuts were examined by using WDXRF system.

Koksal et al. [18] determined the mineral contents of hazelnut varieties grown in the Black Sea Region of Turkey by using atomic absorption spectrophotometry (AAS). The researchers did not take care of farming regimes. They have found K, Mn, Mg, Ca, Fe, Zn, Na and Cu levels to be 6.64 mg/770 mg, 1.43 mg/770 mg, 1.33 mg/770 mg, 0.043 mg/770 mg, 0.032 mg/770 mg, 0.022 mg/770 mg, 0.020 mg/770 mg and 0.017 mg/770 mg, respectively. The present findings clearly revealed that only Ca level (0.13 mg/770 mg) determined in organic farming area was higher than the levels reported by Kocsal [18], and the other seven elements were determined in lower concentrations.

In addition to this study, Alasalvar et al. [19] examined the Al, Cd, Cl, Cr, Co, Cu, Fe, Pb, Mg, Mn, Ni, P, K, Se, Ag, Na, V and Zn element contents of Tombul (Round) hazelnut, grown in the Giresun province of Turkey by using AAS. Similarly, these researchers did not aim on farming regimes. They have determined the Cr, Se and Zn levels as 0.00007 mg/770 mg, 0.0004 mg/770 mg and 0.0149 mg/770 mg, respectively. Herein, these 3 elements were found in higher levels in organic farming regime area compared to Alasalvar et al. [19], but Al, Cl, Cu, Fe, Mg, Mn, Ni, P, K and Na levels were found to be lower. However, due to differences of the applied techniques, the concentrations of some elements including Cd, Co, Pb, Ag and V, could not be detected in the present study.

The element profile of Turkish hazelnuts was investigated by inductively coupled plasma mass spectrometry and atomic absorption spectroscopy techniques, and reported to be an important microelement source for human nutrition and health [20]. In this investigation, we found statistically important alterations in the element contents of hazelnuts grown under organic and conventional farming regimes. Similarly, Beyhan et al. [21] compared the Cu, Mn, Ni, Co, Fe, Zn contents of hazelnut varieties near and far from an industrial area, by using a flame and graphite furnace atomic absorption spectrometry technique. Their findings showed that Mn and Co concentrations in hazelnuts of both areas were generally correlated with the degree of trace element contamination in the environment. Also, paddy plants grown by an organic development program were compared with paddies grown by conventional farming methods, and it was found out that organic paddy was richer in elements, such as N, P, K, Ca and Mg, and was highly balanced nutritionally [22]. Likewise, it was reported that large differences in the elemental balances of vegetal products between organic and conventional dairy farming exist [23, 24].

The WDXRF analysis of this study indicated that Ca, Fe, Mn, F, P, Cl, K, Mg, Br, Rb, Na, Zn and Se contents were higher in hazelnut samples grown under organic farm-

ing regime. This is consistent with analyses of Worthington [25] who also found that organic crops contained significantly more Fe, Mg and P than conventional ones. Again, Gundersen et al. [26] compared the Ca, Mg, Rb and Se contents of onions (*Allium cepa*) from conventionally and organically cultivated sites, and determined significantly different levels between both onion groups. Adotev et al. [27] indicated that the concentration of essential elements in foodstuffs of one region might vary from the other since food supplies are affected by various agricultural practices, type of soil, type of fertilizers and chemicals used, as well as type of pesticides and herbicides sprayed. Therefore, the differences of the applied practices could cause the determined increases of major elements (such as Na, Mg, P, Cl, K and Ca) and some minor ones (Mn, Fe, Zn and Se) in the hazelnuts grown under organic farming regime. On the other hand, food due to the introduction of mechanized farming, ever increasing use of chemicals, sprays, preservatives, food processing, canning etc., are likely to be further contaminated with toxic elements [28]. Previous reports indicated that Al was accepted to be toxic to plants, fish, and higher animals [29, 30]. Likewise, Ni and Cr are toxic to plants and do not play any essential role in plant growth and metabolism [31, 32]. In our study, Al, Cr and Ni were found at higher concentrations (but in permitted levels) in hazelnut samples grown under conventional farming regime. In accordance with our finding, Santos et al. [33] reported that chemicals used in traditional technological coffee farms might cause increase of toxic metal concentrations, such as Cr and Ni in crops and crop soil, being taken up by the plants and entering the food chain.

In conclusion, the determined weight percent concentrations of Ca, Fe, Mn, F, P, Cl, K, Mg, Na, Zn and Se elements (essential for human health) were higher, and the amounts of toxic metals (Al, Cr and Ni) were lower in hazelnut samples grown under organic farming regime. Thus, we could suggest that this farming regime is crucial for the nutritional value of hazelnuts. In addition, from the results obtained in the present study, the usage of WDXRF analysis is an efficient and useful technique which deserves attention for interdisciplinary studies in food science.

REFERENCES

- [1] Çakmakçı, R., Erdoğan, Ü.G. (2008). Organic Farming. 2nd ed. Ataturk University Faculty of Agriculture Publications, Erzurum, Turkey, pp. 355-359.
- [2] Garry, V.F., Schreinemachers, D., Harkins, M.E. and Griffith, J. (1996). Pesticide applicators, biocides and birth defects in rural Minnesota. Environ Health Persp, 104, 394-399.
- [3] Schreinemachers, D.M. (2000). Cancer mortality in four northern wheat-producing states. Environ Health Persp, 108, 873-881.
- [4] Schreinemachers, D.M., Creason, J.P. and Garry, V.F. (1999). Cancer mortality in agricultural regions of Minnesota. Environ Health Persp, 107, 205-211.

- [5] Ward, N.I. (1997). Assessment of chemical factors in relation to child hyperactivity. *J Nutr Environ Med*, 7, 333-342.
- [6] Curl, C.L., Fenske, R.A. and Elgethun, K. (2003). Organophosphorus pesticide exposure of urban and suburban preschool children with organic and conventional diets. *Environ Health Persp*, 111, 377-382.
- [7] Melero, S., Porras, J.C., Herencia, J.F. and Madejon, E. (2006). Chemical and biochemical properties in a silty loam soil under conventional and organic management. *Soil Till Res* 90, 162-170.
- [8] Marinari, S., Mancinelli, R., Campiglia, E. and Grego, S (2006). Chemical and biological indicators of soil quality in organic and conventional farming systems in Central Italy. *Ecol Indic*, 6, 701-711.
- [9] Aberoumand, A. and Deokule, S.S. (2010). Elements evaluation of some edible vegetables and fruits of Iran and India. *Asian J Agric Sci*, 2, 35-37.
- [10] Zahir, E., Naqvi, I.I. and Udin, S.M. (2009). Market basket survey of selected metals in fruits from Karachi City (Pakistan). *J Basic Appl Sci*, 5, 47-52.
- [11] Potts, P.J., Ellis, A.T., Kregsamer, P., Marshall, J., Strel, C., Weste, M. and Wobrauschek, P. (2002). Atomic spectrometry update. X-ray fluorescence spectrometry. *J. Anal. At. Spectrom*, 17, 1439-1455.
- [12] Krishna, A.K., Mohan, K.R. and Dasaram, B.A. (2009). Qualitative application in quantitative determination of major and trace elements in plant species using wavelength dispersive x-ray fluorescence spectrometry. *Atomic Spectroscopy*, 30, 208-217.
- [13] Yigit, D., Akar, F. and Baydas, E. (2010). Elemental composition of various mulberry species. *Asian Journal Chem.*, 22, 3554-3560.
- [14] Erdal, S., Dumlupinar, R. and Cakmak, T. (2010). Determination of some inorganic element concentration changes in germinating chickpea seeds exposed to progesterone and beta-estradiol by using WDXRF spectroscopic technique. *Fresenius Environ Bull*, 19, 507-515.
- [15] Ercisli, S., Demir, F. and Budak, G. (2009). Determination of elemental variations in tea leaves (*camellia sinensis* l) in different harvest time by WDXRF spectrometry. *Asian J Chem*, 21, 1313-1317.
- [16] Camas, N., Karabulut, B. and Karabulut A. (2007). Elemental analysis of some important tobacco varieties (*Nicotiana tabacum* L.) by WDXRF spectroscopy. *Asian J Chem*, 19, 3971-3978.
- [17] Dumlupinar, R., Demir, F. and Bostan, H. (2007). Determination of chilling temperature effects on inorganic element composition and distribution in beans using WDXRF-spectroscopic technique. *Fresenius Environ Bull*, 16, 548-554.
- [18] Köksal, A.I. Artik, N., Şimşek, A. and Güneş, N. (2006). Nutrient composition of hazelnut (*Corylus avellana* L.) varieties cultivated in Turkey. *Food Chem*, 99, 509-515.
- [19] Alasalvar, C., Shahidi, F., Liyanapathirana, C.M. and Ohshima, T. (2003). Turkish tombul hazelnut (*Corylus avellana* L.). 1. compositional characteristics. *J Agric Food Chem*, 51, 3790-3796.
- [20] Simsek, A. and Aykut, O. (2007). Evaluation of the microelement profile of Turkish hazelnut (*Corylus avellana* L.) varieties for human nutrition and health. *Int J Food Sci Nutr*, 58, 677-688.
- [21] Beyhan, O., Elmastas, M. and Genc, N. (2010) Trace elements in some hazelnut varieties near industrial area and far from industrial area in Turkey. *Asian J Chem*, 22, 4040-4044.
- [22] Hasegawa, H., Furukawa, Y. and Kimura, S.D. (2005). On-farm assessment of organic amendments effects on nutrient status and nutrient use efficiency of organic rice fields in Northeastern Japan. *Agr Ecosyst Environ*, 108, 350-362.
- [23] Bengtsson, H., Oborn, I. and Jonsson, S. (2003). Field balances of some mineral nutrients and trace elements in organic and conventional dairy farming - a case study at Ojebyn, Sweden. *Eur J Agronom*, 20, 101-116.
- [24] Gustafson, G.A., Salomon, E. and Jonsson, S. (2006). Barn balance calculations of Ca, Cu, K, Mg, Mn, N, P, S and Zn in a conventional and organic dairy farm in Sweden. *Agric Ecosyst Environ*, 119, 160-170.
- [25] Worthington, V. (2001). Nutritional quality of organic versus conventional fruits, vegetables, and grains. *J Altern Compl Med*, 7, 161-173.
- [26] Gundersen, V., Bechmann, I.E., Behrens, A. and Sturup, S. (2000). Comparative investigation of concentrations of major and trace elements in organic and conventional Danish agricultural crops. 1. Onions (*Allium cepa* Hysam) and Peas (*Pisum sativum* Ping Pong). *J Agric Food Chem*, 48, 6094-6102.
- [27] Adotey, D.K., Serfor-Armah, Y., Fianko, J.R., and Yeboah, P.O. (2009). Essential elements content in core vegetables grown and consumed in Ghana by instrumental neutron activation analysis. *African J Food Sci*, 3, 243-249.
- [28] Mannan, A., Waheed, S., Ahmad, S. and Qureshi, I.A. (1992). Dietary evaluation of toxic elements through integrated diet. *J Rad Nucl Chem*, 162, 111-123.
- [29] Seaborn, C.D. and Nielsen, F.H. (1994). High dietary aluminum affects the response of rats to silicon deprivation. *Biol Trace Elem Res*, 41, 295-304.
- [30] Geyikoglu, F., Turkez, H. and Keles, S.M. (2005). The role of fruit juices in the prevention of aluminum sulphate toxicity in human blood in vitro. *Fresenius Environ Bull*, 14, 878-883.
- [31] Seregin, I.V. and Kozhevnikova, A.D. (2006). Physiological role of nickel and its toxic effects on higher plants. *Rus J Plant Physiol*, 53, 257-277.
- [32] Zeng, F., Ali, S., Qiu, B., Wu, F. and Zhang, G. (2010). Effects of chromium stress on the subcellular distribution and chemical form of Ca, Mg, Fe, and Zn in two rice genotypes. *J Plant Nutr Soil Sci*, 173, 135-148.
- [33] Santos, J.S., Santos, M.L.P. and Conti, M.M. (2010). Comparative study of metal contents in Brazilian coffees cultivated by conventional and organic agriculture applying principal component analysis. *J Braz Chem Soc*, 21, doi: 10.1590/S0103-50532010000800009.

Received: November 02, 2010

Revised: February 22, 2011

Accepted: March 29, 2011

CORRESPONDING AUTHOR

Uğur Akbaba

Ministry of National Education

Abdurrahman Gazi

Ilköğretim Okullu

Su deposu

25100 Palandöken, Erzurum

TURKEY

Phone: +90 0442 316 56 85

Fax: +90 0442 236 09 48

E-mail: ugurakbaba@hotmail.com

PROTECTIVE ROLE OF TWO LICHENS IN HUMAN LYMPHOCYTES *IN VITRO*

Lokman Alpsoy¹, Ali Aslan², Elif Kotan³, Guleray Agar^{3,*} and Mustafa Anar²

¹ Fatih University, Faculty of Art and Science, Department of Biology, Istanbul 34500, Turkey

² Ataturk University, Education Faculty of Kazim Karabekir, Department of Biology Teacher Training, Erzurum 25240, Turkey

³ Ataturk University, Faculty of Science, Department of Biology, Erzurum 25240, Turkey

ABSTRACT

In this study, the antagonistic effects of methanol extracts of *Rhizoplaca chrysoleuca* (RME) and *Lecanora muralis* (LME) were studied against effects of aflatoxin B₁ (AFB₁)-induced oxidative stress and genotoxicity in human lymphocytes *in vitro*. Results showed that 5 and 10 µM concentrations of aflatoxin B₁ increased the frequencies of sister chromatid exchange (SCE), micronuclei (MN) and malondialdehyde (MDA) level, whereas superoxide dismutase (SOD) and glutathione peroxidase (GPx) activities decreased. However, when 5 and 10 µg/ml concentrations of LME and RME were added to AFB₁, the frequencies of SCE, MN and MDA level decreased but SOD and GPx activities increased. The results of this experiment have clearly shown that LME and RME have strong anti-oxidative and antigenotoxic effects, and may play a role in the anti-genotoxic activity mechanisms.

heavy and radioactive metals. The role of photoactive lichen substances in photosynthesis has been examined in environmental pollution [5].

In addition to this, second metabolites isolated from lichens have been reported to show a wide variety of biological activities, including antifungal, antiviral, antiprotozoal, antiproliferative, antibiotic, antitumor, allergenic, antipyretic, plant growth inhibitory, antiherbivore, antigenotoxic and enzyme inhibitory effects [6-13].

In addition, many metabolites obtained from about 60 lichen species are present in different types of antimicrobial, anticancer, antiallergen, immunological, and expectorant drugs [14]. For example; protolichesterinic acid isolated from *Cetraria islandica* L. (Ach.) inhibited the growth of malignant cell lines [15]. On the other hand, usnic acid, another compound isolated from *Rhizoplaca* species, has been used widely in the pharmaceutical and cosmetic industries because of its high antimicrobial and antioxidant activity [16]. These naturally occurring compounds also act as inhibitors of mutagenesis and cytotoxicity, or environmental carcinogen protectors like polysaccharide CFP-2 from lichen species reduced the viability of HL-60 and K562 cells due to apoptotic pathway and telomerase activity, suggesting their possible therapeutic potential against cancer [17, 18].

Therefore, investigation of the antimutagenic properties of these substances becomes a very important strategy for prevention or treatment of various diseases related to mutagenesis. Besides, reactive oxygen species (ROS) damage membrane proteins by causing lipid peroxidation and, by attaching to unsaturated fatty acids, the damage to membrane proteins decreases its permeability as well as activities of enzymes and receptors, and activation of cells. When free radicals attack DNA, cancer-causing mutations may occur. Therefore, antioxidant defense systems including antioxidant enzymes are important in the prevention of many diseases [19]. Antioxidants may also play an important role in the prevention of genotoxic damage. So, in the present study, we aimed to determine whether LME and RME have any protective effects against AFB₁-induced SCE and MN frequencies change in human lymphocyte cell

KEYWORDS: *Rhizoplaca chrysoleuca*, *Lecanora muralis*, anti-genotoxicity, anti-oxidant enzymes.

1. INTRODUCTION

Lichens, which grow on rocky coasts, soil and plant covers, exist from an association with a heterotrophic mycobiont (a fungus) and an autotrophic photobiont (an alga or a cyanobacterium) [1, 2]. These mutualistic symbionts have various characteristic properties different from their basic components. These properties enable lichens to be used in various areas. For example, some of them are used in the perfume and dye industry but also used for the removal of toxic metals from different substances like water, air etc. [3, 4]. Many of them have been used as a biomonitor to measure air pollution by detecting SO₂ as well as

* Corresponding author

cultures *in vitro*, the role of mechanisms underlying their chemo-protective and anti-genotoxic effects by measuring SOD, GPx activities and MDA levels in human blood culture.

2. MATERIALS AND METHODS

2.1. Plant material

Lichen samples (*Rhizoplaca chrysoleuca*, *Lecanora muralis*) were collected from one station in July 2009 (Giresun province, Turkey). The species were collected on soil and identified in the laboratory of lichenology at the Department of Biology (Atatürk University) by Dr. Aslan using various flora books and different papers [20-25]. The lichen sample is stored in the herbarium of Kazım Karabekir Education Faculty, Atatürk University, Erzurum.

2.2. Preparation of methanol extracts

Air-dried and powdered lichens (10 g) were extracted with 250 ml of methanol using the Soxhlet extractor (Iso-pad, Heidelberg, Germany) for 72 h at a temperature not exceeding the boiling point of the solvent [26]. The extract was filtered (Whatman filter paper no. 1) and then concentrated in vacuum at 40 °C using a rotary evaporator (Buchi Labortechnic AG, Flawil, Switzerland) yielding a waxy material. The extract was then lyophilized and kept in the dark at + 4°C until being tested.

2.3. Microscopic evaluation

Peripheral blood lymphocytes were taken from 4 (age: 28, 26) non-smoking healthy individuals. Lymphocyte cultures were set up by adding 0.5 ml of heparinized whole blood to RPMI-1640 chromosome medium supplemented with 15% heat-inactivated fetal calf serum, 100 IU/ml streptomycin, 100 IU/ml penicillin, and 1% L-glutamine. Lymphocytes were stimulated to divide by 1% phytohemagglutinin. AFB₁ (5 and 10 µM), *Rhizoplaca chrysoleuca* methanolic extract (RME) and *Lecanora muralis* methanolic extract (LME) (5 and 10 µg/ml) were added to the cultures just before incubation. The experiments were performed in 11 groups as follows:

- Group 1: Control
- Group 2: 5 µM AFB₁
- Group 3: 10 µM AFB₁
- Group 4: 5 µM AFB₁ + RME1 (5 µg/ml)
- Group 5: 5 µM AFB₁ + RME2 (10 µg/ml)
- Group 6: 10 µM AFB₁ + RME1 (5 µg/ml)
- Group 7: 10 µM AFB₁ + RME2 (10 µg/ml)
- Group 8: 5 µM AFB₁ + LME1 (5 µg/ml)
- Group 9: 5 µM AFB₁ + LME2 (10 µg/ml)
- Group 10: 10 µM AFB₁ + LME1 (5 µg/ml)
- Group 11: 10 µM AFB₁ + LME2 (10 µg/ml)

For SCE demonstration, the cultures were incubated at 37 °C for 72 h, and 5-bromo 2-deoxyuridine at 8 mg/ml was added at the initiation of cultures. All cultures were maintained in the darkness. Next, 0.1 mg/ml of colcemide was added 3 h before harvesting to arrest the cells at metaphase. The cultures were centrifuged at 800g for 10 min. The supernatants were used for enzyme analysis. Cells were harvested and treated for 30 min with hypotonic solution (0.075M KCl) and fixed in a 1:3 mixture of acetic acid/methanol (v/v). Bromodeoxyuridine-incorporated metaphase chromosomes were stained with fluorescence plus Giemsa technique as described by Perry and Evans [27]. In SCE study, by selecting 30 satisfactory metaphases, the results of SCE were recorded on the evaluation table. One hundred metaphases per subject were also scored to determine the proportion of cells that undergo first, second, and third divisions. For each treatment condition, well-spread second division metaphases containing 42–46 chromosomes in each cell were scored, and the values obtained were calculated as SCEs per cell.

For MN analysis, Cytochalasin B was added 44 h after PHA stimulation to a final concentration of 3 g/ml. Twenty-eight hours later (after 72-h cultivation), the cells were harvested by centrifugation (900g x 10 min). The supernatant was removed, the cells were mixed thoroughly and 5 ml of cold hypotonic solution (0.05 M KCl) was added. The cells were subsequently incubated at 37 °C for 20 min and centrifuged again (900g x 10 min). The pellet was mixed thoroughly and 5 ml fresh fixative (1:3 acetic acid:methanol) was added dropwise. This fixation procedure was repeated three times and the tube was centrifuged again. The cell pellet was then resuspended in 1 ml of fresh fixative, dropped onto a clean microscope slide, incubated at 37 °C or at room temperature overnight, and stained with Giemsa dye. Coded slides were scored blind by two independent individuals. Only binucleated cells were scored for MN analysis. For each subject, at least 2000 binucleated cells were analyzed for the presence of MN. For the MN scoring, the micronucleus criteria described by Countryman and Heddle [28] were used: a diameter less than 1/3 of the main nucleus, non-refractility, not touching, and with the same colour as the nucleus or lighter.

2.4. Biochemical analysis

The cell homogenates were prepared at a 1:10 (w/v) dilution in 10 mM potassium phosphate buffer, pH 7.4. Samples were centrifuged at 3000 rpm for 10 min at 4 °C, and the supernatants were collected and immediately assayed for enzyme activities. Cu, Zn-SOD and GPx activity as well as MDA levels in the cell culture supernatant were measured by the methods of Ohkawa et al. [29], Sun et al. [30] and Paglia and Valentine [31], respectively. All samples were measured 6 times.

2.5. SOD assay

Cu, Zn-SOD activity in the cell culture supernatant was detected by the method of Sun et al. [30]. 2.45 ml of

assay reagent [0.3 mM xanthine, 0.6 mM Na₂EDTA, 0.15 mM nitroblue tetrazolium (NBT), 0.4 M Na₂CO₃, 1 g/L bovine serum albumin] was combined with 100 µl of the sample. Xanthine oxidase (50 µl, 167 U/L) was added to initiate the reaction, and the reduction of NBT by superoxide anion radicals, which are produced by the xanthine-xanthine oxidase system, was determined by measuring absorbance at 560 nm. Cu, Zn-SOD activity was expressed in units of SOD per mg protein, where 1 U is defined as that amount of enzyme causing half-maximal inhibition of NBT reduction.

2.6. GPx assay

GPx activity in the cell culture supernatant was measured by the method of Paglia and Valentine [31]. Briefly, 50 µl of sample was combined with 100 µl of 8 mM NADPH, 100 µl of 150 mM reduced GSH, 20 µl of glutathione reductase (30 units/ml), 20 µl of 0.12 M sodium azide solution, and 2.65 ml of 50 mM potassium phosphate buffer (pH 7.0, 5 mM EDTA), and the tubes were incubated for 30 min at 37 °C. The reaction was initiated with the addition of 100 µl of 2 mM H₂O₂ solution, mixed rapidly by inversion, and conversion of NADPH to NADP was measured spectrophotometrically for 5 min at 340 nm. The enzyme activity was expressed as units per g protein using an extinction coefficient for NADPH at 340 nm of 6.22 × 10⁻⁶.

2.7. MDA assay

MDA levels in the cell culture supernatant were determined spectrophotometrically according to the method described by Ohkawa et al. [29]. A mixture of 8.1% sodium dodecyl sulphate, 20% acetic acid, 0.9% thiobarbituric acid was added to 0.2 ml of sample, and distilled water was added to the mixture to bring the total volume up to 4 ml. This mixture was incubated at 95 °C for 1 h. After incubation, the tubes were left to cool under cold water and 1 ml distilled water with 5 ml n-butanol/ pyridine (15:1, v/v) was added, followed by mixing up. The samples were centrifuged at 4000g for 10 min. The supernatants were removed, and absorbance was measured with respect to a blank at 532 nm. 1,1,3,3-Tetraethoxypropane was used as the standard. Lipid peroxide levels were expressed as µmol/L MDA. Protein concentrations in the cell culture supernatant were determined by the Bradford method [32]. All photometrical measurements were performed with a DU 530 spectrophotometer (Beckman Instruments, Fullerton, California, USA) in a quartz cuvette.

2.8. Statistical analysis

The statistical analysis of MN frequencies was performed by use of the χ^2 -test. A p value of ≤ 0.05 was regarded as indicative of statistical significance for all tests used. For statistical analysis of biochemical parameters and analysis of SCE values, Mann–Whitney U-test was used. A value of P less than 0.05 was accepted as statisti-

cally significant. Results were expressed as means ± SD. For these procedures, SPSS 11.5 version for Windows (SPSS Inc, Chicago, Illinois, USA) was used.

3. RESULTS

SCE frequencies and MN frequencies (as means±SD) of the experimental groups are given in Fig. 1. All concentrations of AFB₁ as seen in Fig. 1 caused an increase in SCE frequency and MN frequency. This increase was statistically significant ($p < 0.05$). However, SCE and MN frequency decreased significantly after treatment with AFB₁ and 5 or 10 µg/ml RME and LME ($p < 0.05$).

The activities of enzymes SOD, GPx and MDA in the control and experimental groups are represented in Tables 1 and 2. Significant reduction in the activities of antioxidant enzymes were found in AFB₁-treated group (5 and 10 µM), and level of MDA was significantly higher when compared with the control as seen in Tables 1 and 2 ($p < 0.001$).

TABLE 1 - Effects of AFB₁ and different concentrations of RME on SOD, GPx and MDA activities. ^ap<0.001 compared with control group, ^bp<0.05 compared with control, ^cp<0.05 compared with AFB₁ (5 µM) group, ^dp<0.001 compared with AFB₁ (10 µM) group, ^ep<0.001 compared with AFB₁ (5 µM) group.

	SOD (U/mg protein)	GPx (U/g protein)	MDA (µmol/L)
Control	8.06±0.12	310±24.22	1.22±1.73
AFB ₁ ; 5µM	6.41±0.27 ^a	194±7.87 ^a	1.47±1.30
AFB ₁ ; 10µM	4.43±0.03 ^a	97±6.35 ^a	1.60±2.29
AFB ₁ ; (5µM)+RME1	5.86±0.29 ^b	260±4.47 ^{bd}	1.43±1.36
AFB ₁ ; (5µM)+RME2	7.01±0.14 ^{bc}	290±5.24 ^c	1.22±1.99
AFB ₁ ; (10µM)+RME1	9.97±0.06 ^d	295±6.18 ^d	1.29±2.52
AFB ₁ ; (10µM)+RME2	7.27±0.09 ^e	300±8.10 ^d	1.23±2.75

TABLE 2 - Effects of AFB₁ and different concentrations of LME on SOD, GPx and MDA activities. ^ap<0.001 compared with control group, ^bp<0.05 compared with control, ^cp<0.05 compared with AFB₁ (5 µM) group, ^dp<0.001 compared with AFB₁ (10 µM) group, ^ep<0.001 compared with AFB₁ (5 µM) group.

	SOD (U/mg protein)	GPx (U/g protein)	MDA (µmol/L)
Control	5.54±0.50	506±30.13	1.21±1.62
AFB ₁ ; 5 µM	5.23±0.10 ^b	79±8.58 ^a	1.60±1.32 ^a
AFB ₁ ; 10 µM	4.55±0.20 ^b	250±5.95 ^b	1.72±2.24 ^a
AFB ₁ ; (5µM)+LME1	8.49±0.40 ^{ac}	350±10.12 ^c	1.24±1.51 ^d
AFB ₁ ; (5µM)+LME2	5.71±0.20	320±4.70 ^c	1.27±1.68 ^d
AFB ₁ ; (10µM)+LME1	4.42±0.50 ^b	500±9.19 ^d	1.23±2.43 ^f
AFB ₁ ; (10µM)+LME2	3.03±0.12 ^b	506±8.02 ^{de}	1.19±2.06 ^f

However, these effects of AFB₁ seen at higher levels decreased after treatment with different concentrations of both lichen extracts (RME and LME).

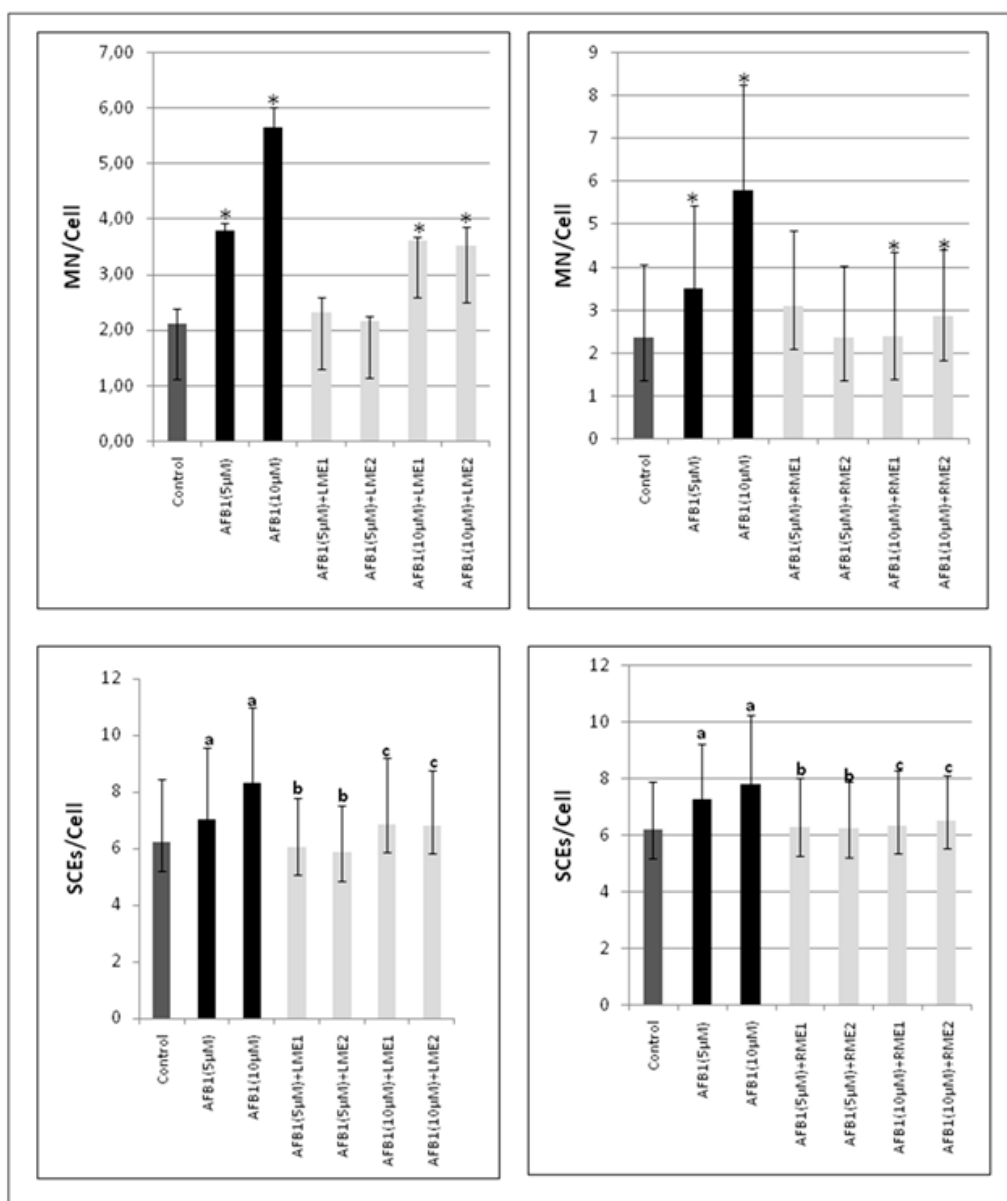


FIGURE 1 - Comparison of the effects on the number of MN and SCEs different concentrations of AFB₁ and different concentrations of RME and LME together with AFB₁ in human peripheral lymphocytes. For SCE: ^ap<0.05 compared with control, ^bp <0.05 compared with AFB₁ (5 µM) group, ^cp<0.05 compared with AFB₁ (10 µM) group. For MN: (*) significant, (*) insignificant.

4. DISCUSSION

According to the results; two different concentrations of AFB₁ used in this study progressively increased the SCE and MN frequencies. Previous studies found that AFB₁ could stimulate the release of free radicals, including reactive oxygen species, which lead to chromosomal aberrations [23, 33]. In addition, the effects of AFB₁ have been reported to be primarily associated with AFB₁-8,9-epoxide, which subsequently binds to nucleophilic sites in DNA, and the major adduct, 8,9-dihydro-8-(N7 guanyl)-9-hydroxy-AFB₁ (AFB₁ N7-Gua) [34-37]. However, these effects of AFB₁ seen at higher levels decreased after treat-

ment with different concentrations of RME and LME. Recently, in several studies, anti-mutagenic effects of lichen extracts with different assays have been reported [17, 38, 39].

In these studies, the antigenotoxic effects of the lichen extract have been linked with lichesterinic acid, protolichesterinic acid, usnic acid, polysaccharide Ci-3, sphaerophorin and pannarin isolated from these lichens [17, 38, 40-42]. Additionally, some research suggested that antigenotoxic activities of lichen extracts may have originated from their antioxidative activity [17, 39, 43]. Therefore, in the present study, SOD, GPx and MDA activities were meas-

ured to examine the antigenotoxic effects of the methanol extracts of RME and LME, in order to understand whether antioxidant properties have any role or not. Our results showed that decrease in AFB₁, SOD and GPX activities caused increasing MDA activities. But these effects of AFB₁ on enzymes decreased after treatment with the methanol extracts of RME and LME. Previous researches have reported on some lichens as well as antioxidant capacity and antioxidant effects of their extracts which have been linked with polyphenolic and non-polyphenolic compounds, such as epigallocatechin gallate, quercetin, gallic acid, curcumin, eugenol, usnic acid, polysaccharide Ci-3, lichesterinic acid, protolichesterinic acid, isolated from these lichens [38, 44-46]. Therefore, our study results indicate that antigenotoxic effects of RME and LME could be related to its antioxidant potential. The fractionation and isolation in crude extracts of lichen samples containing the active components responsible for anti-genotoxic and anti-oxidant activities have been carried out to test this hypothesis.

ACKNOWLEDGEMENTS

This study was supported by grants from the Research Funds appropriated to Ataturk University and Fatih University (Project no: P50031005_2).

REFERENCES

- [1] Lange, O.L., Leisner, J.M.R. and Bilger, W. (1999). Chlorophyll fluorescence characteristics of the cyanobacterial lichen *Peltigera rufescens* under field conditions II. Diel and annual distribution of metabolic activity and possible mechanisms to avoid photoinhibition. *Flora* 194, 413-430.
- [2] Jeon, H.S., Lokos, L., Han, K.S., Ryu, J.A., Kim, J.A., Koh, Y.J. and Hur, J.S. (2009). Isolation of Lichen-forming Fungi from Hungarian Lichens and Their Antifungal Activity against Fungal Pathogens of Hot Pepper Anthracnose. *Plant Pathology Journal* 25, 38-46.
- [3] Bingol, A., Aslan, A. and Cakici, A. (2009). Biosorption of chromate anions from aqueous solution by a cationic surfactant-modified lichen (*Cladonia rangiformis* (L.)). *J Hazard Mater* 161, 747-52.
- [4] Ugur, A., Ozden, B.O., Sac, M.M. and Yener, G. (2003). Biomonitoring of 210Po and 210Pb using lichens and mosses around a uraniumiferous coal-fired power plant in western Turk. *Atmospheric Environment* 37, 2237-2245.
- [5] Speta, F. (1986) Flechten in Oberosterreich-einst und heute, 5, Flechten bedrohte Wunder der Natur. Landesverlag Linz, Linz.
- [6] Behera, B.C., Verma, N., Sonone, A. and Makhija, U. (2006). Determination of antioxidative potential of lichen *Usnea ghattensis* in vitro. *Lwt-Food Science and Technology* 39, 80-85
- [7] Ingolfsdottir, K., Hjalmarsdottir, M.A., Sigurdsson, A., Gudjonsdottir, G.A., Brynjolfsdottir, A. and Steingrímsson, O. (1997). In vitro susceptibility of *Helicobacter pylori* to protolichesterinic acid from the lichen *Cetraria islandica*. *Antimicrob Agents Chemother* 41, 215-7.
- [8] Muller, K. (2001). Pharmaceutically relevant metabolites from lichens. *Appl Microbiol Biotechnol* 56, 9-16.
- [9] Perry, N.B., Benn, M.H., Brennan, N.J., Burgess, E.J., Ellis, G., Galloway, D.J., Lorimer, S.D. and Tangney, R.S. (1999). Antimicrobial, antiviral and cytotoxic activity of New Zealand lichens. *Lichenologist* 31, 627-636.
- [10] Yamamoto, Y., Kinoshita, Y., Matsubara, H., Kinoshita, K., Koyama, K., Takahashi, K., Kurokawa, T. and Yoshimura, I. (1998). Screening of biological activities and isolation of biological active compounds from lichens. *Phytochemistry* 2, 23-34.
- [11] Wei, X., Jeon, H.S., Han, K.S., Koh, Y.J. and Hur, J.S. (2008). Antifungal activity of lichenforming fungi against *Colletotrichum acutatum* on hot pepper. *Plant Pathology Journal* 24, 202-206.
- [12] Gulluce, M., Aslan, A., Sokmen, M., Sahin, F., Adiguzel, A., Agar, G. and Sokmen, A. (2006). Screening the antioxidant and antimicrobial properties of the lichens *Parmelia saxatilis*, *Platismatia glauca*, *Ramalina pollinaria*, *Ramalina polymorpha* and *Umbilicaria nylanderiana*. *Phytomedicine* 13, 515-21.
- [13] Huneck, S. (1999). The significance of lichens and their metabolites. *Naturwissenschaften* 86, 559-70.
- [14] Kirmizigul, S., Koz, O. and Boke, N. (2007). Constituents of Apolar Extracts Including Essential Fatty Acidsof Some Turkish Lichens. *Chemistry of Natural Compounds* 43, 462-464.
- [15] Ogmundsdottir, H.M., Zoega, G.M., Gissurarson, S.R. and Ingolfsdottir, K. (1998). Anti-proliferative effects of lichen-derived inhibitors of 5-lipoxygenase on malignant cell-lines and mitogen-stimulated lymphocytes. *J Pharm Pharmacol* 50, 107-15.
- [16] Cansaran, D., Cetin, D., Halici, M.G. and Atakol, O. (2006). Determination Of Usnic Acid in Some Rhizoplaca Species From Middle Anatolia and Their Antimicrobial Activities. *Zeitschrift Fur Naturforschung Section C-A Journal Of Biosciences* 6, 47-51.
- [17] Zeytinoglu, H., Incesu, Z., Tuylu, B.A., Turk, A.O. and Barutca, B. (2008). Determination of genotoxic, antigenotoxic and cytotoxic potential of the extract from lichen *Cetraria aculeata* (Schreb.) Fr. in vitro. *Phytother Res* 22, 118-23.
- [18] Lin, X., Cai, Y.J., Li, Z.X., Chen, Q., Liu, Z.L. and Wang, R. (2003). Structure determination, apoptosis induction, and telomerase inhibition of CFP-2, a novel lichenin from *Cladonia furcata*. *Biochim Biophys Acta* 1622, 99-108.
- [19] Yen, G. and Hsieh, C. (1998). Antioxidant Activity of Extracts from Du-zhong (*Eucommia ulmoides*) toward Various Lipid Peroxidation Models in Vitro. *J. Agric. Food Chem* 46, 3952-3957.
- [20] Purvis, O.W., Coppins, B.J., Hawksworth, D.L., James, P.W. and Moore, D.M. (1992) The lichen flora of Great Britain and Ireland, Natural History Museum Publications in association with The British Lichen Society. London.
- [21] Wirth, V. (1995) Die Flechten Baden-Württembergs. Ulmer: Stuttgart.
- [22] Poelt, J. (1974) Bestimmungsschüssel europäischer Flechten. Cramer: Vaduz.
- [23] Amstad, P., Levy, A., Emerit, I. and Cerutti, P. (1984). Evidence for membrane-mediated chromosomal damage by aflatoxin B1 in human lymphocytes. *Carcinogenesis* 5, 719-23.

- [24] Aslan, A. (2000). Lichens from the Region of Artvin, Erzurum and Kars (Turkey). Israel Journal of Plant Sciences 48, 143-155.
- [25] Aslan, A., Yazici, K. and Karagoz, Y. (2002). Lichen flora of the Murgul district, Artvin, Turkey. Israel Journal of Plant Sciences 50, 77-81.
- [26] Lin, J., Opoku, A.R., Geheeb-Keller, M., Hutchings, A.D., Terblanche, S.E., Jager, A.K. and van Staden, J. (1999). Preliminary screening of some traditional zulu medicinal plants for anti-inflammatory and anti-microbial activities. J Ethnopharmacol 68, 267-74.
- [27] Perry, P. and Evans, H.J. (1975). Cytological detection of mutagen-carcinogen exposure by sister chromatid exchange. Nature 258, 121-5.
- [28] Countryman, P. I. and J. A. Heddle (1976). "The production of micronuclei from chromosome aberrations in irradiated cultures of human lymphocytes." Mutat Res 41(2-3): 321-32.
- [29] Ohkawa, H., Ohishi, N. and Yagi, K. (1979). Assay for lipid peroxides in animal tissues by thiobarbituric acid reaction. Anal Biochem 95, 351-8.
- [30] Sun, Y., Oberley, L.W. and Li, Y. (1988). A simple method for clinical assay of superoxide dismutase. Clin Chem 34, 497-500.
- [31] Paglia, D.E. and Valentine, W.N. (1967). Studies on the quantitative and qualitative characterization of erythrocyte glutathione peroxidase. J Lab Clin Med 70, 158-69.
- [32] Bradford, M. M. (1976). "Rapid and Sensitive Method for Quantitation of Microgram Quantities of Protein Utilizing Principle of Protein-Dye Binding." Analytical Biochemistry 72(1-2): 248-254.
- [33] Alpsoy, L., Agar, G. and Ikbal, M. (2009). Protective role of vitamins A, C, and E against the genotoxic damage induced by aflatoxin B1 in cultured human lymphocytes. Toxicol Ind Health 25, 183-8.
- [34] Sharma, R.A. and Farmer, P.B. (2004). Biological relevance of adduct detection to the chemoprevention of cancer. Clin Cancer Res 10, 4901-12.
- [35] Klein, P.J., Van Vleet, T.R., Hall, J.O. and Coulombe, R.A., Jr. (2002). Biochemical factors underlying the age-related sensitivity of turkeys to aflatoxin B(1). Comp Biochem Physiol C Toxicol Pharmacol 132, 193-201.
- [36] Towner, R.A., Qian, S.Y., Kadiiska, M.B. and Mason, R.P. (2003). In vivo identification of aflatoxin-induced free radicals in rat bile. Free Radic Biol Med 35, 1330-40.
- [37] Sohn, D.H., Kim, Y.C., Oh, S.H., Park, E.J., Li, X. and Lee, B.H. (2003). Hepatoprotective and free radical scavenging effects of *Nelumbo nucifera*. Phytomedicine 10, 165-9.
- [38] Russo, A., Bonina, F., Acquaviva, R., Campisi, A., Galvano, F., Ragusa, N. and Vanella, A. (2002). Red orange extract: effect on DNA cleavage. Journal of Food Sciences 67, 2814-2818
- [39] Geyikoglu, F., Turkez, H. and Aslan, A. (2007). The protective roles of some lichen species on colloidal bismuth subcitrate genotoxicity. Toxicol Ind Health 23, 487-92.
- [40] Ingolfsdottir, K. (2002). Usnic acid. Phytochemistry 61, 729-36.
- [41] Turk, A.O., Yilmaz, M., Kivanc, M. and Turk, H. (2003). The antimicrobial activity of extracts of the lichen *Cetraria aculeata* and its protolichesterinic acid constituent. Z Naturforsch C 58, 850-4.
- [42] Orange, A., James, P.W. and White, F.J. (2001) Microchemical Methods for the Identification of Lichens, British Lichen Society. London.
- [43] Bucar, F., Schneider, I., Ogmundsdottir, H. and Ingolfsdottir, K. (2004). Anti-proliferative lichen compounds with inhibitory activity on 12(S)-HETE production in human platelets. Phytomedicine 11, 602-6.
- [44] Odabasoglu, F., Aslan, A., Cakir, A., Suleyman, H., Karagoz, Y., Halici, M. and Bayir, Y. (2004). Comparison of antioxidant activity and phenolic content of three lichen species. Phytother Res 18, 938-41.
- [45] Gulcin, I., Oktay, M., Kufrevioglu, O.I. and Aslan, A. (2002). Determination of antioxidant activity of lichen *Cetraria islandica* (L) Ach. J Ethnopharmacol 79, 325-9.
- [46] Halici, M., Odabasoglu, F., Suleyman, H., Cakir, A., Aslan, A. and Bayir, Y. (2005). Effects of water extract of *Usnea longissima* on antioxidant enzyme activity and mucosal damage caused by indomethacin in rats. Phytomedicine 12, 656-62.

Received: November 17, 2010

Revised: December 06, 2010

Accepted: February 11, 2011

CORRESPONDING AUTHOR

Guleray Agar

Ataturk University

Faculty of Science

Department of Biology

Erzurum 25240

TURKEY

E-mail: gagar@atauni.edu.tr

MODELLING THE INFLUENCE OF SALINITY AND WATER DEFICIENCY ON GROWTH AND BIOMASS OF *GROENLANDIA DENSA* (POTAMOGETONACEAE)

Dilek Demirezen Yilmaz^{1,*} and Kadiriyе Uruc Parlak²

¹Erciyes University, Faculty of Science, Department of Biology, 38039, Kayseri, Turkey

²Ibrahim Çeçen University, Faculty of Arts and Sciences, Department of Biology, Agri, Turkey

ABSTRACT

The role of the effects of salinity and different hydrological regimes on growth in *Groenlandia densa* (*Potamogetonaceae*) was investigated under laboratory conditions. The experiment consisted of three treatments of hy-drological regimes (severe, moderate and well watered) and five levels of salinity (0, 125, 250, 375 and 500 mol.m⁻³ which are equivalent to 0, 25, 50, 75 and 100 % sea water salinity). Survival, lengths of shoots and roots and dry matter production were measured. Our results suggested that the growth of roots was significantly reduced at salinity of 250 mol m⁻³ and significantly enhanced at 500 mol m⁻³ compared to a freshwater control. Both salinity and water deficiency significantly impacted root and shoot dry weights. Plants exhibited maximum reduction in dry mass production in response to increasing salt stress. Additionally, leaf chlorosis occurred in plants under increased salinity and water deficiency conditions which may be related to the adverse effects of salinity on plant nutrient status. In this study, a simple model was created according to data from the literature. The model suggested that crowding is an im-portant factor in limiting *G.densa* growth.

KEYWORDS:

Hydrological regimes, Dry matter, *Groenlandia densa*, Salt stress.

1. INTRODUCTION

Water deficiency and salinity are widespread problems around the world; plant growth and seedlings are negatively affected by these conditions [1, 2]. Salinity and water deficiency are two of the most important factors limiting growth and production of both aquatic and terrestrial plants [3].

* Corresponding author

Salinity in soil or aquatic ecosystems depends upon various factors like the amount of evaporation (causing salt concentration to increase), or the amount of precipitation (causing salt concentration to decrease). Weathering of rocks also affects salt concentration in these areas [1, 4].

Salinity can damage the plant through its osmotic effect, which is equivalent to a decrease in water activity through specific toxic effects of ions and by disturbing the uptake of essential nutrients [5-9]. There are much different type of salts in the environment and in plant organs, plant tissues and cells at different developmental stages exhibit varying degrees of tolerance to these kinds of stresses.

A major consequence of NaCl stress in plants is the loss of intracellular water. Another physiological effect of water deficiency on plants is the reduction in vegetative growth, in particular shoot growth [1, 10]. *Groenlandia densa* is restricted to shallow waters, but this species can occur in large rivers on resistant rock and the species has a wide distribution. With increasing flow, *G. densa* is lost first from the environment [11]. Opposite leaved pondweeds have a cosmopolitan distribution in marshlands in most areas of the world. These plants are known to accumulate heavy metal in their tissues, so they can be called biological indicators that determine environmental pressures [12].

The objective of this study was to understand the response of the *G.densa* to salinity and fluctuating water levels. As water deficiency arises during drought conditions, the concomitant salinity changes have a major impact on the submerged macrophyte community [2]. Because a submerged macrophyte area cover is reduced by a lower water level, food sources, habitat and refuge areas for juvenile fauna and other small prey species are also reduced [3].

2. MATERIALS AND METHODS

2.1. Material

Groenlandia densa (*Potamogetonaceae*) green vascular plants that grow rapidly under favorable conditions were supplied from Kayseri, Turkey. The plants used in this experiment were collected the previous autumn. The biomass growth rate of this plant was determined under laboratory conditions (such as: 23 °C and a 14-hour photoperiod). Preliminary tests for plant density were performed to determine the appropriate seedling density for test plants. So, ten seedlings of *G.densa* per pot were used for each treatment. In this study, two experiments (water deficiency and salinity) were separately conducted in the laboratory.

2.1. Water deficiency experiment

The experiments were arranged in a randomized complete block design with five replications per treatment (in total, 250 different plant samples were used) [13]. Water control is shown in Table 1. The seedlings of *G. densa* were grown in glass cylinders (20x50x18 cm) which were filled with an 8 liter medium solution. The plants were grown in a liquid medium according to methods from Smart and Barko [14]. After day 5, the cylinders were replaced with fresh medium. At the start of the test and every day, as well as at test termination, changes in plant development, root and shoot length, appearance and necrosis–chlorosis were recorded.

TABLE 1 - Irrigation methods for *G.densa*. (+) represents irrigated samples, (-) represents non-irrigated samples. 25 ml water was added for irrigation every time.

Water situation	Irrigation period			
	At day 5	At day 10	At day 15	At day 20
Severe drought	-	-	-	-
Moderate drought	-	+	-	+
Well watered	+	+	+	+

The experiment lasted for 25 days at the end of which the plants were harvested and shoot and root length and total biomass (dry weight) were recorded. The initial dry weight was calculated using the dry weight to fresh weight ratio at the end of the experiment.

2.2. Salinity experiment

In this study, sodium chloride (NaCl) was used without further purification for salinity treatments. The salt solutions were prepared by mixing the appropriate amount of sodium chloride to a suitable volume of deionised water in each case. A total of five different salinity concentrations (0, 125, 250, 375 and 500 mol.m⁻³ which are equivalent to 0, 25, 50, 75 and 100 % sea water salinity) were tested [15]. A total of 10 healthy *G.densa* were chosen for each test container and tests for each treatment, five replicates were applied (in total, 250 different plant samples were used). The pH of the samples was measured daily during the experiments and after day five, the water and solutions in each of the treatment were replaced with fresh

solutions. At the start of the test and every day, as well as at test termination, changes in plant development, root and shoot length, appearance and necrosis–chlorosis were recorded. The experiment lasted for 25 days at the end of which the plants were harvested and then root and shoot length and total biomass (dry weight) were recorded.

The initial dry weight was calculated using the dry weight to fresh weight ratio at the end of the experiment.

2.3. Modelling

In this study, a simple model created by Driever *et al.* [16] was constructed to explain the effect of crowding, temperature and nutrients:

$$\frac{dB}{dt} = Brf(T, B, N, P) - lB$$

The variation of the *G.densa* biomass was modeled as the function of the maximum growth rate (r). The gross production was modified by a limitation function (f(T, B, N, P)), which was a function of air temperature (T), biomass (B) and nutrients (N and P). Additionally, the production of plants was corrected for the loss (l), which included mortality [16]. The limitation function (f(T, B, N, P)) was defined as:

$$f(T, B, N, P) = (T - T_{min} / T_{opt} - T_{min}) \cdot (N / N + hN) \cdot (P / P + hP) \cdot (hB / B + hB)$$

Temperature (T) limitation was assumed to be linear from the minimum temperature (T_{min}, 5 °C) up to the optimum temperature (T_{opt}, 26 °C) [16]. According to statements of Lüönd [17], nutrient limitation of ammonia and nitrate (N) and phosphate (P) were also modelled as Monod-type functions (with the following half saturation values: hN = 0.04 mg N L⁻¹ and hP = 0.05 mg P L⁻¹) [17]. The restrictive effect of biomass was simply assumed to be another Monod-type function dependent on biomass B and with half saturation (hB) determined during this study [16].

2.4. Statistical analysis

Relative growth (weight), root and shoot length were subjected to one-way analysis of variance (ANOVA) using Statistical Package for the Social Sciences (SPSS). Individual means of each treatment were compared using Tukey's test. Results were considered significant at a P level < 0.001. Correlations between growth and salt concentrations and between growth and water level were determined.

3. RESULTS AND DISCUSSION

A one-way ANOVA indicated that the salinity and water deficiency treatment significantly decreased all the growth attributes such as plant height, root and shoot length of *G.densa* (F = 11.99; d.f. = 5, P < 0.001). In other words, *G.densa* growth rates decreased with increasing salinity and water deficiency (Figure 1-A). The visual symptoms of salinity and water deficiency observed in the

current study corroborate with those found by Subramanian *et al.* [18].

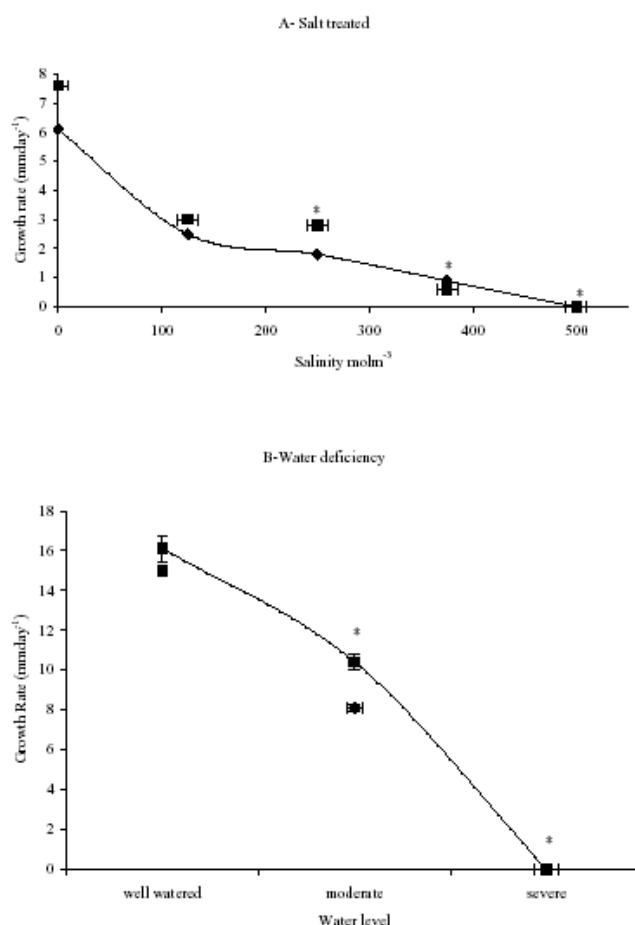


FIGURE 1 - Growth rate (salt-treated and water deficiency) of *Groenlandia densa* both laboratory-scale experiment and simple model. Dots represent the described growth rate by the models and the solid line represents the measured growth rate. Error bars show standard deviations. Values represent mean \pm S.E. ($n = 5$). Asterisks indicate significant differences between control and treatments at $P < 0.001$. Different letters indicate significant differences between treatments at $P < 0.001$.

For example, the growth rate of *G.densa* plants were significantly inhibited at salinity of 500 mol m^{-3} (Figure 1-A). This may be due to the greater sensitivity of plants to the physiological stress of salinity compared to the control plants. Additionally, salinity levels of lower concentrations (125 mol m^{-3}) did not significantly ($P > 0.001$) affect the length of roots and shoots compared to the control. Figure 2-A shows that on average root extension for the control group was taller than those of at the 500 mol m^{-3} salinity levels. It means the highest salinity level causes significant inhibition of roots growth (Figure 2-A). Compared with the control treatment, average root extension was inhibited by 50%. Furthermore, roots of affected plants (375 mol m^{-3} and 500 mol m^{-3} NaCl) were also noticeably thinner than those in the control and other treatments. In these treatments, especially at 500 mol m^{-3} , total root loss

was also more apparent. Tozlu *et al.* [19] obtained that the death of fine roots of *Poncirus trifoliata* was in response to an increasing concentration of NaCl, [19].

The results of shoot length for each treatment also showed a similar patterns with mean length decreasing significantly ($P < 0.001$) from 16 mm in the control down to 12 mm in the 375 mol m^{-3} and 10 mm in the plants exposed to 500 mol m^{-3} NaCl (Fig. 2-A). No significant effects were observed for the 125 mol m^{-3} treatments relative to the control. Also, salt stress significantly ($P < 0.001$) affected the size of leaves in *G. densa*. The leaf injury could be a result of the accumulation of toxic levels of Cl and Na, ion imbalance, nutrient deficiencies and water stress.

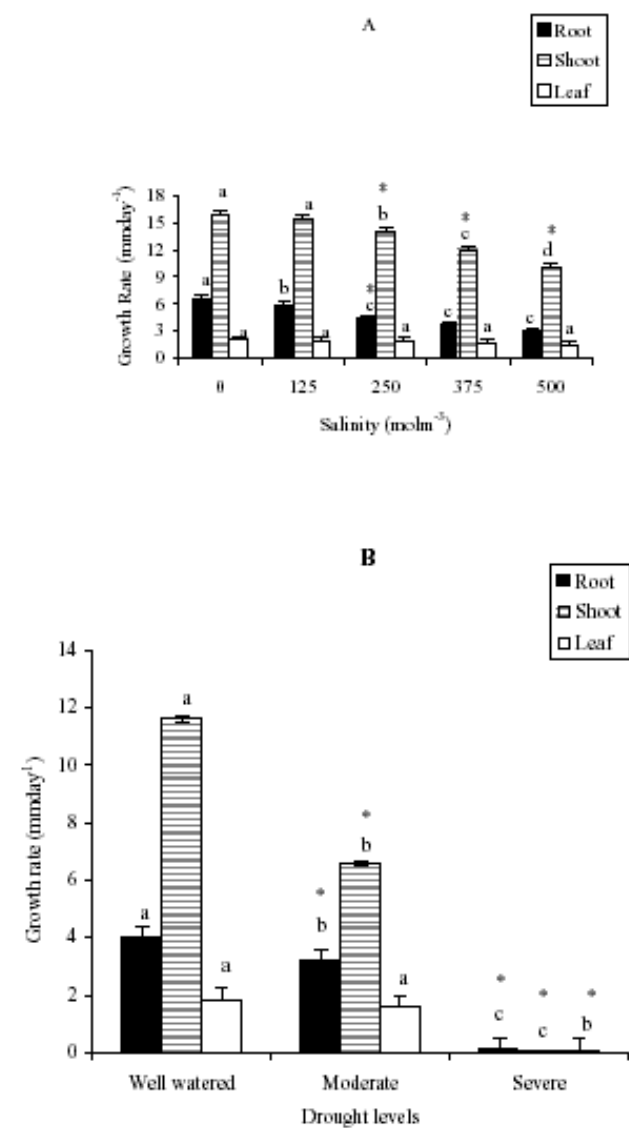


FIGURE 2 - Root and shoot length and leaf size density profile of *G.densa* in response to different salinities (A) and water deficiency treatments (B). Values represent mean \pm S.E. ($n = 5$). Asterisks indicate significant differences between control and treatments at $P < 0.001$. Different letters indicate significant differences between treatments at $P < 0.001$.

It is believed that salinity reduces plant growth by water stress in the root zone, or salt toxicity in the plants tissue [20]. In our experiment, salinity influenced the growth of *G. densa* similarly to its effects on many other species [21-23]. The plants responded to salinity by decreased relative growth rate. According to Koyro [15] and Shannon and Grieve [24], the highest salinity leads to a decrease in the proportion of shoot biomass in the total biomass of *Plantago sp.*. Similar findings have been reported by Ashraf and Mc-Neily [25], Francois *et al.* [26] and Hampson and Simpson [27] for negative effect of salinity on seedling dry weight. Similar patterns were also observed from results of this study (Figure 3B).

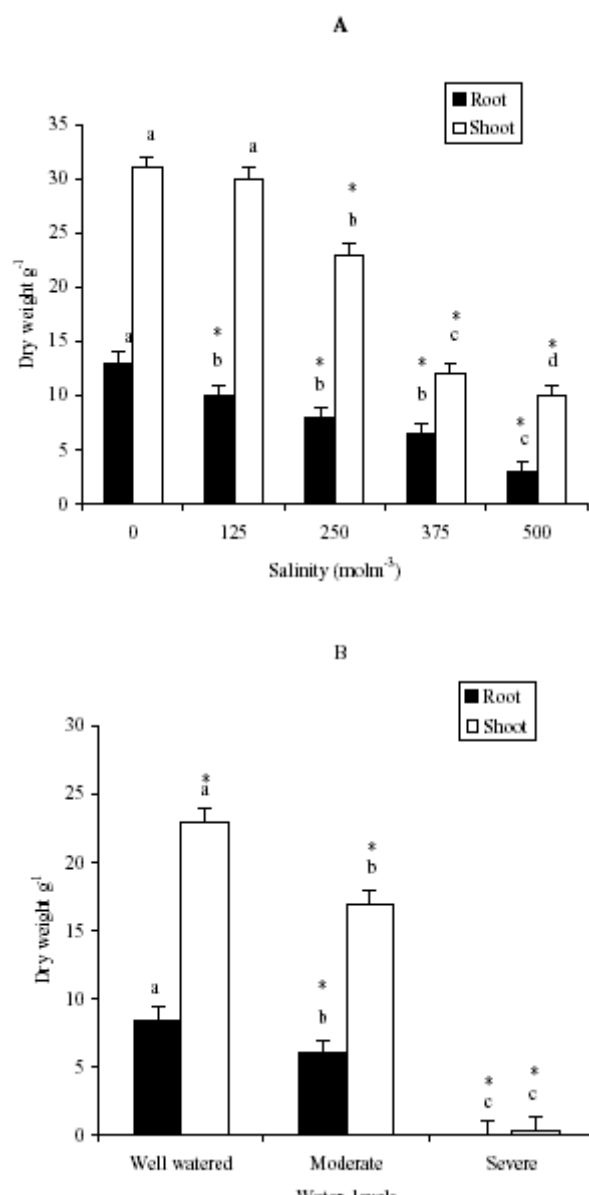


FIGURE 3 - Root and Shoot biomass of *G. densa* in response to different salinities (A) and water deficiency treatments (B). Values represent mean \pm S.E. ($n = 5$). Asterisks indicate significant differences between control and treatments at $P < 0.001$. Different letters indicate significant differences between treatments at $P < 0.001$.

The studies of plant morphogenesis showed that root length was remarkably reduced by an increase of drought stress (Figure 2-B). Additionally, the highest growth rate was observed in well watered plants in this study. Results from the present study agree with those obtained from different plants by different investigators [28, 29].

Furthermore, higher water deficiency caused a reduction in the survival rate of *G. densa* in this study (Figure 3B). For example, water deficiency decreased survival to 41 %. In addition, under increased water deficiency conditions leaf chlorosis and browning were observed in plant samples.

Kramer [30] reported that plants subjected to different kinds of water stress show a general reduction in size and dry matter production. Glenn and Brown [31] indicated that a plant exposed to both increased salinity and drought will suffer from increasing levels of water stress as well as osmotic stress [31]. Drought conditions can change the sulphide concentration within the soil or sediment. Increased soil or sediment sulphide has been shown to affect root respiration as well as inhibit overall plant growth in many wetland species [32-34]. However, some wetland plants are able to modify the environment of the rhizosphere by releasing oxygen through their roots thereby influencing both soil redox potential and sulphide concentrations [35]. In this study, leaf chlorosis was seen in some leaves exposed to higher salinity and water deficiency conditions. According to Raven *et al.* [36], this situation may be due to a magnesium deficiency because magnesium is phloem-mobile, and younger leaves are able to withdraw nutrients from older leaves. It means drought conditions cause a decrease in both leaf (foliar) and root uptake of magnesium. Similar results obtained by Brown *et al.* [37] stated that both salinity and drought treatment significantly affected root uptake of magnesium for *Spartina alterniflora*. Pezeshki *et al.* [33] also stated that the drought conditions and the resulting changes in water level and salinity in the marshlands would damage root functioning, reduce plant nutrient uptake, photosynthetic activity, and impact many other physiological functions. Additionally, both temperature and water are important factors that directly affect plant growth, either as resources or as resource regulators.

Both factors significantly ($P < 0.001$) affected root and shoot mass and the root-shoot ratio of *G. densa* plants measured at harvest (Figure 3 A-B). For example, severely drought stressed conditions caused lower biomass production (Figure 3-B). Additionally, dry weight obtained from *G. densa* significantly decreased ($P < 0.001$) for whole plants in response to an increasing concentration of salt in the water (Figure 3-A). A negative relation was observed between dry weight of plants and salt concentrations ($r = -0.634$, $P < 0.001$). In contrast, Brown *et al.* [37] observed that dry weight components in *Spartina alterniflora* showed no interaction between salinity and soil drying [37]. Additionally, they also stated that both salinity and soil drying significantly impacted root and shoot dry weights.

Results from this study suggest that water deficiency and salt stress decrease mean plant biomass. This is supported by earlier studies conducted at fields or in laboratories [13, 38-40].

Using a combination of a laboratory-scale experiment and a simple model, we obtained insight in the growth dynamics of *G.densa* in the field even though processes were neglected or oversimplified in the model. For example, the model assumed that the plants were homogenous distributed over the pot. In actuality, as a consequence of wind, animals and birds this situation is not true in nature [41]. Furthermore, the laboratory experiment showed that there is relationship between salinity and growth rate and between water deficiency and growth rate for *G.densa*.

Driever *et al.* [16] and Landolt [42] stated that in this model the loss (*I*) was assumed to be constant for all pots, and it included respiration, grazing and mortality implicitly; however, it has neglected the fact that respiration is strongly dependent on temperature [16, 42]. In addition, there is also no information about the influence of grazing pressure by birds or other animals, temperature, crowding and decomposition on mortality. Therefore it could not be accounted for in the mortality rates. Dale and Gillespie, [43] stated that temperature can vary widely between water, air and within floating plants. Furthermore, Driever *et al.* [16] indicated that the temperature of the leaves in the upper layers is better described by the maximum air temperature than by the water temperature, so we used air temperature for model calculations in this study.

Despite these difficulties, the negative effect of salinity and water deficiency on growth rate of *G.densa* was accurately described in the model.

4. CONCLUSION

Both salinity and water deficiency significantly impacted root and shoot dry weights of *G. densa*. Furthermore, leaf chlorosis and browning was seen in plants under increased salinity and water deficiency conditions. Future research involving comparative field studies of *G.densa* and other salt marsh species with regard to the combined effects of increasing salinity and water deficiency is needed.

REFERENCES

- [1] Shilpi, M. and Narendra, T. (2005) Archives of Biochemistry and Biophysics, 444: 139–158.
- [2] Taylor, R., Adams, J.B. and Haldorsen, S. (2006) Primary habitats of the St Lucia Estuarine System, South Africa, and their responses to mouth management, Afr. J. Aquat. Sci. 31 (1): 31–41.
- [3] Gordon, N., Adams, J.B. and Bate, G.C. (2008) Epiphytes of the St. Lucia Estuary and their response to water level and salinity changes during a severe drought, Aquatic Botany, 88:66-76.
- [4] Mer, R.K., Prajith, P.K., Pandya, D.H. and Pandey, A.N. (2000) Effect of Salts on Germination of Seeds and Growth of Young Plants of *Hordeum vulgare*, *Triticum aestivum*, *Cicer arietinum* and *Brassica juncea* J.Agron,Crop.Sci., 185: 209-217.
- [5] Ramoliya, P.J., Patel, H.M. and Pandley, A.N. (2004) Effect of salinization of soil on growth and macro- and micro-nutrient accumulation in seedlings of *Salvadora persica* (Salvadoraceae), Forest Ecology and Management, 202:181-193.
- [6] Laučchi, A. and Epstein, E. (1990) Plant responses to saline and sodic conditions. In: Tanji, K.K. (Ed.), Agricultural Salinity Assessment and Management. American Society of Civil Engineers, New York, pp. 113–137.
- [7] Marschner, H. (1995) Mineral Nutrition of Higher Plants, second ed. Academic Press, London.
- [8] Dorais, M., Papadopoulos, A.P. and Gosselin, A., (2001) Greenhouse Tomato Fruit Quality, Hortic. Rev. 26:239–319.
- [9] Brady, N.C. and Weil, R.R. (1996) The nature and properties of soils 11. th ed. Prentice-Hall, Eglewood Cliffs, NJ.
- [10] Schuppler, U., He, P.H., John, P.L.C. and Munns, R. (1998) Effect of Water Stress on Cell Division and Cdc2-Like Cell Cycle Kinase Activity in Wheat Leaves, Plant Physiol. 117: 667–678.
- [11] Haslam, S.M. (1987) River Plants of Western Europe, Cambridge University Press.
- [12] Demirezen, D. and Aksoy, A. (2006) Common Hydrophytes as Bioindicators of Iron and Manganese Pollutions, Ecological Indicators, 6:388-393.
- [13] Du, Y.J., Li, Z. and Li, W.L. (2006) Effect of different water supply regimes on growth and size hierarchy in spring wheat populations under mulched with clear plastic film Agricultural Water Management. 79: 265–279
- [14] Smart, R.M. and Barko, J.W. (1985) Laboratory culture of submersed freshwater macrophytes on natural sediments, Aquat. Bot., 21:251–263.
- [15] Koyro H.W. (2006) Effect of salinity on growth, photosynthesis, water relations and solute composition of the potential cash crop halophyte *Plantago coronopus* (L.), Environmental and Experimental Botany. 56(2) (2006) 136-146.
- [16] Driever, S.M., van Nes, E.H. and Roijackers, R.M.M. (2005) Growth limitation of *Lemna minor* due to high plant density , Aquatic Botany, 81: 245–251.
- [17] Lüönd, A. (1980) Effects of nitrogen and phosphorus upon the growth of some Lemnaceae. In: Landolt, E. (Ed.). Bio-systematic Investigations in the Family of Duckweeds (Lemnaceae), vol. 1. Veroeff. Geobot. Inst. ETH Zürich, Zürich, pp. 118–141.
- [18] Subramanian, K.S., Santhanakrishnan, P. and Balasubramanian, P. (2006) Responses of field grown tomato plants to arbuscular mycorrhizal fungal colonization under varying intensities of drought stress Scientia Horticulturae. 107: 245–253

- [19] Tozlu, I., Moore, G.A. and Guy, C.L. (2000) Regulation of growth and differential tissue dry mass accumulation by *Citrus gandis*, *Poncirus trifoliata*, Aust.J. Plant Physiol., 27: 35–42.
- [20] Ho, L.C. (2003) Interaction between Root and Shoot Environmental Factors on crop. Yield Acta Hortic., 609: 121–126.
- [21] Adam, P. (1990) Salt marsh Ecology. Cambridge University Press, Cambridge.
- [22] Deegan, B., Harrington, J. and Dundon, P. (2005) Effects of salinity and inundation regime on growth and distribution of *Schoenoplectus triquetus*, Aquatic Botany. 81:199–211.
- [23] Parida, K.A. and Das, B.A. (2005) Salt tolerance and salinity effects on plants: a review Ecotoxicol. Environ. Saf. 60: 324–349.
- [24] Shannon, M.C. and Grieve, C.M. (1999) Tolerance of vegetable crops to salinity. Hort. 78: 5–38.
- [25] Ashraf, M. and McNeily, T. (1988) Variability in Salt Tolerance of Nine Spring Wheat Cultivars, J. Agron. Crop Sci. 160:14–21.
- [26] Francois, L.E., Maas, E.V., Donovan, T.J. and Youngs, V.L. (1986) Effects of salinity on grain yield and quality, vegetative growth and germination of semi-dwarf and durum wheat, Agron. J. 78:1053–1058.
- [27] Hampson, C.R. and Simpson, G.M. (1990) Effect of Salinity Stress on Germination and Seedling Properties in Canola Cultivars (*Brassica napus* L.), Can.J.Bot. 68:524–528.
- [28] Auge', R.M., Duan, X., Ebel, R.C. and Stodola, A.J.W. (1994) Nonhydraulic signaling of soil drying in mycorrhizal maize, Planta. 193:74–82.
- [29] Ruiz-Lozano, J.M., Go'mez, M. and Azco'n, R. (1995) Influence of different *Glomus* species on the time-course of physiological plant responses of lettuce to progressive drought stress periods, Plant Sci. 110: 37–44
- [30] Kramer, P.J. (1983) Water relations of plants, Academic Press, New York.
- [31] Glenn, E. and Brown, J. (1998) Effects of soil salt levels on the growth and water use efficiency of *Atriplex canescens* (Chenopodiaceae) varieties in drying soil, Am. J. Bot. 85:10–16.
- [32] Mendelsohn, I.A. and McKee, K.L. (1988) *Spartina alterniflora* die-back in Louisiana: Time-course investigation of soil waterlogging effects, Journal J. Ecol. 76: 509–521.
- [33] Pezeshki, S.R., Pan, S.Z., DeLaune, R.D. and Jr Patrick, W.H. (1988) Sulfide-induced toxicity: Inhibition of carbén assimilation in *Spartina alterniflora*, Photosynthetica, 22: 437–442.
- [34] Koch, M.S., Mendelsohn, I.A. and McKee, K.L. (1990) Mechanism for the hydrogen sulfide-induced growth limitation in wetland macrophytes, Limnol. Oceanogr. 35: 399–408.
- [35] Jaynes, M.L. and Carpenter, S.R. (1986) Effects of vascular and nonvascular macrophytes on sediment redox and solute dynamics, Ecology. 67: 875–882.
- [36] Raven, P.H., Evert, R.F. and Eichhorn, S.E. (1999) Biology of Plants, sixth ed. W.H. Freeman and Co., New York.
- [37] Brown, C.E., Pezeshki, S.R. and DeLaune, R.D. (2006) The effects of salinity and soil drying on nutrient uptake and growth of *Spartina alterniflora* in a simulated tidal system, Environmental and Experimental Botany. 58(1-3): 140–148.
- [38] Duan, S.S. and Zhao, S.L. (1996) Study on propagula hierarchy and sibling competition in spring wheat populations under semi-arid conditions. In: Zhao, S.L. (Ed.), Arid Physioecology of Spring Wheat. Shanxi Scientific and Technology Publishing House, Xian, (in Chinese), pp. 179–272.
- [39] Xin, X.P., Wang, G. and Zhao, S.L. (1998) Size hierarchy and its genetic analysis in spring wheat population under different water conditions, Acta Phytoecol. Sinica. 22: 157–163.
- [40] Wu, D.X. and Wang, G.X. (1999) The dynamics of size inequality in spring wheat populations under semi-arid conditions and its physioecological basis, Acta Ecol. Sinica. 19: 254–258.
- [41] Duffield, A.N. and Edwards, R.W. (1981) Predicting the distribution of *Lemna* spp. in a complex system of drainage channels. In: Proceedings of the Association of Applied Biologists Conference Aquatic Weeds and their Controls, pp. 59–65.
- [42] Landolt, E. (1986) Biosystematic Investigations in the Family of Duckweeds (Lemnaceae) (vol. 2), the Family of Lemnaceae—A Monographic Study, vol. 1. Veroff. Geobot. Inst. ETH, Zurich.
- [43] Dale, H.M. and Gillespie, T. (1976) The influence of floating vascular plants on the diurnal fluctuations of temperature near the water surface in early spring, 49: 245–256.

Received: September 27, 2010

Accepted: November 23, 2010

CORRESPONDING AUTHOR

Dilek Demirezen Yilmaz

Erciyes University

Faculty of Sciences

Department of Biology

Kayseri
TURKEY

Phone: (90.352) 4374901-33063

Fax: (90.352) 4374933

E-mail: demirez@erciyes.edu.tr

FEB/ Vol 20/ No 7/ 2011 – pages 1667 – 1672

ASSESSMENT OF RIVER LANDSCAPES IN TERMS OF PRESERVATION AND USAGE BALANCE: A CASE STUDY OF THE BARTIN RIVER FLOODPLAIN CORRIDOR (WESTERN BLACK SEA REGION, TURKEY)

Bülent Cengiz^{1,*}, Richard C. Smardon² and Yalçın Memlük³

¹ Department of Landscape Architecture - Faculty of Forestry - Bartın University 74200 Bartın, Turkey
² SUNY-ESF Department of Environmental Studies - 211B Marshall Hall - 1 Forestry Drive Syracuse, NY 13210-2787 USA
³ Department of Landscape Architecture - Faculty of Agriculture - Ankara University 06100 Dışkapı-Ankara, Turkey

ABSTRACT

The objective of the study is to develop new river landscape planning strategies to meet the residential needs of local people and to provide land use and development alternatives that would both protect natural and cultural resources, and ensure sustainable growth and development of the Bartın River. The research methods consist of site inventory, analysis, and synthesis through site documents that include maps and IKONOS satellite images. In this study, the natural and cultural landscape characteristics of Bartın River are defined by use of Geographical Information System (GIS) to determine the environmental issues in the research area, as well as core, buffer and usage zones for landscape planning and alternative land use. Specific development of zoning and recommendations are proposed for: environmental problem solution sets, alternative land use planning and broad scale Bartın River landscape planning. As a result of the study, Bartın River is found to have significant potential for preservation and land use balance of river landscapes as well as promote future planning of the region in terms of environmental health and aesthetics. It is essential that flood risk and other environmental threats be minimized in consort with comprehensive land use planning for the Bartın River Floodplain Corridor.

KEYWORDS: River revitalization, flood risk, urban river landscape planning, floodplain corridor, Bartın River

1. INTRODUCTION

River floodplain corridor landscapes are extremely important [1]. Throughout history, people have settled next to

* Corresponding author
waterways because of the advantages they offer for transportation, commerce, energy, water supply, soil fertility, and even waste disposal. In spite of these benefits, historic attraction to settling along rivers and streams is not without drawbacks. Human uses of floodplains are associated with dangers both to humans and to the natural functions of the riparian or floodplain environment [2].

For developing countries like Turkey, which is still on the way to economical development, urbanization triggered by industrialization and sector diversity greatly increases the variety and intensity of human activities in several parts of river basins. This development pressure destroys the hydrological stability in the entire basin, which leads to devastating floods resulting in life and property losses. The land use changes with the construction of new residential areas, and transportation network extending in the river basins, which are important outcomes of rapid and uncontrolled urbanization, as it drastically destroys meadows and forests [3].

The Bartın River is the only river in Turkey allowing water transportation for a distance of 12 km from the Black Sea to the Bartın City center. Due to this value, the role of the trade on the Bartın River was a determining factor in the development of Bartın, which is the center of its environs especially in the Ottoman Empire period. In addition to its rich natural resources, Bartın City has important cultural landscape characteristics, as well [4]. Therefore, Bartın River is a special river at regional and national scales and it was chosen as the research area for this study. Protection of landscape characteristics of Bartın River and landscape planning studies has many benefits to future generations in view of rising population and urbanization pressure. The main aims of planning studies at various scales are to meet the increasing demands of future population growth and to develop protection strategies for

flood damage and landscape characteristics of the Bartın River [5]. Therefore, landscape characteristics of Bartın River Floodplain Corridor should be evaluated and assessed to protect its valuable natural and cultural resources and to maintain balanced land use and development.

Within this paper, after describing urban and rural landscape characteristics of research area with Geographical Information Systems (GIS), some planning principles and recommendations are utilized to address the factors adversely impacting the river landscape. These factors will be important for reducing flood risk, improving water transportation and connecting natural, cultural and historical environments of the Bartın River so as to enable landscape protection and tourism development, as well. Planning processes related to river landscapes are developed for the research area where such destruction occurs. Thus, it is intended to revive the Bartın River and to propose aims and strategies regarding the transformation of the riverbank and urban enhancement areas. It is hoped that this study will contribute to the economics of the country and the region for a long period of time by combining preservation and land use balance while conserving landscape characteristics of the Bartın River.

2. MATERIALS AND METHODS

2.1. Research Area

The Bartın River is located in the Western Black Sea Basin in northern Turkey. It is the second largest river

basin in the region (the first one is Filyos River Basin) [6]. The Lower Bartın River in Western Black Sea Region was chosen as the research area, which is 3340 ha in area (Fig. 1).

The total drainage area of Bartın River is approximately 2100 km² with a long term mean total annual precipitation of 1034 mm. Bartın City, established on Bartın River, is susceptible to major floods which are considered as flash floods due to the small catchment area [7]. The flow velocity of Bartın River is 720 meters per hour (m/h) and it drains one billion m³ water into the sea per year. The average depth of the river is 4-5 meters. With these characteristics, the Bartın River is a significant source of water transportation, enabling the transportation of goods from the Black Sea to Bartın City center. Moreover, it allows recreational trips with rowboats and motor-driven sea vehicles and sport fishing as well as commercial transportation such as freighters [8].

The Bartın River is situated within a roughly east-west trending asymmetric basin (See Fig. 1). This basin is delimited to the north by an east-west trending mountain range, which separates the basin from the Black Sea [9]. Bartın City and its environs consist of low hills, which are 250-300 m high with long and wide ridges. Among these hills, the dominant views of the topography are the valleys, reaching 2-3 km in width. The eroded surface of the ridges and hills are significant in the area. The valleys eroding these surfaces have slight slopes.

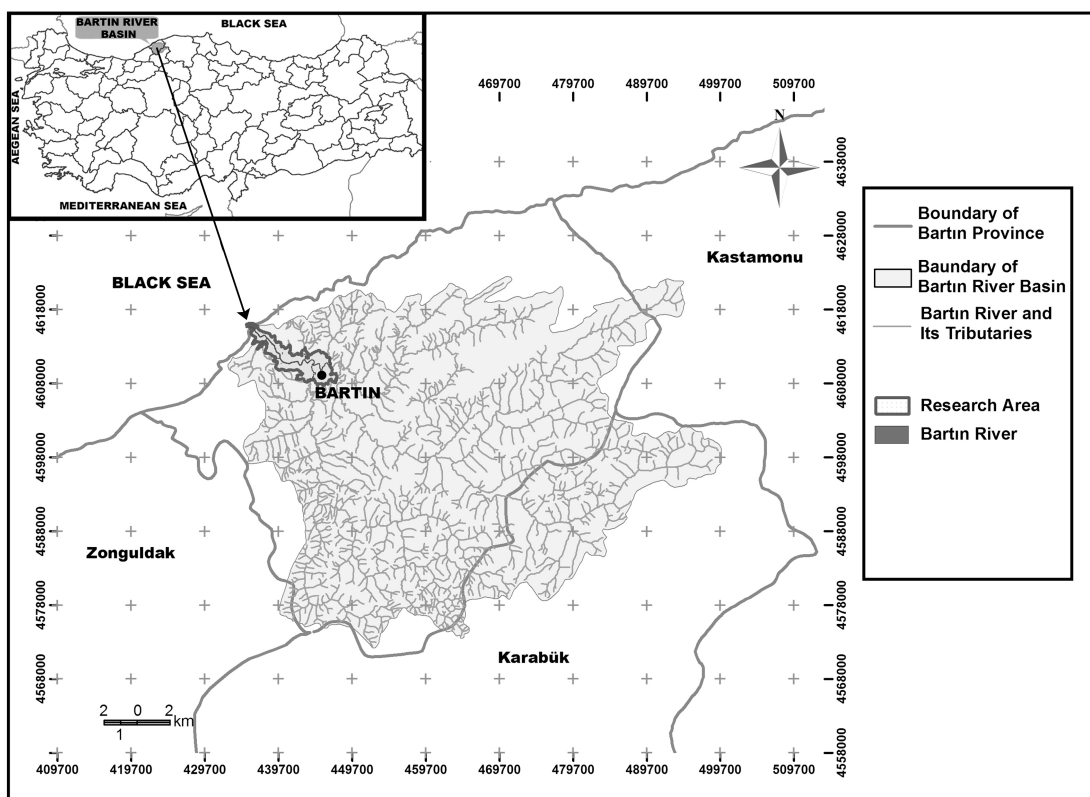


FIGURE 1 - Research area.

Due to the topography, local people use the floodplains of rivers located in narrow valleys both for settlement within urban areas, and agriculture within rural areas. In order to control the floods, local municipalities asked the central government to help them build the longitudinal dikes on both banks of the river crossing the urban areas. Since the fertile land is very limited to the narrow valleys, it is very valuable and utilized under high-risk flood conditions. Water is mainly used for irrigation of agricultural lands in the region [7].

The distribution of the current land use in the research area is as follows: urban settlement areas (29.20%), forests (26%), agricultural lands (20.55%), rural settlement (4.99%), open rivers (4.24%), transportation (3.96%), industry (3.33%), sand-pebble and stone-soil mines (2.91%), military (1.44%), meadow (1.17%), afforestation areas (0.86%), cemeteries (0.60%), recreational areas (0.48%), waste storage areas (0.12%), Bartın Port (0.08%), and artificial lake (0.05%). The types of current land usage are shown in Table 1 and Fig. 2 [5].

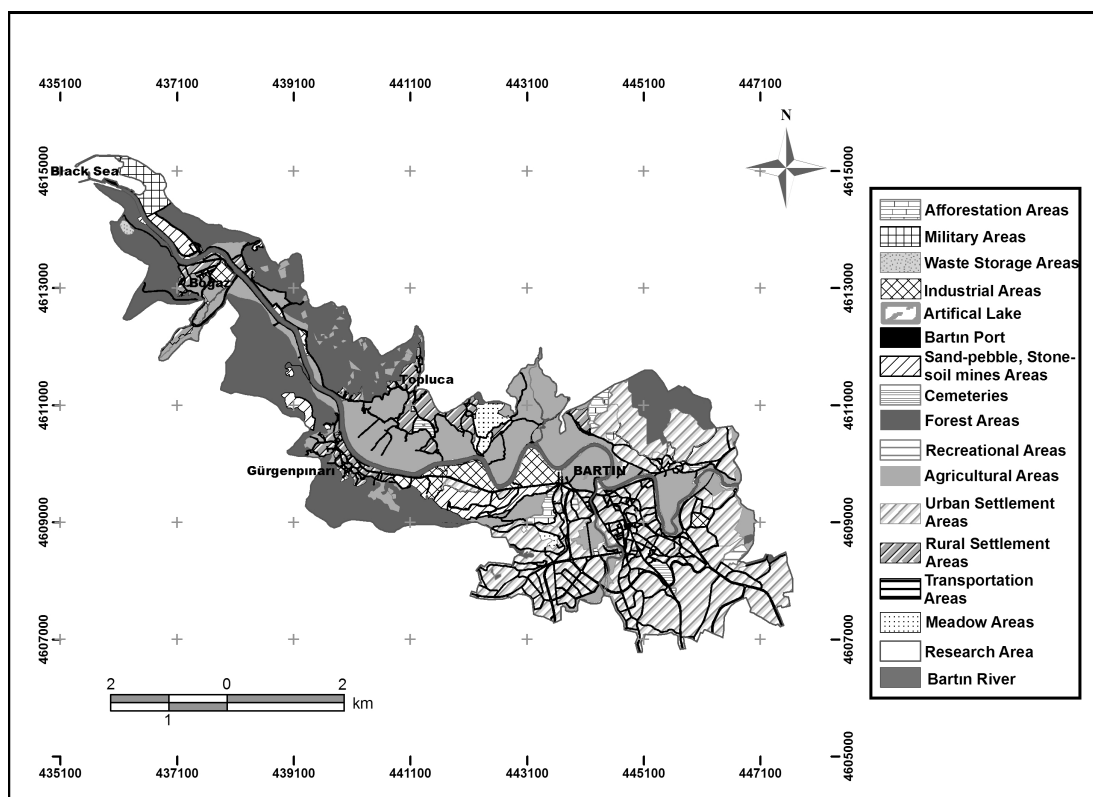


FIGURE 2 - Distribution of current land use within the Bartın Floodplain Corridor.

TABLE 1 - Types and distributions of current land use within the Bartın Floodplain Corridor.

Type	Area (m ²)	%
Afforestation areas	286305	0.86
Military areas	481585	1.44
Waste storage areas	39476	0.12
Industrial areas	1111185	3.33
Artificial lake	15785	0.05
Bartin Port	28048	0.08
Sand-pebble, stone-soil mines	972525	2.91
Cemeteries	201351	0.60
Forest areas	8682550	26.00
Recreational areas	160481	0.48
Open river areas	1419102	4.24
Agricultural areas	6860534	20.55
Urban settlement areas	9750366	29.20
Rural settlement areas	1667382	4.99
Transportation areas	1322045	3.96
Meadow areas	391992	1.17

2.2. Research methodology

The method used in the research has three general stages; (1) determining the boundaries of the research

area; (2) preparing the baseline maps for the research area; (3) and evaluating the landscape characteristics within the research area (Fig. 3).

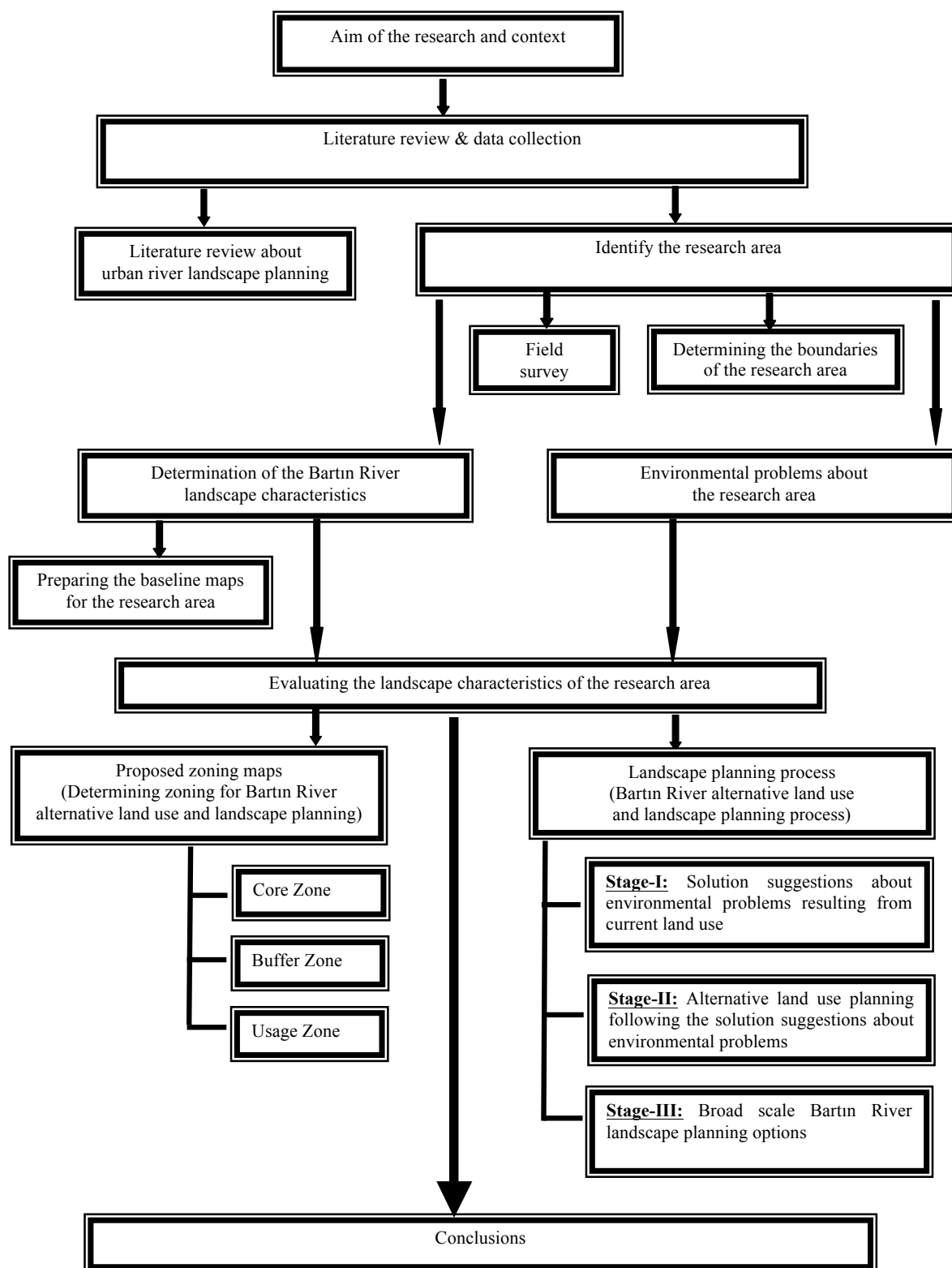


FIGURE 3 - Research methodology.

2.3. The method used for determining the boundaries of the research area

Administrative boundaries are used in the planning process. In ecological assessments, boundaries related to natural processes are utilized, while artificial (or non-physical) boundaries are omitted [10]. There should be important determinations to improve usage decision taking into account ecological processes in accordance with the principle of “design with nature” developed by McHarg [11]. In this study, both administrative and physical breaks were used to determine the boundaries of the research area. Thus, while the plan decisions were intended to be applicable in a managerial way, the major plan decisions were undertaken considering natural factors.

The following criteria were utilized regarding the preservation and land usage balance to determine the boundaries of the research area. According to this process, physical boundaries (overflow boundary and erosion process) and administrative boundaries were evaluated [5].

Biophysical impact areas: The river is the main determinant natural landscape factor of the research area. The continuity of the river system, the processes and the dynamics of its ecosystem, as well as the overflow and erosion processes were determinant natural phenomena in identifying the physical breaks. Overflow boundary and erosion processes were evaluated to identify the primary impact area of the river [10] (See Fig.).

The overflow boundary is defined as the river impact area. It was evaluated considering the following studies in

the literature on landscape planning: Cook [1], Smardon et al [2], Morris [12], Riley [13], Hulse and Gregory [14], Otto et al. [15], Marsh [16], and Anonymous [17]. The evaluation was conducted within a 100-year flood boundary area.

Based on these data, the boundary of Bartın River overflow area was determined in accordance with the following information. The settlements within old urban areas of Bartın are located in inclined ridges formed during the Eocene over 20 m. The natural breaks are physical boundaries, which decrease the risks of overflow and high groundwater [18]. River terraces of 0-20 m height and with about 0.1% are located in the Bartın River Basin. These areas are defined as the “Flood Plain” of the Bartın River [19]. The floodplain of Bartın River and the 100-year old historical overflow boundary area of the river overlap to a great extent with the impact area of the flood that occurred in May 1998 [20]. The above mentioned reasons were used to calculate the areas between 0-20 m levels of the Bartın River, plus the flood area border for the last 100 years [5; 20] (Fig. 4).

Hill slope erosion processes contribute to nonpoint water pollution affecting the river water quality [5]. Therefore, Bartın River hill slope erosion process was evaluated with regard to primary and secondary degree impact areas within the research area. For this evaluation, drainage canals, which directly join the Bartın River and have two bifurcations at most or micro-basins of short seasonal rivers were analyzed. There is a high risk of erosion in these micro-basins and especially for seasonal river flows (natural drainage ca-

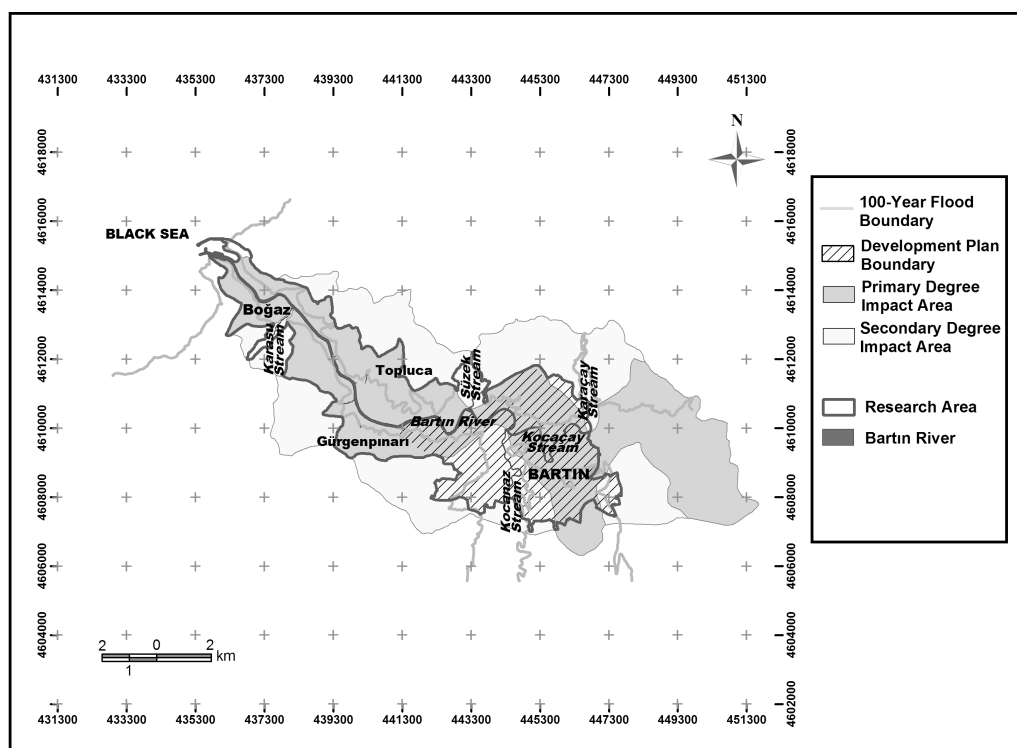


FIGURE 4 - Biophysical impact areas and administrative boundaries.

nals). According to the Şahin and Beşişoğlu [21], a research area boundary was set to merge the micro-basins within the regional boundary position. This boundary constitutes a primary degree impact area in terms of flooding and erosion. On the other hand, drainage canals which directly join the Bartın River and have more than two bifurcations or micro-basins for short flow seasonal rivers and adjacent brooks were evaluated as secondary degree impact areas. Bartın River and its tributaries (Kocanaz and Kocaçay), and physical breaks (topographical and geomorphologic breaks as well as water surfaces) forming primary degree impact areas of these rivers were utilized in the determination of erosion processes impact areas (See Fig. 4).

Administrative boundaries: The physical breaks in the semi-rural area between the Black Sea and Bartın City center (Gazhane Cape) enable the exact definition of the boundaries of the research area. On the other hand, the physical breaks in the city center have disappeared due to the expansive land use practices and flooding zone spreading into the neighboring areas. So, the inter-city crossing of the Bartın River cannot be defined clearly compared to its semi-rural crossing. Therefore, Bartın City zoning borders were taken into consideration for the inter-city crossing (Kocanaz and Kocaçay tributaries) and physical breaks were considered for the semi-rural crossing of the Bartın River. The boundaries of the research area composed of these two borders are given in Fig. 4.

In brief, the research area consists of the biophysical impact areas (primary degree impact area of the Bartın River and a 100-year historical flood boundary) and administrative boundary (Bartın City Development Plan Boundary) (Fig. 4).

2.4. The method used in preparing the baseline maps for the research area

Maps were obtained from various institutions to determine natural and cultural landscape characteristics of the research area and digitized in ArcView 9.2. Because the maps related to the research area have different projection systems and software, the projection of all bases were transformed to Universal Transverse Mercator (UTM) 6 degree and prepared according to UTM coordinate system and D_European_1950 Datum.

1/25000 scaled topographical, soil, geological and forest management and 1/1000-1/5000 scaled cadastral and reconstruction maps were superimposed. Moreover, the files with the extension ncz were transformed into dxf so as to obtain raster data, which was then digitized in GIS. Although the pixels of topographical maps and cadastral maps with a UTM projection are the same, the pixels of place coordinated cadastral maps are on different projection bases. The pixels of development maps of the city are different from the UTM base. A base with a single projection was produced in accordance with the aim and the content of the

study so that all map layers could be combined. Map pixels at 1/5000 and 1/1000 scales were used by Bartın Municipality in development plans was taken as a standard basis. Therefore, the base with a single projection was used for the research area, alternative land use and landscape planning processes.

The method used in evaluating the landscape characteristics of the research area

In this part of the study, the zones relating to Bartın River alternative land use and landscape planning were determined and their processes were described.

2.5. Data Used

The 1/25000-scaled Topographic Maps belonging to the General Command of Mapping [2005] were used to determine the research area boundary, the slope, the promontory groups, the peaks, the aspects and the water body type (wet brook, valley and seaside). The 1/25000-scaled Soil Maps belonging to the General Directorate of Rural Affairs (2004) were used to determine the land groups, the land use capacity classes and the status of erosion in the research area.

The 1/25000-scaled Geology Maps belonging to the General Directorate of Mineral Research and Exploration [2005] were used to determine the geological structure and fault status of the research area. The 1/100000-scaled morphology maps produced by Turoğlu and Özdemir [2005] were used to show the morphological structure of the research area. The 1/25000-scaled Forest Management Planning Map belonging to the General Directorate of Forestry [2005] was used to determine the forest existence within the research area. 1/5000-2500-2000-1000 scaled Cadastral Maps produced in different years were used to determine the land ownership patterns in the research area. IKONOS satellite image [2006] and cadastral maps were used to demonstrate the current land use types and their distribution in the research area.

Maps in various scales obtained from natural, archeological, urban site, urban site impact passage and wild animal habitat areas that are protected under the present laws and managed by government agencies were utilized for the research area.

Maps produced by the State Hydraulic Works were used to determine the hydrology of the Bartın River and the areas having the risk of potential flooding.

Proposed zoning maps (Determining zoning for Bartın River alternative land use and landscape planning): In accordance with the data types obtained via screening the literature of river landscapes and research areas, a method was developed to determine the zones relating to alternative land use and landscape planning (Table 2). Sub-factors constituting the natural and cultural landscape characteristics of the research area were classified into zones and subzones. Factors affecting the landscape char-

acteristics of the area obtained as a result of the grouping of these sub-factors were determined in order to build the preferred zoning map. Then, suggestions were made separately for each zone. In the development of this method (Table 2) the

TABLE 2 - Determining zoning for Bartın River alternative land use and landscape planning.

ZONES	SUB-ZONES	LANDSCAPE CHARACTERISTICS (factors)	TYPES OF LANDSCAPE CHARACTERISTICS (sub-factors)	Recommendations / Priorities of action and measures
CORE	I	Protected and Conserved Areas	Cultural Landscape	<ul style="list-style-type: none"> • Urban Site Area • Semi-Urban Site Area • Archeological Sites • Traditional Architecture Examples • Registered Cemeteries
			Natural Landscape	<ul style="list-style-type: none"> • Natural Site Area • Wild Animal Habitat Area
		Agricultural Landscape		<ul style="list-style-type: none"> • Agricultural Areas Alluvial soils 1st and 2nd class cultivated areas • Meadow Areas
		Forest Landscape		<ul style="list-style-type: none"> • Forest Areas • Endemic Plants Areas
	II	Areas of Outstanding Scenic Quality		The areas with a unique landscape quality and characteristics whose townscape is not spoilt should be protected under natural protected area status and suggestions about public usage should be developed. This zone contributing to urban ecosystem functionally, aesthetically and economically should be evaluated only as a public usage area with recreational aims. This zone should be integrated with Bartın River and urban open and green area system should be formulated.
		Extraordinary Morphological Structure		<ul style="list-style-type: none"> • Hills
	III	Urban Green Areas	<ul style="list-style-type: none"> • Parks • Squares • Recreational Areas • Afforestation Areas • Cemeteries Areas 	Urban ecosystem functional, aesthetic and economic contribution of the people of this zone only as a recreational space for public use should be assessed. This zone is integrated with Bartın River creation of urban open and green areas system must be provided.
BUFFER	I	Areas of Natural Disasters such as Flood, Earthquake, Soil Erosion, etc.	<ul style="list-style-type: none"> • Earthquake Zone • Flood Risk Areas • Landslides 	This zone is important in terms of risk and river restoration considering earthquake, flood, and erosion. Limited usages and urban rehabilitation projects should be allowed after protective measures are taken in the zone. Especially, when the shores of Bartın River are turned to public area, the city has the potential to form the backbone of open and green area system. From this regard; Bartın River is possible to be evaluated in terms of landscape design project and recreational usage of public. Special usage types should be determined for the areas that cannot be turned to public area.
		Areas of Improvement Works of the Bartın River	<ul style="list-style-type: none"> • State Hydraulic Works (DSİ) TEFER Project Area 	
	II	Industrial Landscape	<ul style="list-style-type: none"> • Industrial Development • Sand-pebble, Stone-soil Mines • Waste Storage Areas 	This zone has environmental problems, which result from inappropriate usage areas. Thus, there should be studies in terms of landscape reclamation for material provision quarries operated without certificate or with expired certificate and solid waste storage area, and alternative area choice for industrial establishments.
USAGE	I	Urban Settlement Areas	<ul style="list-style-type: none"> • Development Plan 	This zone consists of urban settlements. The area within development border is urban settlement. This zone includes suitable areas for settlement. Urban rehabilitation projects should be implemented in this zone to vitalize current urban settlement areas.
	II	Rural Settlement Areas	<ul style="list-style-type: none"> • Contiguity Boundary 	This zone consists of (semi) rural settlements. The area outside development border is (semi) rural areas because it is in contiguous area. This zone includes suitable areas for settlement. Planned and controlled structuring should be allowed in this zone. Especially, farmhouses compatible with nature should be spread in rural landscape.

TABLE 3 - Landscape planning process (Bartın River alternative land use and landscape planning process).

ZONING		STAGE-I	STAGE-II	STAGE-III
ZONES	SUB-ZONES	SOLUTION SUGGESTIONS ABOUT ENVIRONMENTAL PROBLEMS RESULTING FROM CURRENT LAND USE	ALTERNATIVE LAND USE PLANNING FOLLOWING SOLUTION SUGGESTIONS ABOUT ENVIRONMENTAL PROBLEMS	BROAD SCALE BARTIN RIVER LANDSCAPE PLANNING OPTIONS
CORE	I-II-III	<ul style="list-style-type: none"> Revision of protected and conserved areas in law (natural sites, wild animal habitat area) Limited usage areas Areas whose scenic quality will be protected 	<ul style="list-style-type: none"> The areas whose agricultural quality will be sustained (Suggested agricultural protected areas) <ul style="list-style-type: none"> Urban agriculture areas The areas whose rural quality will be protected The areas whose forestry areas will be protected The areas whose wildlife areas will be protected 	<ul style="list-style-type: none"> Improve public access to the riverside Provide urban open and green area system along the Bartın River Develop river transportation
BUFFER	I-II	<ul style="list-style-type: none"> Misuse areas (Industrial development and waste storage areas etc) Landscape reclamation areas Urban rehabilitation areas 	<ul style="list-style-type: none"> River recreation areas River rehabilitation / restoration areas Afforestation areas Urban forest areas Urban greenway areas 	
USAGE	I-II	<ul style="list-style-type: none"> Landscape design project areas 	<ul style="list-style-type: none"> Proposed urban park areas Proposed landscape design (Urban design) project areas 	

methods of previous researchers including Smardon et al. [2], Morris [12], Otto et al. [15], Ateş [22], Tzolva [23], Kuiper [24], Fisher et al. [25], and Anonymous [26] were compared. As a result of changes and improvements made on these methods, a field-specific method was prepared for this study [5].

Landscape planning processes (Bartın River alternative land use and landscape planning processes): As a result of determining the zones relating to alternative land use and landscape planning, Bartın River alternative land use and landscape planning processes included three stages. In the development of this method (Table 3): the methods of Smardon et al. [2]; Morris [12]; Otto et al. [15]; Anonymous [17]; Fisher et al. [24]; Anonymous [25] were synthesized. Considering the zoning developed in accordance with Table 2, the suggested Bartın River landscape plan and the process were prepared in 3 stages. These are [5];

Stage-I / Solution suggestions for environmental problems resulting from current land use;

Stage-II / Alternative land use planning following solution suggestions for environmental problems; and

Stage-III / Broad scale Bartın River landscape planning options.

3. RESULTS AND DISCUSSION

3.1. Landscape characteristics

In the evaluation of Bartın River landscape characteristics, some strategies concerning alternative land use and landscape planning are developed. In this regard, the maps were prepared to inventory the landscape characteristics and constraints of the research area within the GIS context.

The sub-factors of Bartın River landscape characteristics were arranged with the help of present data in Table 2 and the study of Smardon et al. [2]. After the sub-factors

were classified, the landscape characteristics of the Bartın River were revealed in map and table formats [5] with the help of the studies of Ateş [22], Tzolva [23], and Anonymous [26].

3.2. Proposed zoning maps (Determining zoning for Bartın River alternative land use and landscape planning)

On the basis of Bartın River landscape characteristics and preservation-usage balance, zoning was proposed to guide decisions about alternative land use concerning river landscape planning. In this context, three main zones were suggested as “core”, “buffer” and “usage” (Table 2) for this research area and a zoning map was developed (See Fig. 5).

The *core zone* is composed of three sub-zones. The primary degree sub zone is composed of protection and conservation areas, agricultural landscape and forest landscape. Protection and conservation areas are comprised of cultural landscape including urban sites, semi-urban sites, archeological sites, samples of traditional architecture, registered cemeteries, and natural landscape including natural sites and wild animal habitats. Agricultural landscape contains 1st and 2nd class cultivated fields, meadows and pasture areas. The forest landscape is comprised of forestlands and areas where endemic plant species are found. Second-degree sub-zone includes the areas with unique landscape and viewpoints with urban silhouette and also the morphologically important areas that contain upper erosion surfaces. Third degree zone includes urban green areas such as parks, squares, recreational areas, afforestation areas, and cemeteries.

The *buffer zone* is composed of two sub-zones. The primary degree sub-zone includes earthquake sensitive areas, flood-overflow areas, areas under earthquake risk, flood-overflow and erosion areas (of which erosion degree is 3rd), and the areas of improvement works of the Bartın River that contain the Turkey Flood and Earthquake Recovery Project (TEFER) area of the Turkish State Hydraulic Works (DSI). Second-degree sub zone includes

the industrial landscape containing industrial development, construction material supply pits and solid waste storage area.

The *usage zone* is composed of two sub-zones. The primary degree sub-zone includes the areas within settlement boundaries and the urban settlements. Second-degree sub-zone includes (semi) rural settlements because the areas are removed from Development Plan Boundaries included in the Contiguity Area.

The core, buffer and usage zones regarding the Bartın River alternative land use planning and landscape planning in terms of the zones improved below are shown on Fig. 5.

3.3. Landscape planning process (Bartın River alternative land use and landscape planning process)

Alternative land use of Bartın River and landscape planning process consists of three phases for reducing flood and erosion damage, improving the water quality, protecting natural waterway, and attracting or enhancing a tourist economy (See Table 3).

Stage-I / Solution suggestions about environmental problems resulting from current land use: The traditional use of Bartın River as recipient of water effluent has obviously negative effects on environment. But it also has other negative effects such as “river regulation” (irrigation, drainage, the construction of navigation channels, reservoirs, dams, etc.); and it damages the habitats of species due to over-exploitation. The current land use types

on both sides of the Bartın River (See Fig. 2) cause environmental problems regarding natural and cultural landscape attributes. The most significant environmental problems may be classified into six groups; air pollution, water pollution, soil pollution, visual pollution, and noise pollution in addition to negative effects on flora and fauna [4; 5; 27]. At this stage, some strategies were proposed for settlement areas, agricultural areas, forest areas, meadows and pasture areas, industrial areas, sand-pebble/stone-soil mines, waste storage areas, recreational areas, protected and conserved areas, existing flora and fauna potential, transportation and planning decisions.

Solutions to problems resulting from the current land use types in *core*, *buffer* and *usage zones* are defined in Table 3. It is intended to make revisions in the regulation of the Protected and Conserved Areas to determine areas on settlement boundaries for controlled (limited) use, and areas with scenic quality that should be protected (keep the urban silhouette). In the *core zone*, following areas should be determined: inappropriate land use areas, landscape reclamation areas and urban regeneration/ transformation areas within the *buffer zone*; in addition, the areas that are proposed as landscape design project areas should also be defined.

Stage-II / Alternative land use planning following the solution suggestions about environmental problems: In stage-II, the alternative land use planning is prepared following the solution suggestions about environmental problems.

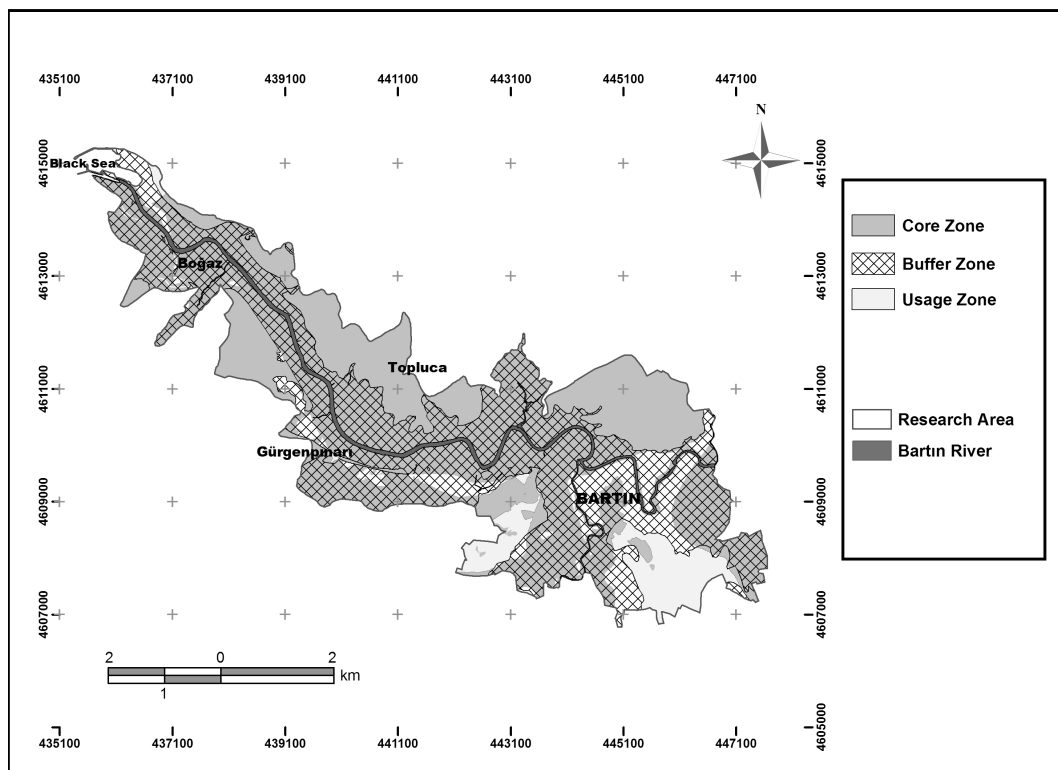


FIGURE 5 - Proposed zoning map for the Bartın River Floodplain Corridor.

There is the Agricultural Site Concept in the *core zone* for stage-II. The areas of 1st, 2nd and 3rd class cultivated areas and alluvial soils should be taken under protection status as protected agricultural areas so as to stimulate continued agricultural usage. Protected agricultural areas should definitely not be allowed to be used except for their highly productive agricultural use. Urban agriculture areas, rural quality and the wooded wildlife areas should be protected to maintain their quality levels.

It is intended to determine specific river recreation areas, afforestation and rehabilitation areas, areas that will be transformed into urban forest and the areas where recreational roads are proposed. Areas need to be transformed into urban park and built-up areas in the *usage zone*, which necessitates landscape design projects.

Fig. 6 is developed according to the alternative land use planning at 1/5000 scale and based on the suggested zones in the research area. As a result of this stage, the following suggestions were put forward:

According to the Fig. 6 recommendation of alternative land use planning (strategies for alternative land use planning):

1. Areas of which the current protection status will be maintained by national law and regulations (Natural site, archeological, urban site, urban site interaction areas, registered buildings and meadows);

2. Ecological restoration areas of Bartın River and its tributaries (Karaçay, Süzek and Karasu Streams);

3. Transforming overflow areas of Bartın River to urban open and green areas (DSI flooding boundary and 100-year flooding boundary);

4. Areas of which the current flora and fauna will be protected;

5. Areas with valuable views and landscapes;

6. Areas of which the rural characteristics will be protected;

7. Areas of which the agricultural characteristics will be maintained;

8. Areas of which the forest asset will be protected;

9. Protection of current afforestation areas and planning/transforming them into city forests;

10. Landscape reclamation areas after mining activities; and

11. Reviving the urban and rural settlement areas and integration with Bartın River.

Stage-III / Broad scale Bartın River landscape planning options:

The following strategies were developed to sustain natural and cultural values of Bartın River, protect flood or overflows, meet the active and passive recreation needs of the city and to positively affect the city climate:

I. Improve public access to the riverside,

II. Provide urban open and green area systems along the Bartın River, and

III. Develop river transportation.

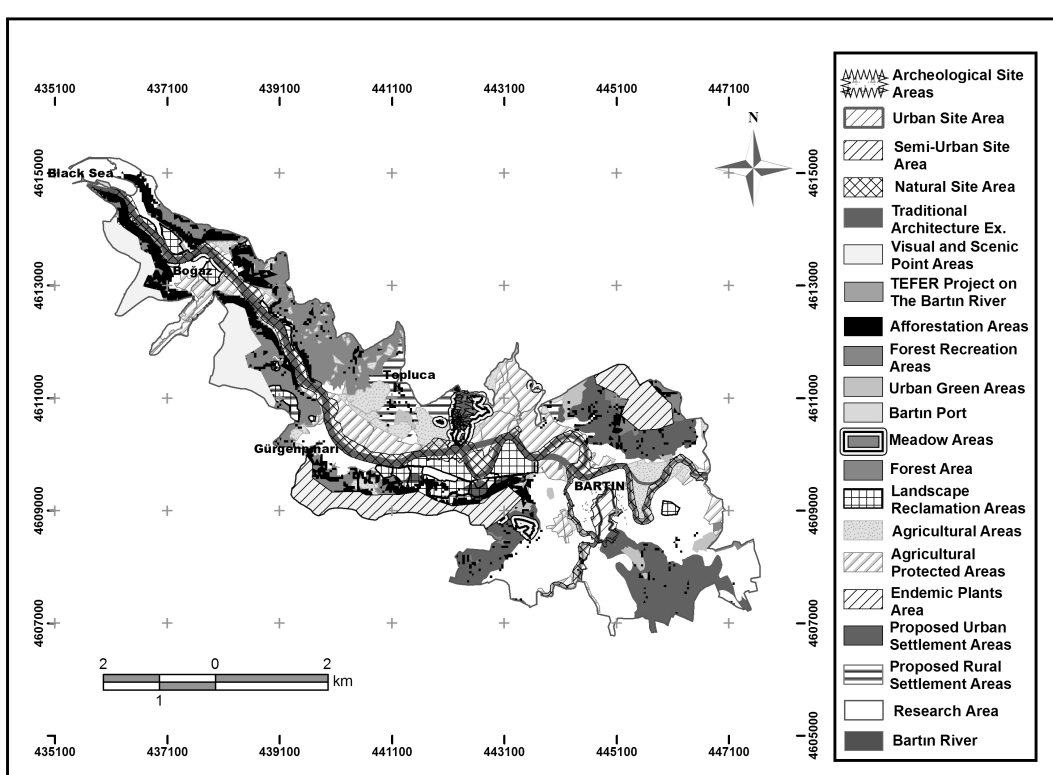


FIGURE 6 - Alternative land use planning for the Bartın River Floodplain Corridor.

4. CONCLUSIONS

A range of problems was encountered with the quality, currency and capacity of data to determine the use of usage for the present study area. These problems were: difficulty in achieving a restoration plan through planning and design studies in Turkey using complex and paradoxical maps of limited utility. That is because, it is very difficult to get updated maps from relevant organizations to use in scientific studies In addition, another important constraint is to obtain necessary metadata for maps prepared under different conditions. Current data should be produced with GIS technology to provide the coordination of relevant organizations so as to overcome these problems. Easier access to these data and metadata should be allowed especially for scientific studies.

In addition to natural and cultural landscape values of the Bartın River, areas with historical significance should be integrated with potential tourism centers in the region to boost river tourism and recreation. Ecological and economical benefits are the main planning objectives of river revitalization studies for Bartın River.

Sustainable ecological characteristics of Bartın River, boundaries of flooding areas (2-5-10-25-50-100-500-year floods) should be determined and handled in the development plans. To evaluate these areas considering public benefit is important in terms of urban open and green space system. So, it could be possible to protect the city against flood and earthquake risks with the help of specifying flooding area boundaries on the shores of Bartın River and to create contemporary places for recreational public use in Bartın city at the same time. According to the European Water Framework Directive (WFD), Basin Management Plans and Urban Flood Risk Management Plans should be prepared. Subsequently, these plans could be integrated into Bartın Development Plans.

It is quite important to protect, develop and use the current landscape characteristics of the river and to convey such characteristics to next generations as a heritage value. The main aim is to carry forward Bartın River to the 21st century by improving its environmental health and aesthetic values, and so utilizing the preservation-usage balance approach. It is an objective to make Bartın City one of the world's prestigious cities cut through by a river with its current natural and cultural landscape characteristics. It is important to protect the landscape characteristics of river and to plan landscape studies so as to convey to future generations and to mitigate against rising population and urbanization pressure. The main aims of planning studies on various scales are to meet increasing demands of future population growth, plus developing strategies to protect the valued landscape characteristics of the river basin. Otherwise, as in many other cities in Turkey, a multifunctional river can be removed from the city landscape.

In this study, a method is developed to determine and assess the landscape characteristics of Bartın River. This

study can be an example for planning urban river landscape revitalization projects for similar hydrologic landscape regions and can be developed further.

ACKNOWLEDGEMENTS

This study was derived from the Ph.D. thesis entitled “A research on the determination and assessment of landscape characteristics of the Bartın River” financially supported by the scientific research grant (ÇAYDAG 104Y190) of the Scientific and Technological Research Council of Turkey (TUBİTAK).

REFERENCES

- [1] Cook, E.A. (1991) Ecosystem modeling as a method for designing synthetic fluvial landscapes: a case study of the Salt River in Arizona. *Landscape and Urban Planning* 20:291-308.
- [2] Smardon, R.C., Felleman, J.P. and Seneca, S. (1995) Protecting floodplain resources: A guidebook for communities. Federal Interagency Floodplain Management Task Force, FEMA publication number 268, Washington, DC.
- [3] Özcan, O., Musaoglu, N., Şeker, D.Z. and Tanik, A. (2008) Determination of flood risk in Sakarya sub-basin using Remotely Sensed data and GIS. *Fresenius Environmental Bulletin*. 17 (11b), 1964-1970.
- [4] Cengiz, B. and Memlük, Y. (2005) The Bartın River (Turkey) and its planning strategies. International Conference on Urban River Rehabilitation. September 21-23, 2005 Dresden, Germany. pp. 296-302.
- [5] Cengiz, B. (2007) A research on the determination and assessment of landscape characteristics of the Bartın River. Ph.D. thesis, Ankara University, Graduate School of Natural and Applied Sciences, Department of Landscape Architecture, Ankara (in Turkish).
- [6] Anonymous (1998) Bartın revised master plan project report. DSİ XXIII. District Office, Kastamonu (in Turkish).
- [7] Gürer, I. and Özgüler, H. (2004) Integrated flood management case study in Turkey: recent flood disasters in North-western Black Sea Region. Technical Support Unit.
- [8] Aşçıoğlu, E. (2001) Bartın. Bartın Trade and Industry Chamber Press, Bartın (original text in Turkish).
- [9] Memlük, Y. and Cengiz, B. (2005) Ecological characteristics of Bartın River. X. European Ecological Congress. Organized by European Ecological Federation Turkish Ecological Society. Ege University Center for Environmental Studies. November 8-13, 2005 Kuşadası, Turkey. pp. 237-248.
- [10] Treweek, J. (1999) Ecological impact assessment. Institute of Terrestrial Ecology, Monks Wood, Komex Clarke Bond, Bristol.
- [11] McHarg, I.L. (1969) Process as values. In design with nature. Published for The American Museum of Natural History, New York.
- [12] Morris, M. (1997) Subdivision design in flood hazard areas. Series: Report (American Planning Association. Planning Advisory Service). No: 473rd Federal Emergency Management Agency, Chicago, IL.

- [13] Riley, A.L. (1998) Restoring streams in cities: a guide for planners, policymakers and citizens. Washington, DC, Island Press.
- [14] Hulse, D.W. and Gregory, S.V. (2001) Alternative futures as an integrative framework for riparian restoration of Large Rivers. Applying ecological principles to land management / edited by Virginia H. Dale, Richard A. Haeuber, Springer-Verlag New York.
- [15] Otto, B., McCormick, K. and Leccese, M. (2004) Ecological riverfront design: restoring rivers, connecting communities. American Planning Association, Planning Advisory Service Report Number: 518-519, Chicago, IL.
- [16] Marsh, W.M. (2005) Landscape planning: environmental applications. 4th Edition. McGraw-Hill Publishers, New York.
- [17] Anonymous (2006) A handbook for stream enhancement & stewardship / The Izaak Walton League of America. Blacksburg, VA. McDonald & Woodward Pub. Co; Gaithersburg, Md.: Izaak Walton League of America.
- [18] Erkin, E. (1978) Bartın (Zonguldak) analytical studies. General Directorate of Bank of provinces, Ankara (in Turkish).
- [19] Turoğlu, H. and Özdemir, H. (2005) Floods and flash floods in Bartın causes, effects, prevention-mitigation. Çantay publisher, İstanbul (original text in Turkish).
- [20] Anonymous (2001) Repair and improvement of flood protection infrastructure in West Black Sea flood region. TEFER project no: 22-23, Rehabilitation of flood protection structures according to 100-year flood in Bartın 1,2. Vol: 1, final report.
- [21] Şahin, Ş. and Bekişoğlu, Ü. (2009) Landscape planning and management strategies for Zir Valley, near Ankara, Turkey. Environmental Geology. 57; 2. pp. 297-305.
- [22] Ateş, V.T. (1985) In the planning of urban green areas system in Ankara Mogan Lake-river system between Lake-Akkopru potential for the environmental determination and evaluation of weight on the research. Ph.D. thesis, Ankara University, Graduate School of Natural and Applied Sciences, Department of Landscape Architecture, Ankara (in Turkish).
- [23] Tzolova, G.V. (1995) An experiment in Greenway analysis and assessment: the Danube River. Landscape and Urban Planning 33:283-294.
- [24] Kuiper, J. (1998) Landscape quality based upon diversity, coherence and continuity: Landscape planning at different planning-levels in the river area of The Netherlands. Landscape and Urban Planning 43:91-104.
- [25] Fisher, B., Gordon D.L.A., Holst, L., Krieger, A., McMillan, G., Rafferty, L. and Schiffman, E.S. (2004) Remaking the urban waterfront. Urban Land Institute, Washington, DC.
- [26] Anonymous (2005) Laws and regulations of the 3194 reconstruction. Ministry of Public Works and Settlement General Directorate of Technical Research and Practice, Ankara (in Turkish).
- [27] Anonymous (2005) Environmental status report of Bartın-2004. Bartın Governorship Provincial Directorate of Environment Bartın Press, Bartın (in Turkish).

Received: September 28, 2010

Revised: March 17, 2011

Accepted: March 18, 2011

CORRESPONDING AUTHOR

Bülent Cengiz

Bartın University
Faculty of Forestry
Department of Landscape Architecture
74200 Bartın
TURKEY

Phone: +90 (378) 223 51 21

Fax: +90 (378) 223 50 62

E-mail: bcengiz@bartin.edu.tr

DEGRADATION OF ORGANIC MATTER AND AMMONIA NITROGEN IN CONSTRUCTED RAPID INFILTRATION SYSTEM

Wenlai Xu^{1,*}, Jianqiang Zhang² and Yun Liu²

¹College of Environment and Civil Engineering, Chengdu University of Technology, Chengdu 610059, China

²College of Environmental Science and Engineering, Southwest Jiaotong University, Chengdu 610031, China

ABSTRACT

Constructed rapid infiltration system (CRIS) belongs to the plug-flow reactor. Some scholars think that owing to the inhibition on the nitrifying bacteria from organics, along the direction of the water flow in the plug-flow reactor, organics is removed firstly and then is NH_4^+ -N. A CRIS analog column was applied to treat the domestic wastewater and the degradation laws of COD and NH_4^+ -N under different hydraulic loads was studied. The results show that in conditions of five different hydraulic loads, the COD removal rates in 0-0.75 m section of CRIS are high and the best filter layer for the COD degradation is 0-0.25 m section. After 0.75m, the COD removal rates become lower and lower with the increase of the filter layer depth. In 0-0.25 m section, since the organic nitrogen is transformed into NH_4^+ -N via action of the heterotrophic bacteria and the ammonifying bacteria, the NH_4^+ -N concentrations rise slightly. After 0.25 m, the NH_4^+ -N removal rates increase rapidly and the best filter layer for removing NH_4^+ -N tends to shift down with the rise of hydraulic load. Though the best filter layer for NH_4^+ -N degradation and the best filter layer for COD degradation are different, the filter layer for NH_4^+ -N degradation and the filter layer for COD degradation have no strict area boundary.

KEYWORDS: COD; NH_4^+ -N; hydraulic load; degradation law; constructed rapid infiltration system

1. INTRODUCTION

Traditional sewage land treating systems have the advantages of requiring simple equipment, easy to operate, low energy consumption and so on, as well as have many limitations, such as the low hydraulic load rate that they can treat, the low wastewater treating capabilities per unit area and the possibility of easy clogging [1-4]. To solve these problems, a constructed rapid infiltration sewage treating system (CRIS) was developed based on the traditional rapid infiltration and the constructed wetland sys-

tems. Here is its working principle: the mixtures of 85% natural sands, 5% marble sands, 5% zeolite sands and 5% magnetite sands are filled in the rapid infiltration pond as the artificial filter material, then the rapid infiltration pond is fed wastewater once every six hours and the water flowing direction within it is vertical down; when wastewater goes through the filter layer, the biofilm will grow on the surface of the filter materials; then the biofilm and the filter medium will retain and adsorb those dissolved substances and suspended materials present in wastewater; meanwhile, the highly concentrated biofilm, attached to the high specific surface area of the filter material, rapidly deputates the pollutants in wastewater [5].

The biomembrane of different dominant species can grow on the surface of the filter material at different depth of CRIS and can perform carbonation, amination, nitrification and denitrification. Therefore, the CRIS can remove diverse pollutants in the same reactor [6]. Some scholars think that because the organics can inhibit the nitrifying bacteria, organic matters and NH_4^+ -N are respectively removed in different areas in the same plug-flow reactor. Along the direction of water flow in plug-flow reactor, organics are removed firstly and then is NH_4^+ -N [7, 8]. CRIS, as a plug-flow reactor, mainly disposes domestic wastewater and polluted rivers [9]. The influent COD concentration of CRIS is relatively low and the heterotrophic bacteria cannot reproduce in large number at top of CRIS [10]. Therefore, the inhibition effect on the nitrifying bacteria by the heterotrophic bacteria is weaker, which let the filter layer for NH_4^+ -N degradation and the filter layer for COD degradation have no strict area boundary. This research applied CRIS analog column to treat domestic wastewater and to study the degradation laws of COD and NH_4^+ -N under different hydraulic loads in CRIS. Research results can optimize the CRIS treatment process and provide a valuable reference for factual design and operation in engineering.

2. MATERIAL AND METHODS

2.1 Experimental device

A CRIS simulation column was constructed in lab. The main body of the reactor was composed of a hard PVC

* Corresponding author

pipe with 200 cm in height and a internal diameter of 21 cm; the filter material consisted of 85% natural sand, 5% ferrous powder, 5% marble sand and 5% zeolite sand, and the height of filter layer was 150 cm. The particle sizes and the relative contents of filler materials are shown in Table 1, the filter porosity is shown in Table 1. There was one sampling port every 0.25 m from top to bottom of filter; CRIS analog column was fed wastewater once every six hours and each feed lasted 20 minutes. A flowmeter was used to control inflow; the water flowing direction within reactor was vertical down. The thumbnail of the experimental installation is shown in Fig. 1.

2.2 Experimental methods

In order to be more close to the fact, the domestic wastewater was adopted as the experimental water sample. The specific water quality indicators are shown in Table 3.

CRIS started up with raw wastewater. Twenty days after the starting-up, the COD removal rate became stable, which indicated a successful membrane hanging. The hydraulic load is an important design and operational parameter in CRIS. In this experiment, the hydraulic load denotes the one day capacity of wastewater disposal per unit area ($m^3/m^2 \cdot d$ or m/d). When the CRIS analog column is mature,

it went on operating under five different hydraulic loads (0.50 m/d, 1.00 m/d, 1.50 m/d, 2.00 m/d and 2.50 m/d) to study the pollutants degradation laws. This experiment took 3 days as one period; every hydraulic load ran for a period and the pollutant indexes were measured once a day. The test ran from April 7 2010 until April 21 2010. Test methods are shown in Table 4.

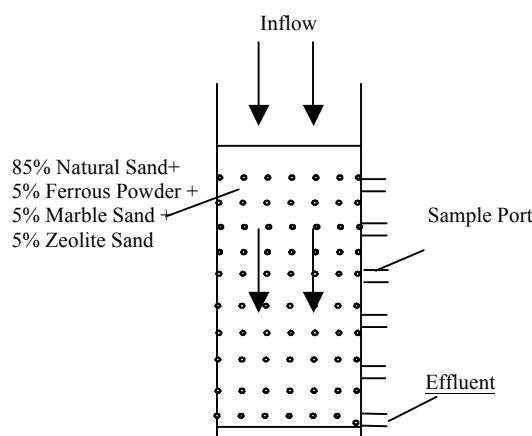


FIGURE 1 - Experimental Installation.

TABLE 1 - The particle sizes and the relative contents of filler materials.

Particle size range (mm)	The relative contents (weight percent %)			
	Natural sand	Ferrous powder	Marble sand	Zeolite sand
>2.0	11	7	15	16
1.0-2.0	28	53	19	21
0.56-1.0	35	26	24	19
0.25-0.56	14	8	22	26
<0.25	12	6	20	18

TABLE 2 - Filter porosity.

Porosity			
Natural sand	Ferrous powder	Marble sand	Zeolite sand
42%	35%	49%	52%

TABLE 3 - Raw water quality indicators.

Water Temperature (°C)	pH	COD (mg/L)	SS (mg/L)	TN (mg/L)	TP (mg/L)	NH ₄ ⁺ -H (mg/L)
21.30	7.60	160.10	60.12	48.40	1.80	36.24

TABLE 4 - Test methods of pollutant indexes.

Index	Test method
Water temperature	Thermometer method
pH	Glass-electrodes method
COD	Potassium dichromate method
NH ₃ -N	Nessler's reagent colorimetry
TN	Alkaline potassium per sulfate digestion-uv spectrophotometric method
TP	Ammonium molybdate spectrophotometric method

3. RESULTS AND DISCUSSION

3.1. COD removal law under different hydraulic loads

It is shown in Fig. 2 that in conditions of five different hydraulic loads, the organic degradation mostly happened in 0-0.75 m section of CRIS. When the hydraulic loads were 0.50 m/d, 1.00 m/d, 1.50 m/d, 2.00 m/d and 2.50 m/d, the total COD removal rates in CRIS were 95.5%, 87.7%, 84.0%, 76.5% and 70.7% respectively. The COD removal rates in 0-0.75 m section were 87.0%, 77.4%, 67.2%, 57.5% and 50% which occupied 91.1%, 88.2%, 80.1%, 75.2% and 70.1% of the total removal rates respectively. The maximal removal rates appeared in 0-0.25 m section: the removal rates in 0-0.25 m section were 48.00%, 43.24%, 36.75%, 26.95% and 21.00% in five different hydraulic loads which occupied 50.3%, 49.3%, 43.7%, 35.2% and 21.00% of the total removal rates respectively. In 0.75-1.50 m section, the growth of organics degradation rate flattened out. The COD removal rates in this section were 9.0%, 10.0%, 16.1%, 19% and 20% which occupied 8.9%, 11.8%, 19.9%, 24.8% and 29.3% of the total removal rates respectively.

The plug-flow structure of the CRIS reactor and the organics removal mechanism caused the above mentioned phenomenon. In CRIS, organic matters were degraded mainly by the heterotrophic aerobic bacteria [11]. The filter layer in 0-0.25 m section is at inlet part where the organics concentration and the oxygen supply are relatively high, therefore, the heterotrophic aerobic bacteria can grow fast that leads to a high COD removal rate in this section. After 0.75 m, owing to the action of the degradation in the former section, the organic concentration became lower and this caused a reduction of the reproduction rate of the heterotrophic aerobic bacteria. In addition, with the decrease of the organic concentrations, the nitrifying bacteria can fight for living space with the heterotrophic aerobic bacteria

[8], which restrains the massive reproduction of the heterotrophic aerobic bacteria and causes the drop of organic degradation rates. When the hydraulic loads are 0.50 m/d, 1.00 m/d, 1.50 m/d, 2.00 m/d and 2.50 m/d, the removal rates under five different hydraulic loads are 9.0%, 10.0%, 16.1%, 19% and 20% in 0.75-1.50 m section respectively. It is indicated in Fig.2 that the organic removal rates increased in 0.75-1.50 m section with the rise of the hydraulic load. Analysis showed that the residence time of the wastewater and the biochemical reaction duration between pollutants and microorganism in CRIS are relatively long in the case of low hydraulic load. At the upper part of the filter, the organic matters were degraded fully. At the bottom part, the organic matter concentration was very low, which constrained the growth of microorganism and led to a lower organic removal rate after 0.75 m section. With the rise of the hydraulic load, the biochemical reaction time between pollutants and microorganism shortened and the organic load per unit area into the CRIS increased. Therefore, more organics could reach the bottom part and the heterotrophic aerobic bacteria could grow to degrade the residual organics from the upper part.

In this experimental condition, when the hydraulic load was 2.50 m/d, the effluent COD concentration was 46.9 mg/L which can meet the A-level of primary standard in *Municipal wastewater treatment plant emission standards* (GB 18918-2002) [12]. Therefore, in order to ensure a high hydraulic load and fine effluent quality, the best hydraulic load was 2.50 m/d.

3.2 NH₄⁺-H removal law under different hydraulic loads

It is shown in Fig. 3 that in CRIS, all NH₄⁺-N removal rates are negative in 0-0.25 m section under five different hydraulic loads. This is caused by the following two main reasons: first, in sewage, some organic nitrogen is converted to NH₄⁺-N under the action of the heterotrophic

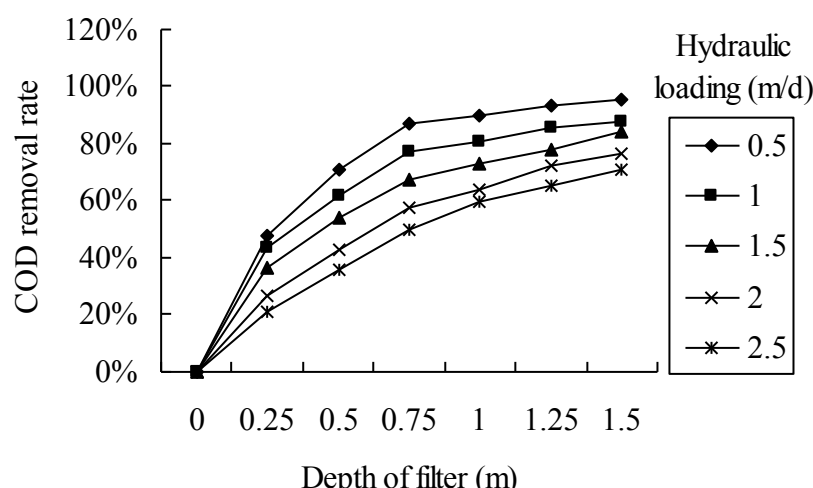


FIGURE 2 - Degradation laws of COD under different hydraulic loads with the change of filter depths in CRIS

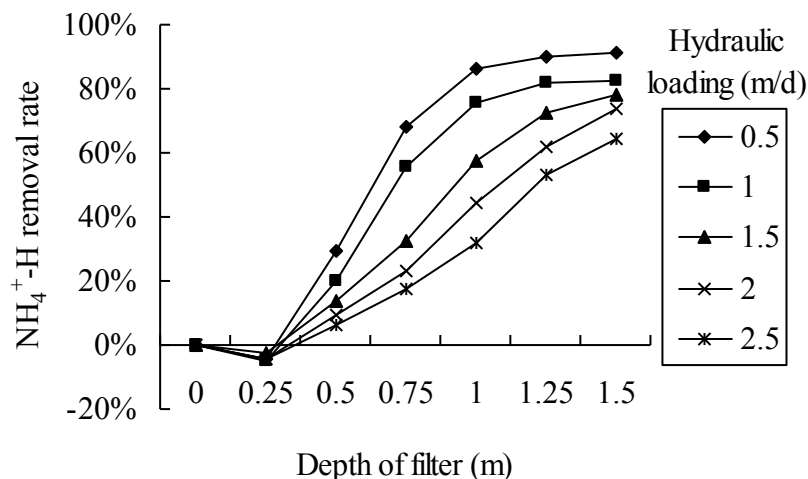
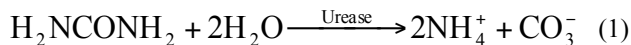


FIGURE 3 - Degradation laws of NH₄⁺-H under different hydraulic loads with the change of filter depths in CRIS.

bacteria and the ammonifying bacteria [13]. Taking the carbamide as an example, the equation for this reaction is as following:



Second, in this section, higher organic matter concentration and a large number of heterotrophic bacteria in the sewage had an inhibition action on the spread of the nitrifying bacteria [8].

From 0.25 m, the NH₄⁺-N removal rates increased rapidly. When the hydraulic loads were 0.50 m/d and 1.00 m/d, the NH₄⁺-N removal rates in 0.25-1.00 m section were 90.77% and 80.13% respectively. In 0.50-0.75 m section, the removal rates were the highest with 38.71% and 35.54%. In 1.00-1.50 m section, the NH₄⁺-N removal rates were only 4.6% and 7.37%. When the hydraulic loads were 1.50 m/d and 2.00 m/d, the NH₄⁺-N removal rates in 0.75-1.00 m section were the highest with 24.83% and 21.30% respectively. The NH₄⁺-N removal rates decreased slightly after 1.00 m: in 1.00-1.25 m section, the removal rates were 15.04% and 17.55% respectively; in 1.25-1.50 m section, the removal rates were 5.51% and 11.81% respectively. When the hydraulic load was 2.50 m/d, the total NH₄⁺-N removal rate was 64.40%, the NH₄⁺-N removal rate increased fast in the 0.25-1.50 m section, and the removal rate in the 1.00-1.25 m section was 21.33% which was the maximal removal rate and occupied 33.12% of the total removal rate.

It is considered that in 0-0.25 m section, the NH₄⁺-N concentrations increased slightly because some organonitrogen in wastewater inverted to NH₄⁺-N with the action of the heterotrophic bacteria and the ammonifying bacteria. Additionally, due to a relatively high organic concentration which brings about a massive growth of the het-

erotrophic bacteria near the inlet section, the nitrification was weak because the heterotrophic bacteria had an inhibition effect on the nitrifying bacteria [14].

On account of the low influent organic concentration and the filtration function of the filter material in 0-0.25 m section, the organics concentration became lower after 0.25 m, which made the heterotrophic bacteria grow slowly. At the same time, the oxygen demand for organics degradation went down. Therefore, a relatively low organic concentration and high dissolved oxygen brought about a massive growth of the nitrifying bacteria, and then a rapid degradation of NH₄⁺-N happened. In addition, the filter materials in the CRIS reactor were suitable for the microorganism to grow, and the heterotrophic bacteria and the nitrifying bacteria could possess different spaces and co-exist. Furthermore, the nitrifying bacteria has a longer generation time than the heterotrophic bacteria [15], once they become mature, they can resist and eliminate interference to work continuously. For the above reasons, when the CRIS treats domestic wastewater, there is no strict boundary between NH₄⁺-N removal area and COD removal area in CRIS, although the best filter layer for NH₄⁺-N degradation is different from that for COD degradation.

With the increase of the hydraulic load and shortening of the hydraulic retention time, the best section of the filter layer for NH₄⁺-N degradation tended to shift down: when the hydraulic loads were 0.50m/d and 1.00m/d, the best section was the 0.50-0.75m section, and removal rates tended to be stable after 1.00 m. Conversely, when the hydraulic load was added to 2.5 m/d, the best section of the filter layer was the 1.00-1.25 m section, and after 1.25 m, the removal rate also maintained growth. If the hydraulic load continued to increase, the filter layer was possible to be broken through by NH₄⁺-N. Compared with

the organic removal, with the increase of the hydraulic load, the NH_4^+ -N removal was much easier to happen at the end of the filter layer. It can be seen from Figure 3 that in this experimental condition, when the hydraulic load was 1.00 m/d, the removal rate of NH_4^+ -N was 82.8% and the effluent NH_4^+ -N concentration was 6.2mg/L. When the hydraulic load was 1.50m/d, the removal rate of NH_4^+ -N was 77.9% and the effluent NH_4^+ -N concentration was 7.9 mg/L. Under the above two conditions, the effluent qualities met the B-level of primary standard in *Municipal wastewater treatmentplant emission standards* (GB 18918-2002) [12]. When the hydraulic load added to 2.00 m/d, the removal rate of NH_4^+ -N was 73.7% and the effluent NH_4^+ -N concentration was 9.4 mg/L which did not satisfy the B-level of primary standard in *Municipal wastewater treatmentplant emission standards* (GB 18918-2002) [12]. Therefore, in order to ensure high hydraulic load and fine effluent quality, the best hydraulic load is 1.50 m/d.

The foregoing analysis showed that the CRIS is an effective technique in removing NH_4^+ -N. However, the correlative literatures [13, 16] show that the TN removal rate is very low in the CRIS. This is because the CRIS runs with the flooding and drying alternate working fashion. This working fashion is good for the oxygen recovery and the nitrification in CRIS, which help to change NH_4^+ -N into Nitrate Nitrogen. However, this operation mode restrains the denitrification, which deters the denitrifying bacteria from changing Nitrate Nitrogen into N_2 . Therefore, the TN concentration in the effluent is high. Regarding the above deficiency, the future research in this field will focus on improving the TN removal efficiency.

4. CONCLUSION

(1) Due to a relatively high organics concentration and sufficient oxygen supply at water inlet area, the heterotrophic aerobic bacteria in 0-0.75 m section can grow fast, which brings about a high COD removal rate in this section. When the hydraulic loads are 0.50 m/d, 1.00 m/d, 1.50 m/d, 2.00 m/d and 2.50 m/d, the total COD removal rates in CRIS are 95.50%, 87.70%, 83.00%, 76.50% and 70.67% respectively and the maximal removal rates appear in 0-0.25 m section.

(2) After the 0.75 m section of the filter layer, organics concentrations in wastewater become low and the nitrifying bacteria can fight for the living space with the heterotrophic bacteria. This restrains the growth of the heterotrophic bacteria. Then the organics removal rate become lower and lower with the increase of the filter layer depth.

(3) In 0-0.25 m section of the filter layer, the organic nitrogen inverts into NH_4^+ -N with the action of the heterotrophic bacteria and the ammonifying bacteria. Therefore, the NH_4^+ -N concentrations rise slightly. After 0.25 m section, the NH_4^+ -N removal rates increase rapidly, and the best filtration layer for removing NH_4^+ -N tends to shift

down with the rise of the hydraulic load. NH_4^+ -N removal is much easier to happen at the end of the filter layer compared with the organics. Therefore, in order to ensure high hydraulic load and fine effluent quality, the best hydraulic load is 1.50 m/d.

(4) When the CRIS disposes domestic wastewater, though the best section of the filter layer for NH_4^+ -N degradation and the best section for COD degradation are different in CRIS, the section of the filter layer for the NH_4^+ -N degradation and the section for the COD degradation do not have an obvious area boundary.

REFERENCES

- [1] Du, X.L., Xu, Z.X. and Wang, S. (2009) Improved ammonia-nitrogen removal in non-planted vertical flow-constructed wetland system by natural oxygen transfer. *Fresenius Environmental Bulletin*, 18(10): 1846-1850.
- [2] Tunçsiper, B., Ayaz, S.C. and Gunes, K. (2009) A serial-operated constructed wetland system to control water pollution. *Fresenius Environmental Bulletin*, 18(9): 1648-1653.
- [3] Bouwer, H. (1985) Recharge of wastewater with rapid infiltration land treatment system, Butterworths, Boston.
- [4] US Environmental Protection Agency. (1994) North American Wetlands for Water Quality Treatment atabase, Vol. 1.0, Washington, DC.
- [5] Xu, W.L. and Zhang, J.Q. (2010) Organic Matter Removal Mechanism in Artificial Soil Rapid Infiltration System. *Geochimica et Cosmochimica Acta*, 74 (12) S1: A1162.
- [6] Liu, C. (2010) Study of Treatment of Raw Water from Wenyu River by Constructed Rapid Infiltration System. *Water & Wastewater Engineering*, 36(3):132-136.
- [7] Fdz-Polanco, F., Garcia, F. and Villaverde, S. (1994) Influence of Design and Operation Parameters on the Flow Pattern of A Submerged Biofilter. *Journal of Chemical Technology & Biotechnology*, 61:153-158.
- [8] Hu, B.W., Cheng, W. and Han, Z. (2010) Experimental Study on Degradation Law of Organic Matter and Ammonia Nitrogen in Biological Aerated Filter. *Shuili Xuebao*, 41(3):374-378.
- [9] Xu, W.L. and Zhang, J.Q. (2009) Dynamic rule of organic matter removal in constructed rapid infiltration. In: 3rd International Conference on Bioinformatics and Biomedical Engineering, Beijing, China.
- [10] Zhang, J.Q. and Xu, W.L. (2010) Treat river sewage by constructed rapid infiltration system. In: 4th International Conference on Bioinformatics and Biomedical Engineering, Chengdu, China.
- [11] Ma, M.C., Li, J.M. Du, Y.P., et al.. (2009) Summarization of Research and Application in Constructed Rapid Infiltration System. *Environmental Engineering*, 27:74-77.
- [12] State Environmental Protection Administration. (2002) Fourth edition of Analytic Methods of Water and Wastewater Monitor, China Environmental Science Press, Beijing.
- [13] Liu, J.B. (2006) Study on contaminant removal mechanism and efficiency of constructed rapid infiltration system, Phy.D.D dissertation, China University of Geosciences, Beijing.

- [14] Cui, C.Y., Ma, L.M, Zhang, X.J., *et al.*. (2007) Mechanism of Contamination Removal in Constructed Rapid Infiltration System. *Environmental Pollution & Control*, 29 (2):95-98.
- [15] Ohashi, A., Silva, D.G. and Mobarrey, B. (1995) Influence of substrate C/N ratio on the structure of multi-species biofilms consisting of nitrifiers and heterotrophs. *Water Science and Technology*, 32(8):75-84.
- [16] He, J.T., Zhong, Z.S. and Tang, M.G. (2001) New method of solving contradiction of rapid infiltration system land use. *Geosciences*, 15: 339-345.

Received: October 26, 2010

Revised: January 31, 2011

Accepted: March 23, 2011

CORRESPONDING AUTHOR

Wenlai Xu

College of Environment and Civil Engineering,
Chengdu University of Technology
No.1 Erxianqiao Road
Chengdu, Sichuan 610059
P.R. CHINA

Phone: +86-13551029646, +86-28-87600602.

Fax: +86-28-87600602

E-mail: xuwenlai1983@163.com

AEROBIC DEGRADATION PROPERTIES AND BACTERIAL DIVERSITY OF TOLUENE DEGRADED BY DIFFERENT ACCLIMATED BACTERIA

Jianghong Guo¹, Yun Qi^{1,*}, Lin Zhao¹, Xiuli Liu² and Xin Tan¹

¹ School of Environmental Science and Engineering, Tianjin University, Tianjin 300072, China

² College of Ren'ai, Tianjin University, Tianjin 300072, China

ABSTRACT

To explore differences in degradation properties of toluene by different acclimated bacteria and determine the factors affecting toluene degradation efficiency, bacteria acclimated by benzene, toluene, ethylbenzene, xylene (BTEX) and BTEX mixture were used to degrade toluene under aerobic conditions. Then degradation properties were explored and bacterial diversity was investigated by polymerase chain reaction-denaturing gradient gel electrophoresis (PCR-DGGE). Bacterial genomic DNA was extracted after cultured by Luria Bertani (LB) medium. 16S rRNA fragments were amplified with universal primers (F357-GC and R518) and analyzed by DGGE. Experimental results demonstrated that five kinds of acclimated bacteria had good effect on degrading toluene, in 54 h, all degradation ratios reached 80% or more. Ethylbenzene acclimated bacteria had the best degradation efficiency, followed by toluene acclimated bacteria. Dominant bacteria and stable community structure were two significant factors to maintain high efficiency of toluene degradation. Longer lag phase would result in lower degradation efficiency. Results and findings gained from this study will be helpful in improving degradation ability of toluene-degrading bacteria.

1. INTRODUCTION

Benzene, toluene, ethylbenzene and xylene (BTEX) contained in petroleum hydrocarbons are hazardous pollutants often resulting from leakage of underground storage tanks and oil pipelines, they have been classified as priority pollutants by many nations including USA [1]. Microbial biodegradation is considered as an efficient and economic method to degrade BTEX compounds, which can be carried out under both aerobic and anaerobic conditions [2]. In recent years, aerobic biodegradation is increasingly applied in BTEX elimination for its faster biodegradation rate [3-5]. In addition, more and more studies focus on isolating high efficient BTEX-degrading bacteria [6]. Basic knowledge about changes of dominant bacteria and community structure in BTEX degradation can yield useful information for bacterial acclimation and isolation [7]. Therefore, it is important and essential to detect BTEX-biodegrading bacteria and their activity in the environment rapidly and accurately.

Modern molecular biology techniques such as restriction fragment length polymorphism, random amplified poly-morphic DNA and ribosomal intergenic spacer analysis have been used to investigate bacterial diversity [8-10]. Especially, denaturing gradient gel electrophoresis (DGGE), based on PCR (polymerase chain reaction)-amplified 16S rRNA, has the advantages of simultaneous analysis of samples obtained at different time and producing results in relatively short time [11, 12]. Recently, Hendrickx et al. [13] applied PCR-DGGE method to assess the diversity of BTEX mono-oxygenase genes at contaminated sites and indicated that different environmental parameters resulted in the diversity of *tmoA*-like genes. Park et al. [14] quantified and modeled the induction kinetics of aerobic toluene biodegradation according to degradation characteristics, which was used for predicting the concentration of toluene. Nicholson and Fathepure [15] used indigenous bacteria at the Great Salt Plains to degrade benzene and toluene under hypersaline conditions and evaluated the degradation potential of the bacteria. Although these re-

KEYWORDS:

Degradation ability, PCR-DGGE, bacterial diversity, acclimation

* Corresponding author

searches have well reported both aerobic degradation characteristics of toluene and bacterial diversity, the factors affecting toluene degradation efficiency still receive little concern.

In this study, differences in toluene degradation of bacteria acclimated by benzene, toluene, ethylbenzene, xylene and BTEX mixture were explored. Moreover, changes of dominant bacteria and community structure in BTEX degradation were investigated using PCR-DGGE analysis and the factors affecting toluene degradation efficiency were determined.

2. MATERIALS AND METHODS

2.1. Enrichment and acclimation of BTEX-degrading bacteria

Soil samples were collected from contaminated sites which were long-term exposed to petroleum in Dagang oil field, located in Tianjin of China. 500 g soil sample was added to 5 L inorganic salt medium. Then the mixture was cultured for 120 days at pH 7.5 and 25°C. In initial 56 days, glucose concentration was 1000 mg/L. From 56 days to 90 days, glucose concentration decreased from 1000 to 0 mg/L, while target pollutants gradually increased from 0 mg/L to saturated concentration (500 mg/L). After 90 days, there were only 500 mg/L of target pollutants. During the whole process, inorganic salt medium was renewed every two days and prepared from the following composition: 1.0 g/L KNO₃; 0.5 g/L KH₂PO₄; 0.7 g/L Na₂HPO₄; 0.03 g/L MgSO₄·7H₂O; 0.01 g/L Fe₂(SO₄)₃; 0.04 g/L MnCl₂·4H₂O; 0.05 g/L ZnSO₄·H₂O; 0.03 g/L CuSO₄·4H₂O; 0.01 g/L CaCl₂; 0.02 g/L (NH₄)₆Mo₇O₂₄·4H₂O.

2.2. Toluene aerobic degradation and determination of related parameters

Toluene aerobic degradation was carried out in a bioreactor with 750 mL of completely sealed volume. After culture medium (150 mL, pH 7.5) and bacterial suspension (1.5 mL) being added from the inlet, air pump was used to fully aerate the solution of the reactor to ensure dissolved oxygen saturation, then the reactor was sealed rapidly. Chromatographic pure target pollutant was added to the medium by a gas-tight syringe to a final concentration of 200 mg/L [16]. The bioreactor was placed in a shaker (150 rpm; 25°C) for continuous incubation.

Absorbance of bacterial suspension at wavelength of 600 nm (OD₆₀₀) and BTEX concentrations in liquid phase were measured. Absorbance was determined by UV-visible spectrophotometer (UV-2800, UNICO (Shanghai) Instruments Co. Ltd.). BTEX concentrations were analyzed by a gas chromatograph (Agilent GC6890N) equipped with a FID detector and a capillary column (HP-5% Phenyl Methyl Siloxane, 0.25 μm×30 m). Column, injector and detector temperature were hold at 40°C, 200°C and 250°C

respectively, H₂ flow rate was 40 mL/min, air flow rate was 550 mL/min [17, 18].

2.3. Extraction of bacterial genomic DNA

1.5 mL of bacterial suspension was obtained from the bioreactor and put in Luria Bertani (LB) medium, then the mixture was cultured under optimal bacterial growth conditions (25°C, pH 7.5) which had been explored at 150 rpm for 24 h. Bacterial genomic DNA was extracted by extraction kit of Biospin (Tianjin Xiangtian Technology Co. Ltd.) according to the manufacturer's instructions and was detected by 1% (w/v) agarose gel electrophoresis with 1×TAE buffer.

2.4. PCR Amplification

Genomic DNA purified was used as templates for PCR amplification with gradient PCR instrument (Eppendorf 5331, Germany). Primers F357-GC (5'-CGCCGCCGC GCGCCCCGGCGCCGGCCCCGGCCCC-3') and R518 (5'-ATTACCGC GGCTGCTGG-3') were employed to amplify the V3 region of 16S rRNA (underlined part was GC clamp). Amplification was performed in 50 μL reactions containing 10–100 ng of template, 5 μL of 10×PCR buffer (Shanghai Sangon Biotech Co. Ltd.), 5 μL of 25 mmol/L MgCl₂, 200 μmol/L of dNTPs (Shanghai Sangon Biotech Co. Ltd.), 0.5 μmol/L of each primer and 2.5 U of Taq DNA polymerase (Promega, USA), and reactions were made up to 50 μL with sterile ultra-pure water. To improve the specificity of the reaction, a “touch-down” PCR was performed. An initial denaturation of 5 min at 94°C, 20 cycles of 1 min at 94°C, 1 min at 65–55°C, 1 min at 72°C (the annealing temperature was set at 65°C initially and then decreased 0.5°C each cycle until it was 55°C), the following 10 cycles of 1 min at 94°C, 1 min at 55°C, 1 min at 72°C, finally, extension of 8 min at 72°C. Amplified products were detected by 2% (w/v) agarose gel electrophoresis with 1×TAE buffer [19, 20].

2.5. DGGE

DGGE analysis of the PCR products was performed as described by Cebron et al. [21] on 8% (w/v) polyacrylamide gels with denaturing gradients ranged from 35% to 55% (where 100% denaturant contains 7 mol/L urea and 40% (w/v) deionized formamide). Electrophoresis was run for 6 h at 150 V in 1×TAE buffer with the DGGE machine (C.B.S. SCIENTIFIC Co., USA). After electrophoresis, the gel was stained with silver nitrate and photographed [22].

2.6. Analysis of DGGE results

Gel-analysis software BIO-RAD Quantity One 4.6.2 was used to process the image of DGGE, and the patterns were carefully checked manually.

Bacterial diversity was investigated by Shannon-Wiener index of diversity (H) [23] calculated as $H = -\sum P_i \ln P_i$. Where P_i is the proportion of the bands in a lane and is calculated by $P_i = n_i / N$. Where n_i is the peak height of lane i and N is the sum of all peak heights of all lanes. The Simpson index of dominance (S) [24] is calculated according to equation $S = \sum P_i^2$. Community similarities were calculated by Dice coefficient (C_s) as $C_s = 2j / (a+b)$. Where j represents the number of bands common to sample A and B, and a and b represent the number of bands detected in sample A and B respectively. Dice coefficient ranged from 0 to 1.0 [25]. Furthermore, a dendrogram was constructed using the unweighted pair group method with arithmetic averages (UPGAMA).

3. RESULTS AND DISCUSSION

3.1. Degradation properties of different acclimated bacteria

Figure 1 shows the growth courses of different acclimated bacteria degrading toluene. Bacterial concentration ratios of ethylbenzene and BTEX acclimated bacteria increased in 4 h, the lag phases were the shortest. However, lag times of other bacteria varied from 16 to 20 h. In experiments undertaken by Berlendis et al. [5], lag time was 25 h at least. Maximum bacterial concentration ratios of all acclimated bacteria were observed after 30 h, in which the ratio value of xylene acclimated bacteria was the highest. One possible explanation is that that xylene acclimated bacteria might use more carbon for assimilation when degrading toluene, while the remaining bacteria transformed more carbon into intermediates.

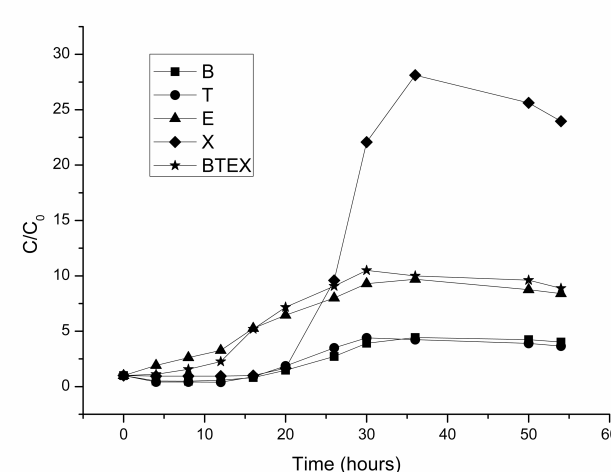


FIGURE 1 - Changes of bacterial concentration ratio during BTEX-degrading bacteria to degrade toluene under different acclimation, where C is the bacterial concentration during degradation process and C_0 is the bacterial initial concentration.

Five kinds of acclimated bacteria had good effect on degrading toluene. In 54 h all degradation ratios reached

80% or more (Figure 2). At 54 h ethylbenzene acclimated bacteria had the highest degradation ratio (95%), followed by toluene acclimated bacteria (93%). A bacterial strain isolated by Yang et al. [26] was employed to degrade toluene with 200 mg/L of initial concentration and the degradation ratio was about 75% at 50 h, confirming that using such acclimated bacteria to degrade toluene is feasible and efficient. It has been reported that long lag time would lead to long biodegradation phase [27]. Shorter lag time of ethylbenzene acclimated bacteria is one reason of its highest degradation efficiency. Results from Deeb et al. [28] suggested that ethylbenzene and toluene were degraded via the same aromatic degradation pathway, while toluene was a more efficient inducer of this pathway, so bacteria acclimated by ethylbenzene may be able to degrade toluene easier than bacteria acclimated by toluene at initial stage, leading to shorter lag time of ethylbenzene acclimated bacteria. Corresponding to bacterial growth curve, degradation rates of ethylbenzene and BTEX acclimated bacteria became fast after 4 h while the others were observed after 16 h.

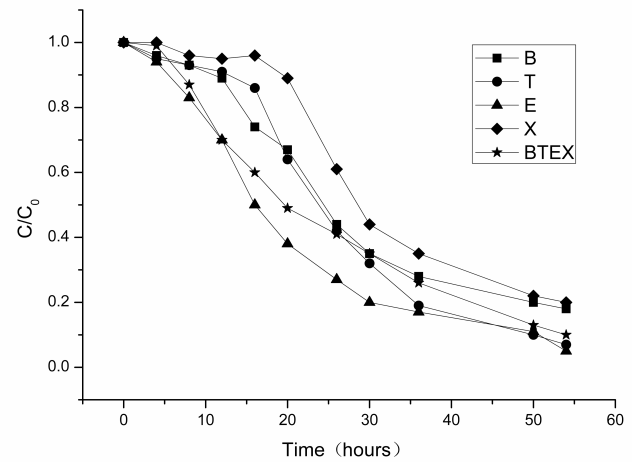


FIGURE 2 - Changes of toluene concentration ratio during BTEX-degrading bacteria to degrade toluene under different acclimation, where C is the toluene concentration during degradation process and C_0 is the toluene initial concentration.

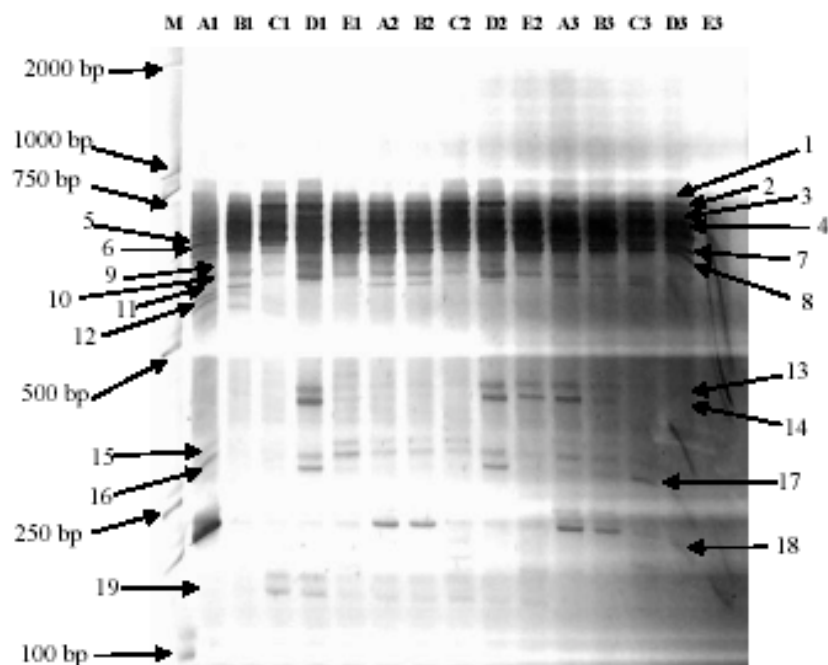
3.2. Analysis of bacterial community in degrading toluene by DGGE

Genomic DNA extracted was detected by 1% agarose gel electrophoresis with 1×TAE buffer, and PCR products were detected by 2% agarose gel electrophoresis, which had proved that genomic DNA extraction and PCR amplification were successful. Then DGGE banding pattern of different acclimated bacteria degrading toluene was performed to investigate the microbial community shifts in degradation process (Figure 3a), and the sketch map of DGGE pattern based on software Quantity One 4.6.2 analysis and manual analysis was presented in Figure 3b.

The length of bands in DGGE pattern ranged from 100 to 750 bp (Figure 3a). Variations of bands' number and position existed at different degradation stages under

different acclimation, so did the relative intensity of bands, which due to different acclimated conditions and changes of degradation environment [29]. The number of bands represents bacterial richness, while the relative in-

(a)



(b)

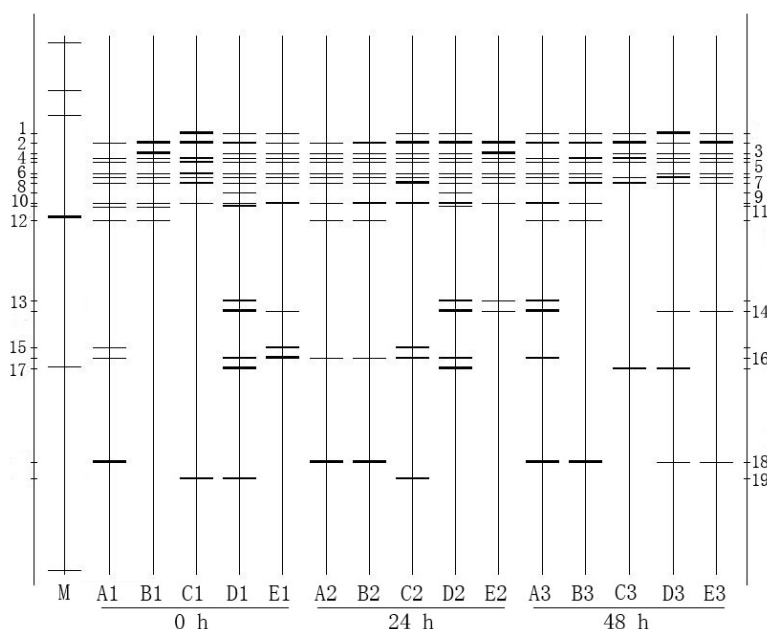


FIGURE 3 - (a) DGGE banding pattern of PCR products from 0 h to 48 h. (b) Sketch map of DGGE pattern. Lane M: Marker; Lane A1, B1, C1, D1 and E1: Samples of benzene, toluene, ethylbenzene, xylene and BTEX acclimated bacteria degrading toluene at 0 h, respectively.

TABLE 1 - Shannon-Wiener diversity index (H) and Simpson index (S) calculated from DGGE pattern.

	A1	B1	C1	D1	E1	A2	B2	C2	D2	E2	A3	B3	C3	D3	E3
H	1.75	1.58	2.08	2.33	1.86	1.84	1.86	2.23	2.34	1.88	2.20	1.92	1.91	1.80	1.63
1/S	3.70	3.86	7.16	8.50	4.84	4.54	5.12	8.07	8.55	5.13	7.47	5.69	5.80	4.55	3.73

tensity of bands represents the number of a certain species [30]. Based on these two aspects, the Shannon-Wiener index of diversity (H) and the Simpson index (S) of dominance (showed as $1/S$) were calculated (Table 1).

Benzene acclimated bacteria (A1, A2, A3) had emerged ten bands that remained dominant position in the whole degradation process. The intensity of band 2, 10 and 16 strengthened after 24 h, suggesting that changes in environment of late degradation phase promoted the growth of the bacterial strains. Meanwhile, bacterial diversity index increased as reaction carried on. Toluene acclimated bacteria (B1, B2, B3) consisted of eight dominant bands during the whole process, while ethylbenzene acclimated bacteria (C1, C2, C3) had six dominant bands. Band 2, 4, 5, and 8 were common dominant bands of all bacteria in all time. Figure 2 shows that the degradation ratios of toluene by ethylbenzene acclimated bacteria was higher than others and the initial 24 h was the main degradation period, it could be seen from Figure 3b that only the relative intensity of band 8 of ethylbenzene acclimated bacteria was stronger than others in entire process and reached the strongest at 24 h, so it can be reasonably inferred that band 8 is the key reason why ethylbenzene acclimated bacteria could degrade toluene with the highest efficiency. Bacterial diversity index of xylene acclimated bacteria (D1, D2, D3) was the highest in initial 24 h for the lowest toxicity of xylene in BTEX [31], however, Shannon-Wiener index decreased sharply from 2.34 to 1.80 after 24 h, demonstrating that part of xylene acclimated bacteria were not able to adjust themselves to adapt to environment of late degradation phase. Changes of BTEX acclimated bacteria was relatively complex, several bands experienced varying degrees of changes throughout the entire degradation process.

3.3. Similarity and cluster analysis

Dice coefficients on DGGE profile of Figure 3b were calculated using Quantity One 4.6.2 to analyze the similarity of bacterial communities (Table 2), and a cluster analysis based on the values of Dice coefficients was constructed and visualized in an UPGAMA dendrogram (Figure 4).

Similarities between A1 and B1, C1, E1 were close, while similarity between A1 and E1 was relatively higher with Dice coefficient of 27.7% resulted from different bacterial acclimation. In initial 24 h, the similarity between D1 and D2 was higher than others, while that between E1 and E2 was the lowest, which indicated that community structure of BTEX acclimated bacteria was relatively stable in early period. Changes of degradation environment resulted in varying degrees of community structure shifts. From 24 h to 48 h, the highest C_s value was observed in B2 and B3, and the lowest in D2 and D3 which due to rapid growth of xylene acclimated bacteria corresponding to sharp increase in bacterial concentration ratio.

From the perspective of the whole process, community structures of toluene, xylene and BTEX acclimated bacteria were unstable, whose C_s values changed from 47.3% to 69.4%, from 86.8% to 28.3% and from 35.7% to 65.0% respectively. Adversely, community structure of benzene and ethylbenzene acclimated bacteria were relatively stable. Stable community structure is one reason of highest degradation efficiency of ethylbenzene acclimated bacteria [32]. However, stable community structure and less dominant bacteria of benzene acclimated bacteria led to its relative low degradation efficiency, which also demonstrated that the effect of dominant bacteria on degradation efficiency was greater than that of community structure.

TABLE 2 - Dice coefficients (%) of community structure of different bacteria degrading toluene.

Lane	A1	B1	C1	D1	E1	A2	B2	C2	D2	E2	A3	B3	C3	D3	E3
A1	100														
B1	21.4	100													
C1	22.3	46.7	100												
D1	21.2	22.6	33.7	100											
E1	31.5	22.8	25.2	39.0	100										
A2	73.7	35.9	25.5	23.3	39.2	100									
B2	68.0	47.3	35.3	34.2	44.2	86.3	100								
C2	28.9	43.4	61.8	45.2	57.2	33.2	46.9	100							
D2	23.1	35.9	35.3	86.8	42.6	31.5	41.9	44.6	100						
E2	21.5	74.6	50.5	41.7	35.7	26.8	40.1	45.0	50.9	100					
A3	61.4	31.1	33.7	53.2	45.5	65.5	68.0	37.9	62.0	49.0	100				
B3	60.4	47.7	50.6	23.0	20.6	62.1	69.4	39.1	31.1	37.1	58.7	100			
C3	21.9	62.8	60.8	37.3	21.0	22.4	35.2	53.5	48.2	58.2	28.8	58.3	100		
D3	16.7	18.4	37.1	23.3	13.9	17.0	15.6	26.2	28.3	15.4	13.4	28.6	43.6	100	
E3	18.6	60.1	44.4	35.2	29.5	15.0	34.7	46.3	38.1	65.0	25.2	37.3	62.2	23.6	100

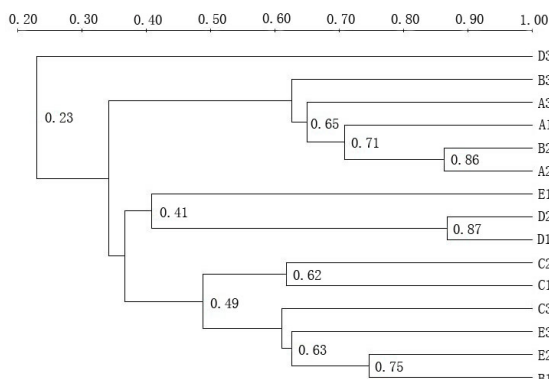


FIGURE 4 - UPGAMA dendrogram constructed with DGGE pattern based on Dice coefficient.

As shown in Figure 4, three major phylogenetic clusters were obtained. D3 displayed the divergent communities from the others, A1, A2, A3, B2, B3 formed a cluster, and the others were grouped into another cluster. The above results indicated that toluene pollutant and changes of degradation environment had affected bacterial structure. Furthermore, C1, C2 and C3 were in one major cluster, so as A1, A2 and A3, suggesting that toluene and changes of degradation environment had little influence on ethylbenzene and benzene acclimated bacteria.

CONCLUSIONS

Different acclimated bacteria in this study had good effect on degrading toluene especially ethylbenzene acclimated bacteria. Dominant bacteria and stable community structure were two significant factors to maintain high efficiency of toluene degradation, the former was more important than the latter, while long lag times would decrease degradation efficiency. However, the study still needs to be further explored in: (1) Sequencing bands of dominant bacteria; (2) isolating high efficient toluene-degrading bacteria and improving degradation ability.

ACKNOWLEDGMENTS

This work was supported by grant from the National Natural Science Foundation of China (50879052), Doctoral Fund of Ministry of Education of China (20090032120039) and National Key Technology R&D Program (2010BAC68B04).

REFERENCES

- [1] Lokhande, P.B., Patil, V.V. and Mujawar, H.A. (2009) Multivariate statistical study of seasonal variation of BTEX in the surface water of Savitri River. Environ. Monit. Assess., 157, 51–61.
- [2] de Mello, J.M.M., de Lima Brandão, H., de Souza, A.A.U., da Silva, A. and de Souza, S.M.A.G.U. (2010) Biodegradation of BTEX compounds in a biofilm reactor-modeling and simulation. J. Petrol. Sci. Eng., 70, 131–139.
- [3] Chiang, C.Y., Salanitro, J.P., Chai, E.Y., Colhart, J.D. and Klein, C.L. (1989) Aerobic biodegradation of benzene, toluene, and xylene in a sandy aquifer-data analysis and computer modeling. Ground Water, 27, 823–834.
- [4] Moreels, D., Bastiaens, L., Ollevier, F., Merckx, R., Diels, L. and Springael, D. (2004) Evaluation of the intrinsic methyl tert-butyl ether (MTBE) biodegradation potential of hydrocarbon contaminated subsurface soils in batch microcosm systems. FEMS Microbiol. Ecol., 49, 121–128.
- [5] Berlendis, S., Cayol, J.L., Verhé, F., Laveau, S., Tholozan, J.L., Ollivier, B. and Auria, R. (2010a) First evidence of aerobic biodegradation of BTEX compounds by pure cultures of *Marinobacter*. Appl. Biochem. Biotechnol., 160, 1992–1999.
- [6] Coates, J.D., Chakraborty, R., Lack, J.G., O'Connor, S.M., Cole, K.A., Bender, K.S. and Achenbach, L.A. (2001) Anaerobic benzene oxidation coupled to nitrate reduction in pure culture by two strains of *Dechloromonas*. Nature, 411, 1039–1043.
- [7] Baldwin, B.R., Nakatsu, C.H. and Nies, L. (2003) Detection and enumeration of aromatic oxygenase genes by multiplex and real-time PCR. Appl. Environ. Microbiol., 69, 3350–3358.
- [8] Berlendis, S., Lascurreges, J.F., Schraauwers, B., Sivadon, P. and Magot, M. (2010b) Anaerobic biodegradation of BTEX by original bacterial communities from an underground gas storage aquifer. Environ. Sci. Technol., 44, 3621–3628.
- [9] Culcu, T., Sozen, E. and Tuylu, B.A. (2010) Determination of genotoxins-induced DNA damage by using RAPD-PCR in human peripheral blood lymphocytes. Fresen. Environ. Bull., 19(10), 2205–2209.
- [10] Hartmann, M., Frey, B., Kölliker, R. and Widmer, F. (2005) Semi-automated genetic analyses of soil microbial communities: comparison of T-RFLP and RISA based on descriptive and discriminative statistical approaches. J. Microbiol. Methods, 61, 349–360.
- [11] Muyzer, G. and Smalla, K. (1998) Application of denaturing gradient gel electrophoresis (DGGE) and temperature gradient gel electrophoresis (TGGE) in microbial ecology. Antonie Van Leeuwenhoek, 73, 127–141.
- [12] Miura, Y., Hiraiwa, M.N., Ito, T., Itonaga, T., Watanabe, Y. and Okabe, S. (2007) Bacterial community structures in MBRs treating municipal wastewater: relationship between community stability and reactor performance. Water Res., 41, 627–637.
- [13] Hendrickx, B., Dejonghe, W., Faber, F., Boënne, W., Bastiaens, L., Verstraete, W., Top, E.W. and Springael, D. (2006) PCR-DGGE method to assess the diversity of BTEX mono-oxygenase genes at contaminated sites. FEMS Microbiol. Ecol., 55, 262–273.
- [14] Park, J., Lang, J., Thamaraiselvi, K., Kukor, J.J. and Abriola, L.M. (2008) Induction kinetics of aerobic toluene degradation as a function of carbon starvation history. Process Biochem., 43, 1345–1351.

- [15] Nicholson, C.A. and Fathepure, B.Z. (2005) Aerobic biodegradation of benzene and toluene under hypersaline conditions at the Great Salt Plains, Oklahoma. *FEMS Microbiol. Lett.*, 245, 257–262.
- [16] Lin, C.W., Yen, C.H., Lin, H.C. and Tran, D.T. (2010) Response surface optimization of dissolved oxygen and nitrogen sources for the biodegradation of MTBE and BTEX. *Biodegradation*, 21, 393–401.
- [17] Liang, C., Huang, C.F. and Chen, Y.J. (2008) Potential for activated persulfate degradation of BTEX contamination. *Water Res.*, 42, 4091–4100.
- [18] Littlejohns, J.V. and Daugulis, A.J. (2008) Kinetics and interactions of BTEX compounds during degradation by a bacterial consortium. *Process Biochem.*, 43, 1068–1076.
- [19] Wu, Q., Zhao, X.H. and Zhao, S.Y. (2006) Application of PCR-DGGE in research of bacterial diversity in drinking water. *Biomed. Environ. Sci.*, 19, 371–374.
- [20] Li, P., Wang, Y.H., Wang, Y.X., Jiang, Z. and Tong, L. (2010) Bioaugmentation of cellulose degradation in swine wastewater treatment with a composite microbial consortium. *Fresen. Environ. Bull.*, 19(12B), 3107–3112.
- [21] Cébron, A., Coci, M., Garnier, J. and Laanbroek, H.J. (2004) Denaturing gradient gel electrophoretic analysis of ammonia-oxidizing bacterial community structure in the lower Seine River: impact of Paris wastewater effluents. *Appl. Environ. Microbiol.*, 70, 6726–6737.
- [22] Zijngje, V., Welling, G.W., Degener, J.E., van Winkelhoff, A.J., Abbas, F. and Harmsen, H.J.M. (2006) Denaturing gradient gel electrophoresis as a diagnostic tool in periodontal microbiology. *J. Clin. Microbiol.*, 44, 3628–3633.
- [23] Gafan, G.P., Lucas, V., Roberts, G.J., Petrie, A., Wilson, M. and Spratt, D.A. (2005) Statistical analyses of complex denaturing gradient gel electrophoresis profiles. *J. Clin. Microbiol.*, 43, 3971–3978.
- [24] Ros, M., Pascual, J.A., Moreno, J.L., Hernandez, M.T. and Garcia, C. (2009) Evaluation of microbial community activity, abundance and structure in a semiarid soil under cadmium pollution at laboratory level. *Water, Air, Soil Pollut.*, 203, 229–242.
- [25] Liu, X.C., Zhang, Y., Yang, M., Wang, Z.Y. and Lv, W.Z. (2007) Analysis of bacterial community structures in two sewage treatment plants with different sludge properties and treatment performance by nested PCR-DGGE method. *J. Environ. Sci. (China)*, 19, 60–66.
- [26] Yang, W.B., Zhu, R.Y., Zhang, L.L., He, D. and Chen, J.M. (2010) Isolation, identification and biodegradation characteristics of a new bacterial strain degrading BTEX. *Huan Jing Ke Xue*, 31, 821–827.
- [27] Zhang, W.X. and Bouwer, E.J. (1997) Biodegradation of benzene, toluene and naphthalene in soil-water slurry microcosms. *Biodegradation*, 8, 167–175.
- [28] Deeb, R.A., Hu, H.Y., Hanson, J.R., Scow, K.M. and Alvarez-Cohen, L. (2001) Substrate interactions in BTEX and MTBE mixtures by an MTBE-degrading isolate. *Environ. Sci. Technol.*, 35, 312–317.
- [29] Zeng, J., Yang, L.Y., Du, H.W., Xiao, L., Jiang, L.J., Wu, J. and Wang, X.L. (2009) Bacterioplankton community structure in a eutrophic lake in relation to water chemistry. *World J. Microbiol. Biotechnol.*, 25, 763–772.
- [30] Boon, N., de Windt, W., Verstraete, W. and Top, E.M. (2002) Evaluation of nested PCR-DGGE (denaturing gradient gel electrophoresis) with group-specific 16S rRNA primers for the analysis of bacterial communities from different wastewater treatment plants. *FEMS Microbiol. Ecol.*, 39, 101–112.
- [31] Schweigert, N., Hunziker, R.W., Escher, B.I. and Eggen, R.I. (2001) Acute toxicity of (chloro-) catechols and (chloro-) catechol-copper combinations in *Escherichia coli* corresponds to their membrane toxicity in vitro. *Environ. Toxicol. Chem.*, 20, 239–247.
- [32] Angenent, L.T., Zheng, D., Sung, S. and Raskin, L. (2002) Microbial community structure and activity in a compartmentalized, anaerobic bioreactor. *Water Environ. Res.*, 74, 450–461.

Received: December 14, 2010

Accepted: April 05, 2011

CORRESPONDING AUTHOR

Yun Qi

School of Environmental Science and Engineering
Tianjin University
Tianjin 300072
P.R.CHINA

Phone: +86-22-27891291

E-mail: qiyun@tju.edu.cn

FEB/ Vol 20/ No 7/ 2011 – pages 1691 – 1697

EFFECT OF INTERMITTENT ALKALI TREATMENT AND POTATO ADDITION ON ANAEROBIC DIGESTION OF SPARTINA ALTERNIFLORA

Jibiao Zhang¹, Yan Luo², Xingzhang Luo¹, Zheng Zheng^{1,*}, Guangyin Chen² and Shiguan Yang³

¹ Department of Environmental Science and Engineering, Fudan University, Shanghai 200433, P.R. China

² State Key Laboratory of Pollution Control and Resource Reuse, School of the Environment, Nanjing University, Nanjing 210046, P.R. China

³National Engineering Laboratory of Biomass Power Generation Equipment,
School of Renewable Energy, North China Electric Power University, Beijing 102206, P.R. China

ABSTRACT

This paper investigated the effect of intermittent alkali treatment and potato addition on *Spartina alterniflora* anaerobic digestion. Laboratory-scale experiments were carried out in the completely mixed reactors of 1.0 L at 35 ± 1 °C. Combined with intermittent alkali treatment, the optimal ratio of potato to fermented *Spartina alterniflora* for gas production was 1:4. The gas yield of first anaerobic digestion of *Spartina alterniflora* was 263.0 ml/g TS while the highest gas yield of second anaerobic digestion of fermented *Spartina alterniflora* was 288.0 ml/g TS. The results showed that combining alkali treatment with potato addition to fermented *Spartina alterniflora* followed by a second anaerobic digestion provided the best result for gas production.

KEYWORDS: *Spartina alterniflora*; anaerobic digestion; intermittent alkali treatment; potato.

1. INTRODUCTION

As a perennial salt marsh grass, *Spartina alterniflora* (*S. alterniflora*) is native to the Atlantic and Gulf coasts of North America [1-3]. In 1979, it was introduced to China at Nanjing University, and 1980 vegetated vigorously in Fujian province [4]. In the following years, more and more *S. alterniflora* plantations were spread quickly in Guangdong, Zhejiang, Jiangsu and Shandong provinces [1, 5]. *S. alterniflora* is a C₄ halophyte whose photosynthesis is higher than respiration, and its average net primary production (NPP) exceeds 1000 g dry mass/m² year [6, 7]. Because of this extensive invasion, a lot of native wetland vegetation was crowding out. In 2003, Environmental Protection Agency of China listed *S. alterniflora* as 1 of the 16 harmful exotic species.

A lot of technologies have been used to control *S. alterniflora*, such as physical, chemical and biological methods [8-13]. However, *S. alterniflora* utilized as a resource for anaerobic digestion was rarely reported. Belonging to lignocellulosic biomass, *S. alterniflora* could be used as a material for anaerobic digestion to produce biogas. Cellulose, hemi-cellulose and lignin are three main biopolymers of lignocellulose [14, 15]. Unfortunately, lignin is highly recalcitrant and only degradable by molecular oxygen [16, 17]. Only 45% of *S. alterniflora* could be biodegraded by anaerobic digestion [18]. In order to improve *S. alterniflora* digestion efficiency and biogas yield, the pretreatment was of great necessity.

Various pretreatment methods have been reported, such as size reduction, steam explosion, fungal biodegradation, ammonification, urea and alkaline treatment. The research showed that NaOH was one of the effective medicaments for alkaline treatment [19]. But NaOH pretreatment had its fatal flaws and required considerable alkali. Furthermore, the lye was easy to induce second pollution. In order to reduce the usage of alkali, intermittent treatment of *S. alterniflora*, firstly fermenting till no gas was produced and then treating by alkali for a second anaerobic digestion, was promising.

Co-digestion as a process had been examined for many waste combinations [20, 21]. It was an interesting and attractive method for biotransformation improvement by diluting the potential toxic compounds, improving balance of nutrients, stimulating synergistic effects of microorganisms, increasing organic loading of digester and improving biogas yield [22, 23]. Also, co-digestion could utilize the nutrients and bacterial diversities in various wastes to optimize the digestion process [22, 24].

The mono-digestion of *S. alterniflora* and co-digestion of potatoes after intermittent NaOH treatment was investigated in this paper to examine the effect of potatoes on *S. alterniflora* anaerobic digestion. Furthermore, the effects of pH value and volatile fatty acids (VFA) on the biogas yield were discussed.

* Corresponding author

2. MATERIALS AND METHODS

2.1. Substrates and inoculums

The samples of *S. alterniflora*, excluding belowground parts, were collected from a plain muddy salt marsh located in Yancheng City ($33^{\circ}36'N$, $12^{\circ}36'E$), Jiangsu Province, P.R. China, on May 21, 2008. The collected *S. alterniflora* was firstly dried in air, then cut into 1-2 cm pieces and stored in airtight bags under ambient temperature. The total solids (TS) and volatile solids (VS) of the *S. alterniflora* used in this study were 88.79 and 81.85%, while C, H, N were 37.11, 5.92 and 2.58%, respectively.

Inoculum was used in this study and taken from the anaerobic reactor treating *S. alterniflora* at mesophilic temperature. TS, VS and pH of the inoculum were 4.62%, 3.08% and 7.2, respectively.

2.2. Experimental design

The reactor used in this study for anaerobic digestion was a cylindrical glass bottle with a sampling outlet and a mouth on the top which was sealed by a rubber stopper with a pipe for transmitting biogas. The reactor was connected to a bottle which was filled with water for gas collection and a beaker was used for collecting water. The whole digestion system was incubated at $35\pm1^{\circ}\text{C}$ in a thermostatically regulated water-bath. Each digester was manually stirred once a day to avoid deposition. Batch anaerobic digestion experiments were performed at initial TS of 8%. *S. alterniflora* was used for the first anaerobic digestion which was terminated when no significant gas production was observed. The fermented *S. alterniflora* after dried at 60°C was treated by NaOH solution at a concentration of 6%, and for 2 days at room temperature for second anaerobic digestion. Second anaerobic digestion was performed for mono-digestion of fermented *S. alterniflora* and co-digestion of fermented *S. alterniflora* and potato was also conducted. The ratios of fermented *S. alterniflora* to potato, based on TS (SA:P), were 6:1, 4:1 and 3:1. The fermented *S. alterniflora* without NaOH solution intermittent treatment was only mixed with potato at SA:P of 4:1 and incubated for biogas production. The total materials were filled in each digester including *S. alterniflora*, inoculum and tap water amounted to 800 g, and then, the digesters were treated by nitrogen-sparging and kept isolated from the atmosphere throughout the experiment. Bio-gas volumes were recorded daily. Before analysis, the samples were centrifuged at a speed of 12,000 rpm, and then supernatants were separated and diluted with ultrapure water. Diluted supernatants were filtrated with a 0.45- μm filter membrane and stored at 4°C for analysis.

2.3. Analytical methods

Standard methods were used to determine VS and TS of feedstock [25]. The C, H and N contents of *S. alterniflora* were analyzed using an element analyzer (Heraeus Co., Germany). Biogas yields were measured at a constant

time every day by the water displacement method. The pH value was measured using a pH-meter (METER 6219) immediately after the sampling process. Methane contents of biogas were measured by gas chromatography (Shimadzu GC-2014) using a Porapak Q (80–100 mesh) column, with Helium as carrier gas at 30 ml/min and a thermal conductivity detector. Volatile fatty acids (VFAs) in fermentation liquor were quantified using gas chromatography (Shimadzu GC-2014), with nitrogen as carrier gas at 40 ml/min.

3. RESULTS AND DISCUSSION

3.1 Biogas yield and composition of the first anaerobic digestion

The daily and cumulative biogas yields during the first digestion of *S. alterniflora* are shown in Fig. 1. During the initial 3 days of digestion, the daily biogas yield decreased sharply. During day 3 to day 5, no biogas was produced because some easily biodegradable organic matter was dissolved and entered the digestion liquid from substrates being converted to VFAs. So, the pH value was reduced rapidly and inhibited the activity of methanogenic bacteria. After pH value was adjusted to 6.5 with 5.0% NaOH solution artificially on day 5, the daily biogas production increased sharply and reached a peak value on day 16 (975 ml/day), followed by a quick decrease. After 23 days of reaction, the daily biogas yield decreased slowly, keep-

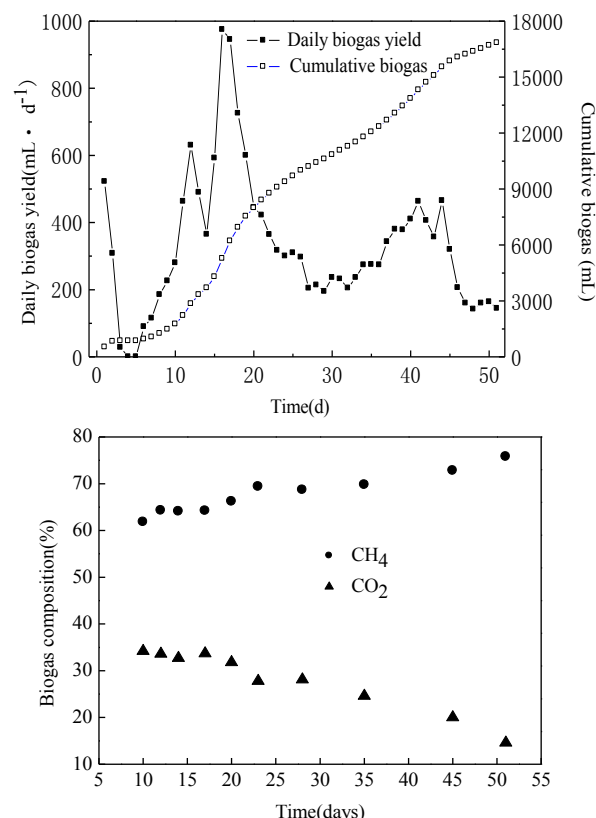


FIGURE 1 - Daily and cumulative biogas yield, biogas composition during anaerobic digestion of *S. alterniflora* at 35 ± 1 °C at TS of 8%.

ing at a low and stable level in the remaining days. The ratio of cumulative biogas to total biogas production was up to 80% in the first 20 days. After 51 days, the cumulative biogas yield reached 263 ml/g TS. However, the initial weight of *S. alterniflora* was 64 g (on TS basis). When the gas production process ceased, it was still 35 g and only 54% *S. alterniflora* was digested. The remainder consisted of non-degradable organic compounds which could not be utilized by microorganism directly.

The biogas composition is also shown in Fig. 1. Methane content increased from 61.8% during the first 10 days to 75.8% during the last 10 days while CO₂ content decreased in the anaerobic digestion process.

3.2 Effect of intermittent NaOH treatment and potato addition on second anaerobic digestion

3.2.1 Change of VFAs and pH value

VFAs containing acetate, propionate and butyrate were important intermediates in the metabolic pathway of methane fermentation and caused microbial stress in high concentrations. It resulted in a decrease of pH value and ultimately led to failure of the digester [26]. Table 1 shows the change of VFAs with the digestion time. As shown in Table 1, the main kind of VFAs generated in three treatments was firstly acetate, then propionate, and finally butyrate. From Table 1 (a), acetate concentration reached the highest value of 1055 mg/L on day 6 while the concentrations of propionate and butyrate were below 300 mg/L.

TABLE 1 (a). Change of VFAs and pH value during the second anaerobic digestion process at SA:P of 4:1 (T1).

Time (days)	Acetate (mg/L)	Propionate (mg/L)	Butyrate (mg/L)	pH
0	967.5	174.4	65.7	8.10
3	973.2	171.6	55.5	6.51
6	1055.8	291.6	128.7	7.19
9	833.7	232.1	162.8	7.70
14	706.2	243.4	169.6	7.49
19	449.8	185.6	105.9	7.54
24	588.7	212.7	141.4	7.54
29	544.5	167.8	113.4	7.46
34	608.3	186.9	122.2	7.46
39	803.8	181.7	117.8	7.40
44	376.8	118.0	65.4	7.61
54	350.1	100.2	70.0	7.52

TABLE 1 (b). Change of VFAs and pH value during second anaerobic digestion under NaOH intermittent treatment (T2).

Time (days)	Acetate (mg/L)	Propionate (mg/L)	Butyrate (mg/L)	pH
0	576.0	125.6	23.3	9.39
3	1388.7	150.3	13.0	7.27
6	3286.5	496.6	294.7	7.24
9	2226.5	516.0	385.4	7.57
14	2149.3	726.6	491.4	7.57
19	844.8	345.6	4.7	7.72
24	981.5	605.7	386.0	7.75
29	800.9	568.1	187.2	7.65

34	663.0	522.0	124.5	7.69
39	1086.8	538.6	153.1	7.93
44	559.0	195.4	56.9	7.53
54	1336.8	350.3	132.0	7.72

TABLE 1 (c). Evolution of VFAs and pH value during second anaerobic digestion under NaOH intermittent treatment and potato addition at SA:P of 4:1 (T3).

Time (days)	Acetate (mg/L)	Propionate (mg/L)	Butyrate (mg/L)	pH
0	355.5	58.4	0.5	9.12
3	1838.1	230.6	363.7	6.22
6	7760.5	1369.3	1096.7	5.84
9	10044.5	2568.0	1035.4	5.88
14	4790.4	2593.3	1324.5	7.43
19	1524.1	1243.8	554.9	7.74
24	984.2	841.7	265.7	7.81
29	915.5	574.5	135.3	7.82
34	2229.6	1051.2	63.3	7.9
39	1130.5	452.4	52.9	7.73
44	546.1	160.5	30.1	7.8
54	296.6	72.0	30.8	7.96

The pH value was kept between 6.51-8.1. From Table 1 (b), acetate reached the highest value (3286 mg/L) on day 6 while on day 14 the concentrations of propionate and butyrate reached maximum values of 726 mg/L and 491 mg/L. The pH value was between 7.24-9.39. From Table 1(c), acetate concentration reached 10044 mg/L on day 9 while both propionate and butyrate reached their maximum values of 2593 mg/L and 324 mg/L on day 14. The pH value was between 5.88-9.12. Propionate had stronger inhibitory effect on methanogenesis than acetate and butyrate [27]. Propionate was disadvantageous to anaerobic digestion process because its degradation process was the slowest and most sensitive process of VFA degradations [28, 29]. In the T1 and T2 treatments, propionate did not show obvious inhibition effects, maybe due to its low concentration. In this study, synergistic effect could be observed during the anaerobic digestion process. NaOH solution in cooperation with potato addition intermittent treatment could accelerate fermented *S. alterniflora*'s hydrolyzation to make more organic nutrients dissolved [30].

3.2.2 Change of the biogas production

As shown in Fig. 2 (a), daily biogas production reached peaks on day 2 which were 650 ml/d, 254 ml/d and 1190 ml/d, respectively. For T1 treatment, daily gas production sharply declined on day 3 and was 80 ml/day but then, daily gas production increased slowly. On day 8, it reached the second peak value of 468 ml/d. After then, daily gas production began to fall again. 10 days of reaction later, only little gas production was observed. In the T2 treatment, daily biogas production increased slowly. On day 9, it reached the second peak value of 635 ml/d, followed by a steady decline. After 21-days fermentation, daily biogas production decreased. In the T3 treatment, daily biogas production decreased rapidly from day 3. Furthermore, the biogas production ceased during day 5 to 10. On day 15, daily biogas production reached a second peak value of 938 ml/d. So, the gas production process was mainly concentrated in the first 20 days. The delayed time

for second peak may be related to VFAs inhibition. After 54 days of reaction, the cumulative biogas yields of T1, T2, and T3 reached 91 ml/d, 218 ml/d, and 288 ml/g TS, respectively.

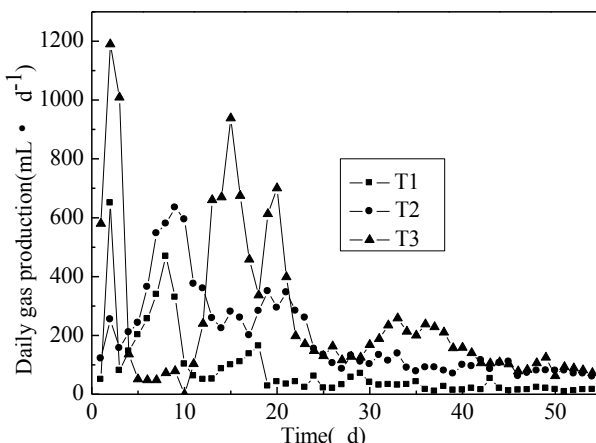


FIGURE 2 (a) - Daily biogas production after intermittent treatment with NaOH solution and addition of potato for second anaerobic digestion.

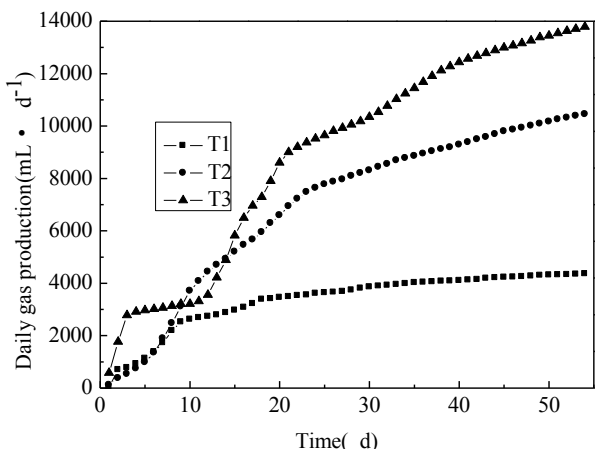


FIGURE 2 (b) - Cumulative biogas productions after intermittent treatment with NaOH solution and addition of potato for second anaerobic digestion.

3.3 Effect of potato addition on anaerobic fermentation

3.3.1 Change of VFAs and pH value with potato addition during the anaerobic fermentation process

As shown in Tables 1 (c), 2 (a) and 3 (b), VFA concentrations were higher with the increase of potato addi-

tion. In the T4 treatment, acetate concentration was between 250 and 4226 mg/L whereas propionate concentration was between 32 and 1445 mg/L. Furthermore, butyrate concentration was between 2 and 752 mg/L, and the minimum pH value was 6.25 on day 6. Acidification did not appear in this treatment. Similar to the results shown before, acid accumulation was observed during the initial time in T3 treatment. From Table 2 (b), the maximal concentrations of acetate, propionate and butyrate were 6338, 1494 and 1324 mg/L, respectively. Because of VFA accumulation, the pH value was reduced quickly during the initial time. From day 3 to 14, the pH value was below 6.0 and biogas production nearly stopped.

TABLE 2 (a) - Change of VFAs and pH value during second anaerobic digestion under NaOH intermittent treatment and potato addition at SA:P of 6:1 (T4).

Time (days)	Acetate (mg/L)	Propionate (mg/L)	Butyrate (mg/L)	pH
0	250.2	32.0	2.0	9.34
3	2226.0	245.2	41.4	6.82
6	4226.6	658.4	289.8	6.25
9	4036.8	1140.4	626.7	6.41
14	2545.8	1255.4	625.3	7.60
19	2020.6	1445.8	752.1	7.80
24	982.2	702.9	355.0	8.04
29	548.3	379.2	120.3	7.87
34	908.4	539.7	145.2	7.86
39	454.0	206.3	52.5	7.69
44	711.0	230.2	74.0	7.68
54	607.8	147.6	50.8	7.87

TABLE 2 (b) - Change of VFAs and pH value during second anaerobic digestion under NaOH intermittent treatment and potato addition at SA:P of 3:1 (T5).

Time (days)	Acetate (mg/L)	Propionate (mg/L)	Butyrate (mg/L)	pH
0	246.6	37.9	0.5	9.08
3	4203.2	686.9	363.7	5.73
6	6338.7	1152.4	1096.7	5.37
9	4504.1	1170.3	1035.4	5.52
14	3318.1	1494.3	1324.5	6.10
19	1511.0	1410.5	554.9	7.74
24	750.4	780.4	265.7	7.82
29	666.3	532.8	135.3	7.66
34	484.5	275.6	63.3	7.78
39	521.8	209.0	52.9	7.83
44	424.6	126.7	30.1	7.85
54	754.8	116.0	30.8	7.60

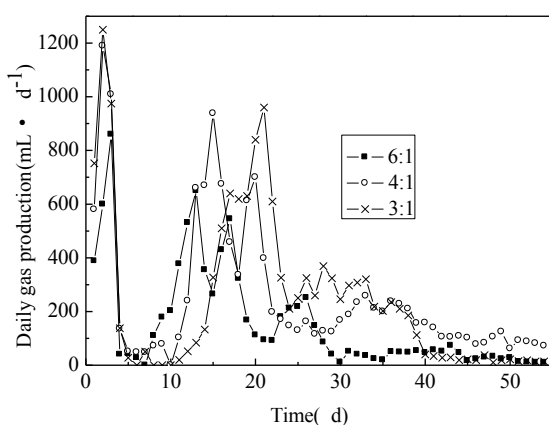


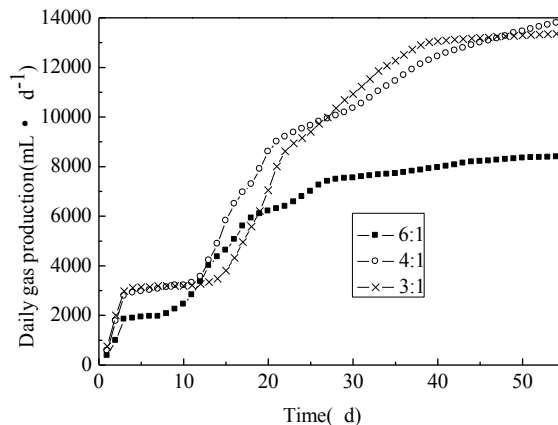
FIGURE 3 - Daily biogas production of co-digestion at SA:P of 6:1, 4:1 and 3:1 (based on TS).

3.3.2 Change of the biogas production

The daily biogas productions of co-digestion at SA:P ratios of 6:1, 4:1 and 3:1 (based on TS) are shown in Fig. 3. Similar trends of daily biogas production curves were found for the three proportions of mixture. The biogas production processes reached their first peak values of 860 ml/d, 1190 ml/d and 1250 ml/d on day 2, day 2 and day 3, respectively. And then, the yields decreased sharply until no biogas was produced. The daily biogas production nearly ceased during day 5 to day 8, day 5 to day 10, and day 5 to day 12 when SA:P was 6:1, 4:1 and 3:1, respectively. With increased proportion of potatoes, the period of acid restraint was prolonged because of potatoes containing too much starch but starch could be dissolved easily. The daily biogas productions reached their second peak values of 650 ml/d, 938 ml/d, 960 ml/d on day 13, day 15 and day 21, respectively. After 30-days reaction, the daily biogas yield decreased slowly and remained at a low and stable level. After 54 days of reaction, the maximum biogas yield of 288 ml/g TS was obtained at SA:P of 4:1. The results of cumulative biogas production showed that fermented *S. alterniflora* could be utilized for biogas production.

4. CONCLUSIONS

This study showed that *S. alterniflora* as feedstock for anaerobic digestion is a practicable alternative for recovering energy in the form of biogas. The results of the anaerobic digestion tests of *S. alterniflora* showed that the cumulative biogas yield reached 263 ml/g TS during the first anaerobic digestion at initial TS of 8%. By intermittent treatment of NaOH and potato addition, substantial gas production was observed and the highest biogas yield of fermented *S. alterniflora* was 288 ml/g TS. The results showed that fermented *S. alterniflora* could be utilized for biogas production after intermittent treatment with NaOH and potato addition.



ACKNOWLEDGEMENTS

This research was funded by the China National Water Special Project (No.2008ZX07101-004) and the Fundamental Research Funds for the Central Universities.

REFERENCES

- [1] Qin P. and Chung, C.H. (1992) Applied studies on *spartina*. Ocean Press, Beijing, 110-128 (in Chinese).
- [2] Daehler C.C. and Strong D.R. (1996) Status, prediction and prevention of introduced cordgrass *Spartina* spp. invasions in Pacific estuaries, USA. Biological Conservation 78 (1-2), 51-58.
- [3] Chung C.H., Zhuo R.Z. and Xu, G.W. (2004) Creation of *Spartina* plantations for reclaiming Dongtai, China, tidal flats and offshore sands. Ecological Engineering 23 (3), 135-150.
- [4] Xu G.W. and Zhuo R.Z. (1985) Preliminary studies of introduced *Spartina alterniflora* Loisel in China I. J. Nanjing Univ. Res. Adv. Spartina, 212-225.
- [5] Chung C.H. (1990) Twenty-five years of introduced *Spartina anglica* in China. In: *Spartina anglica: A Research Review*-Gray, A.G. and Benham, P.E.M., Editors, 1990. ITE research publication No. 2, HMSO, London, 72-76.
- [6] Pomeroy L.R. and Wiegert R.G. (1981) The Ecology of a Salt Marsh. Springer-Verlag, New York, 39-67.
- [7] Mann K.H. (1982) Ecology of Coastal Waters. University of California Press, Berkeley, 322.
- [8] Daehler C.C. and Strong D.R. (1995) Impact of high herbivore densities on introduced smooth cordgrass, *Spartina alterniflora*, invading San Francisco Bay, California. Estuaries 18 (2), 409-417.
- [9] Farber S.C., Costanza R. and Wilson M.A. (2002) Economic and ecological concepts for valuing ecosystem services. Ecological Economics 41 (3), 375-392.
- [10] Grevstad F.S., Strong D.R., Garcia-Rossi D., Switzer R.W. and Wecker M.S. (2003) Biological control of *Spartina alterniflora* in Willapa Bay, Washington using the planthopper *Prokelisia marginata*: agent specificity and early results. Biological Control 27 (1), 32-42.

- [11] Fisher A.J., DiTomaso J.M. and Gordon T.R. (2005) Intraspecific groups of *Claviceps purpurea* associated with grass species in Willapa Bay, Washington, and the prospects for biological control of invasive *Spartina alterniflora*. *Biological Control* 34 (2), 170-179.
- [12] Hastings A., Hall R.J. and Taylor C.M. (2006) A simple approach to optimal control of invasive species. *Theoretical Population Biology* 70 (4), 431-435.
- [13] Thomas M.B. and Reid A.M. (2007) Are exotic natural enemies an effective way of controlling invasive plants?. *Trends in Ecology Evolution* 22 (9), 447-453.
- [14] Zhang Y.H. and Lynd L.R. (2004) Toward an aggregated understanding of enzymatic hydrolysis of cellulose: noncomplexed cellulase systems. *Biotechnology and Bioengineering* 88 (7), 797-824.
- [15] Ding S.Y. and Himmel M.E. (2006) The maize primary cell wall microfibril: a new model derived from direct visualization. *Journal of Agricultural and Food Chemistry* 54 (3), 597-606.
- [16] Pavlostathis S.G. and Giraldo-Gomez E. (1991) Kinetics of anaerobic treatment: a critical review. *Critical Reviews in Environmental Science and Technology* 21 (5-6), 411-490.
- [17] Komilis D.P. and Ham R.K. (2003) The effect of lignin and sugars to the aerobic decomposition of solid waste. *Waste Management* 23, 419-423.
- [18] Yang S.G., Li J.H., Zheng Z. and Meng Z. (2009) Characterization of *Spartina alterniflora* as feedstock for anaerobic digestion. *Biomass and Bioenergy* 33 (4), 597-602.
- [19] Yang D.Y., Li X.J., Gao Z.J. and Wang Y.W. (2003) Improving biogas production of corn stalk through chemical and biological pretreatment: a preliminary comparison study. *Transactions of the Chinese Society of Agricultural Engineering* 19 (5), 209-212.
- [20] Rushbrook P.E. (1990) Co-disposal of industrial wastes with municipal solid wastes. *Resources, Conservation and Recycling* 4 (1-2), 33-49.
- [21] Tafdrup S. (1994) Centralized biogas plants combine agricultural and environmental benefits with energy-production. *Water Science Technology* 30 (12), 133-141.
- [22] Parawira W., Murto M., Zvauya R. and Mattiasson B. (2004) Anaerobic batch digestion of solid potato waste alone and in combination with sugar beet leaves. *Renewable Energy* 29 (11), 1811-1823.
- [23] Agdag O.N. and Sponza D.T. (2007) Co-digestion of mixed industrial sludge with municipal solid wastes in anaerobic simulated landfilling bioreactors. *Journal of Hazardous Materials* 140 (1-2), 75-85.
- [24] Ahring B.K., Angelidaki, I. and Johansen K. (1992) Anaerobic treatment of manure together with industrial waste. *Water Science and Technology* 25 (7), 311-318.
- [25] APHA (1995) Standard methods for the examination of water and wastewater, 19th ed. American Public Health Association, Washington D C, USA.
- [26] Buyukkamaci N. and Filibeli A. (2004) Volatile fatty acid formation in an anaerobic hybrid reactor. *Process Biochemistry* 39 (11), 1491-1494.
- [27] Siegert I. and Banks C. (2005) The effect of volatile fatty acid additions on the anaerobic digestion of cellulose and glucose in batch reactors. *Process Biochemistry* 40 (11), 3412-3418.
- [28] Zhao J.H., Zhang B. and Cai W.M. (2005) Research progress on propionic acid accumulation and control in anaerobic digestion system. *China Water and Wastewater* 21 (3), 25-27 (in Chinese).
- [29] Oktay S., Cokgor E.U., Zengin G.E., Aksit E.A. and Orhon D. (2004) Effect of mixing on primary sludge fermentation products. *Fresenius Environmental Bulletin* 13 (10) 1024-1027.
- [30] Ardic I. and Taner F. (2005) Effects of thermal, chemical and thermochemical pretreatments to increase biogas production yield of chicken manure. *Fresenius Environmental Bulletin* 14 (5), 373-380.

Received: January 10, 2011

Accepted: February 24, 2011

CORRESPONDING AUTHOR

Zheng Zheng

Department of Environmental Science and
Engineering
Fudan University
200433 Shanghai
P.R. CHINA

Phone: +86-21-65643342

Fax: +86-21-65642948

E-mail: zzhenghj@fudan.edu.cn

DISTRIBUTION AND CONTAMINATION STATUS OF HEAVY METALS IN SEDIMENTS OF BUNA RIVER AND ADRIATIC SEA

Alma Shehu* and Pranvera Lazo

University of Tirana, Faculty of Natural Sciences, Department of Chemistry, Tirana, Albania

ABSTRACT

The environmental status of Buna River system due to heavy metal distribution and contamination in sediments was investigated. Samples were collected in different depths along the river, beginning from its mouth toward the Adriatic Sea. All samples have been subjected to “acqua regia” digestion technique and analyzed for major and trace elements (Fe, Mn, Cu, Pb, Cr, Zn, As, Ni and Cd) via atomic absorption spectroscopy technique. Geoaccumulation indexes and enrichment factors were calculated in order to assess the origin of the heavy metal levels observed (natural or contaminated occurrence). Enrichment factor (EF) values <1, when compared with Fe, indicated that elements in the sediments studied originated predominantly from crustal material or terrestrial one, except for Ni. This study showed that a positive correlation was found between Fe, Mn and Cr, Mn and Zn, Ni and Cu, Cr, Mn and Zn whereas negative correlations resulted between Ni, Cd - As, Cr, Cd, Cu - Cd, and As, Zn - Cd, Pb, calculated for the average content of heavy metals at each station.

The role of background value was very important in environmental classification of the studied area. All the samples resulted to be classified mostly in Class 0 or 1 (background concentrations or unpolluted) for all the metals, except for Ni and As, when using METRANAL™-1 certified reference material as background. Stations B1-B4 were classified in Class 2 (as moderately polluted) and B5 in Class 3 (as polluted) when regarding Ni, whereas only station B1 fell in Class 2 (moderately polluted) with respect to As.

KEYWORDS: Surface sediments, heavy metals, geo-accumulation index, enrichment factor; Buna River, Adriatic Sea.

1. INTRODUCTION

Studies on sediments have been increasingly highlighted internationally because of their negative influence on the quality of the aquatic environment. Aquatic sediments represent an open, dynamic, and heterogeneous biogeochemical system, formed by the accumulation of particulate matter introduced to the aquatic environment from a variety of sources. Sediments are a structured accumulation of particulate mineral matter, inorganic matter of biogenic origin, organic matter in various stages of decomposition or synthesis, and water [1].

Metals in river and marine environments have both natural and anthropogenic origins. Sediments of industrial areas are the largest repository and potential source of metal pollutants in the aquatic environment. The metals of considerable environmental impacts are As, Pb, Hg, Cd, Zn and Cu. Other metals, such as Ni, Cr and Co, may reflect as well anthropogenic input, according to local quarrying and industrial activities [2]. Some elements may have background concentrations below or near the limit of detection for the chemical analysis [3]. Undisturbed sediments accumulate chemical compounds, becoming sinks and eventually, reservoirs for many contaminants potentially toxic to aquatic organisms [4]. Assessing the input of metals in the environment, as a result of human activity is complicated by the very large natural input (i.e. erosion of ore-bearing rocks, wind-blown dust, and volcanic activity or forest fires. Factors that influence metal concentration in the sediments are related to: (1) mineralogical and granulometric composition; (2) red-ox state of the metal; (3) pH and Eh of environment; (4) adsorption and surface precipitation processes [5].

Soil characteristics and environmental properties, such as climate, topography, and vegetation, are the major factors that control the movement of pollutants in soils. Nature of the pollutant is another factor on the transport of chemicals in the soil matrix [6].

In order to differentiate between natural and anthropogenic loads of a metal, it is necessary to understand the sedimentological regime of the region studied, and to normalize the concentration obtained to the regional background values. Iron (Fe) has been successfully used for

* Corresponding author

normalization in several studies [7-9]. However, it has been suggested that remobilization and precipitation can lead to changes in the pollutant/Fe ratio in anoxic sediments [9].

The objective of the present study was to analyze heavy metals in bottom sediments of the Buna River and Adriatic Sea, aiming to evaluate the factors controlling metals occurrence in these environments.

1.1. Study Area

Albania lies entirely within the Alpine Orogenic Belt; the belt of rocks deformed and uplifted by the mountain building episodes that formed the European Alps. In Albania, the belt comprises Palaeozoic sediments and metamorphic rocks; volcanic and plutonic rocks chiefly of Mesozoic age; and thick sequences of younger sedimentary rocks. The north-eastern portion of the belt within Albania is prospective for minerals, such as chromium, copper, zinc, nickel, gold and platinum group metals. The south-western portion of the belt is prospective for oil sands and gas [10].

The northern and eastern portion of the Alpine Orogenic Belt in Albania includes widespread ophiolite sequences. Albania's ophiolites represent a 4-8 km thick sheet of oceanic crust that was thrust up onto and over the adjacent continental crust during a collisional phase of the Alpine Orogeny. These ophiolites were emplaced during the Late Jurassic - Early Cretaceous.

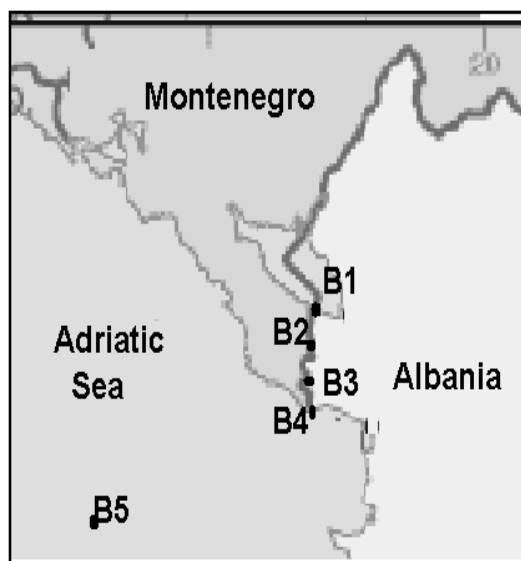


FIGURE 1 - The map of sampling area.

The Buna River is 41 km long and flowing through Albania and Montenegro into the Adriatic Sea. An outflow of Lake Skadar, measured from the source of the lake's longest tributary, the Morača-Lake Skadar-Bojana system is 183 km long [11]. Despite being short, the river has quite a large watershed, covering 5,187 km², because the whole drainage area of Lake Scutari, the largest lake in southeastern Europe, is also a part of it. Also, thanks to the waters from the Great Drin, the Buna ranks second

place among all tributaries to the Adriatic, measured by the annual discharge, after the Po River in Italy (with 352 m³/s).

After the 90's, the activity of mines and chemical industry in Albania has been minimal but the residues of them in environment posed a risk for human health [12].

2. MATERIALS AND METHODS

Sediment samples were collected in three different depths (0-2, 12-14 and 28-30 cm) at different stations along Buna River, beginning from its mouth toward the Adriatic Sea (Fig. 1). Sampling was carried out during May 2009, and 6 stations (four belonging to the river, one to the Adriatic Sea (sample 5) and one to the Ionian Sea (sample 6 used as background)) have been chosen for this study. A representative portion of each sample was powdered for chemical analysis using an agate mortar.

The total metal content was determined after the treatment of each sample with 14 ml aqua regia (HCl/HNO₃, 3:1) using Teflon vessels, until wet salts were reached. Samples were diluted to 25 ml with deionized water and stored at 4 °C until analysis. All reagents employed were of Suprapure-grade (Merck). The determination of heavy metal contents in sediment samples was carried out using the Flame AAS System for Fe, Cr, Ni, Zn, Mn and Cu determination as well as ETA-AAS System for As, Pb and Cd determination. Flame measurements were conducted using a Varian SPECTRA AA 10-Plus atomic absorption spectrophotometer whereas furnace measurements were carried out using the NOVAA 400, Analytik Jena spectrometer. Chemical modifiers, such as Pd(NO₃)₂ and NiSO₄·2H₂O, were used for Cd, Pb and As determination, respectively, when working with ETA-AAS system.

The detection limits for trace elements were 0.1 µg·ml⁻¹ for Pb and As; 0.01 µg·ml⁻¹ for Zn, 0.07 µg·ml⁻¹ for Ni, 0.05 µg·ml⁻¹ for Cr; 0.02 µg·ml⁻¹ for Cd, and 0.05 for Cu. Analytical blanks were run in the same way as the samples and concentration was determined using standard solutions prepared in the same acid matrix. Results are expressed in mg·kg⁻¹ dry sediment. SDM-2/TM marine sediment and METRANAL-1, river sediment were used as reference materials for quality control of total metal analyses of sediments. Obtained results were in good agreement with the certified values given in respective certificates of the CRM-s.

3. RESULTS AND DISCUSSION

3.1. Distribution patterns of elements

The concentration of heavy metals in each point was calculated as the mean value of the content of the metal in three different depths, and expressed in mg·kg⁻¹ dry weight (Table 1). The total concentration of the most toxic metals, such as Cd and Pb, was found to be very low in all sam-

pling sites whereas Fe and Mn resulted to be the metals representing highest contents. Results of the distribution of heavy metals at different stations of sediments showed that, except for As, their content increased from river towards the sea, indicating a potential transport of these elements from river toward the coastal sediments. Concentration of most toxic elements, such as Pb and Cd, resulted to be higher in sediments sampled at the mouth and delta of Buna River, Skadar Lake, indicating the influence of human activity in this area.

The variation in element levels in the sediments of the Buna river, could be partly related to the presence of different sediment types/and or ex-mining industry of Cr and Cu-Ni developed in the past decades near this area.

In order to explore possible associations existing between different variables, simple statistical analysis was applied to the data obtained. Figure 2 shows the correlation matrix for all stations regarding the average content of heavy metals, while Table 2 shows the correlation matrix for all metals.

TABLE 1 - The mean content of heavy metals in sediments of each station ($\text{mg} \cdot \text{kg}^{-1}$).

Sample	Cr	Cu	Ni	Pb	Zn	Cd	Mn	As	Fe
B1	92.8	39.5	243.3	5.9	33.2	0.4	1109.3	6.0	46496.8
B2	113.1	51.4	401.2	2.7	33.4	0.3	771.9	3.5	36882.7
B3	124.2	53.8	421.2	1.4	42.3	0.4	683.8	1.8	48262.7
B4	96.6	54.5	371.9	6.5	36.6	0.3	1084.3	2.4	42940.3
B5	128.3	48.8	431.5	1.0	41.9	0.2	959.6	3.2	47399.7
B6 Ionian Sea	90.48	29.8	269.9	9.64	80.38	0.18	623.23		3020
Igneous Rocks ¹	198.0	97.0	80.0	16.0	80.0	0.19	937.0		4220.0
Metranal	93.0	91.2	35.4	82.4	465.0	2.7	1330.0	24.1	25500.0

¹ Ion Sea (Shehu et.al. [13], Lazo et.al. [14], 2 Igneous Rocks (Grant & Middleton [15]))

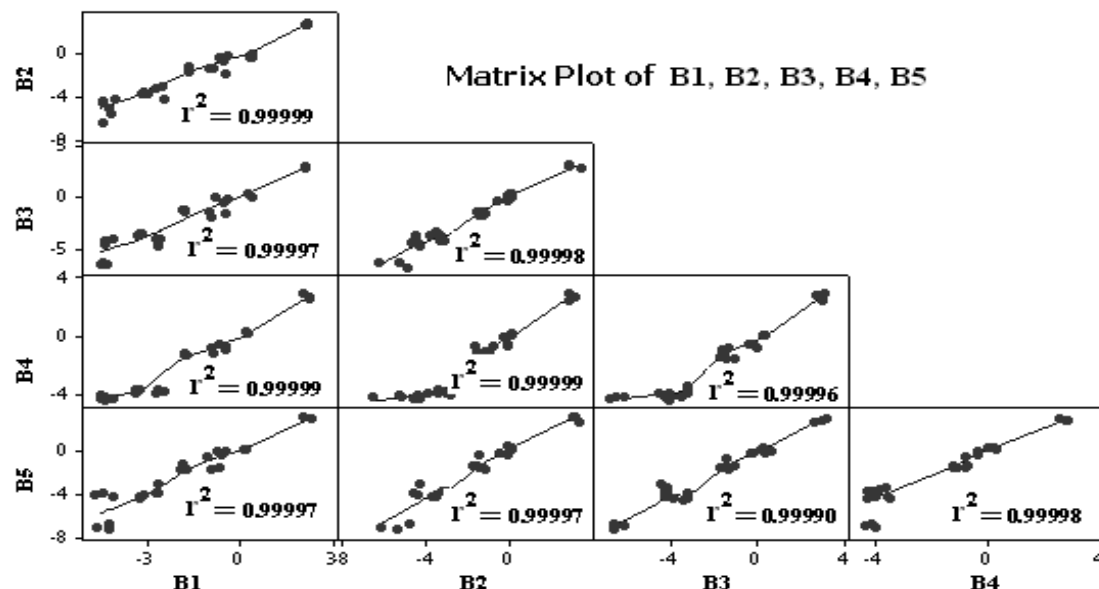


FIGURE 2 - Matrix plot of correlation matrix B1 to B5.

TABLE 2 - Correlation matrix for all metals.

	Fe	Mn	Ni	Cr	Cu	Zn	Pb	Cd
Mn	0.493							
Ni	-0.190	0.133						
Cr	0.674	0.673	0.544					
Cu	-0.459	0.057	0.896	0.223				
Zn	0.503	0.736	0.620	0.967	0.327			
Pb	-0.165	-0.111	-0.601	-0.650	-0.209	-0.694		
Cd	0.015	-0.662	-0.794	-0.690	-0.693	-0.835	0.533	
As	0.521	0.540	-0.761	0.001	-0.730	-0.034	0.437	0.252

All the stations appear to have significant correlation coefficients ($r^2 \geq 1$), confirming the fact that the distribution of the most elements in these stations derives from the same origin.

Results of correlation coefficients of heavy metals show that some of them were well correlated. The most noticeable positive correlations were found between Ni and Cu ($r^2 = 0.896$), Cr and Zn ($r^2 = 0.967$) as well as Mn and Zn ($r^2 = 0.736$), suggesting that these elements derive from the same origin. Meantime, noticeable negative correlations were found for Zn and Cd ($r^2 = -0.835$), for Ni and Cd and As ($r^2 = -0.79$) confirming the different origin of these elements. Concentration of elements deriving from mining industry, such as Cr, Cu and Ni, indicate efficient transport of these elements from Buna and Drini River to the sea sediments, even though decreasing in recent years [16].

3.2. Index of geo-accumulation

For a better estimation of grain size input, the index of geo-accumulation (I_{geo}), first given by Muller (1979) [17] regarding the content of heavy metals in particles with a granulometry < 2 mm, was calculated for each element according to the formula:

$$I_{geo} = \log_2 \frac{C_n}{1.5B_n}$$

where C_n is the measured concentration in the sediment for the metal n , B_n is the background value for the same metal, and the factor 1.5 is used because of possible variations of the background data due to lithological variations.

I_{geo} factors were calculated using three different samples considering to have background values as follows: first one) regional background values determined in Ionian Sea sediment samples, analyzed in our laboratory on the less than $63 \pm 65 \mu\text{m}$ sediment fraction, the second one) METRANAL™-1 certified reference material (river sediment), and as the third one) the global average shale data (crustal concentration of each element [18]).

Classification of the environmental situation based on the index of geoaccumulation consists of seven grades or classes (Table 3 given from Singh et al. [19]).

Similar classifications were obtained when using crustal content or regional values as background concentrations for each element. Obtained results showed that all samples belong to Classes 0 or 1 (classified as background concentrations or non-polluted) for all metals except Ni, for which the I_{geo} values made all samples to be classified in Class 2 (moderately polluted to polluted).

Different classification results were obtained when using METRANAL™-1 certified reference material as background concentration for each element. In this case, all the samples belong to Class 0 or 1 (background concen-

TABLE 3 - Classification of environmental situation based on the index of geoaccumulation, I_{geo} .

Geoaccumulation index	Class	Pollution Intensity
0	0	Background concentration
0-1	1	Unpolluted
1-2	2	Moderately to polluted
2-3	3	Moderately polluted
3-4	4	Moderately to highly polluted
4-5	5	Highly polluted
>5	6	Very highly polluted

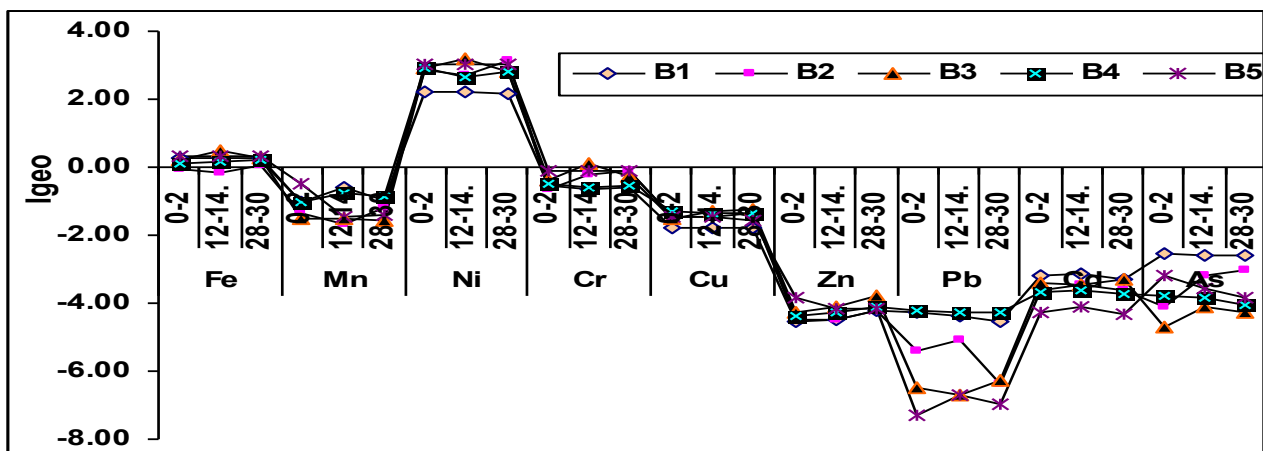


FIGURE 3 - I_{geo} distribution (using METRANAL™-1 CRM as background values).

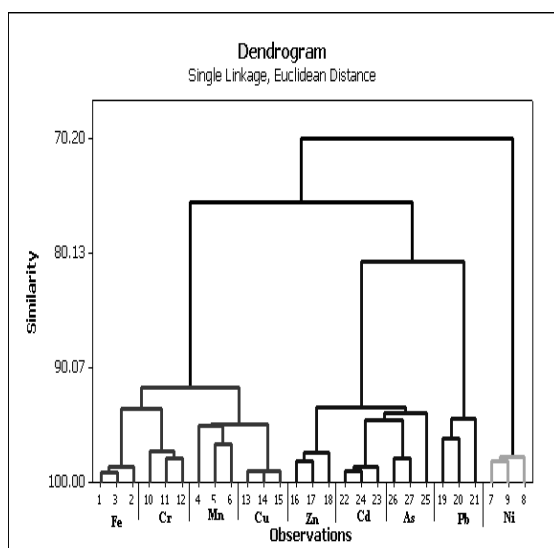


FIGURE 4 - Cluster analyses of elements.

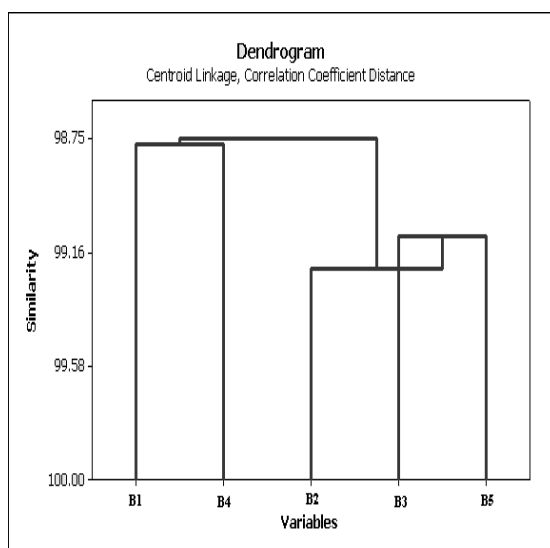


FIGURE 5 - Cluster analyses of stations studied.

trations or unpolluted) regarding all, except for Ni. Consequently, stations B1-B4 fall within Class 2 (classified as moderately to unpolluted); station B5 within Class 3 (classified as moderately polluted) regarding Ni content, whereas only station B1 falls within Class 2 (classified as moderately to unpolluted) regarding As, when using crustal content or regional values as background concentrations. These results suggest the important role of the background values chosen in such calculations, in order to be used in environmental classifications.

Enrichment factor (EF)

For a better estimation of possible anthropogenic input, the enrichment factor (EF) was also calculated for each element, by the ratio of their concentration on the sediment samples to the concentration of normalizing element divided by the same ratio found in the chosen baseline. Iron was used as normalizing element in our study. Three

different samples (sediment from Ion Sea analyzed in our laboratory, CRM sediment METRANAL-1 and crustal abundance (D. Hem [18]) were used for calculation, employing the following equation:

$$EF = \frac{(C_{Me}/C_{Fe})_{sample}}{(C_{Me}/C_{Fe})_{background}}$$

where $(C_{Me}/C_{Fe})_{sample}$ and $(C_{Me}/C_{Fe})_{crust}$ are the relative concentrations of the respective element as well as iron in the sediment and in the background material, respectively (Molinari et al. [20]; Kremling et al. [21]). An enrichment factor close to 1 would indicate a crustal origin, while factors greater than 10 are considered to have non-crustal sources, such as weathering rocks and leaching of soils, being responsible for a part of heavy metal concentrations in sediments (Yunus et al. [22]).

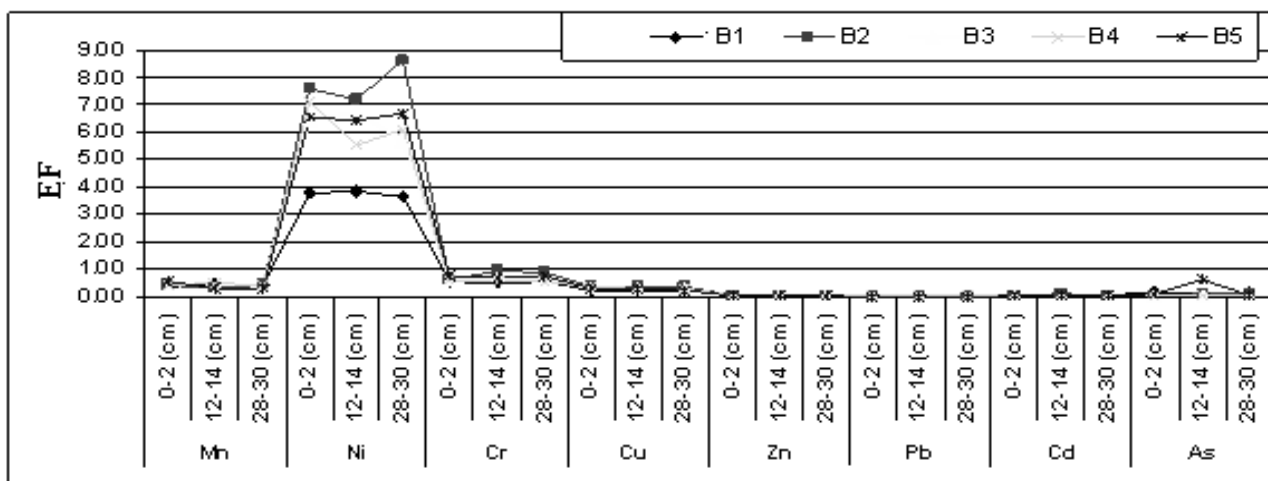


FIGURE 6 - EF distribution (METRANAL™-1 as background).

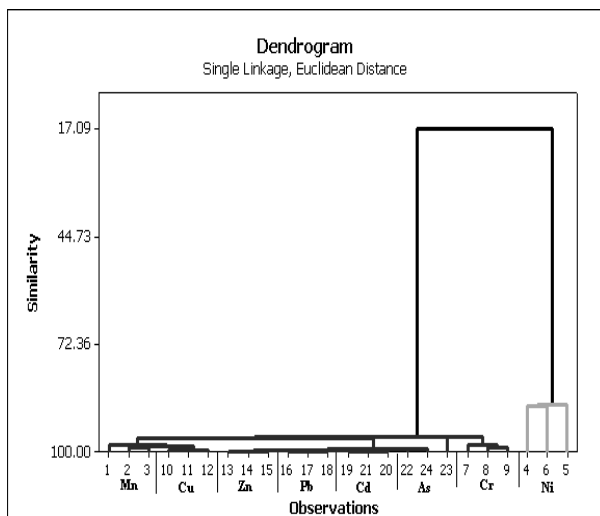


FIGURE 7 - Cluster analyses of elements.

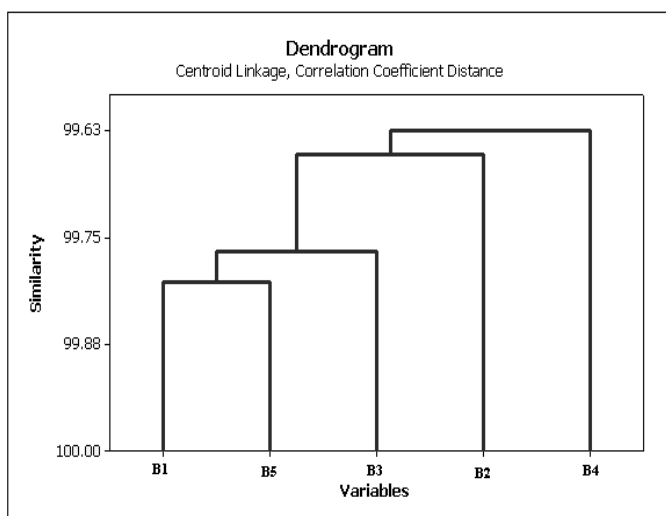


FIGURE 8 - Cluster analyses of stations.

Results presented in Fig. 6 show that all elements, (excluding Ni), despite from the nature of background sample used, represent EF values smaller or close to the unit. Therefore, it can be concluded that heavy metals are considered to be predominantly derived from natural origin (values close to the background levels) and not influenced by any anthropogenic activity. EF values of Ni were found to be within the range 3-9, indicating the influence of the anthropogenic activity in the area. The Relative EF, RE = $(C_{As}/C_{Li(\text{or Fe})\text{sample}})/(C_{As}/C_{Li(\text{or Fe})\text{background}})$ [23] produced similar results with those obtained from Igeo valuation.

4. CONCLUSIONS

Metal concentrations in the sediment of Buna River were mostly influenced by natural processes. From the I_{geo} and EF calculation, it was concluded that the concentrations of the selected elements (except Ni) were not influenced by anthropogenic activities, but moderately occurred naturally. Anthropogenic sources, such as fishing activities and industrial estate, may be the main reasons contributing insignificant heavy metal to the sediment of river. In brief, it can be concluded that there were no serious heavy metal contaminations in sediments of Buna River and Adriatic Sea compared with the world average level of shale values.

It was found that the role of background level was very important in environmental classification of the area. Accordingly, all the samples resulted to fall within Class 0 or 1 (background concentrations or unpolluted) for all metals except Ni, when using METRANALTM-1 certified reference material as background concentration. Consequently, stations B1-B4 fall within Class 2 (classified as moderately to unpolluted); station B5 falls within Class 3 (classified as moderately polluted) regarding Ni content, whereas only station B1 falls within Class 2 (classified as

moderately to unpolluted) for As, when using crustal distribution or Ion Sea site as background values.

No significant difference was found between the contents of heavy metals in different depths (0 to 30 cm) at each station.

REFERENCES

- [1] Ure, A.M., Quevauviller, P.H., Muntau, H. and Griepink B. (1992). Speciation of heavy metals in soils and sediments. an account of the improvement and harmonization of extraction techniques undertaken under the auspices of the BCR of the Commission of the European Communities. *Inter. J. Chem. 51*, 135-151.
- [2] Karageorgis, A. P., Nikolaidis N. P., Karamanos, H. and Skoulikidis, N. (1998). Water and sediment quality assessment of the Axios River and its coastal environment. *Fresenius Environmental Bulletin 7*, 631-634
- [3] Quevauviller, Ph., Muntau, H., Ure, A.M., Griepink, B., Rauert, G., Rubio, R., Fiedler, H.D. and Lopez-Sanchez, J.F. (1994). Evaluation of a sequential extraction procedure for the determination of extractable trace metal contents in sediments. *Fresenius J. Anal. Chem.*, 349, 808.
- [4] Martínez-Sánchez, J.M., Luz García-Lorenzo, M., Pérez-Sirvent, C., and Marimón, J. (2008). Use of marble cutting sludges to immobilize heavy metals and decrease toxicity of contaminated soils. *Fresenius Environmental Bulletin 17* (10), 1672-1678
- [5] Loring, D.H., Rantala, R.T. (1992). Manual for the geochemical analyses of marine sediments and suspended particulate matter, *Earth. Sci. Rev.*, 32, 235-238.
- [6] Dilek Atasoy, A. (2008). Environmental problems in vertisol soils: the example of the Harran Plain. *Fresenius Environmental Bulletin 17* (7a), 837-843.
- [7] Rule, J.P. (1986). Assessment of trace element geochemistry of Hampton Roads Harbor and lower Chesapeake Bay area sediments. *Environmental Geology and Water Science*, 8: 209-219.

- [8] Sinex, S.A. and Wright, D.A. (1988). Distribution of trace metals in the sediments and biota of Chesapeake Bay. *Marine Pollution Bulletin* 19, 425–431.
- [9] Schiff K. and Weisberg, S. (1997). Iron as a reference element for determining trace element enrichment in Southern California coastal shelf sediments. pp. 68–78 in: S. Weisberg and D. Hallock (eds.), *Southern California Coastal Water Research Project 1996 Annual Report*. Westminster, CA.
- [10] Mathison, I. (2009). Technical report on Albanian exploration projects. BSc (Hons Geol), MAusIMM
- [11] Bekteshi, A., Beka, I. and Neziri, A. (2002). The physico-chemical characteristics of waters of the Buna River. *Bul. Shkenc.*, 52: 35-41.
- [12] Miho, A., Cullaj, A., Hasko, A., Lazo, P., Kupe, L., Bachofen, R., Brandl, H., Schanz, F. and Baraj, B. (2005). Environmental state of some rivers of Albanian Adriatic lowland. Evaluation Report of the Swiss National Science Foundation through the Scientific Cooperation between Eastern Europe and Switzerland program.
- [13] Shehu, A. and Lazo, P. (2010). Heavy Metal Speciation in Some Albanian Coastal Sediments. *J. Int. Environmental Application & Science*, Vol. 5 (2): 175- 180.
- [14] Lazo, P., Lubonja, F., Arapi, A. and Pjeshkazini, L. (2004). An evaluation of heavy metals content in Orikumi, Dukati Bay-Ionian Sea – Albania, *International Journal of Chemistry*, (IJCS) Vol.2(1), 101-107
- [15] Grant, A. and Middleton, R. (1990). An assessment of metal contamination of sediments in the Humber Estuary, U.K. *Estuarine Coast. Shelf Sci.* 31 71-85.
- [16] Lazo, P., Cullaj A. and Baraj B. (2003). An evaluation of Hg, Cr and heavy metals pollution in seawater and sediments of Durres Bay, Adriatic Sea – Albania, *J.Phys. IV France*, 107, 715-720
- [17] Müller, G. (1979). Schwermetalle in den Sedimenten des Rheins – Veränderungen seit 1971. *Umschau* 79, 778-783.
- [18] Hem, J. D (1985). Study and Interpretation Of The Chemical Characteristics Of Natural Water, Third Edition, U.S Geological Survey Water-Supply Paper 2254.
- [19] Singh, K.P., Mohan, M., Singh, V.K. and Malik, M. (2005). Studies on distribution and fractionation of heavy metals in Gomati river sediment—a tributary of the Ganges, India. *J. Hydrol.* 312, 14–27
- [20] Molinari, E., Guerzoni, S. and Rampazzo, G. (1993). Contribution of saharan dust to the central Mediterranean Basin. *Geological Society of America, Special Paper* 284: 303- 312.
- [21] Kremling K. and Streu, P. (1993). Saharan dust influence trace element fluxes in deep North Atlantic Subtropical Waters. *Deep Sea Research* 40: 1155-1168.
- [22] Yunus, K and Chuan, O. M (2009). Geochemical Proxy of Some Chemical Elements in Sediments of Kemaman River Estuary, Terengganu, Malaysia. *Sains Malaysiana* 38(5): 631– 636)
- [23] Loring, D.H. (1990). Lithium – a new approach for the granulometric normalization of trace metal data. *Mar. Chem.*, 29, 155-168.

Received: January 10, 2011

Accepted: April 05, 2011

CORRESPONDING AUTHOR

Alma Shehu

University of Tirana
Faculty of Natural Sciences
Department of Chemistry
Tirana
ALBANIA

E-mail: a.shehu@albnet.net

RELATIONSHIP BETWEEN SOIL NUTRIENTS AND SOIL MICROBIAL BIOMASS, STRUCTURE AND DIVERSITY UNDER DIFFERENT TILLAGE MANAGEMENT IN WHEAT-CORN DOUBLE-CROPPING SYSTEM

Ying Wang^{1,2}, Chunsheng Hu^{1,*} and Wenxu Dong¹

¹Key Laboratory of Agricultural Water Resources, Center for Agricultural Resources Research, Institute of Genetic and Developmental Biology, Chinese Academy of Sciences, Shijiazhuang 050021, China

²Graduate University of the Chinese Academy of Sciences, Yuquanlu, Beijing 100049, China

ABSTRACT

Frequent tillage generally results in soil organic matter loss, microbial activity suppression, and soil structure deterioration. In this study, we have used polymerase chain reaction (PCR) based on 16/18S rRNA sequences, followed by denaturing gradient gel electrophoresis (DGGE) to assess the effect of different tillage managements on soil microbial populations. Soil samples were collected in June 2008 at depths of 0-10 cm and 10-20 cm at Luancheng Agroecosystem Experimental Station, Chinese Academy of Sciences. The three treatments with three replicates were: conventional tillage (CT), rotary tillage (RT) and no-tillage (NT), which represent the typical tillage systems in the North China Plain. Our results suggest that the soil microbial community structure varies under different tillage managements. The community diversities of bacteria were higher in soils under RT and NT than that under the CT in the 0-10 cm layer, whereas there was no significant difference in the community diversity of bacteria within the three treatments in the 10-20 cm layer soil. As for the soil fungi, the community diversities were obviously higher in soils under RT and NT than in the CT in both the 0-10 cm and 10-20 cm layers. These results indicate the sensitivity of soil microbial community to tillage and the necessity of considering the effects of agricultural managements on the soil microbial community when assessing changes in soil microbial community structure and diversity.

KEYWORDS:
conservation tillage; soil microbial community; DGGE

1. INTRODUCTION

Tillage is a common agricultural management used worldwide in arable soil. Therefore, the effects of different tillage managements, especially the conservation tillage practices, on the soil physical, chemical and biological properties are studied extensively [1]. The primary effect of tillage is to physically disturb the soil profile [2]. Different tillage systems will disturb the physical framework of the soil to different degrees and affect changes in organic matter levels, mineral concentrations and physical parameters [3]. The two extreme extents of physical disruption were represented by comparisons of soil parameters associated with conventional and conservation tillage systems. The latter is commonly referred to as no-tillage, or reduced tillage, and connections have been made between conservation tillage systems and beneficial effects on soil micro-organisms. The wetter, denser and cooler conditions typically associated with reduced tillage systems resulted in higher amounts of organic matter and greater microbial activity/biomass, principally in the upper layers of the soil [4]. Consequently, conservation tillage practices could have a beneficial and effective impact on the soil properties and agricultural system. The tillage-induced disruption of soil regulates the existence and function of soil micro-organisms.

The North China Plain (NCP) is one of China's major agricultural regions (3.3×10^5 km²) with a population of about 130 million. Winter wheat and summer corn are the staple grain crops in the NCP. Soil in the NCP has been intensively cultivated for thousands of years, while most crop residues were moved from the fields and used as fuel for cooking and heating [5]. The tillage technique of intensively ploughing with no crop residues retention previously used in this area is disadvantageous to the long-term sustainable agriculture. However, the application of modern conservation tillage techniques has developed quickly in the NCP. Recent years, rotary tillage and no-tillage have

* Corresponding author

represented the typical conservation tillage systems in this region. Simultaneously, most residues are now returned to soil as a part of conservational tillage practice. Thus 12–14 t ha⁻¹ of residues (4.8–5.6 t ha⁻¹ of C) are incorporated into the upper soil or covered on the soil surface after harvest [5].

Soil microorganisms play a crucial role in the cycling of almost all major plant nutrients and the energy flow of either natural or anthropogenically altered soils. Soil microbial biomass is both a labile nutrient pool and an agent for transformation and cycling of organic matter and plant nutrients in soil; therefore, it is one of the most important microbiological properties. Population size and community structure of soil microorganisms are sensitive to changes in soil physical and chemical properties [6]. The soil microbial community and functioning may respond to agricultural management and land use and any changes they experience are likely reflected in the functional integrity of soil [7]. The microbial community plays a key role in soil aggregate stability, soil organic matter formation, and the potential for substrate metabolism from the degradation of plant residues, organic amendment, and xenobiotics [8]. Soil microbial diversity is a crucial measure of sustainable soil ecosystems. The diversity of soil microbial community is important for sustainable agriculture because microorganisms perform diverse ecological services in agricultural systems, including recycling of plant nutrients, maintenance of soil structure, detoxification of noxious chemicals, and the control of plant and animal pests [6, 9]. New molecular techniques, targeting small subunit rRNA sequences by PCR amplification, coupled with the rDNA-fragment analyses by denaturing gradient gel electrophoresis (DGGE) [10–13], have recently been developed for rapidly studying soil microbial diversity.

In this study, we collected soil samples from 10-year conservation tillage experimental field located in North China Plain, and examined the soil main properties and soil microbial community structure and diversity under different tillage practices. Our objective was to evaluate the changes in soil microbial community, and the effects of long-term conservational tillage managements on the soil microbial community.

2. MATERIALS AND METHODS

2.1. Study site description

The field experiment was located in Luancheng Agro-ecosystem Experimental Station, Chinese Academy of Sciences (37°53'N, 114°41'E, elevation 50 m), Hebei province, which was at the piedmont of the Taihang Mountains, in the North China Plain. The area was characterized by a temperate semi-wet semi-dry monsoon climate with mean annual temperatures of 12.5°C and mean annual rainfall of about 480 mm, 70% of which was in the period from July to September. The soil type of the area was predominantly silt loam. The principal cropping system in the area

was a winter wheat-corn double-cropping system (two crops harvested in any single year) without fallow between crops.

The field experiment was established since 2001. The three treatments were: conventional tillage (CT); rotary tillage (RT); no-tillage (NT), with three replicated plots. The cultivation depths were about 20 cm and 10 cm for the CT and RT, respectively. The different treatments represented the typical tillage systems in the North China Plain. The RT and NT were prevalent conservation tillage practices in this area. The fertilizer and irrigation were identical for all tillage treatments. The fertilizers used were urea and diammonium hydrogen phosphate. Before winter wheat sowing, fertilizers were applied at the rate of 130 kg ha⁻¹ N and 121 kg ha⁻¹ P. In addition, both wheat and corn received 138 kg ha⁻¹ N by surface broadcast shortly after jointing. The crops were generally flood-irrigated with pumped groundwater. All plots were irrigated at sowing. Additional three or four irrigations for wheat and two or three irrigations for corn were applied using a sprinkler system. Irrigation schedule was determined depending on soil moisture. Irrigation was applied when the soil moisture in the root zone was declined to 60–65% of field capacity.

2.2. Sample collection and preparation

Soil samples were collected from 0–10 cm and 10–20 cm surface soil respectively. Five soil cores (5 cm diameter) were collected from each plot and mixed immediately.

The 18 samples were transported on ice to the laboratory and sieved through a 2-mm mesh. Each sample was separated into three portions. The first portion was air dried for soil chemical analysis. The second portion was stored at 4°C for microbiological analysis. The third portion was stored at -20°C for DNA extraction.

2.3. DNA extraction

Genomic DNA was extracted from 0.5 g of fresh soil using a MoBio UltraClean™ soil DNA isolation kit (San Diego, CA) according to the manufacturer's instructions. DNA was finally eluted with 50 µl of the DNA elution buffer included in the kit and stored at -20°C before use.

2.4. PCR amplification for DGGE

The universal bacterial primers [14], F357-GC: 5'-CGC CCG CCG CGC GCG GCG GGC GGG GCG GGG GCA CGG GGG GCC TAC GGG AGG CAG CAG-3' (GC clamp underlined) and R518: 5'-ATT ACC GCG GCT GCT GG-3', located at the V3 region of the 16S rRNA genes, were used to amplify the variable V3 region of 16S rDNA. A GC clamp attached to the forward primer prevented the complete melting of the PCR products during subsequent separation in DGGE. Amplification was performed in 50 µl reaction mixtures including 5 µl 10×PCR buffer (with MgCl₂), 400 µM each dNTP, 20 µM of each primer, 500 µg ml⁻¹ of BSA and 2.5 U Ex Taq DNA polymerase (TaKaRa). The PCR was performed with

the following reaction conditions: initial denaturation at 94°C for 2 min, followed by 35 cycles of denaturation at 94°C for 30s, annealing at 56°C for 30s, extension at 72°C for 1 min, and a final extension at 72°C for 7 min.

The fungal 18S rDNA was amplified with the forward primer FUNG-GC: 5'-CGC CCG CCG CGC CCC GCG CCC GGC CCG CCG CCC CCG CCC CAT TCC CCG TTA CCC GTT G-3' (GC clamp underlined) and reverse primer NS1: 5'-GTA GTC ATA TGC TTG TCT C-3' [14]. PCR was performed in a total volume of 50 µl using the following protocol: initial denaturation at 94°C for 2 min, followed by 35 cycles of denaturation at 94°C for 30s, annealing at 56°C for 30s, extension at 72°C for 1 min, and a final extension at 72°C for 7 min.

The products of both the 16S rDNA and the 18S rDNA were checked on 1% (w/v) agarose gel and stained with ethidium bromide (EB).

2.5. Denaturing gradient gel electrophoresis analysis

Denaturing gradient gel electrophoresis analysis of PCR products was performed with the DCode Universal Mutation Detection System (Bio-Rad Laboratories, Hercules, USA). PCR products of 16S rDNA and 18S rDNA were loaded onto 6% polyacrylamide gel (Acrylamide/Bisacrylamide 37.5:1) with a denaturing gradient of 35-60% and 15-40% (100% denaturant contains 7 M urea and 40% formamide) respectively. Electrophoreses were run at 65 V for 16 h at 60°C in 1×TAE buffer. The gels were stained with 1:10000 SYBR Gold Nucleic Acid Gel Stain (Invitrogen 20 Molecular Probes, Eugene, USA) for 30 min, and visualized with a Bio-Rad Gel Doc documentation system.

2.6. Cloning and sequencing

Numbered bands in the DGGE gel were excised for clone and sequencing analysis. The dominant bands in the DGGE gel were excised and suspended in 50µl of Tris-HCl buffer (pH 8.0) for 12 h, and reamplified with the primers (not with the GC clamp). The purified reamplified PCR products were ligated into the pGEM-T Easy Vector (Promega, Madison, WI, USA), and the resulting ligation mix transformed into Escherichia coli JM109 com-

petent cells following the instructions of the manufacturer. The positive clones were amplified using the above primers with GC clamp and checked by DGGE. The correct one was selected for sequencing.

2.7. Statistical analysis

Data (means ± SD, n=3), except DGGE gel imaging, were analyzed with the software SPSS 13.0 for windows. One-way ANOVA was used to check for quantitative differences between treatments at $P<0.05$.

The DGGE gel image was analyzed using the software Quantity One (Bio-Rad Laboratories). The genetic diversity of soil microbial communities was analyzed by Shannon indices (H) and Evenness (E_H) according to the following equations:

$$H = -\sum_{i=1}^S p_i \ln p_i = -\sum_{i=1}^S (N_i/N) \ln(N_i/N)$$

$$E_H = H / H_{\max} = H / \ln S$$

Here N_i is the abundance of the i th ribotype, N is the total abundance of all ribotypes in the sample (lane of DGGE gels) and S is the number of ribotypes.

3. RESULTS

3.1. Soil properties

The pH of treated soils increased from 0-10 cm layer to 10-20 cm layer (Table 1). The bulk density showed an increasing trend with the depth of soil. The soil bulk density of RT was significantly higher than that of CT and NT soil in the 10-20 cm layer, while there was no obvious difference within treatments in the 0-10 cm layer. In the 0-10 cm layer soil, the RT samples had the highest concentrations of soil organic carbon, and then the NT samples, the CT samples had the lowest concentrations of soil organic carbon. In the 10-20 cm layer soil, there was no significant difference in soil organic carbon between different treatments. The variation of total N and MBC showed a similar trend with soil organic carbon. The Olsen P concentrations of RT and NT soils were obviously higher than those of CT in both soil layers.

TABLE 1 - Major soil characteristics under conventional tillage (CT), rotary tillage (RT) and no-tillage (NT) in the layers of 0-10 cm and 10-20 cm.

Layer	Tillage treatment	pH	Bulk density (g cm ⁻³)	Organic C (mg g ⁻¹)	Total N (mg g ⁻¹)	C/N	Olsen P (mg kg ⁻¹)	MBC (mg kg ⁻¹)	MBN (mg kg ⁻¹)
0-10 cm	CT	8.22±0.03ab	1.34±0.02c	16.2±0.01c	1.14±0.01bc	14.26±0.16a	7.9±0.01b	208±0.07b	63.3±0.07a
	RT	8.16±0.01c	1.36±0.04c	20.9±0.06a	1.38±0.01a	15.11±0.07a	10.2±0.02a	269±1.16a	77.2±0.13a
	NT	8.19±0.02bc	1.36±0.09c	18.0±0.11b	1.30±0.01a	13.96±0.12a	11.1±0.02a	264±1.62a	72.5±0.11a
10-20 cm	CT	8.24±0.04a	1.34±0.04c	15.9±0.12c	1.13±0.01bc	14.11±0.09a	5.9±0.02c	231±0.64ab	60.9±0.05a
	RT	8.20±0.02abc	1.59±0.03a	15.5±0.10c	1.04±0.01c	15.37±0.06a	8.6±0.03b	247±0.09a	65.3±0.22a
	NT	8.23±0.02ab	1.45±0.02b	16.9±0.07bc	1.25±0.01ab	13.60±0.15a	8.9±0.02b	259±1.50a	73.7±0.15a

Means of 3 replicates ± standard error. Values in the same columns followed by different letters indicate significant difference ($P<0.05$) as determined by the LSD test.

3.2. DGGE profiles of microbial communities

DGGE analysis was used to examine the effects of the different tillage managements on soil microbial communities in greater detail. DNA was successfully extracted from all the soil samples and prepared for PCR-DGGE analysis. PCR amplification of 16/18S rDNA fragments successfully generated 230-390-bp products that were visible as strong bands in the agarose gel after electrophoresis (data not shown). The DGGE profiles of bacterial and fungal communities contained a large number of sequence types (bands). Differences between samples were either in terms of the presence/absence of each DGGE band or in terms of the intensity of co-migrating band.

Comparing the bacterial DGGE profiles (Fig. 1) revealed that bacterial communities are almost similar with regard to the intense bands that may represent numerically dominant bacterial species. Together with these intense

bands, abundant fainter bands presented in the profiles; these were all considered when the community diversity was calculated. In contrast, considering fungal DGGE profiles revealed obvious differences within the CT, RT and NT treatments and bands F1-F16 were excised and sequenced (Fig. 2). Some faint bands disappeared, and some bands became strong in DGGE profiles from 0-10 cm layer to 10-20 cm layer. The numbers of detectable bands in the profiles of the RT and NT samples were obviously higher than those of CT samples in the 0-10 cm layer. Moreover, bands F3 and F14 were unique to 0-10 cm layer RT treatment; whereas F15 was unique to 0-10 cm layer NT treatment. Although some bands (F2, F7-F13, F16) were present in the profiles of most samples, their intensity was discrepant. For example, F4 and F5 presented the high intensity in the 0-10 cm layer RT and NT samples, while faint in the 10-20 layer CT and RT samples, disappeared in the 0-10 cm layer CT and 10-20 cm NT samples.

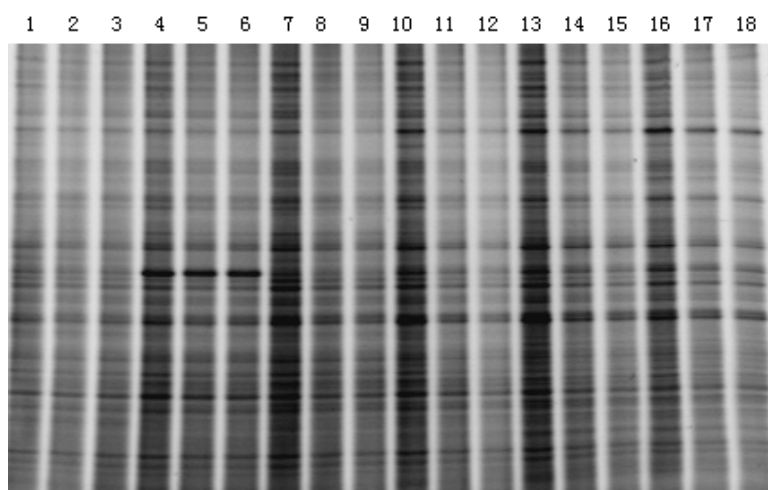


FIGURE 1 - DGGE profiles of soil bacterial community. Lane 1-3: 0-10 cm layer soil under conventional tillage (CT); Lane 4-6: 0-10 cm layer soil under rotary tillage (RT); Lane 7-9: 0-10 cm layer soil under no-tillage (NT); Lane 10-12: 10-20 cm layer soil under conventional tillage (CT); Lane 13-15: 10-20 cm layer soil under rotary tillage (RT); Lane 16-18: 10-20 cm layer soil under no-tillage (NT).

TABLE 2 - Shannon-Weaver diversity and evenness indices of the bacterial and fungal community in soils under conventional tillage (CT), rotary tillage (RT) and no-tillage (NT) in the layers of 0-10 cm and 10-20 cm.

Layer	Treatment	Bacterial		Fungal	
		Shannon-Weaver index (H)	Evenness (E)	Shannon-Weaver index (H)	Evenness (E)
0-10 cm	CT	3.21±0.02c	0.96±0.01ab	2.89±0.05d	0.96±0.02b
	RT	3.39±0.07a	0.95±0.01b	3.38±0.02a	0.98±0.01a
	NT	3.38±0.03a	0.97±0.01a	3.36±0.02a	0.98±0.01a
10-20 cm	CT	3.30±0.04b	0.96±0.01ab	3.18±0.02c	0.96±0.01b
	RT	3.33±0.03ab	0.95±0.01b	3.23±0.01b	0.97±0.01ab
	NT	3.30±0.03b	0.97±0.01a	3.26±0.02b	0.98±0.01ab

Means of 3 replicates ± standard error. Values in the same column followed by different letters (a-c) are significantly different ($p<0.05$).

TABLE 3 - Bivariate correlations between soil properties and Shannon-Weaver diversity indices

	pH	BD	SOC	TotN	C/N	OslP	MBC	MBN	H _B	H _F
pH	1.00									
BD	-0.12	1.00								
SOC	-0.06	-0.29	1.00							
TotN	0.44	-0.41	0.76**	1.00						
C/N	0.33	0.31	0.32	-0.34	1.00					
OslP	0.42	0.07	0.61**	0.62**	0.04	1.00				
MBC	0.50*	0.22	0.60**	0.59*	0.06	0.72**	1.00			
MBN	0.30	0.19	0.34	0.53*	0.13	0.65**	0.67**	1.00		
H _B	-0.15	0.10	0.56*	0.51*	0.08	0.61**	0.82**	0.78**	1.00	
H _F	-0.09	0.19	0.54*	0.52*	0.06	0.59**	0.86**	0.80**	0.88**	1.00

SOC = soil organic carbon, TotN = total nitrogen, OslP = Oslen P, MBC = microbial biomass carbon, MBN = microbial biomass nitrogen, H_B = Shannon-Weaver diversity indices of the bacterial community, H_F = Shannon-Weaver diversity indices of the fungal community. Numbers with * are significant ($P<0.05$) correlations; numbers with ** are significant ($P<0.01$) correlations, n = 3.

To determine microbial community diversity, the Shannon-Weaver index of diversity (H) and evenness (E) were calculated on the basis of the number and relative intensities of bands in a lane (Table 2). Samples of RT and NT had significantly higher diversity of bacterial and fungal communities than those of CT in the 0-10cm layer. As for the 10-20 cm layer, the fungal community diversities of RT and NT samples were significantly higher than those of CT samples, while no obvious differences in bacterial community diversity were observed within treatments. The evenness index of the bacterial communities were lowest in CT samples, and the evenness index of fungal communities in RT and NT samples were significantly higher than those in CT samples in the 10-20 cm layer.

The correlations between soil properties and the Shannon-Weaver index of bacteria diversity (H_B) and fungi diversity (H_F) were calculated to reflect the relationship

between soil nutrients and soil microbial diversity (Table 3). There were significant correlations ($p<0.05$) between H_B and SOC, H_B and total N, and the correlation coefficients were respectively 0.56 and 0.51. There were highly significant correlations ($p<0.01$) between H_B and Olsen P, H_B and MBC, H_B and MBN, and the correlation coefficients were 0.61, 0.82 and 0.78, respectively. The correlations between soil properties and the Shannon-Weaver index of fungi diversity (H_F) were similar with the correlations between soil properties and the Shannon-Weaver index of bacteria diversity (H_B) (Table 3).

3.3. Sequence analysis of the dominant fungi

For the identification of major fungal populations, prominent DGGE bands derived from the soils under three tillage treatments were excised and used for nucleotide sequence analysis (numbered DGGE bands in Fig. 2).

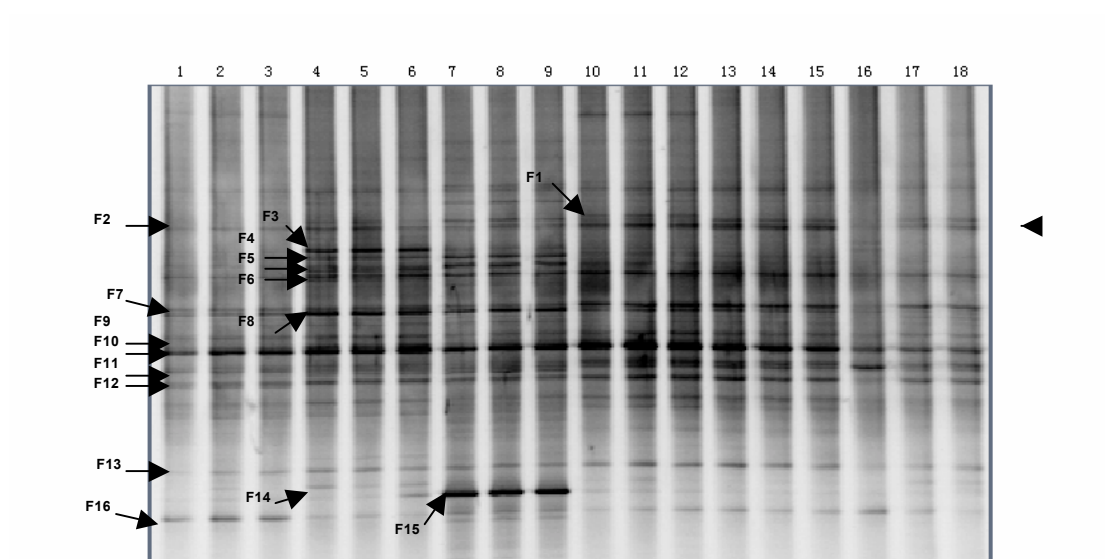


FIGURE 2 - DGGE profiles of soil fungal community. Lane 1-3: 0-10 cm layer soil under conventional tillage (CT); Lane 4-6: 0-10 cm layer soil under rotary tillage (RT) ; Lane 7-9: 0-10 cm layer soil under no-tillage (NT) ; Lane 10-12: 10-20 cm layer soil under conventional tillage (CT); Lane 13-15: 10-20 cm layer soil under rotary tillage (RT) ; Lane 16-18: 10-20 cm layer soil under no-tillage (NT) .

TABLE 4 - Characteristics of 18S rDNA fragments obtained from DGGE gel

DGGE band	Seauence length (bases)	Closest relative	Identity (%)	Accession No.
F1	324	<i>Mucro fragilis</i>	98	HM246420
F2	320	<i>Pheosporales</i> sp.	97	HM246421
F3	318	<i>Leuconeurospora pulcherrima</i>	98	HM246422
F4	322	<i>Cryptococcus</i> sp.	98	HM246423
F5	323	<i>Cryptococcus</i> sp.	97	HM246424
F6	320	<i>Lopharia mirabilis</i>	98	HM246425
F7	328	<i>Cryptococcus</i> sp.	98	HM246426
F8	332	<i>Penicillium</i> sp.	97	HM246427
F9	326	<i>Herpotrichia parasitica</i>	96	HM246428
F10	322	<i>Cucurbitaria</i> sp.	95	HM246429
F11	322	<i>Fusarium</i> sp.	93	HM246430
F12	333	<i>Fusarium</i> sp.	97	HM246431
F13	327	<i>Leuconeurospora pulcherrima</i>	98	HM246432
F14	314	<i>Leuconeurospora pulcherrima</i>	92	HM246433
F15	325	<i>Trichosporon pullulans</i>	97	HM246434
F16	314	<i>Trichosporon pullulans</i>	98	HM246435

Comparison of the 18S rDNA sequences in the study with sequences available in the GenBank database revealed high similarity between the fungal isolates. The dominant bands (F2, F6-F13) that appeared in all the samples were analyzed for general information regarding the dominant species, as shown in Table 4. The derived sequences from these bands confirmed that F2 was related to *Pheosporales* sp., F6 was related to *Lopharia mirabilis*, F7 was related to *Cryptococcus* sp., F8 was related to *Penicillium* sp., F9 was related to *Herpotrichia parasitica*, F10 was related to *Cucurbitaria* sp., F11 and F12 were related to *Fusarium* sp., and F13 was related to *Leuconeurospora pulcherrima*. F3 and F14 represented two of the dominant species in the 0-10 cm soil under RT treatment and were disappeared in the other treated samples. Their sequences closely matched that of *Leuconeurospora pulcherrima*. F15 represented one of the dominant species in the 0-10 cm layer soil under NT management and was absent in the other samples; this band was related closely to *Trichosporon pullulans*. The intensity of F16 was high in the 0-10 cm layer soil under CT treatment and was faint in the other samples; this band was also related closely to *Trichosporon pullulans*. F4 and F5 represented two of the dominant species in the 0-10 cm soil under RT and NT treatments and were faint in the other treated samples; the sequences of the two bands were closely matched that of *Cryptococcus* sp. F1 was appeared in all the samples except in the 0-10 cm layer soil under CT treatment and the sequence was related to *Mucro fragilis*.

4. DISCUSSION

Conservation tillage systems improve soil chemical, physical, and biological properties, especially in the surface layer. Soils under conservation tillage treatments have greater crop residues and higher soil organic carbon in the surface layer, which result in increased infiltration and higher water holding capacity than soils under conven-

tional treatment. Thus, soils under conservation tillage not only have high available substrate concentrations, but also wetter, cooler and less fluctuating in moisture and temperature. In our study, conservation tillage practices resulted in significant increases in soil organic carbon and microbial biomass carbon at the surface layer, hence, improved soil quality. These results supported the findings that no-till systems resulted in the surface enrichment of SOC [4, 15] and microbial biomass C [5, 16], as well as in reduced tillage systems [17]. Conservation till practices improved soil aggregation and increased soil organic carbon, especially in the surface layer [18]. Qin et al. (2010) reported that the accumulated soil organic carbon under conservation tillage was labile and mainly located in sand fractions [19]. In addition, the enzyme activities and nutrient contents observed were significantly higher under conservation tillage [20-21]. These results indicated that the increased soil organic carbon associated with conservation tillage practices not only improved soil structure and water retention, but also served as a nutrient reservoir for plant growth and a substrate for soil microorganisms.

DGGE patterns of soil fungi community shifted under different tillage treatments. The increase of microbial diversity was detected in the conservation tillage treatments (RT, NT) while compared to the conventional tillage treatment (CT). Reduction of microbial diversity with conventional tillage systems were reported in previous studies by other approaches [22-23]. Tillage practices have been shown to alter the composition and substrate utilization of the microbial community both in the current study, and elsewhere [18, 23]. The relationship between soil nutrients and soil microbial community was complicated and diversified [23-25]. Increased soil organic carbon content under long-term conservation tillage practices caused the variation of soil bacterial and fungal community structures. The soil microbial diversity had the highly significant correlations with MBC and MBN. The tillage effect has been attributed to, among other reasons, the soil disturbance. The soil disturbance may affect the organisms

through desiccation, mechanical destruction, soil compaction, reduced pore volume and disruption of access to food resources. Soil moisture is another tillage-related factor that affects microbial community. These conditions could stimulate the growth and activity of soil microorganisms. Therefore, the conservational tillage practice could enhance the ventilation and humidity of the soil and consequently promoted the microorganisms to decompose the organic matter and accelerate the growth of microorganisms. Furthermore, the conservational tillage with chopped residues incorporated into soil could make the soil uniformly mixed with the residues and significantly increased the quality and quantity of soil organic carbon and consequently provide more energy resources.

5. CONCLUSIONS

This study demonstrated statistically significantly higher soil organic carbon in the conservational tillage (RT, NT) than in the conventional tillage treatment (CT). DGGE patterns also showed the bacterial and fungal communities shifted among the different tillage treatments, indicating that the soil microbial community showed an adaption to the varying environment. The diversity of microbial community in the conservational tillage was higher than that in conventional tillage treatment. These results could indicate that the conservation tillage treatments and conventional tillage treatment have different effects on the soil nutrients and microbial community, whereas the soil nutrients and microbial community have different correlations.

ACKNOWLEDGMENTS

This work was supported by the National Natural Science Foundation of China (30970534) and Innovation Knowledge Project of the Chinese Academy of Sciences (grants KZCX2-YW-449).

REFERENCES

- [1] Piovanelli, C., Gamba, C., Brandi, G., Simoncini, S., and Bastistoni, E. (2006) Tillage choices affect biochemical properties in the soil profile. *Soil and Tillage Research* 90, 84-92.
- [2] Young, I.M. and Ritz, K. (2000) Tillage, habitat space and function of soil microbes. *Soil and Tillage Research* 53, 201-213.
- [3] Peixoto, R.S., Coutinho, H.L.C., Madari, B., Machado, P., Rumjanek, N.G., Van Elsas, J.D., Seldin, L., and Rosado, A.S. (2006) Soil aggregation and bacterial community structure as affected by tillage and cover cropping in the Brazilian Cerrados. *Soil and Tillage Research* 90, 16-28.
- [4] Qin, S.P., He, X.H., Hu, C.S., Zhang, Y.M., and Dong, W.X. (2010) Responses of soil chemical and microbial indicators to conservational tillage versus traditional tillage in the North China Plain. *European Journal of Soil Biology* 46, 243-247.
- [5] Dong, W., Hu, C., Chen, S., and Zhang, Y. (2009) Tillage and residue management effects on soil carbon and CO₂ emission in a wheat-corn double-cropping system. *Nutrient Cycling in Agroecosystems* 83, 27-37.
- [6] Lupwayi, N.Z., Arshad, M.A., Rice, W.A., and Clayton, G.W. (2001) Bacterial diversity in water-stable aggregates of soils under conventional and zero tillage management. *Applied Soil Ecology* 16, 251-261.
- [7] Insam, H. (2001) Developments in soil microbiology since the mid 1960s. *Geoderma* 100, 389-402.
- [8] Acosta-Martinez, V., Mikha, M.M., and Vigil, M.F. (2007) Microbial communities and enzyme activities in soils under alternative crop rotations compared to wheat-fallow for the Central Great Plains. *Applied Soil Ecology* 37, 41-52.
- [9] Yan, F., McBratney, A.B., and Copeland, L. (2000) Functional substrate biodiversity of cultivated and uncultivated A horizons of vertisols in NW New South Wales. *Geoderma* 96, 321-343.
- [10] Krave, A.S., Lin, B., Braster, M., Laverman, A.M., van Straalen, N.M., Roling, W.F.M., and van Verseveld, H.W. (2002) Stratification and seasonal stability of diverse bacterial communities in a *Pinus merkusii* (pine) forest soil in central Java, Indonesia. *Environmental Microbiology* 4, 361-373.
- [11] Ronn, R., McCaig, A.E., Griffiths, B.S., and Prosser, J.I. (2002) Impact of protozoan grazing on bacterial community structure in soil microcosms. *Applied and Environmental Microbiology* 68, 6094-6105.
- [12] Forney, L.J., Zhou, X., and Brown, C.J. (2004) Molecular microbial ecology: land of the one-eyed king. *Current Opinion in Microbiology* 7, 210-220.
- [13] He, J.Z., Xu, Z.H., and Hughes, J. (2005) Analyses of soil fungal communities in adjacent natural forest and hoop pine plantation ecosystems of subtropical Australia using molecular approaches based on 18S rRNA genes. *Fems Microbiology Letters* 247, 91-100.
- [14] Qu, X.H. and Wang, J.G. (2008) Effect of amendments with different phenolic acids on soil microbial biomass, activity, and community diversity. *Applied Soil Ecology* 39, 172-179.
- [15] Ding, G., Novak, J.M., Amarasinghe, D., Hunt, P.G., and Xing, B.S. (2002) Soil organic matter characteristics as affected by tillage management. *Soil Science Society of America Journal* 66, 421-429.
- [16] Hungria, M., Franchini, J.C., Brandão-Junior, O., Kaschuk, G., and Souza, R.A. (2009) Soil microbial activity and crop sustainability in a long-term experiment with three soil-tillage and two crop-rotation systems. *Applied Soil Ecology* 42, 288-296.
- [17] Jacobs, A., Rauber, R., and Ludwig, B. (2009) Impact of reduced tillage on carbon and nitrogen storage of two Haplic Luvisols after 40 years. *Soil and Tillage Research* 102, 158-164.
- [18] Feng, Y., Motta, A.C., Reeves, D.W., Burmester, C.H., van Santen, E., and Osborne, J.A. (2003) Soil microbial communities under conventional-till and no-till continuous cotton systems. *Soil Biology and Biochemistry* 35, 1693-1703.
- [19] Qin, S.P., Hu, C.S., He, X.H., Dong, W.X., Cui, J.F., and Wang, Y. (2010) Soil organic carbon, nutrients and relevant enzyme activities in particle-size fractions under conservational versus traditional agricultural management. *Applied Soil Ecology* 45, 152-159.

- [20] Qin, S.P., Dong, W.X., and Hu, C.S. (2010) Tillage affecting the turnover rate of soil urease: implications for enzyme assays and ecological modeling. *Fresenius Environmental Bulletin* 19, 717-720.
- [21] Qin, S.P., Hu, C.S., Wang, Y.Y., Li, X.X., and He, X.H. (2010) Tillage Effects on Intracellular and Extracellular Soil Urease Activities Determined by an Improved Chloroform Fumigation Method. *Soil Science* 175, 568-572.
- [22] Jackson, L.E., Calderon, F.J., Steenwerth, K.L., Scow, K.M., and Rolston, D.E. (2003) Responses of soil microbial processes and community structure to tillage events and implications for soil quality. *Geoderma* 114, 305-317.
- [23] Cookson, W.R., Murphy, D.V., and Roper, M.M. (2008) Characterizing the relationships between soil organic matter components and microbial function and composition along a tillage disturbance gradient. *Soil Biology and Biochemistry* 40, 763-777.
- [24] Xue, D., Yao, H., and Huang, C. (2006) Microbial Biomass, N Mineralization and Nitrification, Enzyme Activities, and Microbial Community Diversity in Tea Orchard Soils. *Plant and Soil* 288, 319-331.
- [25] Marschner, P., Kandeler, E., and Marschner, B. (2003) Structure and function of the soil microbial community in a long-term fertilizer experiment. *Soil Biology and Biochemistry* 35, 453-461.

Received: January 21, 2011

Accepted: March 25, 2011

CORRESPONDING AUTHOR

Chunsheng Hu

Key Laboratory of Agricultural Water Resources
Center for Agricultural Resources Research
Institute of Genetics and Developmental Biology
The Chinese Academy of Sciences
Shijiazhuang 050021
P.R. CHINA

Phone: +86-311-85814360

Fax: +86-311-88150953

E-mail: sweetwy@hotmail.com

SUBJECT INDEX**A**

absolute diagnosis	1598
acclimation	1691
accumulation response	1583
Adriatic Sea	1704
aerobic process	1649
anaerobic digestion	1698
anaerobic process	1649
anti-genotoxicity	1661
anti-oxidant enzymes	1661
antscale magnetic treatment	1617
artificially constructed flora	1649
assessment indicator	1598

B

bacterial diversity	1691
Bartin River	1673
biological pretreatment	1611
Buna River	1704

C

carbon dioxide emissions	1629
Çatalağzı	1642
cationic polymer	1611
CdS-C ₆₀ /TiO ₂	1589
cell disruption	1649
cement industry	1629
coagulation	1611
COD	1685
conservational tillage	1711
constructed rapid infiltration system	1685
conventional farming	1655
coupled	1649

D

degradation ability	1691
degradation law	1685
degradation	1624
DGGE	1711
dissolved organic nitrogen (DON)	1611
dry matter	1667

E

electricity generation	1629
elemental analysis	1655
enrichment factor	1704

F

Fe ³⁺ -AgNbO ₃	1624
flood risk	1673
floodplain corridor	1673

G

geo-accumulation index	1704
<i>Groenlandia densa</i>	1667
growth	1583

H

hazelnut	1655
heavy metals	1704
hydraulic load	1685
hydrological regimes	1667

I

industrial sector	1629
intermittent alkali treatment	1698

J

Jiangsu offshore ecosystem health	1598
-----------------------------------	------

L

lead	1583
<i>Lecanora muralis</i>	1661

M

magnetic water softening	1617
magnetic water treatment (MWT)	1617
methylene blue (MB)	1589

N

NH ₄ ⁺ -N	1685
---------------------------------	------

O

organic farming	1655
-----------------	------

P

<i>Panicum maximum</i>	1583
PCR-DGGE	1691
photocatalytic	1589
photocatalytic	1624
potassium	1642
potato	1698
pressure	1598
projection pursuit cluster model - principal component analysis method (PPCM-PCAM)	1598

Q

quantitative determination	1655
----------------------------	------

R

radioactivity	1642
radium	1642
refineries	1629
relative comparison	1598
<i>Rhizoplaca chrysoleuca</i>	1661
river revitalization	1673

S

salt stress	1667
scanning electron microscopy (SEM)	1589
soil microbial community	1711
soil	1642

AUTHOR INDEX**S**

- Spartina alterniflora* 1698
surface sediments 1704

T

- thorium 1642
transmission electron microscopy (TEM) 1589
Turkey 1642

U

- urban river landscape planning 1673

W

- wastewater treatment 1649

A

- Agar, Guleray 1661
Akbaba, Uğur 1655
Al Ott, Riad 1617
Alpsoy, Lokman 1661
Anar, Mustafa 1661
Aslan, Ali 1661
Aytekin, Hüseyin 1642

B

- Baldık, Rıdvan 1642

C

- Cao, Peng 1649
Cengiz, Bülent 1673
Chen, Guangyin 1698
Cho, Kwang-Youn 1589
Chu, Kejian 1598

D

- Dai, Benlin 1598
Dong, Wenxu 1711

F

- Fan, Zihong 1611

G

- Ge, Chengjun 1583
Gu, Li 1598
Gu, Li 1611
Guo, Jianghong 1691

H

- He, Yulong 1598
Hu, Chunsheng 1711
Hua, Zulin 1598

K

- Kaldellis, John K. 1629
Kotan, Elif 1661

L

- Lazo, Pranvera 1704
Li, Cheng 1583
Li, Chun 1649
Li, Huaming 1624
Li, Yunzhen 1598
Liu, Bing 1611
Liu, Ling 1624
Liu, Xiuli 1691
Liu, Yun 1685
Luo, Xingzhang 1698
Luo, Yan 1698

M

- Mantelis, Nikolaos 1629

M	
Memlük, Yalçın	1673
Meng, Ze-Da	1589
N	
Ni, Jinren	1649
O	
Oh, Won-Chun	1589
Q	
Qi, Yun	1691
S	
Şahin, Yusuf	1655
Shakhatreh, Saleh	1617
Shehu, Alma	1704
Smardon, Richard C.	1673
Sun, Guangsong	1624
T	
Tan, Xin	1691
Tang, Wenhao	1583
Tong, Yanbin	1649
Türkez, Hasan	1655
U	
Uruç Parlak, Kadiriye	1667
W	
Wang, Ying	1711
Wen, Shumei	1649
Wu, Xiangyang	1624
X	
Xu, Hui	1624
Xu, Wenlai	1685
Xu, Yuanguo	1624
Y	
Yang, Shiguan	1698
Yilmaz, Dilek Demirezen	1667
Yu, Huamei	1583
Yu, Xin	1611
Z	
Zafirakis, Dimitris	1629
Zhang, Huining	1611
Zhang, Jianqiang	1685
Zhang, Jibiao	1698
Z	
Zhao, Lin	1691
Zheng, Zheng	1698
Zhu, Lei	1589